UNIVERSITY OF RIJEKA FACULTY OF BIOTECHNOLOGY AND DRUG DEVELOPMENT

Robert Kolman

THE FUNCTION OF VPS34 IN THE CELLULAR RESPONSE TO NUCLEOLAR STRESS DURING MEGAKARYOPOIESIS

DOCTORAL THESIS

UNIVERSITY OF RIJEKA FACULTY OF BIOTECHNOLOGY AND DRUG DEVELOPMENT

Robert Kolman

THE FUNCTION OF VPS34 IN THE CELLULAR RESPONSE TO NUCLEOLAR STRESS DURING MEGAKARYOPOIESIS

DOCTORAL THESIS

Mentor: Prof. Antonija Jurak Begonja, PhD

Rijeka, 2025.

SVEUČILIŠTE U RIJECI FAKULTET BIOTEHNOLOGIJE I RAZVOJA LIJEKOVA

Robert Kolman

FUNKCIJA VPS34 U STANIČNOM ODGOVORU NA NUKLEOLARNI STRES TIJEKOM MEGAKARIOPOEZE

DOKTORSKI RAD

Mentor: prof. dr. sc. Antonija Jurak Begonja

Rijeka, 2025.

Mentor doktorskog rada : prof. dr. sc. biotehnologije i razvoja lijekova, Sveučilište u	
Doktorski rad obranjen je dana	u/na
	_, pred povjerenstvom u sastavu:
1.	
2.	
3	

Zahvale / Acknowledgments

Abstract

Megakaryopoiesis involves the differentiation of hematopoietic progenitors into megakaryocytes (MKs), which are the largest cells in the bone marrow (BM) that produce platelets. A key feature of the MK lifecycle is its maturation, preceding platelet formation. This process involves regulated cell growth, polyploidization, and cytoplasmic expansion. To meet the increased demands for protein synthesis and platelet production, MKs depend heavily on their ribosomal machinery and nucleolus. Besides ribosome production, the nucleolus also coordinates cellular stress responses. Vps34, the only class III Pl3K, produces phosphatidylinositol 3-phosphate (Pl3P) and plays a role in vesicular trafficking, autophagy, and lysosomal functions. Although mainly cytoplasmic, Vps34 has been found in the nucleus and nucleolus of MKs, suggesting novel roles in stress adaptation. This thesis explores how inflammatory signals and Vps34 activity influence MK maturation, nucleolar responses, and DNA damage during cellular stress.

Interleukin-1 alpha (IL-1a) was previously identified as an alternative regulator of platelet release. In this study, murine BM-derived MKs cultured with IL-1a and thrombopoietin (TPO) showed faster maturation, increased cell size, and higher ploidy levels. IL-1α changed proplatelet morphology; they were more fragile, had larger tips, and generated more platelet-like particles that were bigger. Flow cytometry and immunoblotting revealed decreased levels of hemostatic proteins, including von Willebrand factor (vWF) and GPIbβ. IL-1α promoted Erk phosphorylation downstream of TPO activation. Blocking Erk reduced IL-1α-driven increases in MK size and ploidy, indicating that the Erk-MAPK pathway is involved in this maturation process. Additionally, IL-1α increased emperipolesis, with more than half of MKs containing neutrophils, and multiple neutrophils were often observed inside a single MK. Proteomic analysis supported these findings: on day 3, IL-1α-treated MKs showed lower levels of hemostatic proteins and higher levels of neutrophil-associated proteins. By day 5, neutrophil proteins remained high, despite low emperipolesis, suggesting that neutrophil material had been transferred to MKs. Although longer culture periods partially restored vWF and GPIbB expression, these changes indicated that specific reprogramming effects of IL-1α lasted longer.

Additionally, proteome analysis revealed that IL- 1α -treated MKs are enriched in ribosomal proteins, particularly in mature MKs at day 5, suggesting heightened ribosome biogenesis or translational capacity. Likewise, nucleolar proteins were more abundant in IL- 1α MKs at days 3 and 5, with crucial nucleolar factors like UBF and B23 being more abundant in early IL- 1α MKs. Immunofluorescence

demonstrated colocalization of Vps34 with UBF in nucleoli, with IL-1 α increasing the number of nucleolar Vps34/UBF foci. Pharmacological Vps34 inhibition disrupted nucleolar structure, dispersed UBF/Vps34 foci, and halted MK growth, confirming Vps34 activity is essential for IL-1 α -induced nucleolar activation. *In vivo*, platelet depletion *via* an anti-GPIb α antibody resulted in short-term reductions in MK size and increased Vps34 fluorescence, with persistent Vps34 foci indicating nucleolar localization.

In human megakaryocytic cell lines (DAMI, HEL, K562), PMA-induced differentiation increased the nucleolar number and colocalization of Vps34 with nucleolar markers. Differentiation was associated with polyploidization and altered nucleolar morphology, with leukemic cell lines showing nucleolar stress phenotypes distinct from primary MKs. The role of Vps34 in DNA damage responses was also examined. Vps34 inhibition induced an increase in DNA damage marker γ-H2A.X and reduced nucleolar UBF expression in DAMI and HEL cells, but not in K562, suggesting lineage-specific vulnerability. PI3P colocalized with γ-H2A.X foci, and Vps34 inhibition reduced PI3P while increasing DNA damage accumulation. Pre-treatment with Vps34 inhibitor attenuated UV-induced γ-H2A.X increase, indicating that Vps34 activity modulates both baseline DNA repair and the response to genotoxic insult.

In summary, this work identified IL-1 α as a regulator of MK maturation, emperipolesis, and proteomic remodeling, while also promoting ribosomal and nucleolar activity. Vps34 emerged as a key mediator of nucleolar organization and DNA damage responses, further linking PI3P signaling to nucleolar stress adaptation. Together, these findings improved our understanding of megakaryopoiesis under stress conditions and provided a mechanistic framework for the interplay between inflammation, nucleolar regulation, and MK stress responses.

Key words: megakaryopoiesis, megakaryocyte maturation, Vps34, nucleolar stress, inflammation, DNA damage

Sažetak

koji uključuje diferencijaciju Megakariopoeza jе proces hematopoetskih progenitorskih stanica u megakariocite (MK), najveće stanice koštane srži (KS) koje proizvode trombocite. Ključna značajka životnog ciklusa MK jest njihovo sazrijevanje koje prethodi formiranju trombocita. Proces sazrijevanja uključuje regulirani rast stanice, poliploidizaciju i rast citoplazme. Kako bi zadovoljili povećane zahtjeve za sintezom proteina i proizvodnjom trombocita, MK u velikoj mjeri ovise o ribosomima i aktivnosti jezgrice (nukleolusa). Osim proizvodnje ribosoma, jezgrica također koordinira stanične odgovore na stres. Vps34, jedina Pl3-kinaza klase III, proizvodi fosfatidilinozitol 3-fosfat (PI3P) i sudjeluje u vezikularnom transportu, autofagiji i funkciji lizosoma. Iako se uglavnom nalazi u citoplazmi. Vps34 je identificirana i u jezgri i jezgrici MK, što sugerira njene do sad neistražene uloge u nukleolarnom odgovoru na stanični stres. Ovaj doktorski rad istražuje kako upalni signali i aktivnost Vps34 utječu na jezgricu, sazrijevanje MK i oštećenje DNA tijekom staničnog stresa.

Interleukin-1 alfa (IL-1α) se prethodno pokazao kao alternativni regulator stvaranja trombocita. U ovom istraživanju, mišji MK izdvojeni iz KS i kultivirani s IL-1α i trombopoietinom (TPO) pokazali su ubrzano sazrijevanje, pojačani rast i višu razinu ploidnosti. IL-1α je promijenio morfologiju protrombocita sa većim vrhovima i generirajući veći broj čestica sličnih trombocitima koje su bile veće. Protočna citometrija i Western blot analiza pokazale su smanjenu razinu hemostatskih proteina, uključujući von Willebrand factor (vWF) i GPIbβ. Mehanistički, IL-1α je povećao fosforilaciju Erk nizvodno od TPO aktivacije, dok je inhibicija Erk onemogućila rast stanice i visoku ploidnost pod utjecajem IL-1α, što implicira uključenost Erk-MAPK puta u ovaj model sazrijevanja. Osim toga, IL-1α je povećao emperipolezu, pri čemu više od polovice MK sadrži neutrofile, a često je unutar jedne stanice uočeno i više neutrofila. Proteomska analiza potvrdila je ove rezultate: na dan 3, IL-1α MK su pokazali niže razine hemostatskih proteina i više razine neutrofilnih proteina. Do dana 5, neutrofilni proteini ostali su povišeni, unatoč rjeđoj emperipolezi, što sugerira prijenos neutrofilnog materijala u MK. Dulje kultiviranje djelomično je obnovilo ekspresiju vWF i GPlbβ, no očito je da neki učinci reprogramiranja IL-1α traju dulje.

IL-1α MK također su pokazali povećane razine ribosomskih proteina, osobito zreli MK na dan 5, što sugerira pojačanu biogenezu ribosoma ili translacijski kapacitet. Nukleolarni proteini također su bili prisutniji u IL-1α MK na danima 3 i 5, s ključnim faktorima poput UBF i B23 povećanim u ranim IL-1α MK. Imunofluorescencija je pokazala kolokalizaciju Vps34 s UBF u jezgrici, a IL-1α je povećao broj nukleolarnih Vps34/UBF fokusa. Farmakološka inhibicija Vps34 omela je strukturu jezgrice,

raspršila UBF/Vps34 fokuse i zaustavila rast MK, potvrđujući ključnu ulogu Vps34 u IL-1α-induciranoj aktivaciji jezgrice. *In vivo*, deplecija trombocita putem protutijela protiv GPIbα rezultirala je kratkotrajnim smanjenjem veličine MK i povećanim fluorescentnim signalom Vps34, pri čemu se Vps34 nalazila u jezgrici tijekom trombocitopenijskog stresa.

U ljudskim megakariocitnim staničnim linijama (DAMI, HEL, K562), PMA-inducirana diferencijacija povećala je broj jezgrica i kolokalizaciju Vps34 s nukleolarnim proteinima. Diferencijaciju stanica je pratila poliploidizacija i promijenjena morfologija jezgrice, pri čemu su leukemične linije pokazale nukleolarne fenotipe stresa različite od primarnih stanica. Ispitana je i uloga Vps34 u odgovorima na oštećenje DNA. Inhibicija Vps34 inducirala je porast markera oštećenja DNA (γ-H2A.X) i smanjila ekspresiju nukleolarnog UBF u DAMI i HEL stanicama, ali ne u K562, što sugerira specifičnu osjetljivost prema staničnoj liniji. PI3P je kolokalizirao s γ-H2A.X fokusima, a inhibicija Vps34 smanjila je nuklearnu razinu PI3P i povećala akumulaciju oštećenja DNA. Pretretman inhibitorom Vps34 smanjio je UV-induciranu ekspresiju γ-H2A.X što ukazuje da Vps34 modulira popravak DNA u osnovnim uvjetima i uvjetima odgovora na genotoksične podražaje.

Ukratko, ovaj doktorski rad je identificirao IL-1α kao regulator sazrijevanja MK, emperipoleze i proteomske preuredbe, istovremeno potičući ribosomalnu i nukleolarnu aktivnost. Vps34 se pokazala ključnom za nukleolarnu organizaciju i odgovore na oštećenja DNA, povezujući PI3P signalizaciju s prilagodbom jezgrice na stres. Ovi rezultati unaprijedili su naše razumijevanje megakariopoeze u uvjetima staničnog stresa te pružili mehanistički okvir koji povezuje upalu, regulaciju jezgrice te megakariocitni odgovor na stanični stress.

Ključne riječi: megakariopoeza, sazrijevanje megakariocita, Vps34, nukleolarni stres, upala, oštećenje DNA

TABLE OF CONTENTS

INTRODUCTION	1
1.1. PLATELETS	1
1.2. DEVELOPMENT OF MEGAKARYOCYTES	2
1.2.1. Megakaryocyte maturation	3
1.3. PLATELET BIOGENESIS	5
1.4. PHOSPHOINOSITIDES AND VPS34 KINASE	8
1.4.1. Phosphoinositide roles in megakaryocytes	10
1.1. THE NUCLEOLUS	13
1.1.1. Nucleolar stress	14
1.1.2. Ribotoxic and non-canonical nucleolar stressors in the contexinflammation	
1.1.3. Impact of nucleolar stress on megakaryopoiesis in diffe	
1.1.4. Nuclear phosphoinositides in the cellular stress response to I damage	
2. THESIS AIMS AND HYPOTHESES	21
B. MATERIALS AND METHODS	22
3.1. MATERIALS	22
3.1.1. Chemicals	22
3.1.2. Cell culture reagents	23
3.1.3. Buffers	24
3.1.4. Primary antibodies	26
3.1.4.1. Evaluation of Vps34 antibody	27
3.1.5. Secondary antibodies	27
3.2. METHODS	28
3.2.1. Mice	28
3.2.2. Isolation, preparation, and culturing of murine BM MKs	28
3.2.3. BM MK culture on Matrigel	29

29	Proplatelet formation assay	3.2.4.
29	BSA gradient-based enrichment of MKs	3.2.5.
30	Immunofluorescence	3.2.6.
30	Immunofluorescence staining of phosphoinositide	3.2.7.
30	Isolation of human mononuclear cells	3.2.8.
31	Fluorescence microscopy and image analysis	3.2.9.
31	Murine blood platelet isolation	3.2.10.
32	Platelet-like-particle count	3.2.11.
32	Flow cytometry of whole bone marrow cultures	3.2.12.
32	Cell lysis and protein extraction	3.2.13.
33	DNA damage induction experiments	3.2.14.
33	Induction of acute thrombocytopenia in vivo	3.2.15.
33	Bone marrow cryosections immunostaining	3.2.16.
34	SDS-PAGE and Western blot	3.2.17.
34	Sample preparation for proteomic analysis	3.2.18.
on35	LC-MS/MS parameters for proteome data acquisi	3.2.19.
36	Data analysis for proteome data	3.2.20.
37	Statistical analysis	3.2.21.
38	SULTS	4. RESU
RESHAPES THE	ITERLEUKIN-1 ALPHA MODULATES I ATION, ENHANCES EMPERIPOLESIS, AND ARYOCYTE PROTEOME	MATURA
	IL-1α increases megakaryocyte size, alters elets, and boosts the release of platelet-like particles	4.1.1. proplate
=	IL-1α alters early megakaryocyte maturation egulation of GPIb β and vWF and increased ploidy	4.1.2. downreg
	IL-1α increases Erk phosphorylation following TP0 receptor expression	4.1.3. altering
ryocytes49	IL-1α promotes emperipolesis in immature megak	4.1.4.
	IL-1α-stimulated terminally mature megakaryocy sion and decrease the rate of emperipolesis	4.1.5. express

4.1.6. IL-1α-mediated megakaryopoiesis results in specific changes in the proteomic signature of megakaryocytes	
4.2. INTERLEUKIN-1 ALPHA ENHANCES RIBOSOMAL AND NUCLEOLA ACTIVITY DURING EARLY MEGAKARYOPOIESIS6	
4.2.1. IL-1α-stimulated megakaryocytes display a trend-based increase ribosomal protein abundance	
4.2.2. IL-1α-stimulated megakaryocytes exhibit modest abundance nucleolar proteins	
4.2.3. IL-1α increases the number of UBF and Vps34 foci in the nucleoli megakaryocytes with a moderate effect on total UBF expression	
4.2.4. Inhibition of Vps34 during early megakaryopoiesis inhibi megakaryocyte growth and disperses nucleolar UBF	
4.3. IN VIVO MODEL OF THROMBOCYTOPENIA DEMONSTRATE CHANGES IN THE NUCLEOLUS AND VPS34 KINASE IN BONE MARROMEGAKARYOCYTES	W
4.3.1. Acute platelet depletion affects the size of bone marro megakaryocytes and increases Vps34 fluorescence intensity	
4.4. CHARACTERIZATION OF THE NUCLEOLUS AND VPS34 KINASE I HUMAN MEGAKARYOCYTIC CELL LINES	
4.4.1. PMA-induced differentiation of DAMI cells leads to an increase nucleolar number and Vps34 localization in the nucleus	
4.4.2. K562 cells respond to PMA by decreasing nucleolar protein expression and subtly increasing the number of nucleoli	
4.4.3. Nucleoli number increases significantly in PMA-differentiated HE cells 93	ΞL
4.4.4. Vps34 localizes in the nucleolus of human mononuclear cells9)5
4.5. VPS34 INHIBITION AFFECTS DNA DAMAGE OUTCOMES AN NUCLEOLAR PROTEIN EXPRESSION AFTER EXPOSURE TO GENOTOXI INSULT	С
4.5.1. Vps34 inhibition alone induces DNA damage and downregulates UB in a time- and dose-dependent manner in DAMI and HEL cells	
4.5.2. PI3P strongly localizes in the nucleus of cells positive for γ-H2A.X10)1
4.5.3. Pre-treatment with Vps34 inhibitor attenuates UV-induced DN damage in DAMI and HEL cells	

			imary megakaryocytes show a slight reduction in γ-F inhibition and before UV exposure	
5.		DISCUSS	SION	107
	5.1. MEG		LEUKIN-1 ALPHA AS A PROINFLAMMATORY MODU	
	5.2. TO II		UCLEOLUS AND VPS34 IN THE MEGAKARYOCYTE IATORY-MEDIATED STRESS AND THROMBOCYTOF	_
		_	ACTIVITY MODULATES THE DNA DAMAGE RES	_
6.	-	CONCLU	JSIONS	120
7.	-	REFERE	NCES	121
8.	-	LIST OF	FIGURES	141
9.	-	LIST OF	TABLES	143
1(0.	LIST OF	ABBREVIATIONS	144
1	1.	BIOGRAF	PHY	146

1. INTRODUCTION

Hematopoiesis is a tightly regulated process through which all blood cells emerge from hematopoietic stem cells (HSCs). It is a vital biological process that ensures a continuous supply of red blood cells (erythrocytes), white blood cells (leukocytes), and platelets. Hematopoiesis is also a spatially distinct process in which a balance between self-renewal, differentiation, and proliferation occurs in the yolk sac and fetal liver during early development, and later within the bone marrow (BM) [1].

1.1. PLATELETS

Platelets are small, discoid-shaped, anucleate blood cells. They typically measure between 1.5 and 3 μ m in diameter and have a lifespan of approximately 8 to 10 days in the bloodstream. To maintain a platelet count of about 150 to 400 \times 10° platelets per liter of blood in a healthy adult, continuous production is required [2]. The ongoing demand for platelets is met through thrombopoiesis, a process that is elaborated upon through several proposed models of platelet biogenesis.

The primary function of platelets is to maintain hemostasis by rapidly responding to vascular injury, adhering to exposed subendothelium, and initiating clot formation to prevent excessive bleeding [3]. This response is driven by platelet adhesion, activation, and aggregation. These processes involve a complex interplay of receptors, signaling pathways, and the release of bioactive molecules [4]. Collectively, this is referred to as primary hemostasis. Platelets are not merely passive responders to vascular injury but actively sense their microenvironment through an array of surface receptors, including integrins and selectins.

In addition to their key role in stopping bleeding during primary hemostasis, recent research suggests that platelets also interact with components of the immune system [5]. Platelets can participate in both innate and adaptive immunity, either directly or indirectly. Under conditions of infection or inflammation, platelets directly interact with leukocytes by altering the expression of P-selectin or the CD40 marker. They are also capable of directly activating dendritic cells and facilitating their antigen presentation to T lymphocytes [6]. Pathological conditions such as sepsis, which involves a systemic infection, are often accompanied by hemostatic disorders due to excessive platelet activation and their immunomodulatory effects on neutrophils and monocytes. These effects include neutrophil degranulation, enhanced phagocytosis, and increased synthesis of pro-inflammatory mediators, among others [7]. These interactions are made possible by various immune receptors that platelets inherit from megakaryocytes.

In addition, platelets interact with leukocytes and endothelial cells, influencing processes such as wound healing, angiogenesis, and host defense [8]. Recent evidence also suggests that platelets play a role in pathological conditions such as atherosclerosis, autoimmune disorders, and even cancer metastasis by promoting tumor cell survival and metastasis [9, 10].

Among the BM lineages, megakaryopoiesis – the formation and renewal of megakaryocytes – plays a central role in maintaining platelet levels.

1.2. DEVELOPMENT OF MEGAKARYOCYTES

Megakaryocytes (MKs) are the largest cells in the BM, measuring 50 to 100 μ m. They are also among the rarest, constituting less than 0.1% of all BM cells [11]. In the hierarchical model of canonical hematopoiesis, MKs are formed through the gradual differentiation of HSCs through several lines of progenitor cells. Long-term HSCs (LT-HSCs) maintain self-renewal capacity and give rise to short-term HSCs (ST-HSCs), which possess limited renewal potential but can differentiate into multipotent progenitors (MPPs). MPPs differentiate into the common lymphoid progenitor (CLP) or the common myeloid progenitor (CMP), giving rise to lymphoid and myeloid lineages. The CMP generates two distinct progenitors: the granulocyte-macrophage progenitor (GMP), which forms granulocytes and monocytes, and the megakaryocyte-erythroid progenitor (MEP), which produces erythroblasts and MKs (Figure 1) [12].

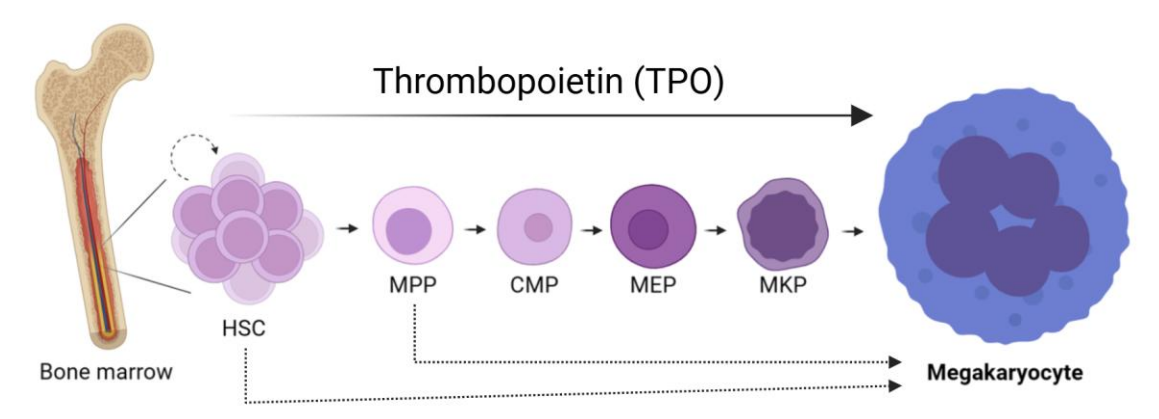


Figure 1. Schematic representation of canonical megakaryopoiesis.

In the BM, MKs originate from HSCs through a series of sequential differentiation steps, from multipotent progenitors to lineage-specific cells. Biased differentiation from HSCs and MPPs accelerates MK production (dotted arrows). Megakaryopoiesis is regulated by thrombopoietin (TPO), the key cytokine that influences all stages of MK development.

However, recent studies have highlighted early progenitor cells with the capacity for direct differentiation into MKs. Both LT-HSCs and MPPs can be biased towards the

MK lineage, allowing for direct differentiation. This accelerates MK production and consequently platelet formation when the body's demand for them is high [13].

Megakaryopoiesis is governed by a range of external factors, such as cytokines, chemokines, and cell adhesion signals, in concert with the regulation by intrinsic transcription factors [14]. The key regulator of steady-state megakaryopoiesis is thrombopoietin (TPO). TPO binds to its receptor, c-MpI (TPO-R), on MKs, triggering several important effects. These include the prevention of MK apoptosis, an increase in MK number, size, and ploidy, enhanced maturation of MKs, and the internalization of the TPO/TPO-R complex [15, 16].

TPO influences the earlier stages of MK development, ensuring a continuous supply of MK precursors capable of responding to physiological demands for platelet production. These precursor cells are well-defined and classified based on morphological characteristics, histochemical staining, and specific biochemical markers. The earliest identifiable MK precursors arise from colony-forming unitmegakaryocytes (CFU-MKs), which commit to the MK lineage. These give rise to megakaryoblasts, the first morphologically distinct cells in MK development. Megakaryoblasts are small, round cells with a high nuclear-to-cytoplasmic ratio, basophilic cytoplasm, and non-lobulated nuclei [17]. As they megakaryoblasts transition into promegakaryocytes, which exhibit increasing cytoplasmic volume, nuclear lobulation, and the onset of platelet-specific granule formation. These cells further mature into fully developed MK, characterized by their large size, extensive polyploid nuclei, and abundant cytoplasm rich in granules and demarcation membranes, which facilitate platelet release [18]. TPO mediates those outcomes through various signaling pathways, including Janus kinases (JAK), signal transducers and activators of transcription (STAT), and mitogen-activated protein kinases (MAPK).

Besides TPO, several interleukins also modulate specific stages of megakaryopoiesis. Interleukin-3 (IL-3) plays a role in the early proliferation of MK progenitors, enhancing their expansion before full commitment to the MK lineage [19]. Interleukin-6 (IL-6) has been shown to synergize with TPO to support MK maturation and platelet production, particularly under inflammatory conditions [20]. Interleukin-11 (IL-11) promotes MK polyploidization and maturation, contributing to an increase in platelet output [21, 22].

1.2.1. Megakaryocyte maturation

One of the most distinctive aspects of megakaryopoiesis is the unique maturation process that MKs undergo before releasing platelets. MK maturation involves highly

specialized cellular processes affecting nuclear and cytoplasmic growth and expansion.

MKs' nuclear maturation implies endomitosis, through which MKs increase their ploidy. It is a specialized form of cell cycle progression where DNA replication occurs without cytokinesis [23]. In humans and mice, MK ploidy follows a distribution ranging from 2N to 64N, with 16N being the most common ploidy level. During fetal development, MKs are consistently smaller and of lower ploidy than their adult counterparts, though there is a gradual shift toward higher ploidy classes and larger MKs as gestation progresses [24]. Despite this relatively low ploidy, fetal MKs display all the cytoplasmic hallmarks of maturity, including α-granules and a well-developed demarcation membrane system, highlighting that cytoplasmic maturation can occur independently of extensive polyploidization [24]. Furthermore, MKs can mature and release platelets at lower ploidy levels, and this has been observed in some pathological conditions, such as myelodysplastic and myeloproliferative syndromes [25, 26]. Polyploidization is a key adaptation that enables MKs to meet the high metabolic and structural demands of platelet biogenesis. Polyploidization leads to functional gene amplification, resulting in a boost in protein synthesis, cytoplasmic expansion, and granule formation that results in cell enlargement [27]. This enhanced biosynthetic capacity ensures that MKs generate sufficient membrane and organelle content to support platelet release.

Another defining feature of mature MKs is the presence of an intricate invaginated demarcation membrane system (DMS), a vast network of interconnected flattened cisternae and tubules that extends throughout the cytoplasm [28]. The formation of the DMS has been a topic of extensive research, with studies suggesting that it originates from plasma membrane invaginations. This system remains continuous with the external environment, and initially, the DMS was thought to define predetermined platelet territories. However, more recent findings indicate that its primary function is to serve as a membrane reservoir that supports the extension of the cytoplasm and proplatelet formation. The development of the DMS follows a stepwise process. It begins with membrane infolding at specific sites, forming an early pre-DMS near the nucleus. This precursor structure subsequently expands as additional material is incorporated from Golgi-derived vesicles and lipid transfer from the endoplasmic reticulum [29]. Besides DMS, MKs also contain a dense tubular system, which is thought to function as the primary site for prostaglandin and thromboxane synthesis within future platelets, playing a crucial role in their biochemical signaling. Additionally, it serves as an intracellular calcium reservoir, which is essential for platelet activation [30].

The rapid expansion and reorganization of the membranes within MK cytoplasm facilitate the biogenesis and proper localization of secretory granules, like α -granules and dense granules. α -granules, the most abundant, contain key proteins for platelet adhesion and vascular repair. They originate from the trans-Golgi network, acquiring proteins through both endogenous synthesis and receptor-mediated uptake [31, 32]. Proteins such as platelet factor 4, β -thromboglobulin, von Willebrand factor (vWF), fibrinogen, integrin α Ilb β 3, and P-selectin (CD62P) are selectively packaged into these granules [33]. Multivesicular bodies act as intermediates in α -granule formation and contain secretory and lysosomal proteins. These structures are more prominent in cultured MKs and serve as key sorting compartments. Dense granules, approximately 250 nm in size, store active molecules such as serotonin, catecholamines, adenosine diphosphate (ADP), adenosine triphosphate (ATP), and calcium, which are released upon platelet activation [34].

1.3. PLATELET BIOGENESIS

After completing their maturation journey, MKs undergo a remarkable transformation to fulfill their primary function: platelet production. Over the years, several mechanisms have been proposed to explain how MKs generate platelets. These include proplatelet formation, platelet budding, and cytoplasmic fragmentation.

The formation of proplatelet extensions from MKs has been proposed as a predominant model of platelet generation. Over a century ago, pseudopod-like projections were identified on the surface of "giant cells", later identified as MKs [35]. The proplatelet model proposes that MKs actively extend microtubule-driven proplatelets into the sinusoidal vasculature, where shear forces accelerate their fragmentation into preplatelets; larger intermediates that can further fragment into reversible [36]. **Preplatelets** barbell-shaped mature platelets undergo transformations before splitting into daughter platelets, and both preplatelets and barbell platelets have been identified in circulation (Figure 2) [37, 38]. Early in vivo imaging confirmed MK extensions into sinusoids, releasing platelets and cytoplasmic fragments, while further studies demonstrated that proplatelets and platelet barbells exist in both in vivo and in vitro conditions [39]. However, platelet generation in vivo appears more efficient than in vitro, likely due to shear stress and endothelial signals, which may play crucial regulatory roles [40, 41].

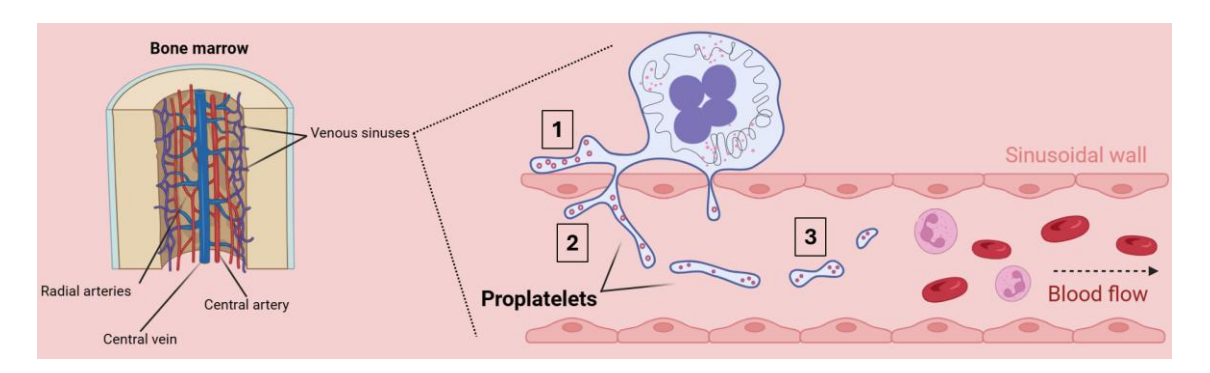


Figure 2. Schematic representation of proplatelet formation.

Within the venous sinuses of the BM, MKs readily elongate their proplatelet protrusions through the sinusoidal vasculature. (1) Proplatelet formation is driven by the active reorganization of the microtubule cytoskeleton, which also contributes to organelle and granule movement from MKs to platelets. (2) Branching of proplatelets is actin-dependent. (3) Final platelet morphogenesis continues in the circulation.

A recent study suggested membrane budding as an alternative model of platelet biogenesis, proposing that platelets form by directly detaching from the MK plasma membrane rather than through proplatelet extension [42]. Intravital microscopy supported this mechanism, suggesting it accounts for nearly 89% of platelet production in the mouse fetal liver and adult BM [42]. Unlike apoptotic fragments, these buds maintain a continuous cytoskeletal connection with the MK and are similar in size to circulating platelets. Although MKs in the BM and spleen are often considered stationary due to their lack of movement or proplatelet formation [28, 43], it has been demonstrated that many actively generate platelets through membrane budding [42]. However, this theory remains contested, as others argue that the observed buds are instead microvesicles, citing morphological and organelle content differences observed *via* transmission electron microscopy [44].

Cytoplasmic fragmentation offers yet another model for platelet production, proposing that platelets are preassembled within designated regions of the MK, known as platelet territories, before the cell ruptures, leaving behind its nucleus [45]. Phase-contrast microscopy has captured this process *in vivo* [45] and several studies suggest that MKs fragment into platelets both in the BM and lungs [46], though much of this evidence comes from *in vitro* research [41, 47-50]. This mechanism also introduces the concept of protoplatelets, these are considered chains of platelet territories released during MK fragmentation [41, 45].

Nishimura *et al.* provided crucial *in vivo* evidence, demonstrating that MKs in the BM can rupture and release platelets directly into the circulation [51]. Their findings suggest that while proplatelet formation maintains physiological platelet production, cytoplasmic fragmentation may serve as a rapid-response mechanism under

conditions requiring an acute platelet release, such as inflammation and thrombocytopenia. Notably, interleukin- 1α (IL- 1α) appears to play a crucial role in triggering emergency thrombopoiesis (**Figure 3**) [51].

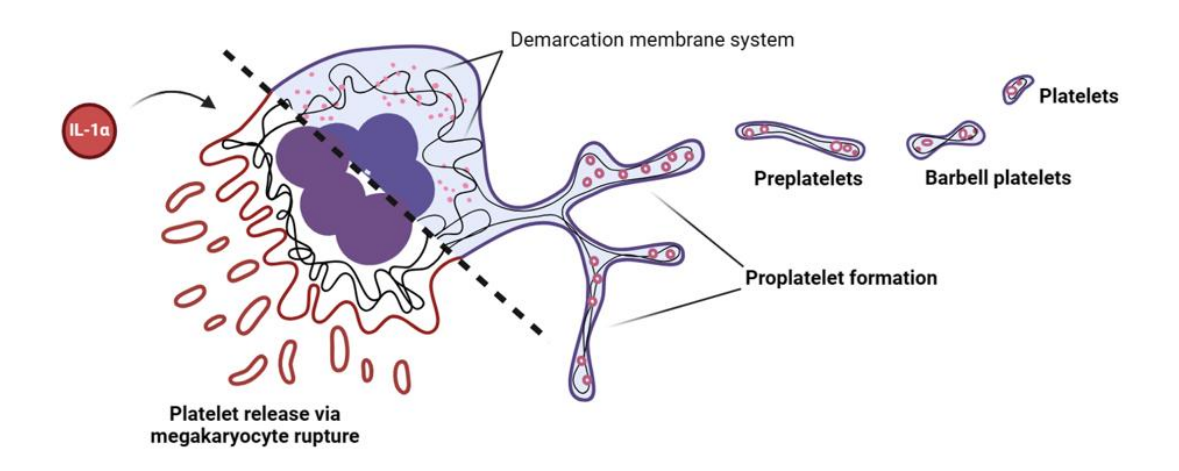


Figure 3. Schematic representation of IL- 1α -mediated cytoplasmic rupture vs. proplatelet formation.

During proplatelet formation, MKs extend their cytoplasmic protrusions, which gradually branch out and reorganize, releasing intermediate stages of platelets (preplatelets and barbell platelets). Conversely, under conditions of acute platelet demand, MKs undergo rupture thrombopoiesis, which is predominantly mediated by $IL-1\alpha$.

IL-1α is a key pro-inflammatory cytokine present in various cell types that acts as an early alarmin released upon cell stress or necrosis, triggering acute inflammatory responses [52-54]. It is synthesized as a 31 kDa precursor (pro-IL-1α) that can shuttle to the nucleus, bind chromatin, and act as a transcriptional regulator before cleavage by proteases such as calpain, elastase, thrombin, or granzyme B into a more receptor-active form [53, 55]. It exerts its effects by binding to IL-1 receptor type I (IL-1R), initiating a signaling cascade that activates as nuclear factor kappa B (NF-κB) and MAPK pathways [53, 55, 56]. IL-1α is produced constitutively by cells, including macrophages, endothelial and epithelial cells, and MKs, and is released especially during acute sterile injury, inflammation, or infection [51, 53, 56, 57].

In MKs, IL-1 α emerged as a key inflammatory signal capable of rapidly shifting MK programming toward rupture-type thrombopoiesis under acute inflammatory or cytopenic stress [51]. Neutralizing IL-1 α impaired platelet recovery during inflammation, and although other cytokines such as IL-1 β , IL-2, IL-6, and IL-11 were also elevated, IL-1 α specifically destabilized the MK plasma membrane [51]. These

effects were shown to be caspase-3 dependent, suggesting that IL-1 α signaling through IL1R1 activates a cascade that alters the cell membrane stability [51].

Other studies also support the role of IL-1 α in recovering from acute thrombocytopenia, particularly through its direct effects on MKs and other BM niche cells [58, 59].

1.4. PHOSPHOINOSITIDES AND VPS34 KINASE

Phosphoinositides (PI) are a small family of phospholipids derived from phosphatidylinositol. Structurally, they consist of a glycerol backbone linked to two fatty acid chains and an inositol ring. Pls can be phosphorylated on positions D3, D4, and D5 of the inositol head group, leading to the formation of distinct phosphoinositide species (Figure 4) [60]. Phosphoinositides are minor components of cellular membranes, comprising approximately 1% of the total cellular phospholipids, with phosphatidylinositol accounting for about 10%. Despite their low concentrations in membranes, phosphoinositides are crucial for the recruitment and/or activation of effector proteins [61]. Additionally, their distribution and levels in specific membranes are regulated by different lipid kinases and phosphatases unique to each membrane. This enables spatiotemporal control of processes linked to membrane dynamics, as each PI plays a unique role in specific cellular compartments [62].

Vacuolar protein sorting 34 (Vps34) is the sole representative of the class III phosphoinositide-3 kinases (PI3K) and is ubiquitously expressed across all eukaryotic cells. Its main function is the phosphorylation of PI to generate phosphatidylinositol 3-phosphate (PI3P) (Figure 4). In mammals, Vps34 forms two heterotetrameric complexes, designated as complex I and II. Complex I comprises Vps34, Vps15, Beclin 1, and autophagy related 14 (ATG14L) subunit. Complex II has a UV irradiation resistance-associated gene (UVRAG) instead of ATG14L (Figure 5) [63, 64]. A single subunit difference determines the distinct localization and activity between the two complexes.

Complex I plays a crucial role in generating PI3P at the phagophore, facilitating the formation of autophagosomes. On the other hand, complex II is involved in a wide range of intracellular processes, such as regulating endocytic sorting, cytokinesis, autophagosome maturation, and lysosome recycling [65].

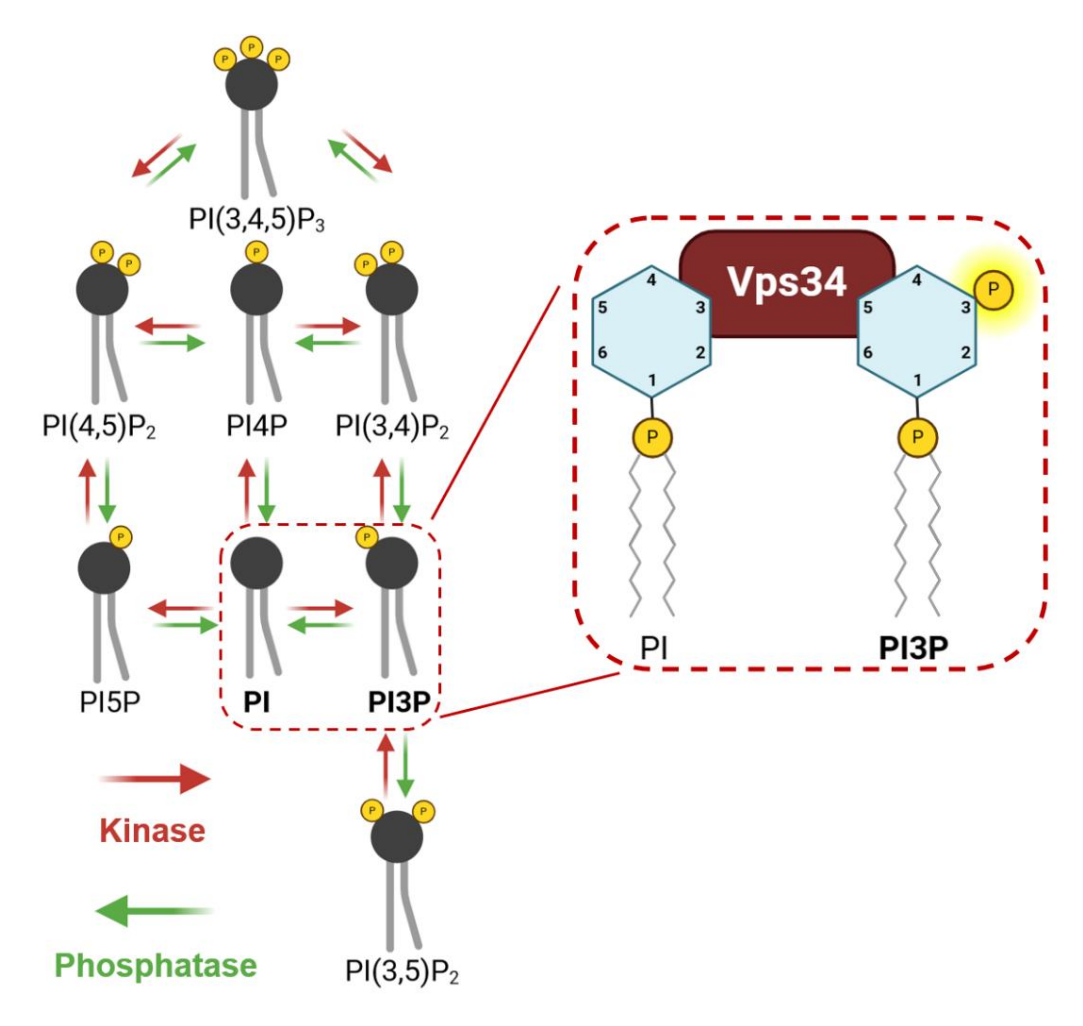


Figure 4. The interconversion of phosphoinositide species.

The inositol head group can be phosphorylated at positions 3, 4, and 5, giving rise to 7 distinct PIs. Each PI can be interconverted with one another through the action of different lipid kinases or phosphatases. Vps34 kinase phosphorylates PI to produce PI3P, an important PI involved in endolysosomal trafficking. (PI3P – phosphatidylinositol 3-monophosphate, PI4P – phosphatidylinositol 4-monophosphate, PI5P – phosphatidylinositol 5-monophosphate, PI(3,4)P₂ – phosphatidylinositol 3,4-bisphosphate, PI(4,5)P₂ – phosphatidylinositol 3,5-bisphosphate, PI(3,4,5)P₃ – phosphatidylinositol 3,4,5-trisphosphate)

Vps34 is the catalytic subunit of the complexes, while Vps15 serves as a regulatory subunit. Specifically, the N-terminal pseudokinase domain of Vps15 plays a crucial role in stabilizing the enzyme, inhibiting basal activity, and facilitating membrane recruitment [63, 64]. Beclin 1 is a component shared between both complexes and is a membrane adaptor. Multiple post-translational modifications regulate its localization and can either promote or inhibit autophagy-related functions of the complex [63, 64]. ATG14L is the defining subunit of the Vps34 complex I. Phosphorylation of specific sites on ATG14L is necessary for the activation of complex I and the initiation of autophagy. This phosphorylation can be triggered by,

for example, deprivation of essential cell nutrients like amino acids and glucose [63, 64]. On the other hand, the key subunit of complex II, UVRAG, is essential in endocytic trafficking and autophagosome maturation. This subunit is believed to possess tumor suppressor activity, since mutations or deletions in the UVRAG gene have been linked to various cancers [63, 64, 66].

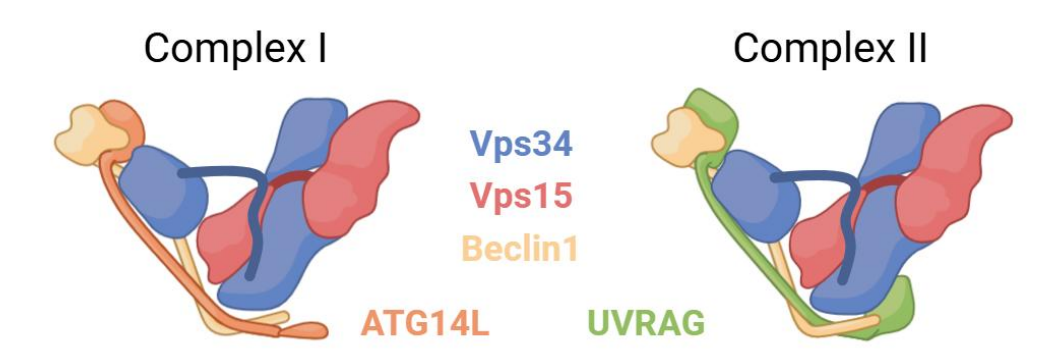


Figure 5. Schematic representation of the structural subunits of Vps34 complexes I and II.

Mammalian Vps34 forms two distinct complexes, each consisting of different subunits, as shown color-coded above. Both complexes share the Vps34, Vps15, and Beclin 1 subunits. The final subunit varies between the two complexes: complex I includes the ATG14L subunit, while complex II contains the UVRAG subunit.

1.4.1. Phosphoinositide roles in megakaryocytes

The dynamics of membranes and intracellular trafficking are essential for MK maturation and the production of platelets. Pls are important in these processes, acting as signaling molecules that govern endosomal trafficking, organize the actin cytoskeleton, and facilitate proplatelet formation [67].

<u>Table 1. Overview of PIs, related enzymes, and their localization and roles in MK</u> biology

PI	Biosynthesis / Enzymes	Localization	Functions in MKs	Ref.
Pls	Synthesized de novo; precursor for all Pls	Membranes	Precursor for phosphorylation into functional PIs	[61, 67]
PI3P	Vps34, PI3KC2α	Early/late endosomes, plasma membrane (cytoplasmic and outer leaflet)	Endosomal trafficking, c-Mpl internalization, DMS formation, MK migration <i>via</i> SDF1α	[68-70]

PI4P	PI4KIIIα (plasma membrane), PI4KIIα (Golgi)	Golgi, plasma membrane Regulates MK size, Golgi remodeling, ar proplatelet formation		[71]
PI5P	PIKfyve or myotubularins (from PI(3,5)P ₂)	Granule membranes	Precursor for PI(4,5)P ₂ ; loss of PIP4Kα impairs DMS development	[72]
PI(4,5)P ₂	PIP5KIγ (cytoskeletal pool), PIP5KIβ (PLC substrate)	Plasma membrane, DMS	Links the plasma membrane to actin <i>via</i> talin; involved in DMS-associated actin regulation	[73, 74]
PI(3,5)P ₂	PIKfyve (from PI3P)	Granule membranes (dense > α)	Maintains α-/dense granule integrity; regulates vesicular trafficking	[72, 75]
PI(3,4)P ₂	SHIP1 (from $PI(3,4,5)P_3$)	Plasma membrane	-	[76]
PI(3,4,5)P ₃	Class I PI3Ks (α, β) from PI(4,5)P ₂	Plasma membrane	Drives Btk/PLCγ2 activation, proplatelet formation, TPO signaling, and migration	[77, 78]

In MKs, PI3P is primarily found in vesicles associated with early and late endosomes, which are identified by early endosomal antigen 1 (EEA1) and lysosomal-associated membrane protein 1 (LAMP1), respectively. As MKs progress in maturation, PI3P transitions from early to late endosomes and is ultimately found at the plasma membrane in larger, mature cells [68]. This lipid is primarily produced by Vps34. which contributes to around 40% of PI3P synthesis in MKs [69]. Vps34 is located in early and late endosomes, the plasma membrane, and occasionally in internal compartments [68]. The pool of PI3P produced by Vps34 regulates endosomal trafficking by controlling the movement of vesicles between early endosomes, late endosomes, and lysosomes. Moreover, it regulates the endocytosis of the TPO receptor, c-Mpl, thus affecting circulating TPO levels [67]. PI3P is critical for forming the DMS, which aids in the translocation and fusion of late endosomes and lysosomes with the plasma membrane. It also promotes proplatelet formation. Additionally, PI3P directs MK migration along a stromal cell-derived factor 1α (SDF1α) gradient, guiding them toward the BM sinusoids for effective platelet release [68, 69]. Disruption of PI3P homeostasis has a substantial effect on thrombopoiesis, as overexpression of 3-phosphatase MTM1 in MKs leads to a decrease in both the number and structural integrity of proplatelets [68].

In an unpublished study of our Laboratory, Bertović et al. demonstrated that Vps34 localizes in the nucleolus [79]. Using primary mouse MKs, BALB3T3 cells, and human mononuclear cells, Bertović et al. showed that Vps34 specifically colocalized with the transcription factor UBF in the fibrillar center of the nucleolus, the key site of rRNA transcription. By using co-immunoprecipitation, they confirmed the presence of Vps34 in a complex with UBF, independent of its cytoplasmic binding partner Vps15, suggesting the existence of a distinct nuclear Vps34 complex. Importantly, Bertović et al. demonstrated that nucleolar localization of Vps34 is dependent on RNA Pol I activity, and inhibition of Vps34 significantly reduced nascent RNA synthesis and 45S pre-rRNA levels, indicating that Vps34 activity is directly required for efficient rRNA transcription. The presence of PI3P in nucleoplasmic and perinucleolar regions further supported the idea that Vps34-derived lipid signaling contributes to nucleolar functions. Functionally, inhibition of Vps34 during early MK development impaired cell growth and decreased expression of the maturation marker GPIbβ, pointing to defective ribosome biogenesis as an underlying mechanism. Collectively, the findings of Bertović et al. established Vps34 as an essential regulator of rRNA transcription and ribosome production in MKs, linking PI signaling to nucleolar function for the first time.

Extensive studies on PIs have primarily concentrated on their roles in membranes and organelles found in the cytosol. However, their discovery in the nucleus has led to a growing body of evidence supporting various functions they perform there [80, 81], including the cellular stress response. For example, some nuclear PIs, such as PI(4,5)P₂ and PI4P, undergo dynamic changes in response to growth factors, stress signals, cell cycle progression, differentiation, and DNA damage [82]. Nuclear PI(4,5)P₂ localizes to speckles and lipid islets, where it regulates RNA Pol II transcription and pre-mRNA splicing [83-86], while PI4P is found at the nuclear envelope, lamina, nucleoli, and speckles, interacting with factors in transcription, splicing, and transport, suggesting broader but less defined nuclear functions compared to PI(4,5)P₂ [87, 88].

Several recent studies report nuclear presence of Vps34 (or its complex subunits) and local accumulation of PI3P at sites of genomic stress: nuclear-targeted PI-binding domains rapidly enrich at DNA-damage foci [89] and Vps34/Vps15 have been detected in nuclear fractions [90]. In plants, a study of carrot suspension and root cells found that the plant homolog of Vps34 exhibits PI3K activity associated with nuclei (internal nuclear matrix) and that this kinase localizes in punctate foci in

the nucleus and associates with sites of active transcription [91]. In *S. cerevisiae*, Vps34 was detected at nuclear pores, and mutants with Vps34 deletion showed impaired transcription elongation [92]. In mammalian cells, in addition to endo/lysosomal pools, Pl3P has been observed within the nucleolus, specifically the dense fibrillar component, consistent with nuclear Pl3K activity and suggesting potential nuclear function [93].

However, while these findings point to a role of nuclear PI3P in genomic stress responses, its functional significance remains largely unknown.

1.1. THE NUCLEOLUS

The nucleolus is a dynamic, membrane-less organelle found within the nucleus, primarily tasked with ribosome biogenesis. In addition to its primary role, the nucleolus participates in the cellular response to stress, the regulation of the cell cycle, and even cellular aging [94-96]. It is a membraneless subnuclear organelle, characterized by its dynamic nature; it is not permanently present within the cell. Rather, it assembles and disassembles in response to the cell's metabolic demands. Nucleoli form around nucleolar organizing regions (NORs), which contain rDNA sequences [97, 98].

The nucleolus consists of three morphologically distinct subcompartments: the fibrillar center (FC), the dense fibrillar component (DFC), and the granular component (GC). The unique organization of the nucleolus illustrates the spatial variations for each stage of ribosomal synthesis: ribosomal RNA (rRNA) transcription, processing, and ribosome assembly [97, 98] (Figure 6).

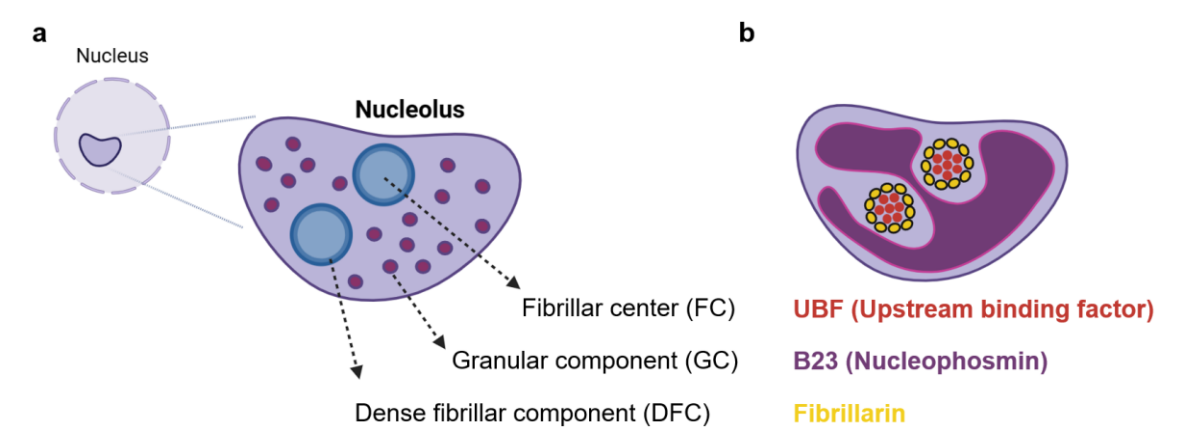


Figure 6. Schematic representation of the nucleolus and nucleolar subcompartments.

The nucleolus is a highly dynamic and membrane-less structure inside the nucleus with the primary function of ribosomal biogenesis. (a) It is organized into three distinct subcompartments: the fibrillar

center (FC), the dense fibrillar component (DFC), and the granular component (GC), each playing a specialized role in the transcription, processing, and assembly of ribosomal RNA (rRNA). **(b)** Specific protein markers are associated with each subcompartment: UBF (Upstream Binding Factor) marks the FC, fibrillarin is a marker for the DFC, and nucleophosmin (B23) is found in the GC.

The FC contains inactive ribosomal DNA (rDNA) and the RNA polymerase I (Pol I) transcription machinery, marking the initiation of rRNA synthesis. Surrounding the FC, the DFC is rich in small nucleolar ribonucleoproteins such as fibrillarin and nucleolin, which aid early stages of rRNA processing and modifications. Lastly, the GC is where late-stage rRNA processing and ribosomal subunit assembly occur, containing proteins like nucleophosmin (B23), crucial for ribosome maturation and export out of the nucleus [97, 98].

Ribosome biogenesis starts in the nucleolus. First, RNA polymerase I (Pol I) transcribes the 47S rRNA precursor (pre-rRNA) within the nucleolus, while RNA polymerase III (Pol III) simultaneously transcribes the 5S rRNA outside of it. The 47S pre-rRNA is then processed and modified to produce three specific rRNA molecules: 28S, 18S, and 5.8S rRNAs. Following this, the 18S rRNA associates with 33 different small ribosomal subunit proteins to create the pre-40S ribosome particle, whereas the combination of 5S, 28S, and 5.8S rRNAs with 48 types of large ribosomal subunit proteins forms the pre-60S ribosome particle. These pre-ribosomal particles exit the nucleolus, travel through the nuclear pores, and enter the cytoplasm, where they assemble and form the mature 80S ribosome, which is capable of translating mRNA [99, 100].

Cells spend a significant portion of their energy (around 80%) on ribosomal biogenesis [101, 102]. Given the high energy demand of this process, it is carefully regulated, and any disruption in one of its three critical stages can result in nucleolar stress [103].

1.1.1. Nucleolar stress

Although initially used to refer to events that disturb the homeostasis of ribosome production, the definition of nucleolar stress has expanded beyond being solely ribosome-related. Generally, it describes the morphological and functional changes in the nucleolus in response to various cellular insults. These disturbances further lead to the activation of p53 or p53-independent stress signaling.

In resting cells, the tumor suppressor protein p53 is predominantly kept inactive through polyubiquitination by the E3 ubiquitin ligase MDM2, marking it for degradation *via* the proteasome [104]. However, during nucleolar stress, several ribosomal proteins are released from the nucleolus and translocate to the nucleoplasm. Proteins such as RPL5, RPL11, and RPL23 bind to MDM2 and inhibit

its ubiquitin ligase activity, preventing p53 degradation [105, 106]. As a result, p53 is stabilized and activated, leading to cell cycle arrest and/or apoptosis.

Even in the absence of p53, cells can still undergo cell cycle arrest or programmed cell death in response to nucleolar stress. This p53-independent response involves alternative signaling pathways, with key regulatory roles played by transcription factors such as E2F-1, MYC, and NF-κB [105]. Like p53, E2F-1 undergoes regulation via MDM2-mediated polyubiquitination and subsequent proteasomal degradation. However, under conditions of nucleolar stress, the interaction between RPL11 and MDM2 leads to a specific outcome. Rather than stabilizing E2F-1, this interaction enhances its polyubiquitination and degradation [105, 107, 108]. As a result, the transcriptional activity of E2F-1 is suppressed, leading to the downregulation of its target genes and triggering cell death through a p53-independent mechanism [105].

These signaling events, however, do not occur in isolation. They are typically preceded or accompanied by characteristic nucleolar changes induced by specific stressors. To better contextualize the triggers of nucleolar stress, some authors have proposed a classification system that divides these stimuli into two broad categories: ribotoxic stressors, which directly impair ribosome biogenesis (canonical insults), and non-canonical cellular insults, which affect nucleolar function more indirectly [109].

1.1.2. Ribotoxic and non-canonical nucleolar stressors in the context of inflammation

Ribotoxic insults can directly interfere with ribosome biogenesis by disrupting various stages of rRNA synthesis, processing, or assembly. A well-known ribotoxic insult is exposure to dactinomycin (actinomycin D or Act.D), a chemotherapeutic agent that inhibits Pol I [110]. It is thought that at high concentrations, Act.D can cause DNA damage and inhibit general transcription. However, at lower doses, it selectively inhibits Pol I and induces ribosomal stress [110, 111]. Inhibition of rRNA transcription leads to reduced levels of 47S pre-rRNA, while inhibiting rRNA processing typically leads to the buildup of precursor rRNA and a decrease in the final products, or both.

Ribotoxic stressors, including ribosome-targeting toxins and translation inhibitors, trigger a highly conserved ribotoxic stress response (RSR) that links ribosome damage to inflammatory signaling. Early work established that ribotoxins such as ricin and Shiga toxins activate stress-activated kinases and inflammatory pathways [112]. Mechanistically, the MAP3K ZAKα acts as the primary sensor of ribosome stalling and collisions, linking ribotoxic stress to the activation of p38 and JNK MAPKs, which then promote inflammatory gene expression and cell-fate decisions [113, 114]. Importantly, this stress pathway is not limited to *in vitro* models. *In vivo*

work demonstrates that RSR activation in response to UV-induced ribotoxic stress drives acute inflammation, cell death, and tissue remodeling in skin, placing the ribotoxic stress response upstream of inflammatory pathology [115].

Exposure to chronic inflammation [116] or treatment of cells with lipopolysaccharide (LPS), poly(I:C), or *E. coli* [117, 118], cause changes the morphology of nucleoli, inducing its hypertrophy. The nucleolus interacts closely with inflammatory signaling networks, particularly the NF-κB pathway [119, 120]. Studies have shown that nucleolar stress influences NF-κB activity through proteins such as TIF-1A, copper metabolism domain containing 1 (COMMD1), and B23, either attenuating or promoting inflammatory gene expression depending on the context [119-121]. Nucleolar stress and its crosstalk with inflammatory pathways have been implicated in the pathogenesis of degenerative diseases characterized by chronic inflammation and oxidative damage [122], such as Parkinson's disease [122, 123].

In response to ribotoxic stress, the nucleolus undergoes several morphological alterations. Unlike membrane-bound organelles, the nucleolus lacks a physical barrier separating it from the surrounding nucleoplasm. Because of this, soluble molecules can move in and out of the nucleolus. This shuttling occurs at a basal, low level when the cell is at rest. However, under stressful conditions, it increases significantly. This movement is a key indicator of nucleolar stress and is best illustrated by the nucleoplasmic translocation of B23.

While Act.D treatment led to the relocation of B23 from the nucleolus to the nucleoplasm [124], this phenomenon isn't limited to ribotoxic insults alone. A wide variety of cellular stressors can be regarded as non-canonical insults, as they do not specifically impair ribosomal biogenesis but instead affect overall cellular homeostasis.

For example, cells starved in serum-free medium showed decreased levels of B23 in the nucleolus and increased levels in the nucleoplasm, as measured by immunofluorescence [125]. Interestingly, when the cells were refed with serum-containing media, B23 was re-imported back into the nucleolus, suggesting that this nucleoplasmic translocation is reversible [125]. Other stressors, such as UV radiation [126, 127], viral infections [126], and conditions like hypoxia [128] and oxidative stress (H_2O_2 exposure) [127, 129], also cause B23 to move from the nucleolus into the nucleoplasm while triggering other cellular stress mechanisms like the DNA damage response.

Various anticancer drugs, including camptothecin (topoisomerase I inhibitor) [130], doxorubicin and daunomycin (topoisomerase II inhibitors) [131], were also found to

induce nucleoplasmic translocation of B23. Of note, camptothecin derivatives (topotecan, irinotecan) and anthracycline topoisomerase II inhibitors such as doxorubicin and daunomycin are well-established causes of chemotherapy-induced thrombocytopenia [132, 133]. The predominant mechanism involves impaired platelet production, as these agents induce DNA damage and apoptosis in proliferating MK progenitors and disrupt MK maturation [132]. In addition, doxorubicin has been shown to exert direct toxic effects on circulating platelets through the generation of reactive oxygen species and caspase activation, leading to premature clearance by macrophages [134].

1.1.3. Impact of nucleolar stress on megakaryopoiesis in different hematological disorders

Hematopoietic cells are among the most energy-demanding cells in the body. They constantly synthesize large amounts of proteins to support their rapid growth, differentiation, and proliferation. This high demand for protein synthesis is directly linked to the continuous production of ribosomes. To meet these needs, hematopoietic cells depend heavily on the nucleolus. Because of this, however, they are highly susceptible to disruptions in these processes.

Diamond-Blackfan anemia (DBA) is a congenital BM failure disorder primarily characterized by anemia, macrocytosis, reticulocytopenia, and a selective reduction of erythroid progenitor cells in the BM [135]. Our understanding of the disease's pathophysiology has evolved significantly with the discovery of a congenital balanced translocation that disrupted the gene encoding ribosomal protein S19 (RPS19) [136]. The 5q- syndrome (also noted as "del(5q)"), first described in 1974, is an acquired BM failure disorder caused by a deletion on the long arm of chromosome 5 [137]. The clinical phenotype of 5q- syndrome is characterized by severe macrocytic anemia, thrombocytosis, and the presence of hypolobated micromegakaryocytes [138]. Patients with this syndrome exhibit haploinsufficiency of RPS14 expression, and much like the findings in DBA, decreased expression of RPS14 impairs erythropoiesis [139]. 5q- syndrome is classified by the World Health Organization as a distinct subtype of myelodysplastic syndrome (MDS) [140]. Dysmegakaryopoiesis, marked by the presence of micromegakaryocytes carrying nuclear abnormalities, is one of the key components in MDS classification [141-143].

DBA and the 5q- syndrome both arise from defects in ribosome biogenesis or its regulators, and although classically defined by erythroid failure, they can also perturb megakaryopoiesis and platelet biology. In DBA, a subset of patients carries germline GATA1 lesions [144]. GATA1 is essential for both erythroid and MK programs, and GATA1-mutant DBA patients show combined erythroid failure with MK dysplasia and

platelet abnormalities [144]. Mouse models harboring mutations found in DBA patients recapitulate BM failure and impaired erythropoiesis and, depending on model and genetic context, show secondary effects on megakaryopoiesis [145]. In GATA1-null mice, the deletion was found to induce maturation arrest of erythroid cells at the proerythroblast stage, thrombocytopenia, and excessive splenic proliferation of MKs [145].

Beyond their diagnostic relevance for e.g. MDS, MKs are biologically intriguing due to their substantial size, rapid growth, and elevated demand for protein synthesis throughout maturation. These features make them a compelling model for investigating how nucleolar function adapts under different stressors. Our previous finding of Vps34 localization in the nucleolus [79] reveals new opportunities to investigate its role in regulating nucleolar integrity and ribosomal biogenesis. Thus, we introduce a previously overlooked aspect of the cellular stress response during megakaryopoiesis.

1.1.4. Nuclear phosphoinositides in the cellular stress response to DNA damage

DNA integrity is essential for the survival of all living organisms, ensuring that genetic information is accurately passed during cell division. Even minor DNA sequence disruptions can be harmful. Cells face continuous challenges from endogenous factors, like reactive oxygen species, and exogenous agents, including ionizing radiation and chemical mutagens. To mitigate these damaging effects, cells have developed a complex surveillance and repair network, collectively known as the DNA damage response (DDR) [146].

DNA double-strand breaks (DSBs) are among the most harmful lesions. When a DSB occurs, one of the first responses in the cell is the recruitment of the MRE11-RAD50-NBS1 (MRN) complex to the damage site [147]. This highly conserved sensor complex serves two essential purposes: it connects the ends of damaged DNA to facilitate repair and acts as a platform to activate the ataxia-telangiectasia mutated (ATM) kinase, a key regulator of DSB response [147, 148]. When the MRN complex binds to the DNA break, ATM undergoes autophosphorylation at serine 1981, transforming from an inactive dimer into active monomers that can phosphorylate various substrates involved in DDR [148, 149].

An important and immediate substrate of ATM is the histone variant H2AX, which quickly undergoes phosphorylation at serine 139 to form γ -H2A.X (**Figure 7**) [149]. The formation of γ -H2A.X foci not only strengthens the DNA damage signal but also

organizes the repair machinery spatially, meaning that downstream repair proteins are recruited and kept at the DNA damage sites [149]. The presence of γ -H2A.X foci can be detected using immunofluorescence, making it a valuable biomarker for monitoring DDR [150-152].

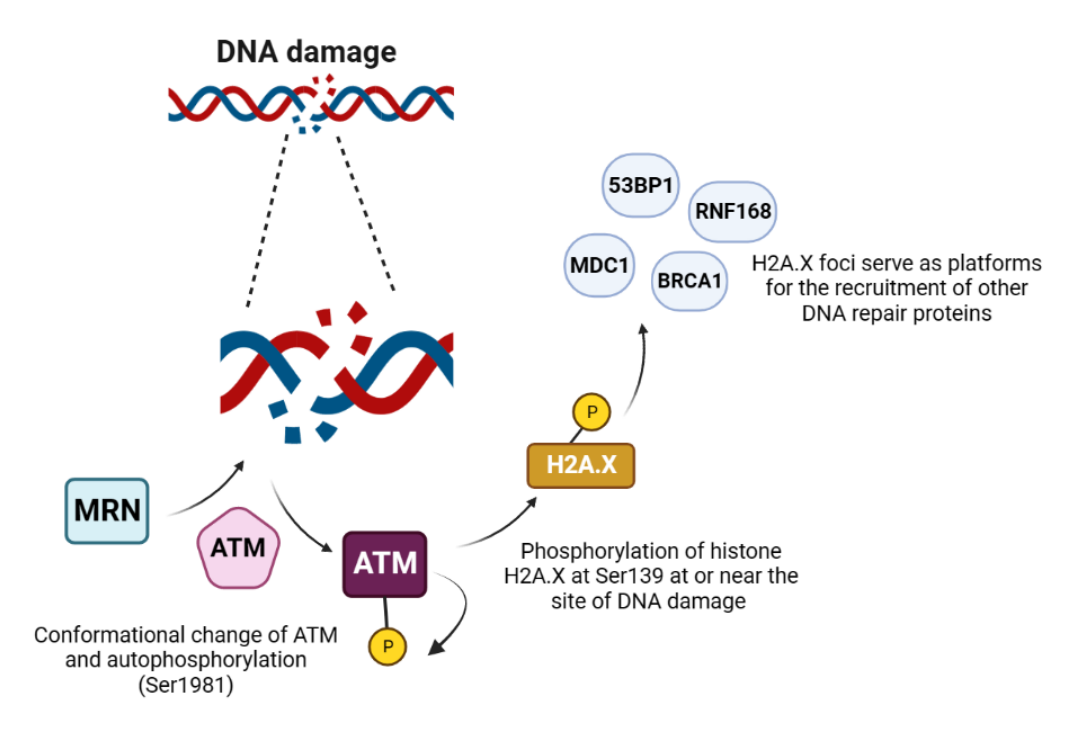


Figure 7. Schematic overview of the mechanism of histone H2A.X phosphorylation in the early phase of DDR.

The MRN complex is recruited to the site of DNA damage, where it helps activate ATM. Autophosphorylation of ATM turns on this kinase, enabling the phosphorylation of key targets involved in DDR, such as the histone variant H2A.X. The formation of H2A.X foci is a crucial step for recruiting other DNA repair proteins, including mediator of DNA damage checkpoint protein 1 (MDC1), breast cancer type 1 susceptibility protein (BRCA1), p53-binding protein 1 (53BP1), and ring finger protein 168 (RNF168).

Emerging evidence highlights the significant roles of nuclear phosphoinositides in DDR [89, 148, 153, 154]. Unlike their cytosolic counterparts, nuclear PIs are associated with both membrane-bound and membraneless structures. Thus far, all PIs except PI(3,5)P₂ have been identified within the nucleus [153, 155]. The discovery that some PI kinases also localize in the nucleus [156, 157] improved our understanding of nuclear PI metabolism and offered better insight into their nuclear functions. Nuclear PIs localize in various sub-nuclear compartments, highlighting their diverse roles in multiple nuclear processes.

Following genotoxic insult, the levels of PI3P in the cell nucleus increased, yet this observation was not explored further [89]. Since this thesis focuses on Vps34, the

kinase that produces PI3P, and nucleolar stress as a specific form of cellular insult, we have emphasized PIs with confirmed nucleolar localization and listed their roles based on how they respond to it **(Table 2)**.

Table 2. Pls that localize in the nucleus and their functions in cellular stress response

PI	Subnuclear localization	Role in the cellular stress response
PI3P	Nucleoli Matrix	Nuclear levels increased in response to genotoxic stress [158]
PI4P	Nucleoli Speckles Matrix Nucleoplasm Chromatin Envelope	Localized to DNA damage sites and played a role in the repair response [89]
PI(3,4)P ₂	Nucleoli Speckles Envelope	Nuclear levels increased in response to oxidative stress [159]
PI(4,5)P ₂	Nucleoli Speckles Matrix Nucleoplasm Chromatin Envelope	Nuclear levels increased in response to genotoxic stress [89, 158] Localized to DNA damage sites [89, 158] Accumulated in nucleoli in response to heat shock [160]
PI(3,4,5)P ₃	Nucleoli Speckles Matrix Nucleoplasm Chromatin	Nuclear levels increased in response to genotoxic stress [89, 158] Localized to DNA damage sites after UV exposure [89, 158]

2. THESIS AIMS AND HYPOTHESES

Vps34 is the sole class III PI3K involved in vesicular transport regulation and autophagy. It localizes in the cytoplasm, endo-lysosomal system, and plasma membrane, but recently it has also been found in the nucleus and nucleolus of primary MKs. The nucleolus is where ribosome biogenesis occurs and is a central hub for cellular stress. Given the importance of Vps34 and PI3P in platelets and MKs, particularly focusing on the yet unexplored role of Vps34 in the nucleolus, the purpose of this thesis is to deepen the understanding of the molecular mechanisms underlying the MK response to stress, as well as the function of nuclear Vps34 in these conditions.

Specifically, this thesis aims to examine the cellular response of MKs to stress under conditions that require increased platelet production through (I) in vitro and (II) in vivo models of thrombocytopenia (mediated by IL-1 α). We also aim to analyze the (III) expression and intracellular localization of nucleolar proteins and Vps34 in different developmental stages of BM MKs in response to IL-1 α , and during differentiation and proliferation of human megakaryocytic cell lines (DAMI, K562, and HEL). Furthermore, we aim to investigate whether (IV) Vps34 modulates the DNA damage response by analyzing the localization of Vps34 and PI3P in relation to DNA-damage sites.

We addressed the following hypotheses:

- **1.** Under thrombocytopenic stress conditions, MKs activate a stress response program characterized by alterations in nucleolar organization and the maturation program.
- **2.** The expression and intracellular localization of Vps34 and nucleolar proteins are dynamically regulated during MK development and differ across proliferative and differentiating stages.
- **3.** Vps34 can influence the DNA damage response in MKs by modulating PI3P levels at or near damage sites.

3. MATERIALS AND METHODS

3.1. MATERIALS

3.1.1. Chemicals

Table 3. List of chemicals

Chemical	Catalog No.	Manufacturer
Acrylamide	3029.2	Carl Roth
Ammonium persulfate (APS)	9592.2	Carl Roth
β-mercaptoethanol	M6250-0100	Sigma Aldrich
Bovine serum albumin (BSA)	T844.2	Carl Roth
Cisplatin	232120	Calbiochem
Citric acid	X863.1	Carl Roth
DAPI (4',6-diamidino-2-phenylindole)	D9542	Sigma Aldrich
Digitonin	BN2006	Invitrogen
EDTA	E6758	Sigma Aldrich
Ethanol	P112001	Gram Mol
Fluoroshield™ with DAPI	F6057	Sigma Aldrich
Glucose	HN06.1	Carl Roth
Glycerol	15523-1L-R	Sigma Aldrich
Glycin	3908.3	Carl Roth
Goat serum	P30-1001	Pan Biotech
HCI	20252.290	VWR chemicals
HEPES	HN77.4	Carl Roth
Isopropanol	34965	Honeywell
KCI	HN02.2	Carl Roth
KH ₂ PO ₄	1112408	Kemika
Liquid Barrier Marker	AN92.1	Carl Roth
Methanol	414816	Carlo Erba
MgCl ₂	KK36.1	Carl Roth
NaCl	3957.1	Carl Roth
Na₂HPO₄	S9390	Honeywell
NaOH	P147090	Gram Mol
NH₄CI	31107	Honeywell
NucRed™	R37106	Thermo Fisher
Paraformaldehyde	0335.3	Carl Roth
Phalloidin-488	A12379	Invitrogen
PIPES	9156.2	Carl Roth
Phorbol 12-myristate 13-acetate (PMA)	P8139	Sigma Aldrich
Poly-L-lysine	P1524	Sigma Aldrich
Sodium dodecyl sulfate (SDS)	0183.2	Carl Roth
Sucrose	4621.1	Carl Roth

TEMED	2367.1	Carl Roth
Tris	4855.3	Carl Roth
Trisodium citrate	HN12.3	Carl Roth
Triton X-100	BP151-100	Thermo Fisher
Tween20	P2287	Sigma Aldrich
Vps34-IN1	17392	Cayman Chemicals

3.1.2. Cell culture reagents

Table 4. List of reagents for cell culture

Reagent	Catalog No.	Manufacturer
BSA	CP84.2	Carl Roth
DMEM	P04-04510	Pan Biotech
FBS	P30-3306	Pan Biotech
HBSS	HBSS-2A	Capricorn Scientific
L-Glutamine	GLN-B	Capricorn Scientific
Sodium pyruvate	P04-43100	Pan Biotech
P/S (penicillin/streptomycin)	P06-07100	Pan Biotech
PBS	P04-36500	Pan Biotech
RPMI-1640	P04-18047	Pan Biotech
Trypsin	R3228	Pan Biotech

Table 5. List of cytokines

Cytokine	Catalog No.	Manufacturer
TPO (recombinant)	315-14	Peprotech
IL-1α	211-11A	Peprotech

Culture medium for murine BM-derived MKs and cell lines

BM progenitors were stimulated with thrombopoietin (TPO; 1% tissue culture supernatant obtained from a cell line modified to produce thrombopoietin [161]. Primary murine bone-marrow-derived megakaryocytes (BM MKs) were cultured in Dulbecco's Modified Eagle Medium (DMEM) containing 4.5 g/L glucose supplemented with 10% (v/v) fetal bovine serum (FBS), 10,000 U/mL penicillin (P), and 10 mg/mL streptomycin (S). This supplemented medium is regarded as a complete medium within the text of this dissertation.

Human megakaryoblastic cell lines, DAMI and HEL, were cultured in Roswell Park Memorial Institute-1640 (RPMI-1640) medium containing 4.5 g/L glucose supplemented with 10% (v/v) FBS, 10,000 U/mL penicillin, and 10 mg/mL

streptomycin. K562 cells were cultured in RPMI-1640 medium containing 4.5 g/L glucose supplemented with 10% (v/v) FBS, 10,000 U/mL penicillin, 10 mg/mL streptomycin, 200 mM L-Glutamine, and 100 mM sodium pyruvate.

3.1.3. Buffers

Table 6. List of buffers used for cell lysis, SDS-PAGE, and Western blot

Buffer	Ingredients		
10X Cell lysis buffer, pH 7.5	0.5 M Tris1.5 M NaCl10% sodium deoxycholate10% Triton X-1001% sodium dodecyl sulfate (SDS)		
3X SDS buffer	200 mM Tris pH 6.7 15% glycerol 6% SDS bromophenol blue 10% β-mercaptoethanol		
1X Running buffer	25 mM Tris 192 mM Glycine 0.1% SDS		
1X Transfer buffer	25 mM Tris 192 mM glycine 20% methanol		
TBS-Tween20, pH 7.5	10 mM Tris-HCl 150 mM NaCl 0.1% Tween-20		
Blocking buffer	3% BSA dissolved in TBS-Tween20		
Resolving gel (10%)	375 mM Tris-HCl pH 8.8 10% acrylamide 0.1% SDS 0.1% APS 0.05% TEMED		
Stacking gel	125 mM Tris-HCl pH 6.8 6% acrylamide 0.1% SDS 0.1% APS 0.1% TEMED		

Table 7. List of buffers used for immunofluorescence staining of BM cryosections

Buffer	Ingredients
Washing buffer	5% FBS and 0.1% Tween-20 in PBS
Permeabilization buffer	0.1% Triton-X-100 in PBS
Blocking buffer	10% goat serum in Washing buffer

Table 8. List of buffers used for immunofluorescence staining of cells

Buffer	Ingredients
Fixation buffer, pH 7.4	4% paraformaldehyde
	43 mM Na2HPO4 x 7H2O
	26.4 mM NaH2PO4
PBS, pH 7.4	137 mM NaCl
	2.7 mM KCl
	10 mM Na2HPO4
	1.8 mM KH2PO4
Buffer A	20 mM PIPES, pH 6.8
	150 mM NaCl
	3 mM KCl
Permeabilization buffers	0.5% Tween-20 in PBS
	Or
	20 μM digitonin in Buffer A
Blocking buffers	5% goat serum in PBS (or Buffer A)

Table 9. List of buffers used for murine platelet isolation

Buffer	Ingredients
Aster Jandl anticoagulant, pH 4.6	100mM trisodium citrate
	70 mM citric acid
	110 mM glucose
Washing buffer, pH 6.0	140 mM NaCl
	5 mM KCl
	12 mM trisodium citrate
	10 mM glucose
	12.5 mM sucrose
Resuspension buffer, pH 7.4	10 mM HEPES
	140 mM NaCl
	3 mM KCI
	0.5 mM MgCl2
	5 mM NaHCO3
	10 mM glucose

3.1.4. Primary antibodies

Table 10. List of primary antibodies

Antigen	Host	Catalog No.	Manufacturer	Application
Akt	Rabbit	9272	Cell Signaling	WB 1:1000
B23	Mouse	60096-1-lg	Proteintech	IF 1:100
β1-tubulin*	Rabbit	In-house	In-house	IF 1:100
CD61	Rat	M030-0	Emfret	IF 1:100
CD61*	Rat	In-house	Emfret	WB 1:1000
CD61-PE	Hamster	553347	BD Pharmingen	FC 1:100
c-Mpl (TPOR)	Mouse	SC-377417	Santa Cruz	WB 1:500
Erk	Rabbit	9102	Cell Signaling	WB 1:1000
Fibrillarin	Mouse	ab218846	Abcam	IF 1:100
GAPDH	Mouse	MAB374	Milipore	WB 1:2000
GPIbα	Rat	M042-0	Emfret	IF 1:100
GPIbβ	Rat	M050-0	Emfret	IF 1:100
GPlbβ	Rabbit	ab192541	Abcam	WB 1:1000
GPIbβ-FITC	Rat	M050-1	Emfret	FC 1:100
GPIX	Rat	M051-0	Emfret	IF 1:100
IL1R1	Rabbit	PA597866	Invitrogen	WB 1:1000
JAK2	Rabbit	3230	Cell Signaling	WB 1:1000
Ly6G	Rat	BE0075-1	Bioxcell	IF 1:100
Ly6G-FITC	Rat	127606	BioLegend	FC 1:1000
P-Akt	Rabbit	9271	Cell Signaling	WB 1:1000
P-Erk	Rabbit	9101	Cell Signaling	WB 1:1000
PI3P	Mouse	Z-P003-2-EC	Echelon	IF 1:100
P-JAK2	Rabbit	3771	Cell Signaling	WB 1:1000
P-STAT3	Rabbit	9131	Cell Signaling	WB 1:1000
P-UBF	Rabbit	ab182583	Abcam	WB 1:1000
STAT3	Mouse	9139	Cell Signaling	WB 1:1000
UBF	Mouse	sc-13125	Santa Cruz	IF 1:100 WB 1:1000
Vps34	Rabbit	NB110-87320	Novus Biologicals	IF 1:100 WB 1:1000
vWF	Rabbit	A008202	Dako/Agilent	IF 1:150 WB 1:1000
vWF-FITC	Rabbit	P150-1	Emfret	FC 1:100
ү-Н2А.Х	Mouse	80312	Cell Signaling	IF 1:100 WB 1:1000

 $^{^{\}star}$ Rabbit anti- β -1 tubulin antibody was a kind gift from Dr. Italiano (Brigham & Women's Hospital, Boston, USA)

* Rat anti-CD61 antibody (clone 57B10) was a kind gift from Dr. Nieswandt (Rudolf Virchow Center for Experimental Biomedicine, Würzburg, Germany).

3.1.4.1. Evaluation of Vps34 antibody

Vps34 antibody validation was performed by Dr. Ivana Bertović (Laboratory of Hematopoiesis, Faculty of Biotechnology and Drug Development, University of Rijeka, Rijeka, Croatia), using transient Vps34 knock-out HEK293 cells, produced by CRISPR/Cas9.

Vps34 antibody evaluation was performed using recombinant Vps34 (#40690, Amsbio) and two Vps34 primary antibodies: #NB110-87320 (Novus Biologicals) and #4263 (Cell Signaling) on Western blot, in addition to samples of primary BM-derived MKs, DAMI cells, and BALB3T3 mouse fibroblasts.

3.1.5. Secondary antibodies

Table 11. List of secondary antibodies

Antigen	Conjugate	Catalog No.	Manufacturer	Application
Anti-mouse Anti-rabbit Anti-rat	HRP	7076 7074 7077	Cell Signaling Cell Signaling Cell Signaling	WB 1:2000
Anti-mouse	AF 488 AF 555 AF 568	A11029 A21424 A21043	Invitrogen Invitrogen Invitrogen	IF 1:500
Anti-rabbit	AF 488 AF 555	A11070 A21429	Invitrogen Invitrogen	IF 1:500
Anti-rat	AF 488 AF 555 Dylight 650	A11006 A21434 SA5-10021	Invitrogen Invitrogen Invitrogen	IF 1:500

3.2. METHODS

3.2.1. Mice

In this dissertation, all experiments were conducted using C57BL/6J strain mice. The animals were bred and maintained at the Laboratory of Mouse Engineering and Breeding Facility, Faculty of Medicine, University of Rijeka. Before euthanasia by cervical dislocation, the mice were anesthetized via intraperitoneal injection of 2% xylazine and 10% ketamine solution diluted in sterile PBS. All animal procedures complied with the European Communities Council Directive (86/609/EEC, 24 November) and adhered to institutional and national ethical guidelines. Experimental protocols were reviewed and approved by the Ethics Committees of the Faculty of Biotechnology and Drug Development and the Faculty of Medicine, University of Rijeka, as well as the Ministry of Agriculture of the Republic of Croatia.

3.2.2. Isolation, preparation, and culturing of murine BM MKs

For bone marrow (BM) isolation, male mice aged 8–12 weeks were used. Following euthanasia, the fur was pre-wetted with 70% ethanol to minimize loose hair dispersion. The femur and tibia were excised using scissors, and any adherent muscle and connective tissue were carefully removed. Bone marrow was extracted by flushing 0.5 mL of pre-warmed medium through the bone lumen using a 25G needle. The resulting suspension was collected in a plate and dissociated into a single-cell suspension by sequential passage (6-8 times) through needles of decreasing gauges (18G, 21G, and 23G). The quality of the single-cell suspension was assessed using a standard light microscope, and larger aggregates or connective tissue were removed using a 70 µm cell strainer. The marrow from all bones was pooled into a single tube, and the cell suspension was centrifuged at 1000 rpm for 5 minutes. The resulting pellet was resuspended in 1 mL of complete medium, then counted using Neubauer's chamber, and BM progenitor cells were seeded at a concentration of 10⁷/mL. Cells were then incubated in a standard humidified incubator at 37°C with 5% CO₂. The plating day was designated as day 0, and the cells were cultured for three or five days, yielding immature or more mature MKs.

In TPO signaling experiments, MKs were deprived of serum in DMEM for 3 hours, then stimulated with murine recombinant TPO at concentrations of 10, 25, or 50 ng/ml for 15 minutes before immediate lysis. For Erk inhibition, we utilized PD0325901, a gift from Dr. Wensveen of the Department for Histology and Embryology at the Faculty of Medicine, University of Rijeka, Croatia. To assess signaling effects, specifically Erk phosphorylation, starved MKs were pretreated with PD0325901 at 0.5 or 1 µM for 30 minutes prior to TPO stimulation at 25 ng/ml. To

examine how ERK inhibition impacts MK development, BM cultures were treated with 0.5 or 1 μ M of the inhibitor for 72 hours, from day 1 to day 3. For proteome analysis, MKs from day 3 or 5 of culture were isolated through two consecutive BSA gradient separations. Purity was verified by immunofluorescence staining for MKs (CD61) and nuclei (DAPI).

3.2.3. BM MK culture on Matrigel

BD Matrigel Matrix Growth Factor Reduced, Phenol Red-Free (#356231, BD Biosciences) was thawed on ice. Glass coverslips were coated with diluted Matrigel (1:6 in DMEM) in a 24-well plate and incubated at 37° C for 1 hour. Any non-polymerized supernatant was carefully removed, and isolated murine BM progenitor cells were seeded in a complete medium supplemented with the required cytokines (TPO or TPO with IL-1 α). After three or five days of culture, cells were pre-fixed by adding 4% PFA to the medium for 15 minutes. The supernatant was then discarded, and cells were fixed again with 4% PFA for an additional 15 minutes. Finally, cells were washed with PBS and immunostained as previously described.

3.2.4. Proplatelet formation assay

To assess the proplatelet formation capacity of BM MKs, cells were isolated and enriched using a BSA gradient on day three or five, then cultured for an additional 18 hours in complete medium. The percentage of proplatelet-forming MKs was determined by calculating the ratio of proplatelet-bearing cells to the total MK population. Imaging was performed using a 40× objective on an Axio Vert.A1 bright-field microscope (Carl Zeiss). Before immunofluorescent staining of proplatelets, cells were centrifuged on PLL-coated coverslips at 1000g for 5 minutes (Heraeus Megafuge, Thermo Fisher Scientific) and then processed according to the immunofluorescence protocol.

3.2.5. BSA gradient-based enrichment of MKs

A 1 mL volume of pre-warmed 3% BSA (in PBS) was pipetted into the bottom of a Falcon tube and carefully overlaid with an equal volume of 1.5% BSA (in PBS). The whole BM culture was collected into a tube and centrifuged at 800 rpm for 5 minutes. The resulting pellet was resuspended in 1 mL of pre-warmed complete medium and layered onto the 1.5% BSA solution. The gradient was allowed to stabilize at room temperature (RT) for 30 minutes. Following this, the top 2.5 mL of the suspension was discarded, while the bottom 0.5 mL, containing enriched MKs, was washed with a complete medium and used for further analysis.

3.2.6. Immunofluorescence

BM MKs, DAMI, K562, or HEL cells were centrifuged onto poly-L-lysine-coated (P1524, Sigma) glass coverslips at 1500 rpm for 8 minutes using a Hettich cytospin centrifuge. Cells were then fixed with 4% paraformaldehyde (PFA) for 15 minutes at RT, then washed once with PBS and permeabilized with 0.5% Tween-20 in PBS for 10 minutes at RT. Following another PBS wash, cells were blocked with 5% goat serum in PBS for 45 minutes at RT. Next, cells were incubated with primary antibodies diluted in the blocking solution for 2 hours at RT, followed by three washes with PBS and incubation with the appropriate secondary antibody, diluted in PBS, for 1 hour at RT. After three additional PBS washes, nuclei were counterstained with either 4',6-diamidino-2-phenylindole (DAPI) at a final concentration of 300 nM for 1 minute at RT or with NucRed dye diluted in PBS for 45 minutes at RT. Finally, coverslips were mounted using Aqua-Poly/Mount mounting medium, stored in the dark, and left to dry. Afterward, coverslips were kept at 4°C.

3.2.7. Immunofluorescence staining of phosphoinositides

For PI3P staining, cells were fixed with 2% PFA and 2% sucrose in PBS for 15 minutes at RT, then briefly washed twice with PBS containing 50 mM NH₄Cl. Permeabilization was performed using 20 μM digitonin diluted in buffer A for 5 minutes, followed by two washes with buffer A. Cells were then blocked with 5% goat serum in buffer A for 45 minutes, and subsequently washed once for 5 minutes with buffer A. PI3P-specific primary antibody was diluted in buffer A containing 5% goat serum in 1:100 ratio and incubated for 2 hours, followed by two 5-minute washes with buffer A. Cells were then incubated with the appropriate fluorescently labeled secondary antibodies, also diluted in buffer A with 5% goat serum in 1:250 ratio, for 1 hour, followed by three additional 5-minute washes with buffer A. Post-fixation was performed with 2% PFA and 2% sucrose in PBS for 5 minutes, followed by one 5-minute wash with PBS containing 50 mM NH₄Cl. Nuclei were counterstained with NucRed dye diluted in buffer A for 45 minutes at RT, then DAPI for 1 minute at RT. Finally, coverslips were mounted using Aqua-Poly/Mount mounting medium and stored in the dark. Afterward, coverslips were kept at 4°C.

3.2.8. Isolation of human mononuclear cells

Human blood was collected from adult, healthy donors under the institutional guidelines and the Declaration of Helsinki. Venous blood was drawn in a syringe containing Aster-Jandl anticoagulant (1/10 of the total drawn blood volume). Anticoagulant-treated blood was diluted with HBSS in a 1:1 ratio, and the following procedures were done according to the manufacturer's protocol for Ficoll-Paque™ PLUS (#17-1440-02, GE Healthcare). Briefly, Ficoll-Paque solution was drawn in

aseptic conditions and added to a centrifuge tube. The diluted blood sample was carefully layered on the Ficoll-Paque solution and centrifuged at 400g for 35 minutes at RT. The upper separated layer of plasma was discarded using a clean Pasteur pipette while making sure not to disturb the lymphocyte layer. Then, the lymphocyte layer was transferred carefully in a clean centrifuge tube and washed with at least 3x volumes of HBSS. The cell suspension was centrifuged at 100g for 10 minutes at RT, and the washing step was repeated twice. Finally, lymphocytes were resuspended in PBS and centrifuged onto PLL-coated coverslips according to the standard protocol before immunofluorescence staining.

3.2.9. Fluorescence microscopy and image analysis

Fluorescence images were captured using a Zeiss Axio Observer Z1 epifluorescence microscope (Carl Zeiss) equipped with a Plan-Apochromat 63x/1.40 oil DIC M27 objective, a 1.6x Tubelens Optovar lens, and an Axiocam 506 imaging device. Confocal images were captured from sequential z-stacks using the LSM880 laser scanning confocal microscope (Carl Zeiss), which is equipped with an Argon laser multiline (458/488/514 nm), HeNe lasers (543 nm and 633 nm). The objective was a Plan-Apochromat 63×/1.40 oil DIC III (Carl Zeiss). To ensure consistency across samples, image acquisition settings (laser intensity) were kept the same. The weighted colocalization coefficients (M1, M2), mean fluorescence intensity (MFI), and cell area were quantified using ZEN Black software (Carl Zeiss). MFI was expressed relative to the area (size) of the cells and reported from maximum intensity projections of z-stack acquired images.

3.2.10. Murine blood platelet isolation

Platelets were isolated from male mice up to 6 months old. The mice were anesthetized, and blood (up to 1000 μ L) was collected via retro-orbital plexus bleeding using heparinized capillary tubes into a tube containing Aster Jandl anticoagulant. The collected blood was centrifuged at 100 g for 8 minutes, after which the supernatant and the buffy coat were carefully transferred to a new tube. Pre-warmed washing buffer was added to the suspension, followed by centrifugation at 100 g for 6 minutes. The resulting supernatant, containing platelet-rich plasma, was transferred to a new tube, and washing buffer was added. The suspension was centrifuged at 1200 g for 5 minutes, and the pellet was resuspended in washing buffer. This step was repeated with another round of centrifugation at 1200 g for 5 minutes, and the final pellet (platelets) was resuspended in a pre-warmed resuspension buffer.

3.2.11. Platelet-like-particle count

BM MKs were cultured for three or five days as previously described. On the day of isolation, MKs were enriched using a BSA gradient and seeded for 18 hours. Cells were then collected, centrifuged at 100g for 5 minutes to pellet MKs. The supernatants containing PLPs were further centrifuged at 1000g, and the pellets were washed twice with 0.5% BSA in PBS. They were stained with CD61-PE, GPIbβ-FITC, or the appropriate isotype control for 30 minutes in the dark. For intracellular staining, PLPs were fixed with 4% PFA, permeabilized with Perm/Wash buffer (per manufacturer's instructions, #51-2091KZ, BD Biosciences), and stained with vWF-FITC antibody. The staining was stopped by adding 200 µL of 0.5% BSA/PBS. Before flow cytometry, 5 µL of Spherotech AccuCount Fluorescent Particles (106/mL. #ACFP-50-5) were added to each sample. Proplatelet formation and PLP release were also monitored after acute IL-1α stimulation (18h, 50 ng/mL) of TPO-cultured day 3 MKs or following Erk inhibition (18h, 1 µM PD0325901) in TPO or TPO/IL-1a day 3 MKs. PLPs were counted with a BD FACSAria™ III cytometer and quantified based on the percentage of CD61-positive events using FACS Diva software (BD Biosciences).

3.2.12. Flow cytometry of whole bone marrow cultures

BM cultures were collected and briefly washed with sterile, filtered 0.5% BSA/PBS. Before staining, cells were washed once with PBS and incubated in the dark at 4°C with fixable viability dye eFluor[™] 450 (#65-0863-14, Invitrogen) for 30 minutes. To prevent nonspecific binding, Fc blocking antibody (anti-CD16/CD32, clone 2.4G2, #553142, BD Biosciences) was added for 5 minutes. Then, cells were stained with primary antibodies in FACS flow buffer (2% FBS, 0.05% NaN₃ in PBS) for 30 minutes at 4°C. After staining, cells were washed again, filtered through a 100 μm cell strainer, and kept on ice until analysis. Dead cells and doublets were excluded based on eFluor[™] 450 dye staining and forward scatter area/height gating. Lastly, cells were analyzed and quantified using a BD FACSAria[™] III cytometer and FlowJo (Treestar) software.

3.2.13. Cell lysis and protein extraction

Cells were washed twice with 1X PBS. After washing, cells were resuspended in PBS, lysed with lysis buffer containing protease inhibitor cocktail (#87785, Thermo Fisher Scientific), and mixed thoroughly with 3X SDS buffer with freshly added β -mercaptoethanol. Lysates were stored at -20°C and heated at 95°C for 5 min before loading the samples on the gels and continuing with SDS-PAGE.

3.2.14. DNA damage induction experiments

Cells were seeded at a concentration of 100,000/mL, and the plate was left open before switching on the UV lamp. TUV 30W/G30 T8 (Philips) lamp irradiated the cells in defined intervals (2, 5, and 10 minutes). Control cells were left in a separate laminar for the same time duration. After the UV treatment, both control and treated cells were left to recover in the incubator at 37°C, 5% CO₂ for 1 hour. After that, cells were either collected and processed for immunofluorescent staining or were lysed and processed further according to sample preparation protocol for SDS-PAGE and Western blot.

3.2.15. Induction of acute thrombocytopenia in vivo

Experiments involving *in vivo* thrombocytopenia were performed with Tea Bruketa and in collaboration with Dr. Markus Bender and Dr. Markus Spindler (Institute of Experimental Biomedicine, University Hospital Würzburg, Rudolf Virchow Center, Würzburg, Germany).

The protocol for inducing acute platelet depletion followed the established study design by Gupta *et al.* [162]. Briefly, WT mice were injected with polyclonal rat antimouse GPIb α antibody (4 µg/g bodyweight; Emfret Analytics, Germany). Control mice were injected with PBS. Platelet levels were measured 6 hours, 24 hours, and 48 hours post-antibody administration. Bone marrow sections were harvested, prepared, and immunostained for MK marker (GPIb β , GPIX) and Vps34.

3.2.16. Bone marrow cryosections immunostaining

The buffers and cryosections were allowed to rest at RT before use. A humid chamber was used for all incubation steps. The Roti®-Liquid Barrier Marker (#AN92.1, Carl Roth) was applied around the film, ensuring it was dry and tightly pressed against the glass to minimize the marker from seeping underneath. The sections were then permeabilized by incubating in the permeabilization buffer for 20 minutes at RT. After permeabilization, the sections were blocked with the blocking buffer for 1 hour at RT, ensuring enough volume to cover the specimen. The blocking buffer was removed, and 150 µL of primary antibody diluted in washing buffer was added. MK markers (GPV or GPIbβ) were incubated for 1 hour at RT, while Vps34 was stained overnight. The primary antibody incubation was done in the dark and was followed by appropriate secondary antibodies that were incubated for 1 hour at RT. The sections were washed three times with washing buffer for 5 minutes each, discarding the buffer between washes. Afterward, the washing buffer was removed, and one drop of Fluoroshield™ with DAPI (#F6057, Sigma Aldrich) was added; then the section was covered with a coverslip, pressing tightly to remove any bubbles. The sections were allowed to dry overnight at RT and stored at 4°C.

3.2.17. SDS-PAGE and Western blot

The samples were separated using a 1X Running buffer in a Mini-PROTEAN Tetra Vertical Electrophoresis Cell (Bio-Rad). A pre-stained protein marker (#26619, Thermo Fisher) was used to determine protein size. The stacking gel was run at 80 V for 15 minutes, while the separating gel was run at 110 V until the loading dye reached the end of the gel. After protein separation in the polyacrylamide gel, proteins were transferred to a nitrocellulose membrane (0.45 µm pore size). During preparation of the gel-membrane transfer sandwich, all components were soaked in 1X Transfer Buffer. The transfer sandwich was placed into a gel holder cassette and positioned in a Mini Trans-Blot Electrophoretic Transfer Cell (Bio-Rad). The transfer was conducted at 850 mA for 90-120 minutes, depending on the protein size. After the transfer, the membrane was blocked with a blocking solution for 45 minutes at RT to minimize non-specific antibody binding. Following blocking, the membrane was incubated with the primary antibody overnight at +4°C, with all primary antibodies diluted in the blocking solution. The next day, the membrane was washed three times with TBS-Tween20 for 10 minutes and then probed with an appropriate HRP-conjugated secondary antibody. After three additional 10-minute washes, the membrane was incubated with ECL™ Prime Western Blotting Detection (RPN2236, GE Healthcare) for 1 minute or with SuperSignal™ West Femto Maximum Sensitivity Substrate (#34095, Thermo Fisher Scientific) for phosphorylated proteins, and developed using the ChemiDoc™ MP Imaging System (Bio-Rad). Band density was measured using ImageJ (Fiji) software [163]. These values were then normalized according to GAPDH loading control or, in the case of phosphorylated proteins, normalized to their respective total protein fractions.

3.2.18. Sample preparation for proteomic analysis

Approximately 100,000/mL of isolated and purified MKs were lysed in 100 μL of lysis buffer (100 mM ammonium bicarbonate, 2% sodium deoxycholate). Protein concentration was determined using the bicinchoninic acid (BCA) assay (Pierce™ BCA Protein Assay Kit, #23225, Thermo Fisher Scientific) following the manufacturer's instructions. Tryptic digestion was performed at a protein-to-protease ratio of 1:100 using the single-pot, solid-phase-enhanced sample preparation (SP3) protocol, as described by Hughes et al. [164]. Peptides were dried using a Savant SpeedVac Vacuum Concentrator (Thermo Fisher Scientific, Waltham, USA) and stored at −80°C until further use. Immediately before measurement, dried peptides were reconstituted in 0.1% formic acid (FA), and their concentration was estimated using a NanoDrop Microvolume Spectrometer (Thermo Fisher Scientific, Waltham, USA). For spectral library generation, 24 μg of peptides were dissolved and fractionated into eight fractions using the Pierce High pH Reversed-Phase Peptide

Fractionation Kit (Thermo Fisher Scientific, Waltham, USA), according to the manufacturer's instructions.

3.2.19. LC-MS/MS parameters for proteome data acquisition

Experiments involving proteomic analysis were conducted in collaboration with Dr. Olga Shevchuk and Dr. Hannah Voß under the supervision of Prof. Dr. Daniel Robert Engel (Department of Immunodynamics, University Hospital Essen, Essen, Germany).

For each sample and fraction, 300 ng of peptides were injected into a NanoElute2 LC system (Bruker Daltonics, Billerica, Massachusetts, USA) and analyzed using a timsTOF flex mass spectrometer (Bruker Daltonics, Billerica, Massachusetts, USA) via a CaptiveSpray ion source set to 1600V. Peptides were first loaded onto a trapping column (5 mm length, 3 µm inner diameter, 5 µm particle size, 100 Å pore size; Thermo Fisher Scientific, Massachusetts, USA) and then separated using a 50minute chromatography gradient on an Aurora C18 capillary column (25 cm length, 75 µm inner diameter, 1.7 µm particle size, 120 Å pore size; IonOpticks, Fitzroy, Australia). The mobile phase consisted of solvent A (0.1% formic acid in H₂O) and solvent B (0.1% formic acid in acetonitrile-H₂O), with a gradient ranging from 0% to 34% B at a flow rate of 300 nL/min. For spectral library generation, the mass spectrometer was operated in data-dependent acquisition (DDA) mode using parallel accumulation-serial fragmentation (PASEF), with ten PASEF scans per topN acquisition cycle and a total cycle time of 1.17 seconds. The accumulation and ramp times for the dual-trapped ion mobility spectrometry (TIMS) analyzer were set to 100 ms at a ramp rate of 9.42 Hz. Scan ranges were configured from m/z 100-1,700 for mass detection and from $1/K_0$ 0.60–1.60 V s⁻¹ cm⁻² for ion mobility at both MS levels. Precursor ions were selected in real-time from TIMS-MS survey scans based on their positions in the m/z-ion mobility plane. Those reaching a target intensity of 20,000 AU were dynamically excluded for 0.4 minutes. Quadrupole isolation width was set to 2 Th for m/z <700 and 3 Th for m/z >800. Collision energy (CE) was ramped linearly from 52 eV at $1/K_0$ 1.6 V s⁻¹ cm⁻² to 20 eV at $1/K_0$ 0.6 V s⁻¹ cm⁻².Individual samples were analyzed in data-independent acquisition (DIA) PASEF mode using similar scan ranges and collision energies. DIA-PASEF cycle time was estimated at 1.8 seconds. Within each cycle, precursor ions in the m/z range of 400–1201 Da and a mobility range of 1/K₀ 0.6–1.6 were fragmented. At the MS1 level, one ramp was executed per cycle. For MS/MS acquisition, 32 fragmentation windows, each with a mass width of 26.0 Da and a mass overlap of 1.0 Da, were distributed across 16 MS/MS ramps

3.2.20. Data analysis for proteome data

LC-MS raw data were processed using Spectronaut (Version 19.1.240806.626, Biognosys, Schlieren, Switzerland). A spectral library was generated from Pulsar based on DDA-PASEF measurements of high-pH reversed-phase peptide fractions, utilizing BSG factory settings. The parameters included trypsin/P as the cleavage enzyme, carbamidomethylation (C) as a fixed modification, and acetylation (protein N-terminal) and methionine oxidation as variable modifications. The library was searched against a reviewed murine UniProt/Swiss-Prot FASTA database (downloaded on October 29, 2024, containing 17,221 target sequences). DIA-PASEF measurements of individual samples were then matched against this spectral library using BSG factory settings, with quantification performed at the MS2 level. Cross-run normalization was enabled and automatically selected. Normalized protein abundances were exported and analyzed in Perseus (Version 2.0.11, MPI, Martinsried, Germany). Protein abundances were log₂-transformed. differentially abundant proteins between phenotypes (TPO and TPO/IL-1α) were identified using Student's t-test. Proteins with a permutation-based false discovery rate (FDR) q-value < 0.05 and at least a 1.5-fold change between groups were considered significant and subjected to further analysis. To identify differentially regulated biological processes, significant proteins were uploaded to the STRING Protein-Protein Interaction database (https://string-db.org) for pathway analysis. Functional enrichment was performed using the REACTOME pathway database (https://reactome.org, accessed January 10, 2025). Gene sets containing fewer than 600 genes and an FDR < 0.05 were considered for further investigation. Additional gene sets (MM14472 and MM15715, Version 2024.1) were obtained from the MSigDB Mouse collection (https://www.gsea-msigdb.org/gsea/msigdb, accessed January 10, 2025). A list of neutrophil marker proteins was retrieved from the Human Protein Atlas immune cell resource (https://www.proteinatlas.org/humanproteome/single+cell/immune+cell, January 10, 2025) [165]. Only genes enriched in neutrophils and at most one additional cell type were considered. Mouse orthologs of selected human genes using identified the g:Orth function in g:Profiler were (https://biit.cs.ut.ee/gprofiler/orth, accessed January 10, 2025) [166]. antimicrobial peptides, a custom gene set focusing on mammalian innate immune system peptides was used [167]. Data visualization, including principal component analysis (PCA), volcano plots, and heatmaps, was performed in R (Version 4.4.2; R Core Team, 2021; https://www.R-project.org), utilizing the ggplot2 (Wickham H, 2016), plotly (Sievert C, 2020), pheatmap (Kolde R, 2019), dplyr (Wickham H, François R, Henry L, Müller K, Vaughan D, 2023), RColorBrewer (Neuwirth E, 2022), and openxlsx (Schauberger P, Walker A, 2024) libraries. For heatmap generation, Euclidean distance was used for both sample and protein clustering, with the Ward.D2 method applied for hierarchical clustering. Prior to heatmap construction, log₂ protein abundance values were centered around the mean for each protein.

3.2.21. Statistical analysis

All experiments were performed at least in three independent experiments and data are represented as mean \pm standard deviation (SD). Data was analyzed by Student's t-test or Analysis of variance (ANOVA) with a post-Bonferroni test using Prism software (GraphPad). Differences were considered significant when P values were < 0.05 (* p < 0.05; ** p < 0.01; *** p < 0.001, **** p < 0.0001).

4. RESULTS

4.1.INTERLEUKIN-1 ALPHA MODULATES MEGAKARYOCYTE MATURATION, ENHANCES EMPERIPOLESIS, AND RESHAPES THE MEGAKARYOCYTE PROTEOME

In a mouse model of thrombocytopenia, the proinflammatory cytokine IL-1 α was identified as a key driver of MK rupture, a process that enables the rapid release of large numbers of platelets compared to proplatelet formation [51]. The effect of IL-1 α was linked to caspase-3 activation, dysregulated tubulin expression, and reduced membrane stability in fetal liver-derived MKs (FL MKs) *in vitro* [51].

Despite the recognized impact of the proinflammatory IL-1 superfamily on MK function [168-172], so far, no work has focused on the specific effects of IL-1 α , particularly in BM MK maturation *in vitro*. Here, we demonstrate that IL-1 α induces significant changes in the phenotype and proteomic profile of murine BM-derived MKs. IL-1 α enhances MK size and ploidy while downregulating the expression of hemostatic proteins. Notably, IL-1 α increases the frequency of emperipolesis, with neutrophil entry found to be IL-1 α -dependent. Furthermore, IL-1 α induces a shift in MK cell programming, as evidenced by a distinct proteomic signature in early and late MKs, characterized by a marked abundance of neutrophilic, antimicrobial, and inflammation-related proteins.

4.1.1. IL-1 α increases megakaryocyte size, alters the morphology of proplatelets, and boosts the release of platelet-like particles

Since IL-1 α has been shown to mediate platelet release through MK rupture both *in vivo* and from FL MKs *in vitro*, we investigated how BM MKs respond to IL-1 α treatment. Murine BM-derived progenitor cells were cultured for 3 days with TPO, either alone or in combination with IL-1 α (TPO/IL-1 α), then assessed for MK size, number, proplatelet formation, and platelet release. MKs grown with IL-1 α were significantly larger than those with only TPO (**Figures 8A, B**). IL-1 α alone did not induce significant MK development, although occasionally smaller MKs could be observed (**Figure 9A**). However, TPO/IL-1 α cultures produced approximately 700,000 more MKs per mL than TPO-only cultures (**Figure 8C**). This increase was further confirmed by flow cytometry analysis of CD61+ (MK marker) cell percentages at various time points (**Figure 9B**).

Next, we examined proplatelet production from cultures, normalized to MK count. BM MKs were cultured until day 3, enriched via a BSA gradient, and equal amounts of MKs for both conditions were then cultured for 18 or 36 hours. Brightfield microscopy showed that IL- 1α had no significant impact on proplatelet formation

after either time point (**Figure 8E, Figure 9C**), although at 36 hours, there was a notable increase in the percentage of proplatelet-forming MKs in both conditions. Immunostaining confirmed that IL-1 α -treated MK cultures produced much shorter proplatelets with minimal branching (**Figure 8D, Figure 9D**), and these had significantly larger tips at both time points (**Figure 8F, Figure 9E**). In IL-1 α samples, proplatelets were rarely attached to cell bodies, indicating increased fragility, despite no differences in β 1-tubulin and F-actin staining.

To measure platelet release under identical culture conditions, we analyzed CD61+ platelet-like particles (PLPs) in supernatants using flow cytometry. We found that BM MKs cultured with IL-1α released significantly more CD61+ PLPs than those cultured with only TPO at both time points (Figure 9G, Figure 9F). Moreover, the PLPs from IL-1α-treated MKs were notably larger at 18 hours, as indicated by increased forward scatter (FSC) (Figure 8H). These findings are consistent with previous reports on the number and size of platelets released from IL-1α-cultured FL-MKs [51]. Next, we investigated whether short-term (acute) IL-1α treatment affects proplatelet formation and platelet release capacity. BM MKs cultured solely with TPO (on day 3 or day 5) were exposed to IL-1α for 18 hours and assessed for proplatelet formation and platelet release. Although there was no statistically significant change in the percentage of proplatelet-bearing MKs (day 3, 18h IL-1α, Figure 9G) or CD61+ PLP release, day 3 MKs stimulated with IL-1α produced a slightly higher number of CD61+ PLPs (Figure 9H). Collectively, these results show that IL-1α induces increased MK and platelet production, possibly by accelerating BM MK maturation and generating more fragile proplatelets.

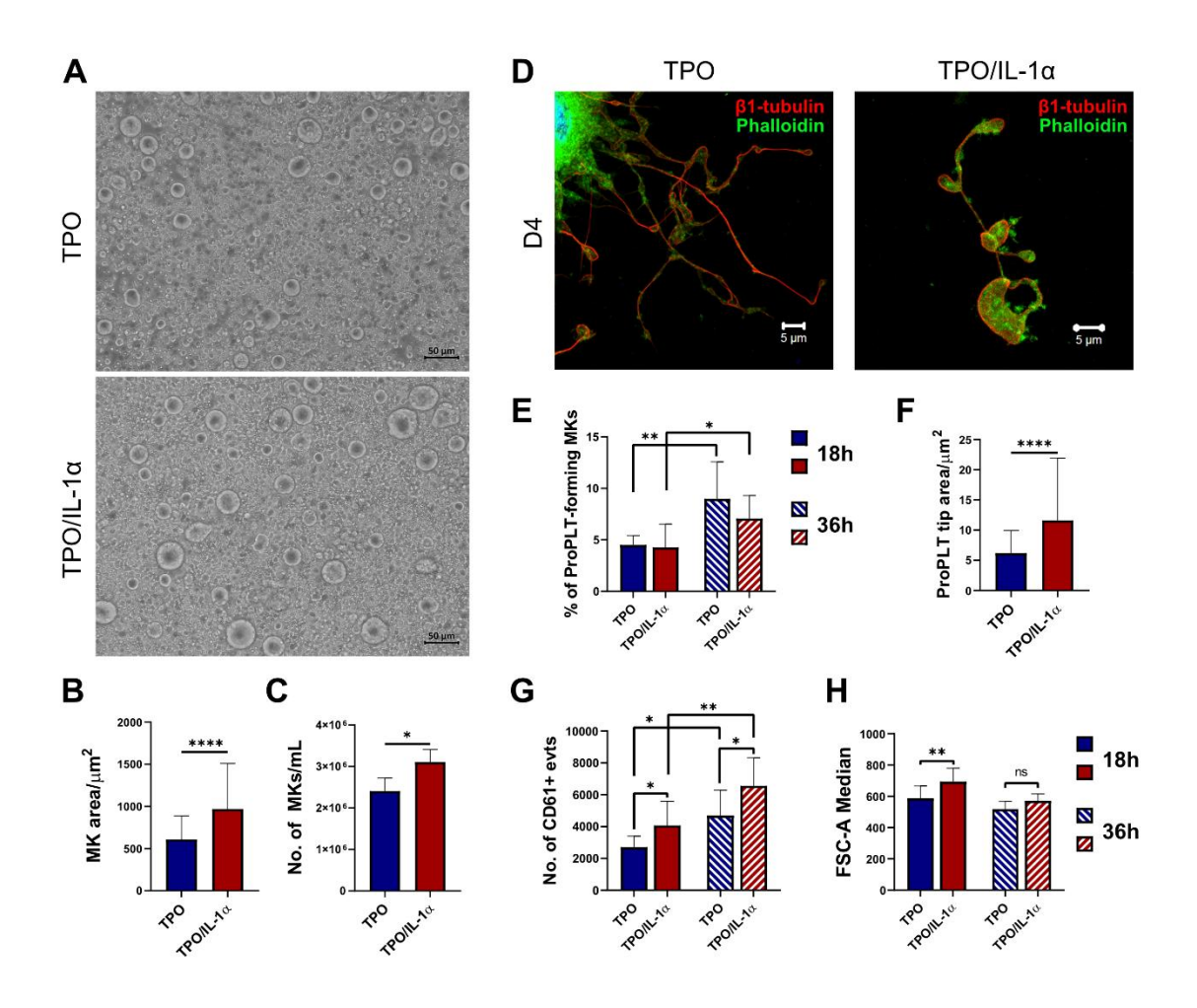


Figure 8. IL- 1α significantly enlarges megakaryocytes, modifies proplatelet structures, and promotes the release of platelet-like particles in vitro.

(A) BM-derived MKs were captured under a 40x objective of the Axio Vert.A1 bright-field microscope (Carl Zeiss) after three days of culture. (B) The graph shows the surface area of MKs on day three, quantified with ZEN 2 software (Carl Zeiss). (C) MKs from TPO and TPO/IL-1α cultures were manually counted with a hemocytometer before BSA gradient enrichment. MK size and number was measured across a minimum of seven independent experiments. (D) MKs were isolated on day 3, enriched over a BSA gradient, and cultured for another 18 hours. Proplatelets were spun onto PLL-coated coverslips, fixed, and immunostained for β1-tubulin and actin (Phalloidin-Alexa Fluor 488). Imaging was done using an LSM880 (Carl Zeiss) confocal microscope with a Plan-Apochromat 63×/1.40 oil DIC III objective. The shown images are maximum projections. (E) The graph indicates the percentage of MKs with proplatelets, with at least 100 MKs counted across three independent experiments. (F) The graph displays proplatelet tip area, measured and analyzed with Zeiss ZEN Black software from three independent experiments (N=205 for TPO, N=139 for TPO/IL-1a). (G) Flow cytometry results show the number of CD61+ events in TPO or TPO/IL-1α culture supernatants after 4 days (D4) and 5 days (D5). (H) Forward scatter (FSC) of released CD61+ PLPs was measured, with median values presented from four independent biological replicates. Data are shown as means, with error bars indicating \pm SD. * p < 0.05, ** p < 0.01, **** p < 0.0001

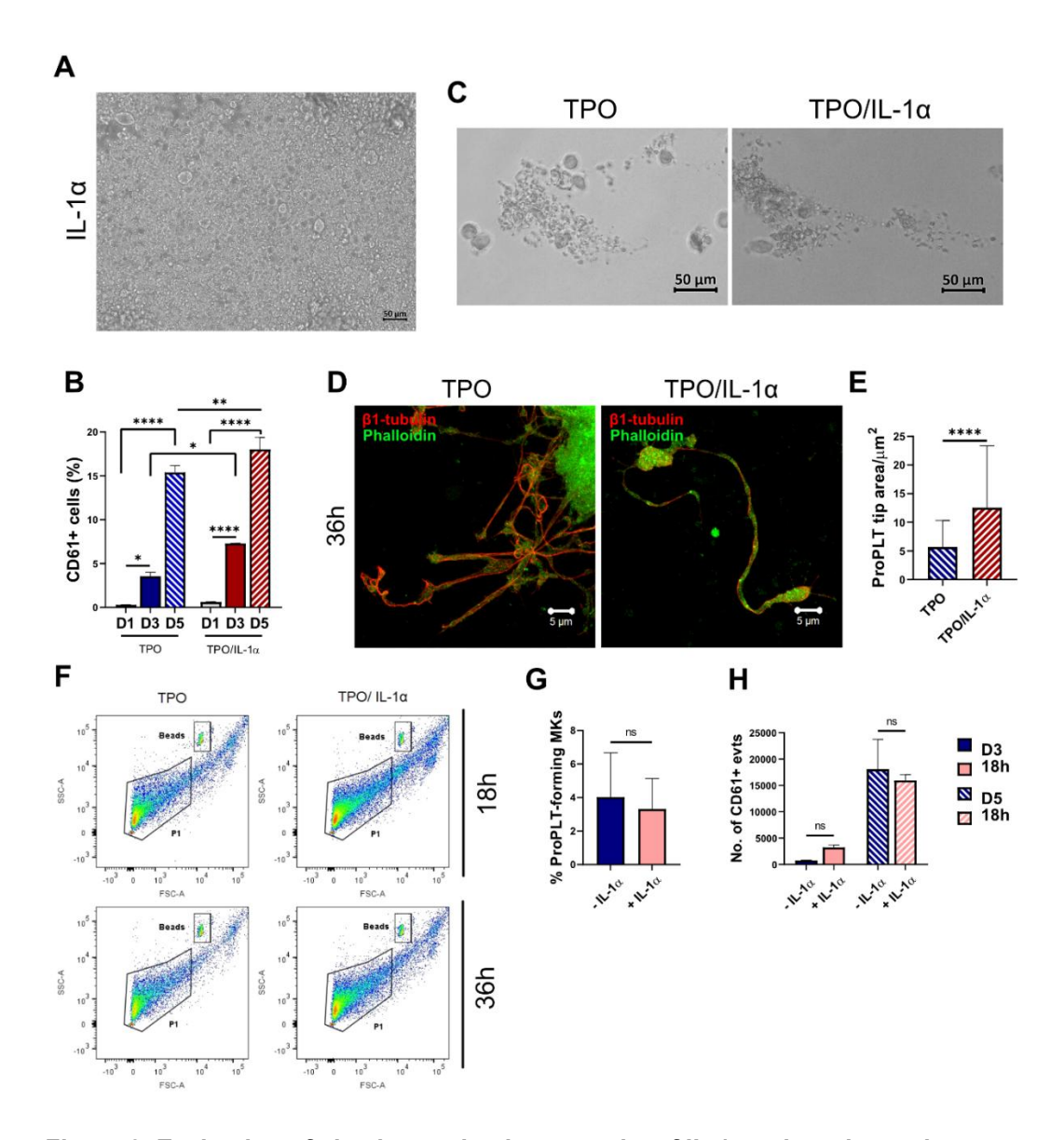


Figure 9. Evaluation of platelet production capacity of IL-1α-cultured megakaryocytes.

(A) BM cultures were prepared as described in Methods and treated solely with IL-1α (50 ng/ml) for 3 days. Cells were visualized with an Axio Vert.A1 bright-field microscope (Carl Zeiss). (B) BM cells cultured with TPO or TPO/IL-1α were analyzed by flow cytometry, as detailed in the Methods. They were stained with viability dye eFluor™ 450 and anti-CD61-PE. The graph shows the percentage of live CD61+ cells on days 1, 3, and 5 (D1, D3, D5). Data are from three independent biological replicates. (C) After 3 days, BM MKs were isolated, enriched over a BSA gradient, and further cultured for 18 hours with TPO or TPO/IL-1α. Images of proplatelet-forming MKs under 40x magnification using Axio Vert.A1 are shown. (D) MKs were cultured for 3 days, then enriched, and cultured for an additional 36 hours with TPO or TPO/IL-1α. Proplatelets were fixed, stained for β1-tubulin and actin (Phalloidin-Alexa Fluor 488), and imaged using a Carl Zeiss LSM880 confocal microscope with Plan-Apochromat 63×/1.40 oil DIC III lens. Maximum projections are displayed. (E) Proplatelet tip areas at 36 hours were measured using Zeiss ZEN Black software across three independent experiments (TPO, N=92; TPO/IL-1α, N=102). (F) Supernatants were stained for CD61, and PLPs were quantified

via flow cytometry with beads. Scatterplots depict PLPs (P1) and beads. **(G)** The proportion of MKs bearing proplatelets was assessed after an 18-hour IL-1α stimulation of MKs previously cultured in TPO for 3 days. About 40 proplatelet MKs were analyzed across five fields in two independent experiments. **(H)** MKs cultured 3 or 5 days in TPO had supernatants collected, then exposed to IL-1α for 18 hours, stained for CD61, and PLPs counted with flow cytometry in two independent experiments. * p < 0.05, ** p < 0.01, **** p < 0.0001, ns – not significant.

4.1.2. IL-1α alters early megakaryocyte maturation, resulting in the downregulation of GPIbβ and vWF and increased ploidy

In addition to growing larger, MKs experience significant cellular transformations during maturation, including protein synthesis and endomitosis. To investigate the impact of IL-1α on these processes, we analyzed the expression and localization of markers, including vWF, GPIbβ, and CD61, as well as MK ploidy levels. vWF is a key component of the most abundant MK granules, α-granules. Granule biogenesis occurs alongside the rapid growth of the MK cytoplasm; therefore, we chose to track vWF as a marker of cytoplasmic maturation [173]. On the other hand, the GPIb receptor complex is one of the most abundant surface receptors on MKs and platelets, and represents membrane maturation. It is composed of four subunits: GPIbα, GPIbβ, GPV, and GPIX [174, 175]. As MKs mature, the GPIb membrane content increases and is later transferred to platelets, where it plays a crucial role in initiating platelet adhesion during primary hemostasis [176]. Western blot results showed that IL-1α-treated MKs had reduced levels of vWF and GPlbβ compared to those cultured with TPO alone (Figure 10A). Since vWF is a large, multimeric protein, we confirmed that decreased expression was not due to changes in multimer composition by measuring the total vWF signal in both TPO and TPO/IL-1α MKs (Figure 10B, C). Next, we examined vWF and GPIbβ content and localization using immunofluorescent staining (**Figure 10F**). Confocal microscopy showed that IL-1αcultured MKs had a significantly reduced MFI for both vWF and GPIbB, while their distribution pattern remained unchanged (Figure 10G). Similar findings were observed for the MK marker CD61, with slightly lower levels on Western blot (Figure **10B, D)** and markedly lower presence in immunofluorescence of immature (day 3) IL-1 α -cultured MKs (**Figure 10E**).

Next, we evaluated the ploidy of MKs by counting nuclear lobes that were visibly separated and stained with NucRed. The modal ploidy was 8N, indicating the immaturity of BM MKs isolated on day 3, consistent with previous observations [177]. Analysis revealed a shift toward higher ploidy after IL-1 α stimulation, with a significantly greater number of MKs reaching 32N and above (**Figure 10H**).

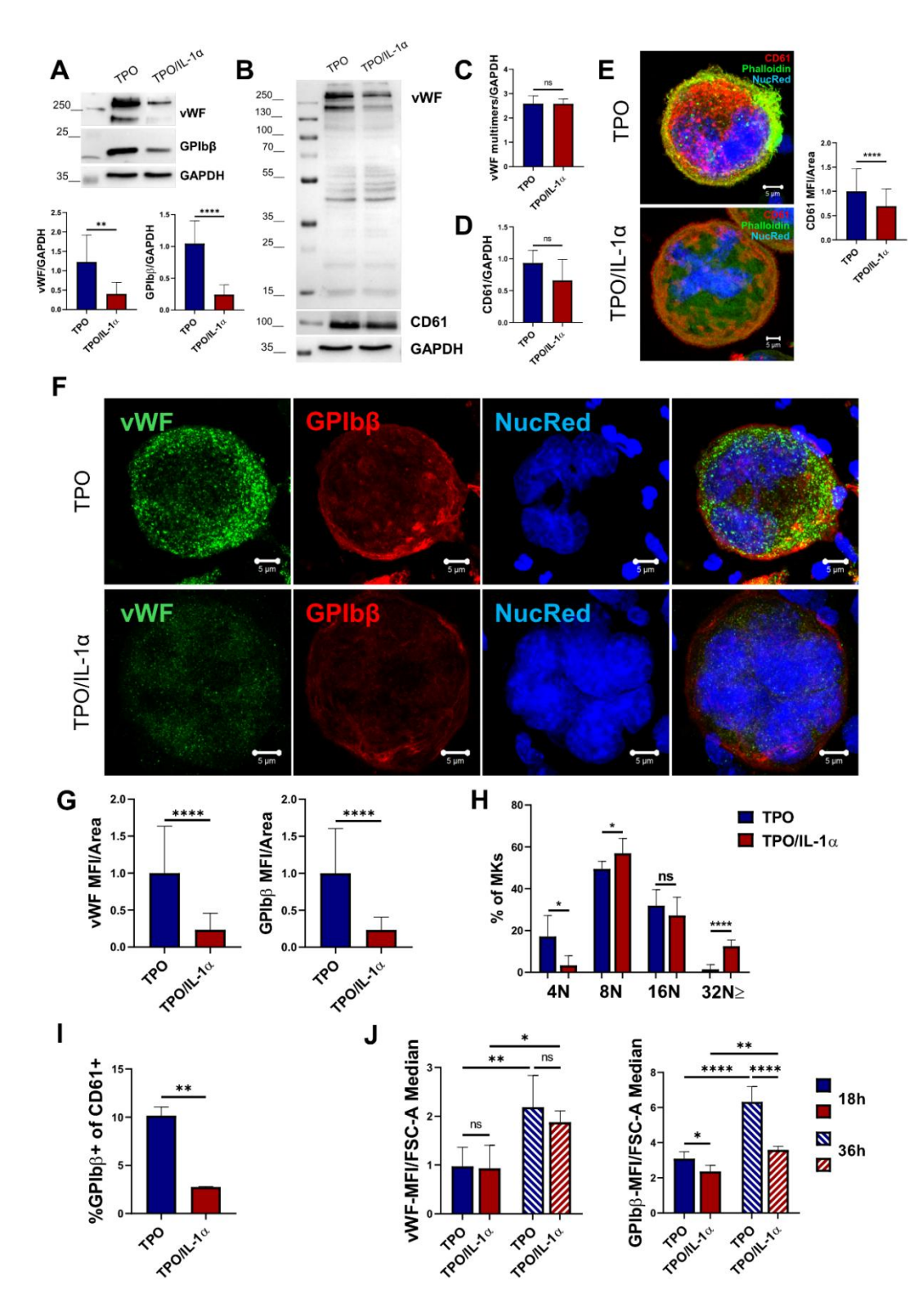


Figure 10. IL-1 α modulates megakaryocyte maturation by decreasing GPIb β and vWF levels while enhancing ploidy.

(A) On day three, BM MK lysates underwent Western blot analysis. The immunoblots display the expression patterns of vWF and GPIbβ, with GAPDH serving as a loading control. Quantification was performed using ImageJ. (B) BM MK lysates were subjected to SDS-PAGE, transferred to nitrocellulose, and probed with specific antibodies. CD61 samples were run under non-reducing conditions. Quantification of (C) vWF multimers (<130 kDa) and (D) CD61 was performed with ImageJ. Data are expressed as means ± SD from at least two experiments. (E) MKs after 3 days in culture were enriched, stained for CD61, F-actin, and NucRed, and imaged with an LSM880 confocal microscope (Carl Zeiss) with Plan-Apochromat 63×/1.40 oil DIC III lens. Fluorescence intensity (MFI) was measured with Zeiss ZEN Black software for 85 MKs per condition across three experiments. (F) Following BSA gradient enrichment on day three of culture, MKs were fixed, immunostained for VWF and Gplbß, and stained with NucRed for nuclei. Imaging was conducted with an LSM880 confocal microscope (Carl Zeiss) equipped with a Plan-Apochromat 63×/1.40 oil DIC III objective; the figure shows representative maximum intensity projections. (G) Mean fluorescence intensity (MFI) was measured with Zeiss ZEN Black software, and results are expressed relative to cell area. (H) Nuclear lobes (stained by NucRed) were counted across z-stack images to determine MK ploidy, calculated as twice the number of lobes. The graphs depict the distribution of ploidy and the percentage of MKs. At least 20 MKs were analyzed per condition for MFI and ploidy measurements across a minimum of six independent experiments. (I) Day 3 whole BM cultures were stained with CD61-PE and GPIbβ-FITC and analyzed by flow cytometry. The graph shows the percentage of GPIbB+ cells within CD61+ MKs from two independent experiments. (J) PLPs were harvested from the supernatant, permeabilized, fixed, stained, and analyzed by flow cytometry. MFI values of permeabilized vWF or surface GPIbβ were normalized to FSC median values. The graph presents data from 18 and 36 hours after MK enrichment over a BSA gradient on day 3 from three independent biological replicates. All results are expressed as means with error bars indicating ± SD. * p < 0.05, ** p < 0.01, **** p < 0.0001, ns – non-significant.

To elaborate on our immunofluorescence results concerning MK maturation, we examined whole BM cultures through flow cytometry and assessed the percentage of GPIbβ+ cells within CD61+ MKs. Consistent with previous findings, TPO cultures showed a significantly higher proportion of GPIbβ+ cells compared to TPO/IL-1α cultures (Figure 10I). Because MKs cultured with IL-1α displayed reduced levels of vWF and GPIbβ, we also investigated whether the released PLPs exhibit a similar pattern. Interestingly, although vWF content remained unchanged, surface GPIbB expression was lower in PLPs from IL-1α MKs, and this difference persisted over time (Figure 10J; MFI values were normalized to PLP size). To rule out the possibility that culture conditions in suspension cause the altered maturation phenotype, we also grew BM MKs on Matrigel. Matrigel is a basement membrane matrix rich in laminin, collagen IV, and growth factors, commonly used to mimic the extracellular environment in vitro. We used it to support cell adhesion and to better replicate physiological conditions during MK differentiation. Interestingly, both vWF and GPIbβ exhibited significantly reduced MFI values in MKs cultured with IL-1α on Matrigel (Figure 11A). Additionally, we examined other GPIb receptor subunits, GPIbα and GPIX, on MKs cultured both in suspension ad Matrigel. Notably, GPIbα and GPIX also showed significantly lower MFI values in MKs cultured with IL-1α compared to those grown in TPO alone, whether in suspension (spun on PLL-coated coverslips) or on Matrigel (Figure 11B, C), further confirming our findings.

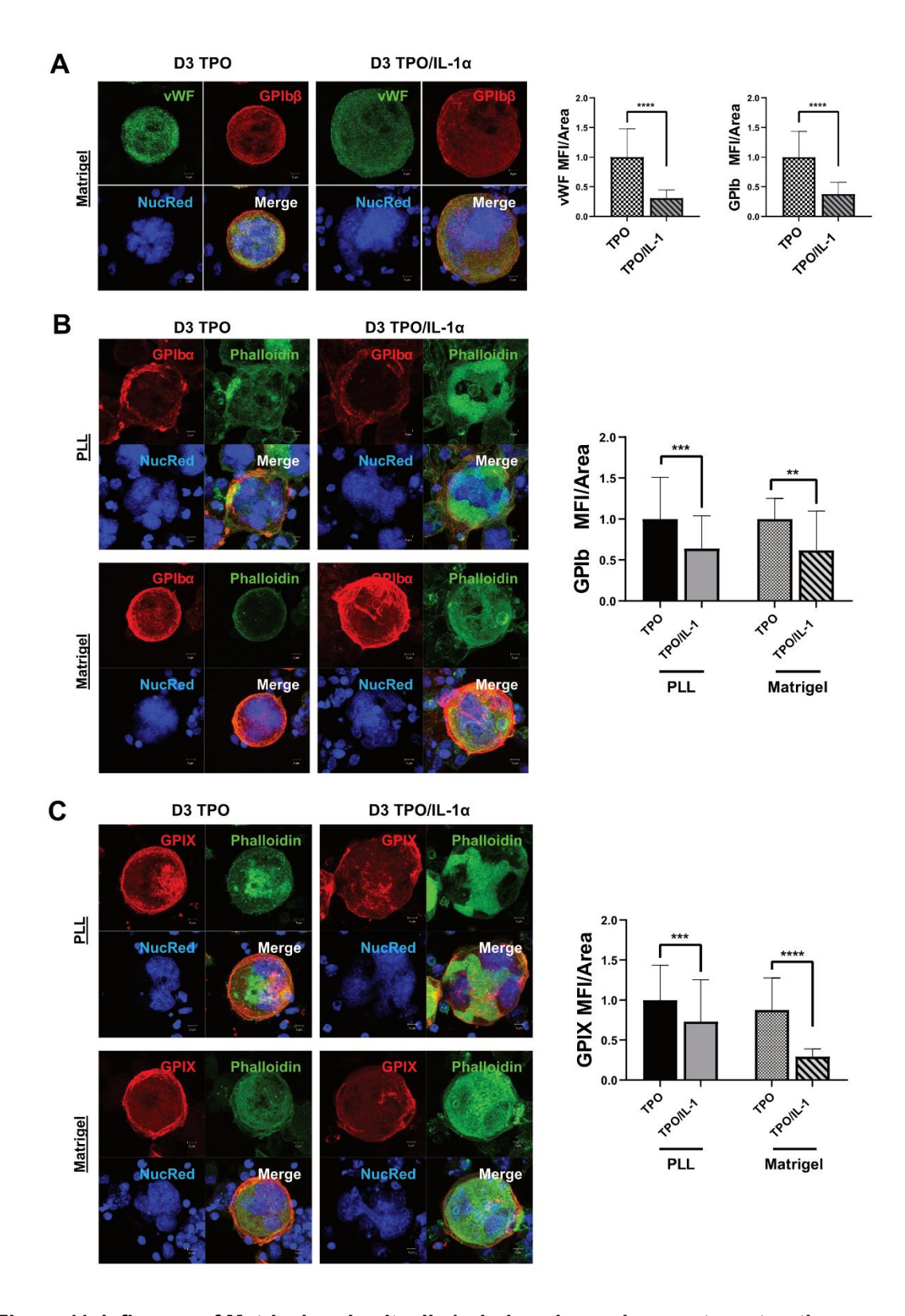


Figure 11. Influence of Matrigel on *in vitro* IL-1α-induced megakaryocyte maturation.

BM MKs were cultured for 3 days under the conditions described in the Methods, and Matrigel was used to evaluate the localization and distribution of GPIb receptor subunits in comparison to suspension cultivation. Confocal microscopy images were captured using an LSM880 (Carl Zeiss) microscope with a Plan-Apochromat $63\times/1.40$ oil DIC III objective. Mean fluorescence intensity (MFI) was quantified using Zeiss ZEN Black software. (A) MFI of GPIb β and VWF, (B) GPIb α , and (C) GPIX was measured relative to cell area in BM MKs fixed and stained on PLL-coated coverslips and compared to those grown on Matrigel-coated coverslips. Representative maximum intensity projections are displayed. A minimum of 15 MKs were measured per condition per experiment. Data are presented as mean values, with error bars representing \pm SD across three independent experiments. ** p < 0.01, *** p < 0.001, **** p < 0.0001.

4.1.3. IL-1α increases Erk phosphorylation following TPO stimulation without altering receptor expression

TPO primarily regulates megakaryopoiesis, and its binding to the TPO receptor (c-Mpl) activates downstream signaling pathways such as JAK2/STAT3 [178]. Since MKs formed in the presence of IL-1 α were larger and had higher ploidy, we investigated whether they expressed higher levels of c-Mpl or IL1R1 receptors and whether TPO signaling was enhanced in IL-1 α -cultured MKs. Analysis of early megakaryopoiesis (day 3 MKs) shows no significant difference in the expression of c-Mpl or IL1R1 receptors between MKs cultured with TPO alone and those cultured with TPO/IL-1 α (**Figure 12A**).

Next, MKs cultured with TPO or TPO/IL- 1α were starved and then stimulated with increasing concentrations of TPO (10, 25, 50 ng/ml) for 15 minutes. Western blot analysis revealed no differences in total JAK2 and STAT3 levels between TPO and TPO/IL- 1α cultured MKs (**Figure 12B**). Both groups showed an increase in P-JAK2 and P-STAT3 in response to TPO stimulation. Although the JAK2 phosphorylation was somewhat lower in TPO/IL- 1α cultured MKs compared to TPO-cultured MKs, this difference was not statistically significant. Next, we investigated other downstream targets of the TPO receptor [178], the mitogen-activated protein kinase (MAPK) and PI3-kinase pathways, by analyzing the phosphorylation of Erk (P-Erk) and Akt (P-Akt), respectively. Interestingly, MKs cultured with IL- 1α exhibited a notably higher rate of P-Erk compared to control MKs, while P-Akt levels stayed the same (**Figure 12B**).

Considering the increased P-Erk in IL-1 α -cultured MKs, we examined how inhibiting P-Erk affects MK development. We applied the PD0325901 Erk inhibitor to BM cells at 0.5 and 1 μ M starting on day 1 (24 hours post-isolation) and assessed the cultures on day 3. Erk inhibition significantly reduced MK size, which was confirmed through confocal microscopy (**Figure 12C, D**). Ploidy analysis showed a decrease in the modal ploidy for both MK groups, with TPO-treated MKs maintaining a modal ploidy

of 4N, while IL-1 α -treated MKs showed a stepwise decline to 8N, and ultimately 4N at the highest inhibitor dose (**Figure 12E**).

Overall, these findings indicate that the changed maturation phenotype after IL-1 α stimulation results, at least partially, from a stronger activation of the Erk-MAPK pathway, which may explain the increased ploidy and size of MKs cultured with IL-1 α .

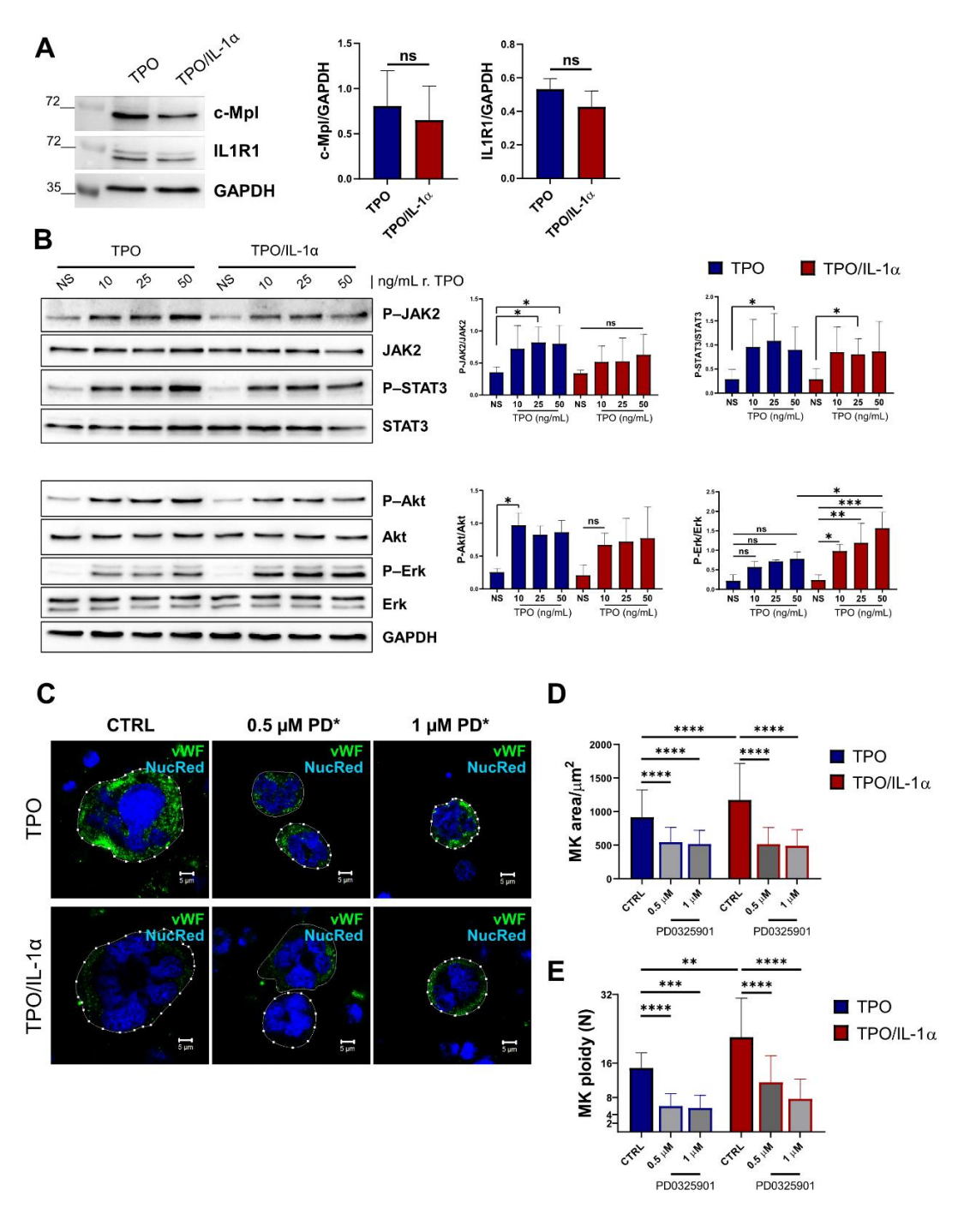


Figure 12. IL-1 α modulates Erk signaling in megakaryocytes following TPO stimulation, and inhibiting Erk leads to halted megakaryocyte growth and ploidy.

(A) BM MK lysates from day 3 were examined using Western blot analysis. Representative immunoblots display the expression patterns of TPO (c-Mpl) and IL-1 α receptor (IL1R1). GAPDH served as a loading control. Blots were analyzed with ImageJ. (B) BM MKs were collected over a BSA gradient on day 3, washed, and starved in serum-free medium for 3 hours. Cells were then treated with varying concentrations of recombinant TPO (10, 25, 50 ng/mL) for 15 minutes and

immediately lysed for Western blot analysis. BM MK lysates were tested for phospho-JAK2 (p-JAK2), JAK2, phospho-STAT3 (p-STAT3), STAT3, phospho-Akt (p-Akt), and phospho-Erk (p-Erk), with GAPDH as a loading control. Quantification was performed using ImageJ. Results are shown as means with error bars indicating \pm SD from five independent experiments. **(C)** MKs were cultured with 0.5 or 1 µM Erk inhibitor (PD*) or vehicle (DMSO; CTRL) for 48 hours (day 1 to day 3), then enriched over a BSA gradient, fixed, and stained for vWF, with nuclei counterstained using NucRed. Maximum projections are shown of confocal images acquired using an LSM880 (Carl Zeiss) microscope with a Plan-Apochromat 63×/1.40 oil DIC III objective. **(D)** Cells were visualized using an Axio Vert.A1 bright-field microscope (Carl Zeiss), and cell size was measured with ZEN 2 software. At least 300 MKs were analyzed per condition. **(E)** MK ploidy was determined by counting NucRed-positive nuclear lobes manually. MKs were categorized into ploidy groups from 2N to 32N, expressed as percentages. Data are presented as means with error bars representing \pm SD from two independent experiments. * p < 0.05, ** p < 0.01, *** p < 0.001, *** p < 0.0001, ns – not significant.

4.1.4. IL-1α promotes emperipolesis in immature megakaryocytes

While examining cells for nuclear staining (NucRed), we observed structures that resembled smaller nuclei inside the MK cytoplasm. These were separate from MK nuclear lobes (white arrows; Figure 13A), suggesting the presence of other cells within the cytoplasm. Previous studies describe a phenomenon of emperipolesis where other cells, primarily neutrophils, can be transiently present within the MK cytoplasm [179]. In our experiments, over 50% of MKs cultured with TPO together with IL-1α showed emperipolesis, compared to about 20% MKs cultured with TPO alone (Figure 13B). The TPO/IL-1α MKs that exhibited emperipolesis had a significantly higher number of other cell nuclei within the cytoplasm, averaging around five per MK. In contrast, TPO-cultured MKs with other cells typically had just one such nuclear structure (Figure 13C). To better identify these internalized cells, we conducted immunostaining for the neutrophil marker Ly6G. About 86% of the cells within the TPO/IL-1α cultured MK cytoplasm tested positive for Ly6G (Figure **13D**). We also examined whether emperipolesis influences the size and ploidy of MKs. When dividing the TPO/IL-1α MKs into emperipolesis-positive (containing Ly6G-positive cells) and emperipolesis-negative (lacking Ly6G staining in the cytoplasm) groups, we observed no significant differences in either MK size (Figure **13F**) or ploidy (Figure 13G). This suggests that the presence of neutrophils inside the MK cytoplasm does not impact their nuclear or cellular growth. Since whole BM cultures were used to differentiate MKs, we aimed to rule out the possibility that IL-1α stimulation caused proliferation of Ly6G+ cells, which could enhance their interaction with MKs and lead to increased emperipolesis. To do this, flow cytometry was performed on whole BM cultures stained for live Ly6G+ cells on days 1, 3, and 5. Results showed that in both cultures, the highest percentage of live Ly6G+ cells (about 27%) was on day 1, decreasing progressively until day 5 (Figure 13E). Notably, because the percentage of live Ly6G+ cells was around 7% on day 3 in both conditions, the greater level of emperipolesis in TPO/IL-1 α cultures could not be due to an increased neutrophil presence. Interestingly, on day 5, TPO/IL-1 α cultures had more Ly6G+ cells (3%) compared to TPO cultures (1.7%).

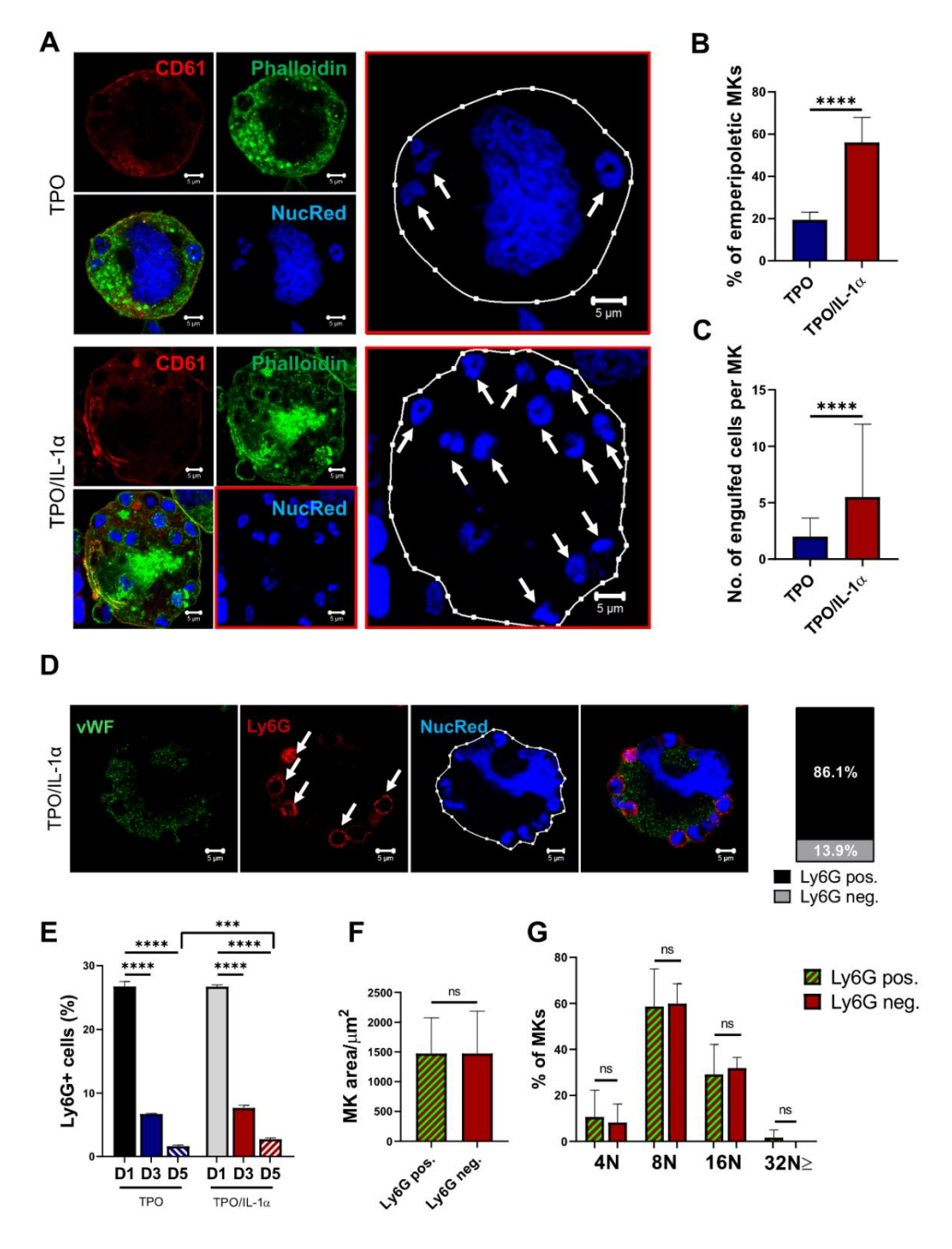


Figure 13. IL-1α induces emperipolesis in megakaryocytes *in vitro*.

(A) After day 3 of culture, following BSA gradient enrichment, MKs were fixed and immunostained for CD61, actin (using Phalloidin-Alexa Fluor 488), and counterstained with NucRed for nuclei. Imaging was performed with an LSM880 (Carl Zeiss) confocal microscope equipped with a Plan-Apochromat 63×/1.40 oil DIC III objective. The image shows the middle plane of the captured z-stack. Cells with more NucRed-positive nuclei were more abundant in IL-1α cultured MKs (indicated by white arrows). (B) MKs were counted and categorized into emperipoletic or non-emperipoletic groups based on the presence or absence of NucRed-positive structures in their cytoplasm. The percentages are shown in the graph. (C) The number of NucRed-positive structures (representing engulfed cells) was quantified in the emperipoletic MK population and displayed graphically. At least 20 MKs were analyzed and categorized based on the above criteria for each experimental condition. A minimum of seven independent experiments was performed. (D) MKs were stained for vWF, an MK marker, and Ly6G, a neutrophil marker, and engulfed cells were characterized by the presence or absence of Ly6G staining. (E) Whole BM cultures were harvested on days 1, 3, and 5 (D1, D3, D5). Cells were stained with viability dye eFluor™ 450 and Ly6G-FITC antibody, then analyzed using a BD FACSAria™ III cytometer (BD Biosciences). The graph shows the percentage of live Ly6G+ cells. Data are presented as means with error bars indicating ± SD from three independent biological replicates. **** p < 0.0001, ns – not significant

4.1.5. IL-1 α -stimulated terminally mature megakaryocytes normalize vWF expression and decrease the rate of emperipolesis

Culturing BM MKs with TPO *in vitro* for 3 days mainly produces immature MKs, whereas extended culture for up to 5 days results in mostly fully mature MKs. [177]. To extend our study to later time points, we examined the long-term effects of IL-1 α stimulation on terminally mature megakaryocytes (cultured for 5 days), focusing on maturation markers and emperipolesis. MKs treated with TPO/IL-1 α until day 5 had sizes comparable to those of TPO controls, with both conditions reaching approximately 2000 μ m² (**Figure 14A, B**). Additionally, the expression levels of vWF and GPIb β were similar to TPO controls. However, the lower band of vWF (representing vWF multimers of lower molecular weight) remained more prominent in TPO-MKs, as confirmed by Western blot analysis (**Figure 14C, D**).

Immunofluorescent staining and confocal microscopy analysis showed comparable MFI values for vWF and GPIb β , along with Western blot results for CD61 (**Figure 15A-D**). There were slightly higher MFI levels of other GPIb subunits, GPIb α and GPIX (**Figure 15E-H**). The modal ploidy of MKs in both conditions was 16N (**Figure 15I**), although a greater percentage of MKs with ploidy \geq 32N was still observed in IL-1 α MKs. Very few emperipoletic cells were seen on day 5, as indicated by the lack of Ly6G+ cells in the MK cytoplasm, supporting the transient nature of this process (**Figure 15J**).

Although the overall GPIb receptor expression normalized, flow cytometry of the entire BM cultures showed that, by day 5, TPO/IL-1 α cultures still had a significantly lower percentage of GPIb β +/CD61+ MKs compared to TPO cultures (**Figure 15K**).

These findings indicate that, despite $IL-1\alpha$ -cultured MKs reaching normalized protein expression levels of GPIb and vWF, they still remain distinct from MKs cultured with TPO.

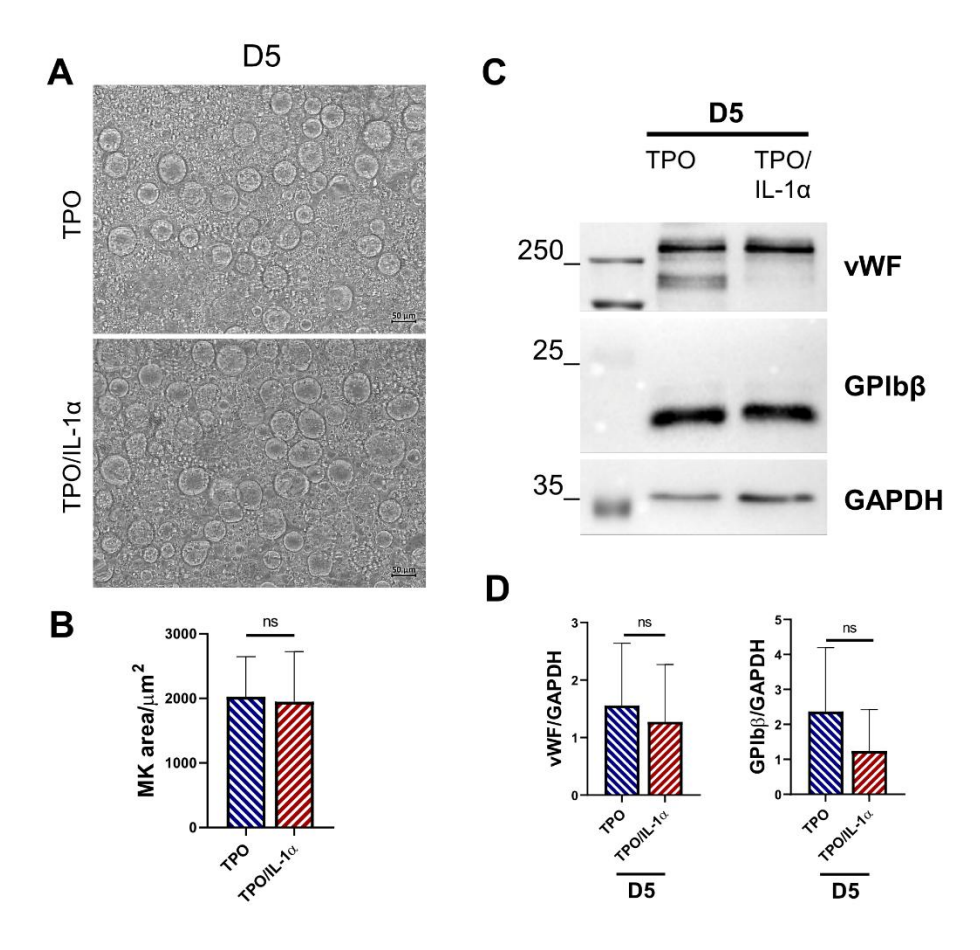


Figure 14. Characterization of megakaryocytes cultured with IL-1α until day 5.

(A) BM MKs were cultured with TPO or TPO/IL-1 α until day 5, as described in Methods. MKs were imaged under a 40x objective of the Axio Vert.A1 bright-field microscope (Carl Zeiss) while still in culture. (B) The surface area of MKs was measured, showing comparable sizes between both groups with no significant differences. MK size was analyzed from at least 50 MKs in a minimum of five different fields of vision across three independent experiments. (C) On day 5, BM MK lysates were collected, analyzed by SDS-PAGE, transferred to a nitrocellulose membrane, and incubated with specific antibodies. Representative immunoblots display the expression of vWF, GPIb β , and GAPDH proteins. (D) Protein levels were quantified using ImageJ, with results normalized to the GAPDH control. Data are presented as mean values, with error bars indicating \pm SD from three independent experiments. ns – non-significant.

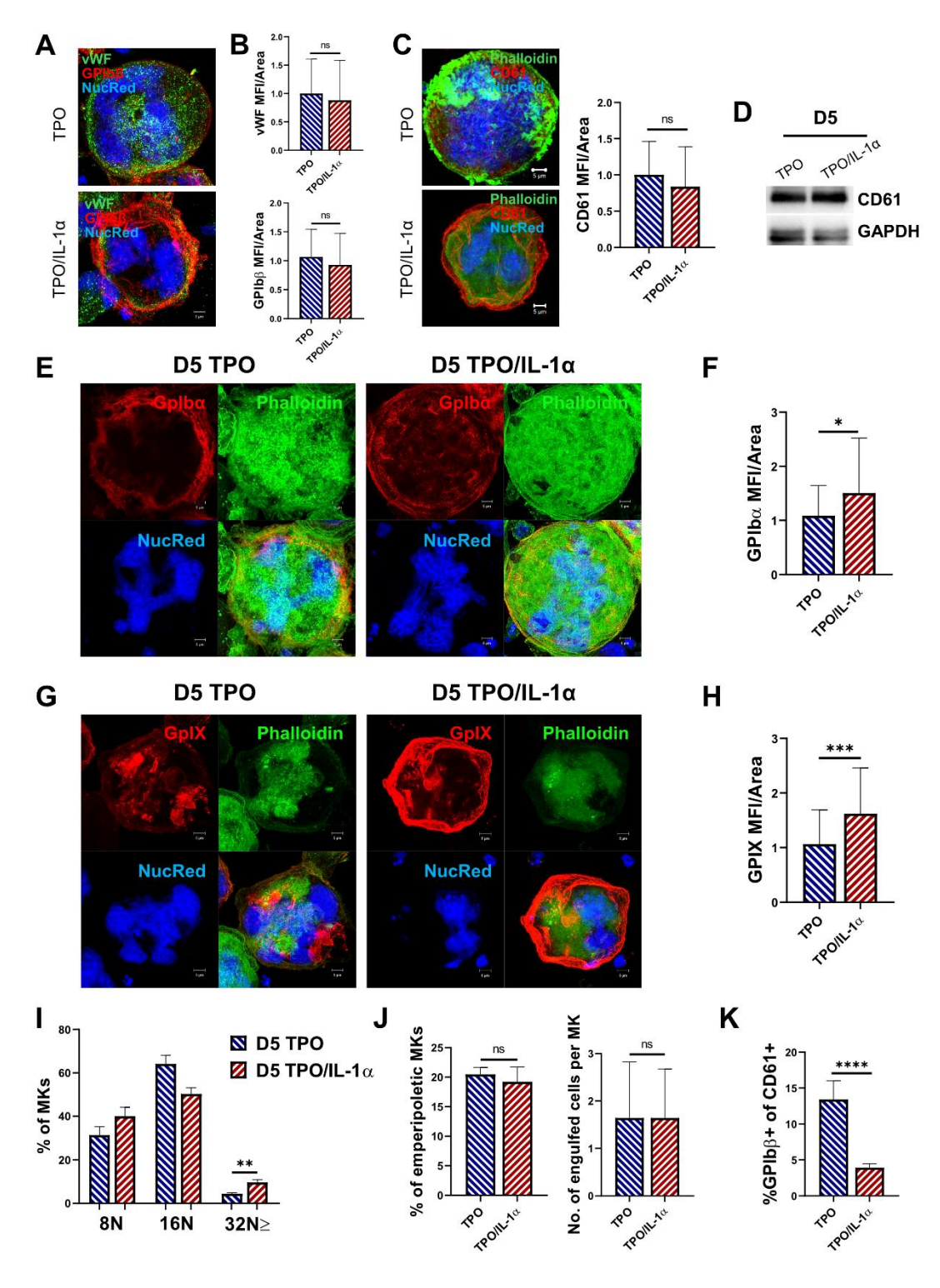


Figure 15. The localization and distribution of the GPIb receptor and CD61 in megakaryocytes cultured with IL-1 α until day 5.

BM MKs were grown in vitro as detailed in the Methods section until day 5. After enrichment via BSA gradient, MKs were fixed, then immunostained for (A) Gplbβ and VWF, (B) with their mean fluorescence intensity (MFI) per area quantified. Cells were imaged using an LSM880 Carl Zeiss confocal microscope equipped with a Plan-Apochromat 63×/1.40 oil DIC III objective and analyzed with Zeiss ZEN Black software to MFI. Representative maximum intensity projections are displayed. A minimum of 20 MKs were analyzed in each condition across four independent experiments. (C) MKs were stained for CD61 and F-actin (using Phalloidin Alexa Fluor-488), then imaged under the same confocal setup. The MFI of CD61 was measured and normalized per cell area, with maximum projections shown from three independent experiments. (D) Lysates from BM MKs collected on day 5 were subjected to SDS-PAGE under non-reducing conditions, and blotted for CD61 and GAPDH. Cells were also immunostained for (E, F) GPIba and (G, H) GPIX, alongside F-actin and NucRed, and imaged with the same confocal microscope. Representative maximum projections and corresponding MFI quantifications are presented per cell surface area. (I) MKs stained with NucRed were counted for nuclear lobes, multiplied by two to determine ploidy, with results displayed as a distribution graph. (J) MKs were sorted into emperipoletic and non-emperipoletic groups based on NucRed-positive structures, with the percentage of emperipoletic MKs plotted and the number of nuclear structures counted. (K) At day 5, whole BM cultures were stained with CD61-PE and GPIbβ-FITC, then analyzed by flow cytometry. The data show the percentage of GPIbβ+ cells among CD61+ MKs. Data are expressed as mean ± SD from a minimum of three biological replicates. Significance levels: * p<0.05, ** p<0.01, *** p<0.001, **** p<0.0001, ns - not significant.

4.1.6. IL-1 α -mediated megakaryopoiesis results in specific changes in the proteomic signature of megakaryocytes

After establishing that the altered maturation phenotype following IL-1 α stimulation results in a reduced hemostatic capacity of early MKs, yet still exhibits high ploidy and interacts with neutrophils, we aimed to explore this further through proteomic analysis. We cultured BM MKs with TPO or TPO/IL-1 α , then isolated them on days 3 and 5 for LC-MS/MS-based proteomics. We identified and quantified a total of 6301 proteins on day 3 and 5670 on day 5.

To evaluate variability in the proteomic data and identify distinct clustering patterns between TPO and TPO/IL-1 α MK populations at day 3, we conducted principal component analysis (PCA) (**Figure 16A**). PCA is a dimensionality reduction technique that transforms high-dimensional data into a smaller number of uncorrelated variables, known as principal components, which capture the most variance in the data. PCA revealed a clear separation between the two groups, with PC1 accounting for 30.56% of the total variance and PC2 accounting for 17.94%, indicating distinct proteome profiles (**Figure 16A**). Student's t-test identified proteins that were significantly differentially abundant between TPO and TPO/IL-1 α -stimulated MKs. A total of 215 proteins were significantly upregulated in TPO MKs after 3 days, while 43 proteins were significantly upregulated in TPO/IL-1 α (q-value < 0.05, fold change > 1.5) (**Figure 16C**). Consistent with these results, we confirmed early findings that vWF and GPIb β were more abundant in TPO-cultured MKs compared to those cultured with IL-1 α (**Figure 16B**), although the abundance of

GPIb β did not meet the statistical significance cutoff. Additionally, other hemostasis-related receptors such as GPIb α , GPIX, CD61 (previously observed by iimunofluorescence), and P-selectin showed higher abundance in TPO-cultured MKs.

To investigate the biological significance of the differentially expressed proteins, we conducted a REACTOME pathway analysis that identified significantly enriched gene sets (FDR < 0.05) in both experimental groups (**Figure 16D**). The most notably enriched process between TPO and TPO/IL-1a MKs was "neutrophil degranulation," followed by pathways involved in platelet functions such as degranulation, activation, signaling, and aggregation, as well as antimicrobial peptides (AMPs) and hemostasis, supporting earlier hypotheses (**Figure 16D**). A heatmap of the top 50 regulated proteins emphasized the enrichment of neutrophil-related proteins and AMPs in IL-1 α MKs (**Figure 16E**). Importantly, proteins like CXCL5, lactoferrin (Ltf), cathelicidin antimicrobial peptide (Camp), S100 calcium-binding protein A9 (S100a9), lipocalin-2 (Lcn2), and peptidoglycan recognition protein 1 (Pglyrp1) were among the top 50 significantly upregulated (**Figure 16E**, also marked in **Figure 16C**).

PCA demonstrated distinct proteome differences between TPO and TPO/IL-1α MKs also on day 5 (Figure 16F), where 165 proteins were significantly upregulated in TPO MKs. In comparison, 131 proteins were upregulated in TPO/IL-1α MKs (q-value < 0.05, Fold change > 1.5). At day 5, MKs showed only a few emperipoletic cells within the cytoplasm of IL-1α-cultured MKs, indicating a normal or low level of emperipolesis, similar to TPO MKs (Figure 15J). The most regulated pathways in MKs at day 5 involved neutrophil degranulation, extracellular matrix organization, collagen interactions, and hemostasis (Figure 18A). The difference in specific neutrophil marker protein abundance between TPO and TPO/IL-1α MKs after 3 and 5 days remained consistent for most relevant proteins, including CXCL5, Ltf, Lcn2, Camp, and S100a9 (Figure 16G, upper right quadrant). Additionally, S100a8, which is thought to be constitutively expressed in neutrophils and monocytes, along with neutrophilic cytosol factor 1 (Ncf1), was found at higher levels in IL-1α-treated cells after 5 days, but not after 3 days (Figure 16G, upper middle quadrant). Another protein exhibiting similar patterns was β1-tubulin (Tubb1), which had been previously identified as upregulated in FL MKs after IL-1α stimulation [51].

In addition to the high levels of neutrophil proteins and AMPs in IL-1α MKs, TPO-cultured MKs still exhibited elevated levels of specific hemostasis-related proteins on day 3 and 5 (**Figure 17, Figure 18A**) such as platelet glycoprotein 4 (CD36), GPV, which meet the fold-change criteria, P-selectin, GPVI, filamin A (FlnA), and vWF. These proteins exhibit significant differences in q-value, despite their smaller

fold-changes, which supports their physiological development (**Figure 18A, C**). Other hemostasis-related receptors, such as GPIb β , GPIX, and CD61, in IL-1 α -cultured MKs had levels that normalized or decreased compared to those in TPO-cultured MKs (in agreement with previously observed results by Western blot or immunofluorescence).

Overall, these findings suggest that IL-1 α influences the MK proteome during early maturation, promoting a high abundance of neutrophil-related proteins and AMPs. Moreover, the decreased emperipolesis on day 5, combined with a high content of neutrophil proteins and the absence of neutrophil cellular structures in MKs, may indicate protein transfer between MKs and neutrophils.

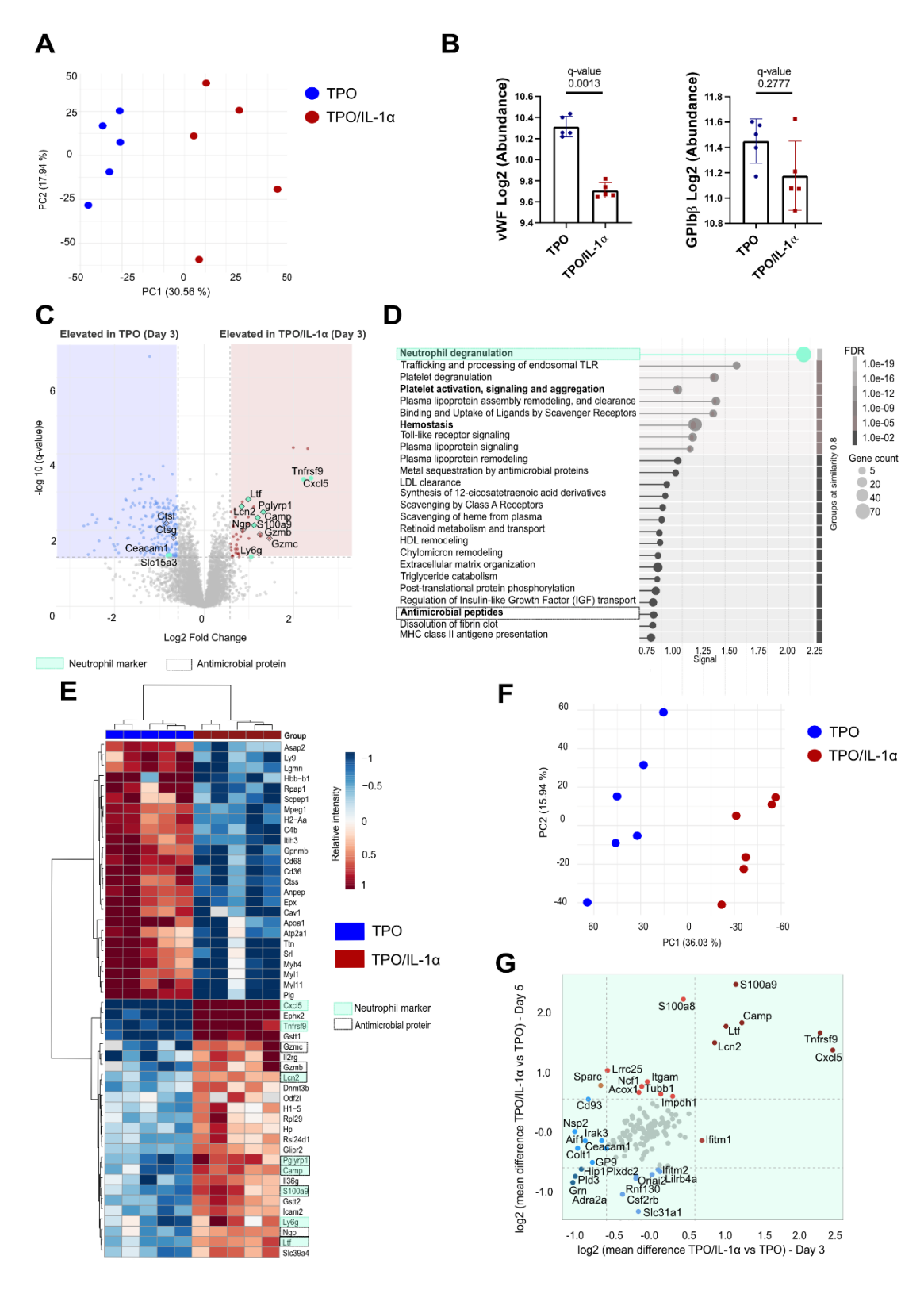


Figure 16. IL-1 α alters the megakaryocyte proteome and protein expression during early maturation.

(A) PCA analysis of 5173 proteins reveals proteome differences in day 3 BM MKs treated with TPO and TPO/IL-1 α . (B) Normalized levels of vWF and GPIbß proteins in TPO versus TPO/IL-1 α treated BM MKs after 3 days. (C) Volcano plot indicates significantly regulated proteins between TPO and IL-1 α -treated BM MKs after 3 days (q < 0.05; > 1.5-fold change). (D) Enriched murine REACTOME gene sets (FDR < 0.05) derived from all regulated proteins (q < 0.05; > 1.5-fold change). (E) Heatmap with hierarchical clustering of 50 significant proteins (q < 0.05) showing the highest fold change after 3 days. (F) PCA of day five BM MKs for TPO and TPO/IL-1 α using 5211 proteins. (G) Scatter plot depicting Log2 mean differences in protein levels between TPO and TPO/IL-1 α -treated BM MKs after 3 and 5 days. The proteomic dataset was generated from LC-MS/MS analysis of five independent biological replicates for each experimental condition on day 3 BM MKs and six independent biological replicates for each condition on day 5 BM MKs.

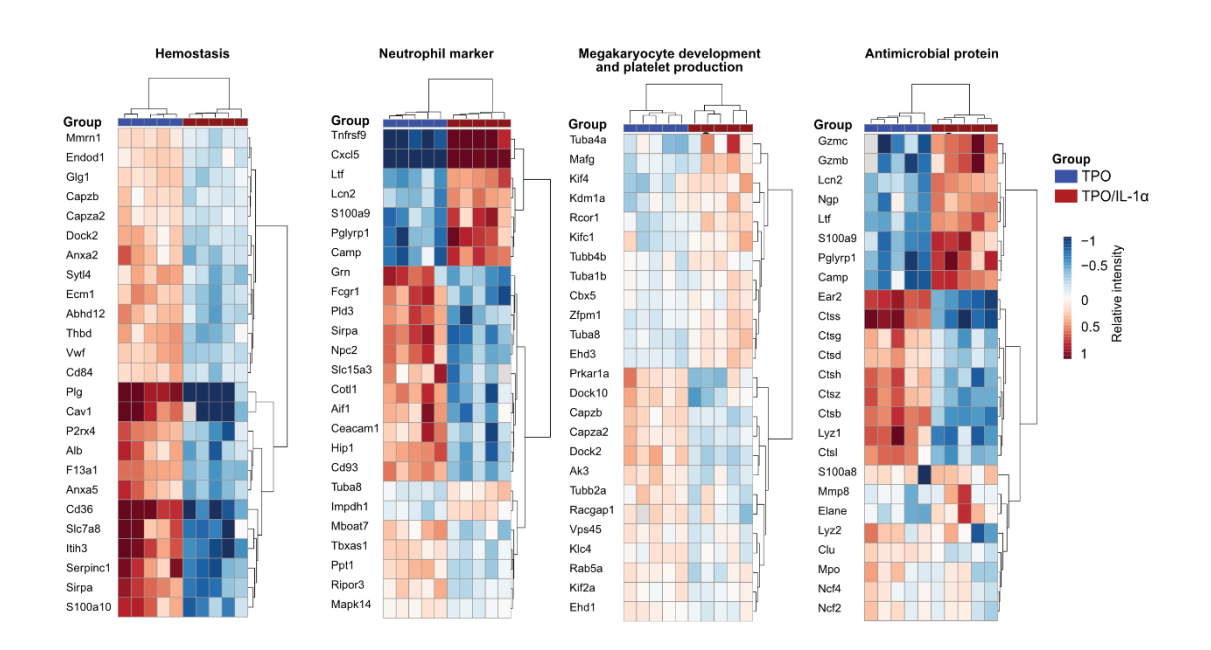


Figure 17. Heatmap of key proteins involved in hemostasis, immunity, and megakaryocyte development in immature megakaryocytes.

Hierarchical clustering based on Euclidean distance for the top 25 significant proteins (FDR < 0.05) comparing TPO and TPO/IL-1 α at day 3, linked to specific gene sets is shown here. Protein levels were normalized, log2-transformed, and centered around their mean across all samples. The proteomic dataset was generated from LC-MS/MS analysis of five independent biological replicates for each experimental condition on day 3 BM MKs.

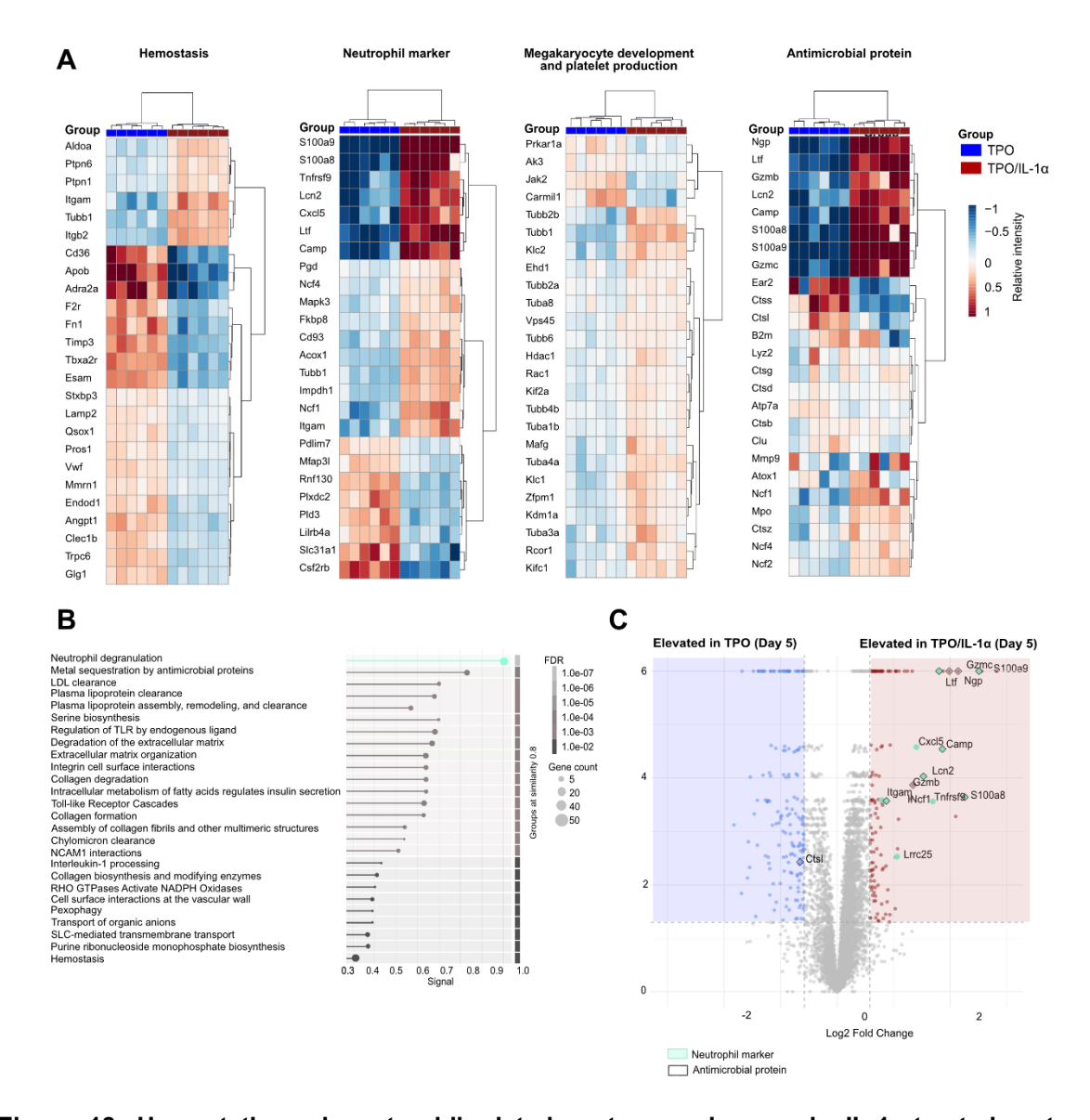


Figure 18. Hemostatic and neutrophil-related proteome changes in IL-1 α -treated mature megakaryocytes.

(A) Hierarchical clustering based on Euclidean distance for the top 25 significant proteins (FDR < 0.05) between TPO and TPO/IL-1a, linked to selected gene sets at day 5. Protein abundances are normalized, log2 transformed, and centered around the mean value across all samples. (B) Enriched murine REACTOME gene sets (FDR < 0.05) from regulated proteins in TPO and TPO/IL-1 α treated BM-MKs after 5 days (q-value < 0.05; difference >1.5-fold). (C) Volcano plot of significantly regulated proteins between TPO and TPO/IL-1 α -treated BM-MKs after 5 days (q-value < 0.05; difference > 1.5-fold change). The proteomic dataset was generated from LC-MS/MS analysis of six independent biological replicates for each condition on day 5 BM MKs.

4.2.INTERLEUKIN-1 ALPHA ENHANCES RIBOSOMAL AND NUCLEOLAR ACTIVITY DURING EARLY MEGAKARYOPOIESIS

Because MKs actively synthesize many proteins during their development, and taking into consideration the functional connections of nucleolar stress and inflammation, we aimed to investigate the effects of IL-1 α -mediated inflammatory insult on nucleolar activity and ribosomal biogenesis in MKs. We discovered that, in addition to an immune proteomic signature, IL-1 α -derived MKs are abundant in ribosomal and nucleolar proteins. Additionally, we found that IL-1 α stimulation results in an increased number of UBF foci, indicating higher nucleolar activity. Vps34 colocalizes with UBF and is found to increase alongside UBF in the nucleolus of IL-1 α -cultured MKs. Vps34 has already been proven crucial for normal MK development; however, we also found that it is essential during IL-1 α -mediated MK maturation, as the inhibition of Vps34 leads to growth arrest and nucleolar dispersion.

4.2.1. IL-1α-stimulated megakaryocytes display a trend-based increase in ribosomal protein abundance

We have shown that IL-1 α stimulation results in larger MKs (**Figure 8B**) with higher ploidy (**Figure 9D**). Given the increased size, cytoplasmic volume, and ploidy, we were interested in investigating the ribosomal and nucleolar proteins within the obtained proteomic data that could indicate translational capacity of IL-1 α MKs. To identify proteins with different abundance between TPO-only and IL-1 α -treated MKs, we used statistical filtering with q-value (< 0.05) to control false discovery rate, as in previous analysis. A fold change threshold (> 1.5; log2(fold change) > 0.6) was applied to define biologically relevant shifts. Although fold change thresholds serve as useful markers for identifying robust differences, biological systems can sometimes exhibit subtle but coordinated shifts in protein abundance, particularly within functionally connected groups such as ribosomal proteins. This was the case in our proteomic dataset, where we found many q-value-significant proteins (q-values are bold in red) exhibiting subtle fold changes in favour of their higher abundance in IL-1 α -cultured MKs at day 3 and 5 (**Table 12, 13**).

We generated volcano plots containing all detected proteins across our two experimental groups (TPO- and TPO/IL- 1α -cultured MKs on day 3) and highlighted 26 ribosomal proteins with differential abundance, listed in **Table 12**. All 26 displayed positive log2 fold changes, indicating higher abundance in IL- 1α -treated MKs (**Figure 19A**). Among them, three proteins (RsI24d1, RpI35, RpI29) surpassed the fold change threshold and were labelled directly on the plot (**Figure 19A**, listed in

orange in **Table 12.**). Of the 26 ribosomal proteins, 16 belong to the large ribosomal subunit, including Rpl35 and Rpl29.

A similar analysis was performed on mature MKs (TPO- and TPO/IL-1 α -cultured MKs on day 5), identifying 93 ribosomal proteins with differential abundance, listed in **Table 13**. Only two proteins, Sbds and Mrps25, had negative log2 fold changes, suggesting higher abundance in TPO-only MKs. The remaining proteins were more abundant in IL-1 α MKs (**Figure 19B**). Proteins that passed both q-value and fold change criteria were Rpl34, Urb1, and Rrp7a, emphasized in the volcano plot (**Figure 19B**, listed in orange in **Table 13**.).

Taken together, these results suggest a consistent shift toward increased ribosomal protein abundance in IL-1 α -treated MKs, particularly pronounced in the mature stage. This trend may reflect enhanced ribosome biogenesis or/and elevated translational capacity in response to IL-1 α -driven megakaryopoiesis.

Table 12. List of q-value significant ribosomal proteins with higher abundance in TPO/IL-1α cultured MKs on day 3

Gene name	Protein description	q-value (IL-1α_TPO)	t-test difference (IL-1α_TPO)
Bop1	Ribosome biogenesis protein BOP1	0.002728744	0.354545116
Mrpl55	Large ribosomal subunit protein mL55	0.040867722	0.421187019
Rpl10	Large ribosomal subunit protein uL16	0.028440727	0.436653519
Rpl10a	Large ribosomal subunit protein uL1	0.014540131	0.22949543
Rpl13	Large ribosomal subunit protein eL13	0.025910881	0.557149887
Rpl15	Large ribosomal subunit protein eL15	0.048111995	0.487460518
Rpl17	Large ribosomal subunit protein uL22	0.027988277	0.354473114
Rpl26	Large ribosomal subunit protein uL24	0.019723694	0.384594345
Rpl27	Large ribosomal subunit protein eL27	0.045997684	0.313212776
Rpl29	Large ribosomal subunit protein eL29	0.041822525	0.758032227
Rpl3	Large ribosomal subunit protein uL3	0.014950584	0.348665619
Rpl32	Large ribosomal subunit protein eL32	0.030898152	0.369252777
Rpl35	Large ribosomal subunit protein uL29	0.03397035	0.605529022
Rpl39	Large ribosomal subunit protein eL39	0.030777705	0.532187462
RpI5	Large ribosomal subunit protein uL18	0.002448067	0.311250496
Rpl6	Large ribosomal subunit protein eL6	0.045951082	0.429566383
Rpl8	Large ribosomal subunit protein uL2	0.021037573	0.455053139
Rps10	Small ribosomal subunit protein eS10	0.01455409	0.240517807
Rps14	Small ribosomal subunit protein uS11	0.012981066	0.364691925
Rps24	Small ribosomal subunit protein eS24	0.046501361	0.576686478

Rps26	Small ribosomal subunit protein eS26	0.044309961	0.511966705
Rps27I	Small ribosomal subunit protein eS27-like	0.0463527	0.353211021
Rps6	Small ribosomal subunit protein eS6	0.016539597	0.486247063
Rps7	Small ribosomal subunit protein eS7	0.045162217	0.33293705
Rrs1	Ribosome biogenesis regulatory protein homolog	0.007340539	0.560053539
Rsl24d1	Probable ribosome biogenesis protein RLP24	0.01110271	0.858288288

Positive q-values indicate higher differential abundance in TPO/IL-1 α cultured MKs on day 3 of culture. Listed in **red** are q-values for proteins satisfying the < 0.05 criteria. Listed in **orange** are log2 fold change values for proteins satisfying the >0.6 criteria.

Table 13. List of q-value significant ribosomal proteins with higher abundance in TPO/IL-1 α cultured MKs on day 5

Gene name	Protein description	q-value (IL-1α_TPO)	t-test difference (IL-1α_TPO)
Bop1	Ribosome biogenesis protein BOP1	0.002642512	0.307711999
Dap3	Small ribosomal subunit protein mS29	0.043600394	0.079066594
Gadd45gip1	Large ribosomal subunit protein mL64	0.016747541	0.286754449
Gfm2	Ribosome-releasing factor 2, mitochondrial	0.006070796	0.284424941
Mrpl11	Large ribosomal subunit protein uL11m	8.00E-05	0.270339171
Mrpl14	Large ribosomal subunit protein uL14m	0.004290389	0.300316175
Mrpl15	Large ribosomal subunit protein uL15m	0.001635294	0.329685291
Mrpl17	Large ribosomal subunit protein bL17m	0.048154139	0.303806067
Mrpl18	Large ribosomal subunit protein uL18m	0.018811285	0.280708392
Mrpl2	Large ribosomal subunit protein uL2m	0.005087041	0.264343659
Mrpl21	Large ribosomal subunit protein bL21m	0.04111359	0.156206449
Mrpl28	Large ribosomal subunit protein bL28m	0.004593035	0.211070935
Mrpl3	Large ribosomal subunit protein uL3m	0.011321429	0.426554759
Mrpl34	Large ribosomal subunit protein bL34m	0.002040377	0.478810946
Mrpl38	Large ribosomal subunit protein mL38	0.000254682	0.324938615
Mrpl39	Large ribosomal subunit protein mL39	0.032413719	0.193398078
Mrpl41	Large ribosomal subunit protein mL41	0.00386906	0.206439336
Mrpl45	Large ribosomal subunit protein mL45	0.01809341	0.509268761
Mrpl46	Large ribosomal subunit protein mL46	0.004461847	0.567153772
Mrpl49	Large ribosomal subunit protein mL49	0.048461248	0.229958455
Mrpl53	Large ribosomal subunit protein mL53	0.000259386	0.362949212
Mrpl57	Large ribosomal subunit protein mL63	0.033889597	0.353161414
Mrpl58	Large ribosomal subunit protein mL62	8.16E-05	0.289176146
Mrpl9	Large ribosomal subunit protein bL9m	0.002685851	0.274793625

Mrps16	Small ribosomal subunit protein bS16m	0.001066667	0.460805416
Mrps24	Small ribosomal subunit protein uS3m	0.024180539	0.27717638
Mrps25	Small ribosomal subunit protein mS25	0.041362304	-0.33962265
Mrps26	Small ribosomal subunit protein mS26	0.015050616	0.16106685
Mrps34	Small ribosomal subunit protein mS34	0.045189714	0.113025904
Mrps35	Small ribosomal subunit protein mS35	0.007386935	0.27302599
Mrps7	Small ribosomal subunit protein uS7m	0.00236272	0.290270567
Mrps9	Small ribosomal subunit protein uS9m	0.005358209	0.192311843
Nsa2	Ribosome biogenesis protein NSA2 homolog	0.047095785	0.267594814
Rack1	Small ribosomal subunit protein RACK1	0.034017999	0.099711418
Rpf2	Ribosome production factor 2 homolog	0.04452123	0.207407633
Rpl11	Large ribosomal subunit protein uL5	0.000273616	0.284265359
Rpl12	Large ribosomal subunit protein uL11	0.000570093	0.220148087
Rpl13	Large ribosomal subunit protein eL13	0.00039759	0.38357687
Rpl13a	Large ribosomal subunit protein uL13	0.022979079	0.189720631
Rpl14	Large ribosomal subunit protein eL14	0.00193956	0.288994789
Rpl18a	Large ribosomal subunit protein eL20	0.001382946	0.375555197
Rpl19	Large ribosomal subunit protein eL19	0.001081967	0.268167337
Rpl21	Large ribosomal subunit protein eL21	0.001942228	0.306814512
Rpl23	Large ribosomal subunit protein uL14	0.000260536	0.368745327
Rpl23a	Large ribosomal subunit protein uL23	0.001049069	0.267149448
Rpl24	Large ribosomal subunit protein eL24	0.037032659	0.151048501
Rpl26	Large ribosomal subunit protein uL24	0.02732169	0.070533593
Rpl27a	Large ribosomal subunit protein uL15	0.044045098	0.346210162
Rpl28	Large ribosomal subunit protein eL28	0.00143951	0.347738107
Rpl3	Large ribosomal subunit protein uL3	0.002912485	0.160173098
Rpl30	Large ribosomal subunit protein eL30	8.42E-05	0.347829819
Rpl31	Large ribosomal subunit protein eL31	0.001419753	0.516712825
Rpl32	Large ribosomal subunit protein eL32	0.018246992	0.454571247
Rpl34	Large ribosomal subunit protein eL34	0.003856085	0.604993661
Rpl35	Large ribosomal subunit protein uL29	0.028764219	0.223680337
Rpl35a	Large ribosomal subunit protein eL33	0.026012651	0.43432951
Rpl37a	Large ribosomal subunit protein eL43	0.004894942	0.348642826
Rpl38	Large ribosomal subunit protein eL38	0.000753036	0.383339723
Rpl4	Large ribosomal subunit protein uL4	0.002644068	0.228143215
RpI5	Large ribosomal subunit protein uL18	0.040130546	0.1014479
Rpl7a	Large ribosomal subunit protein eL8	0.00510704	0.254569689
Rpl7l1	Large ribosomal subunit protein uL30-like 1	0.005247148	0.389089346
Rpl8	Large ribosomal subunit protein uL2	0.032581507	0.124176025

Rplp0	Large ribosomal subunit protein uL10	0.000465608	0.22947979
Rps10	Small ribosomal subunit protein eS10	0.010198309	0.215479056
Rps11	Small ribosomal subunit protein uS17	0.000745491	0.343710899
Rps13	Small ribosomal subunit protein uS15	0.000291139	0.468662103
Rps15a	Small ribosomal subunit protein uS8	0.028147404	0.15983359
Rps16	Small ribosomal subunit protein uS9	0.000731006	0.347004096
Rps17	Small ribosomal subunit protein eS17	0.018662461	0.219990095
Rps18	Small ribosomal subunit protein uS13	0.004357724	0.1989247
Rps19	Small ribosomal subunit protein eS19	0.000430939	0.355285327
Rps2	Small ribosomal subunit protein uS5	0.000758893	0.330819925
Rps20	Small ribosomal subunit protein uS10	8.51E-05	0.410146713
Rps23	Small ribosomal subunit protein uS12	0.005380465	0.327730179
Rps25	Small ribosomal subunit protein eS25	0.000617391	0.389801979
Rps26	Small ribosomal subunit protein eS26	0.023457788	0.464748224
Rps28	Small ribosomal subunit protein eS28	0.001972603	0.360473156
Rps3	Small ribosomal subunit protein uS3	0.001530643	0.239141305
Rps3a	Small ribosomal subunit protein eS1	0.000555024	0.353625774
Rps4x	Small ribosomal subunit protein eS4	0.002246506	0.268473625
Rps5	Small ribosomal subunit protein uS7	0	0.418534597
Rps6	Small ribosomal subunit protein eS6	0.020103704	0.18794028
Rps7	Small ribosomal subunit protein eS7	0.002775801	0.321369966
Rps8	Small ribosomal subunit protein eS8	0.012354136	0.239004453
Rps9	Small ribosomal subunit protein uS4	0.001905556	0.294075966
Rpsa	Small ribosomal subunit protein uS2	0.005527675	0.201946259
Rrp1b	Ribosomal RNA processing protein 1 homolog B	0.006046181	0.447003444
Rrp7a	Ribosomal RNA-processing protein 7 homolog A	0.03512	0.715787172
Rrs1	Ribosome biogenesis regulatory protein homolog	0.005283019	0.363188505
RsI1d1	Ribosomal L1 domain-containing protein 1	0.000951351	0.413763841
Sbds	Ribosome maturation protein SBDS	0.003068927	-0.13729461
Urb1	Nucleolar pre-ribosomal-associated protein 1	0.00517195	0.634692589

Positive q-values indicate higher differential abundance in TPO/IL-1 α cultured MKs on day 5 of culture. Listed in **red** are q-values for proteins satisfying the < 0.05 criteria. Listed in **orange** are log2 fold change values for proteins satisfying the > 0.6 criteria. Negative fold change values indicate that the protein is more abundant in TPO cultured MKs.

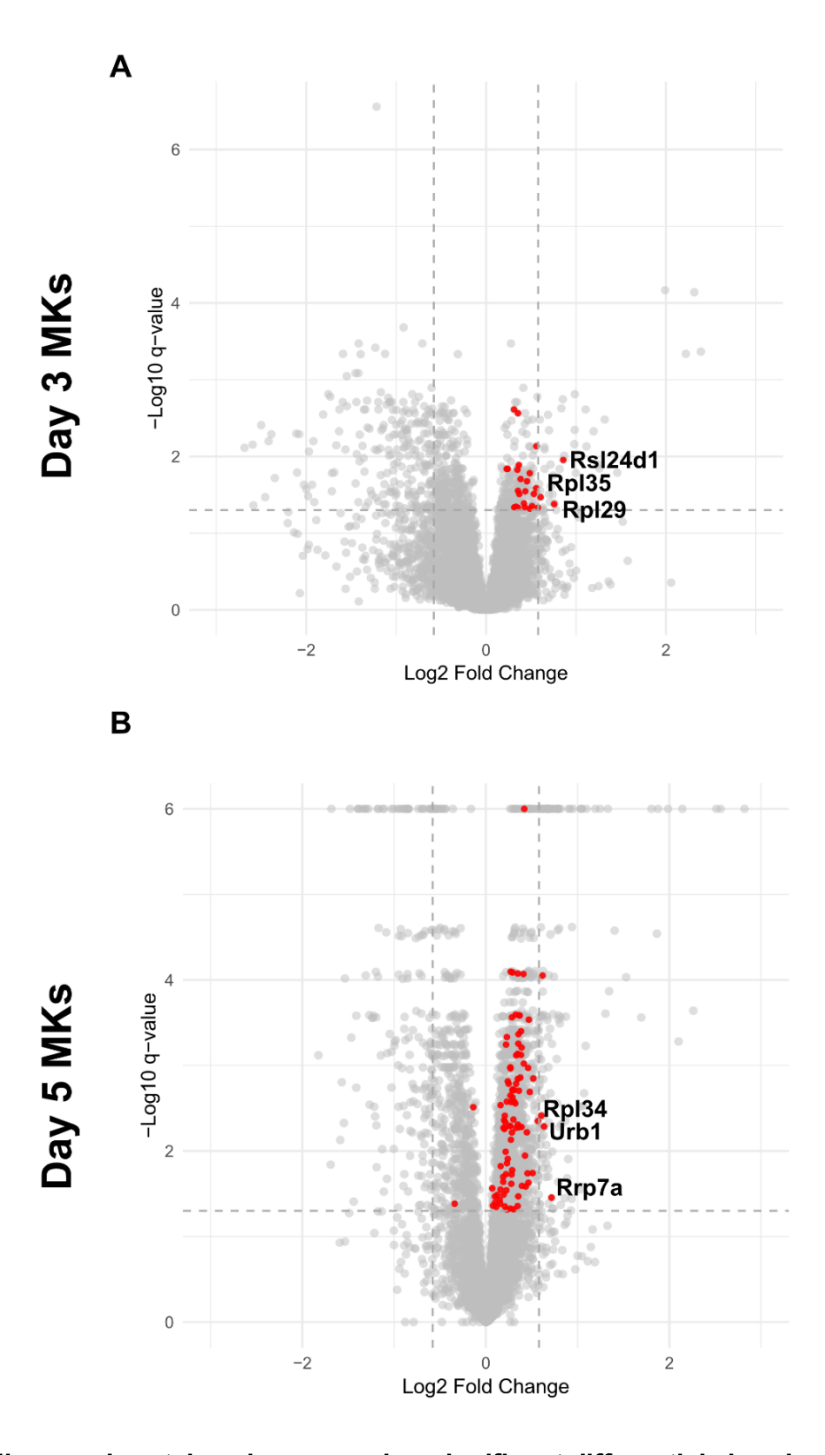


Figure 19. Ribosomal proteins show a q-value-significant differential abundance in IL-1α MKs.

(A) Volcano plot showing log2 fold changes versus -log10 q-values for proteins quantified in immature MKs (day 3). Ribosomal proteins are highlighted, with those passing both q-value (< 0.05) and fold change (> 1.5) thresholds marked in bold and labelled. (B) A volcano plot displaying log2 fold changes against -log10 q-values for proteins quantified in mature MKs (day 5). Ribosomal proteins are highlighted, with those satisfying both q-value (< 0.05) and fold change (> 1.5) thresholds marked in bold and labelled.

4.2.2. IL-1α-stimulated megakaryocytes exhibit modest abundance of nucleolar proteins

Given that cellular translational capacity depends on ribosomal machinery and that ribosome biogenesis is tightly linked to nucleolar function, we next examined the abundance of nucleolar proteins and proteins associated with nucleolar activity in IL- 1α -stimulated MKs. We used the same proteomic dataset and reproduced our q-value (< 0.05) and fold-change thresholds (> 1.5; log2(fold change) > 0.6), as above. To guide our analysis, we used a previously published reference describing functionally important nucleolar proteins [180]. By cross-referencing this list with our proteomic dataset, we identified and extracted 61 nucleolar proteins detected in our day 3 MK samples (**Table 14**, **Figure 20A**). Out of 61 proteins, 13 were significantly more abundant in IL- 1α MKs as evidenced by their q-values (**Table 14**, marked bold in red), while 51 of them had positive fold-change values, further supporting their abundance in IL- 1α MKs. Among the nucleolar proteins detected in immature MKs, Noc3l stood out, as it passed both the q-value and fold change thresholds, indicating significantly higher abundance in IL- 1α -treated MKs (**Figure 20A**).

To explore whether the maturation status of MKs also shapes nucleolar protein abundance, we next investigated the same panel of 61 proteins in mature MKs (day 5, **Table 15**, **Figure 20B**). We identified 32 proteins with significant q-values, indicating their abundance in IL-1α MKs (**Table 15**, marked in bold red), and all of them exhibited a positive fold-change. However, some proteins previously identified in day 3 MKs were not detected in day 5 samples (Table 15, marked as "NaN"). Missing values in proteomic datasets are common and may result from low protein abundance or true biological absence. In our case, undetected nucleolar proteins in mature MKs could reflect reduced expression at later stages of development, although the overall higher number of abundant proteins in IL-1α MKs on day 5 may suggests enhanced nucleolar activity. In mature IL-1α-stimulated MKs, two nucleolar proteins (Nol8 and Urb1) showed differential abundance based on both statistical significance and fold change (Figure 20B). Functionally important nucleolar proteins (often used as markers), such as UBF (Ubtf) and B23 (Npm1), which we have characterized in detail using other methods in our next experiments and previously (Bertović et al., unpublished data), are also significantly more abundant in IL-1α MKs on day 3. The abundance of UBF persists on day 5, while the fold-change remains moderate.

Table 14. List of nucleolar and functionally related proteins identified in the day 3 MK proteome with corresponding q-values and fold changes (TPO/IL-1α vs. TPO)

Gene name	Protein description	q-value (IL-1α_TPO)	t-test difference (IL-1a_TPO)
Ep300	Histone acetyltransferase p300	0.752294331	0.094482994
Ddx21	Nucleolar RNA helicase 2	0.01601193	0.485241318
Fbl	rRNA 2'-O-methyltransferase fibrillarin	0.101562597	0.301403809
Gnl2	Nucleolar GTP-binding protein 2	0.298684914	0.198999882
lmp3	U3 small nucleolar ribonucleoprotein protein IMP3	0.8147062	0.071942806
lmp4	U3 small nucleolar ribonucleoprotein protein IMP4	0.217266092	0.173745728
Knop1	Lysine-rich nucleolar protein 1	0.52255	0.893850406
Lyar	Cell growth-regulating nucleolar protein	0.099248538	0.398365307
Mphosph10	U3 small nucleolar ribonucleoprotein protein MPP10	0.238426244	0.191981411
Ncl	Nucleolin	0.115414399	0.308007622
Nepro	Nucleolus and neural progenitor protein	0.705451802	0.21372215
Nifk Noc2l	MKI67 FHA domain-interacting nucleolar phosphoprotein Nucleolar complex protein 2 homolog	0.393566564 0.368101346	0.255862236 0.320966244
Noc3l	Nucleolar complex protein 3 homolog	0.012741635	0.718553543
Noc4l	Nucleolar complex protein 3 homolog	0.012741033	0.611133862
Nol10	Nucleolar protein 10	1	0.010403156
NoI10	Nucleolar protein 11	0.102865242	0.255552959
NoI12	Nucleolar protein 12	0.752881159	-0.177959919
NoI4I	Nucleolar protein 4-like	0.504903975	0.174304485
NoI6	Nucleolar protein 6	0.504903973	0.134185219
NoI7	Nucleolar protein 7	0.675995642	0.144307899
Nol8	Nucleolar protein 8	0.016275019	0.495849705
NoIc1	Nucleolar and coiled-body phosphoprotein 1	0.009679525	0.520320702
Nom1	Nucleolar MIF4G domain-containing protein 1	0.887115921	0.079571056
Nop14	Nucleolar protein 14	0.306910966	0.242160511
Nop16	Nucleolar protein 16	0.078321833	0.286071301
Nop56	Nucleolar protein 56	0.099488683	0.262959671
Nop58	Nucleolar protein 58	0.186368915	0.193222427
Nop9	Nucleolar protein 9	0.169628266	0.412354946
Npm1	Nucleophosmin	0.02424793	0.42359581
Nusap1	Nucleolar and spindle-associated protein 1	1	0.009452415
Pml	Protein PML	0.025910881	-0.301905632
Polr1g	DNA-directed RNA polymerase I subunit RPA34	0.005122778	0.45043726

	DNA-directed RNA polymerase I subunit		
Polr1h	RPA12	0.040502282	0.513595676
	DNA-directed RNA polymerases I, II, and III		
Polr2h	subunit RPABC3	0.484128956	-0.426909065
Pram1	PML-RARA-regulated adapter molecule 1	0.17548835	0.850159681
Rad51ap1	RAD51-associated protein 1	0.118620807	-0.602935934
-	Replication protein A 70 kDa DNA-binding		
Rpa1	subunit	0.217448659	0.180926514
Rpa2	Replication protein A 32 kDa subunit	0.257296062	0.217364597
Rpap1	RNA polymerase II-associated protein 1	0.004707032	-1.633804131
Rrp9	U3 small nucleolar RNA-interacting protein 2	0.400190842	0.174557781
Ruvbl1	RuvB-like 1	0.03786732	0.298216248
	Structural maintenance of chromosomes		
Smc1a	protein 1A	0.049306609	0.185341263
Snrpa	U1 small nuclear ribonucleoprotein A	0.309313027	0.139921951
Snrpa1	U2 small nuclear ribonucleoprotein A'	0.85362812	0.059340477
Srp9	Signal recognition particle 9 kDa protein	0.557133934	-0.142769146
Srp14	Signal recognition particle 14 kDa protein	0.796494733	0.066659164
Srp19	Signal recognition particle 19 kDa protein	0.997388484	-0.012814045
Srp54	Signal recognition particle subunit SRP54	0.47733729	0.093083382
	Signal recognition particle receptor subunit		
Srpra	alpha	0.12416042	0.274899769
	Signal recognition particle receptor subunit		
Srprb	beta	0.609910141	0.103248215
Tial1	Nucleolysin TIAR	0.735972269	-0.067841816
Ubtf	Nucleolar transcription factor 1	0.038404013	0.289357758
Urb1	Nucleolar pre-ribosomal-associated protein 1	0.354529753	0.269777489
	Probable U3 small nucleolar RNA-associated		
Utp11	protein 11	0.020189412	-0.137248611
	U3 small nucleolar RNA-associated protein	0.0400=====	
Utp14a	14 homolog A	0.819655823	-0.060380459
11645	U3 small nucleolar RNA-associated protein	0.440040700	0.007040040
Utp15	15 homolog	0.110019738	0.397816849
1.16m.4.0	U3 small nucleolar RNA-associated protein	0.0147000	0.056604054
Utp18	18 homolog	0.8147062	0.056631851
Htn2F	U3 small nucleolar RNA-associated protein 25 homolog	0.421682501	0.265876484
Utp25	0	0.421002001	0.203070404
Utp4	U3 small nucleolar RNA-associated protein 4 homolog	0.372291346	0.148681927
Otp4	U3 small nucleolar RNA-associated protein 6	0.312231340	0.140001821
Utp6	homolog	0.355390027	0.314050102
	Honolog		

Positive q-values indicate higher differential abundance in TPO/IL-1 α cultured MKs on day 3 of culture. Listed in **red** are q-values for proteins satisfying the < 0.05 criteria. Listed in **orange** are log2 fold change values for proteins satisfying the > 0.6 criteria. Negative fold change values indicate that the protein is more abundant in TPO cultured MKs.

Table 15. List of nucleolar and functionally related proteins identified in the day 5 MK proteome with corresponding q-values and fold changes (TPO/IL- 1α vs. TPO)

Gene name	Protein description	q-value (IL-1α_TPO)	t-test difference (IL-1α_TPO)
Ep300	Histone acetyltransferase p300	0.012298028	0.431482871
Ddx21	Nucleolar RNA helicase 2	0.058613738	0.177633286
Fbl	rRNA 2'-O-methyltransferase fibrillarin	0.002510379	0.193180561
Gnl2	Nucleolar GTP-binding protein 2	0.678432888	0.050647179
lmp3	U3 small nucleolar ribonucleoprotein protein IMP3	0.001003584	0.300696294
lmp4	U3 small nucleolar ribonucleoprotein protein IMP4	0.004466332	0.374860048
Knop1	Lysine-rich nucleolar protein 1	NaN	NaN
Lyar	Cell growth-regulating nucleolar protein	0.57418626	0.040751775
Mphosph10	U3 small nucleolar ribonucleoprotein protein MPP10	0.001967213	0.52750047
Ncl	Nucleolin	0.006464471	0.273182074
Nepro	Nucleolus and neural progenitor protein	NaN	NaN
Nifk	MKI67 FHA domain-interacting nucleolar phosphoprotein	0.158810003	0.173386176
Noc2l	Nucleolar complex protein 2 homolog	0.00236409	0.320647955
Noc3l	Nucleolar complex protein 3 homolog	0.759746966	-0.051654975
Noc4l	Nucleolar complex protein 4 homolog	NaN	NaN
NoI10	Nucleolar protein 10	0.367168556	0.220349773
NoI11	Nucleolar protein 11	0.028555003	0.352760792
NoI12	Nucleolar protein 12	NaN	NaN
Nol4l	Nucleolar protein 4-like	0.136894069	0.504523039
NoI6	Nucleolar protein 6	0.000422764	0.395922105
NoI7	Nucleolar protein 7	0.003167604	0.326370557
Nol8	Nucleolar protein 8	0.000559036	0.720583836
NoIc1	Nucleolar and coiled-body phosphoprotein 1	0.00197551	0.432876428
Nom1	Nucleolar MIF4G domain-containing protein 1	NaN	NaN
Nop14	Nucleolar protein 14	0.004700297	0.367490768
Nop16	Nucleolar protein 16	0.443597068	0.141202211
Nop56	Nucleolar protein 56	0.02327381	0.204984506
Nop58	Nucleolar protein 58	0.955323974	-0.00576671
Nop9	Nucleolar protein 9	0.008211726	0.306316058
Npm1	Nucleophosmin	0.25050297	0.155445894
Nusap1	Nucleolar and spindle-associated protein 1	NaN	NaN
Pml	Protein PML	0.872914048	-0.01306502
Polr1g	DNA-directed RNA polymerase I subunit RPA34	0.910485401	0.017020623

	DNIA directed DNIA melymerates I subscrib		
Polr1h	DNA-directed RNA polymerase I subunit RPA12	NaN	NaN
FOILIU	DNA-directed RNA polymerases I, II, and III	INAIN	INAIN
Polr2h	subunit RPABC3	0.008479871	-0.46757706
Pram1	PML-RARA-regulated adapter molecule 1	NaN	NaN
Rad51ap1	RAD51-associated protein 1	NaN	NaN
Rausiapi	Replication protein A 70 kDa DNA-binding	INAIN	ivaiv
Rpa1	subunit	0.000138528	0.457569043
Rpa1	Replication protein A 32 kDa subunit	0.000138328	0.383557161
Rpap1	RNA polymerase II-associated protein 1	NaN	0.303337 101 NaN
Rrp9	U3 small nucleolar RNA-interacting protein 2	0.000389381	0.325900237
	RuvB-like 1		
Ruvbl1	1.12.2	0.00240796	0.1648043
Cma1a	Structural maintenance of chromosomes	0.404407607	0.047740757
Smc1a	protein 1A	0.404407687	0.047713757
Snrpa	U1 small nuclear ribonucleoprotein A	0.022989247	0.185125192
Snrpa1	U2 small nuclear ribonucleoprotein A'	0	0.42803208
Srp9	Signal recognition particle 9 kDa protein	NaN	NaN
Srp14	Signal recognition particle 14 kDa protein	0.000781955	0.355186701
Srp19	Signal recognition particle 19 kDa protein	0.036023001	0.212783813
Srp54	Signal recognition particle subunit SRP54	0.001586924	0.196786722
	Signal recognition particle receptor subunit		
Srpra	alpha	0.016016064	0.258497397
	Signal recognition particle receptor subunit		
Srprb	beta	0.000752852	0.186782837
Tial1	Nucleolysin TIAR	0.005289225	0.145004114
Ubtf	Nucleolar transcription factor 1	0.005543796	0.277607282
Urb1	Nucleolar pre-ribosomal-associated protein 1	0.00517195	0.634692589
	Probable U3 small nucleolar RNA-associated		
Utp11	protein 11	0.112862056	0.331420978
	U3 small nucleolar RNA-associated protein		
Utp14a	14 homolog A	0.003350993	0.272215128
	U3 small nucleolar RNA-associated protein		
Utp15	15 homolog	0.139830451	0.166356405
-	U3 small nucleolar RNA-associated protein		
Utp18	18 homolog	0.756088552	-0.031835953
-	U3 small nucleolar RNA-associated protein		
Utp25	25 homolog	NaN	NaN
	U3 small nucleolar RNA-associated protein 4		
Utp4	homolog	0.048519603	0.348012288
•	U3 small nucleolar RNA-associated protein 6		
Utp6	homolog	0.117138517	0.231106122
	J		

Positive q-values indicate higher differential abundance in TPO/IL-1 α cultured MKs on day 5 of culture. Listed in **red** are q-values for proteins satisfying the < 0.05 criteria. Listed in **orange** are log2 fold change values for proteins satisfying the > 0.6 criteria. Negative fold change values indicate that the protein is more abundant in TPO cultured MKs. NaN indicates missing values.

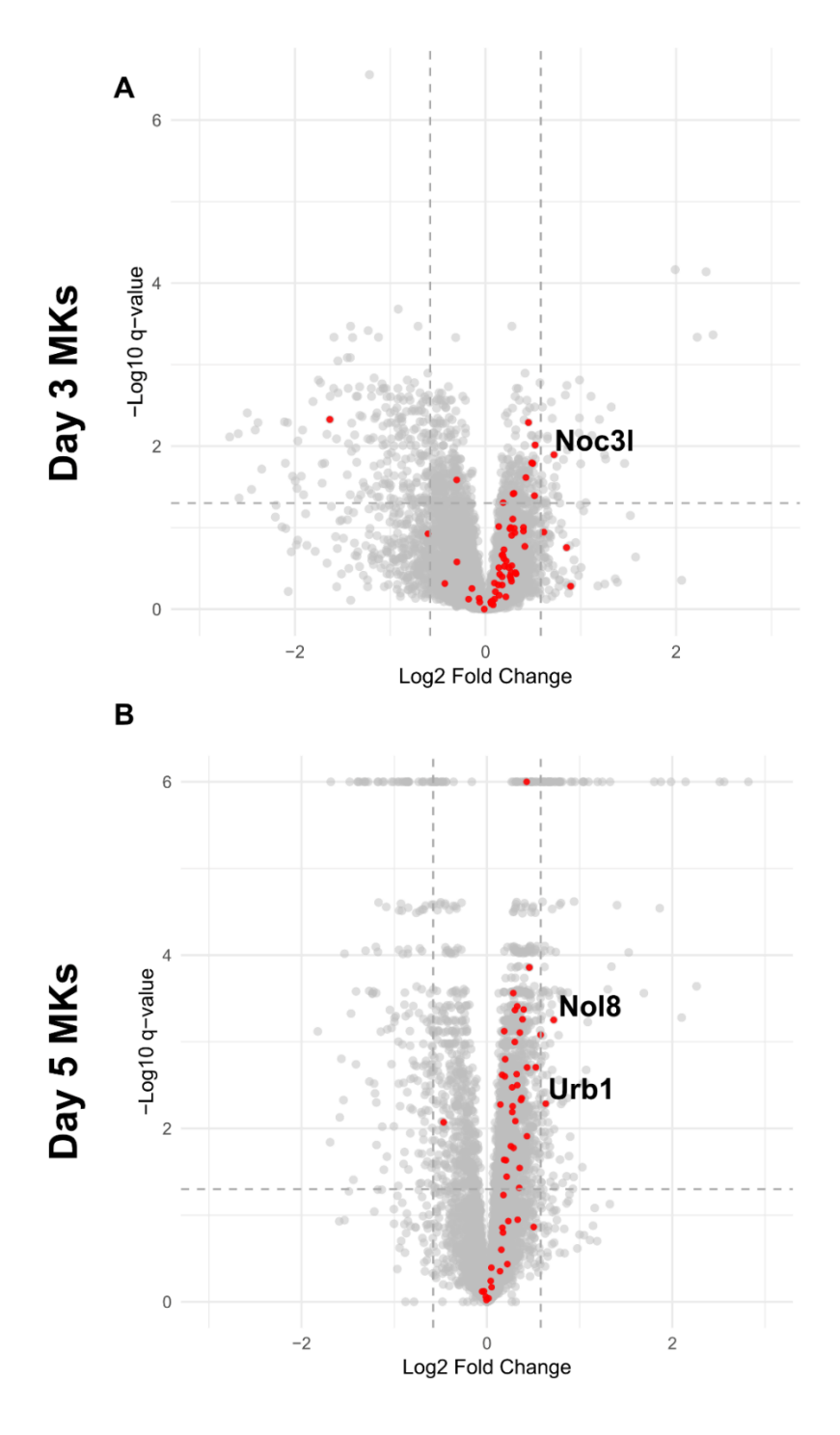


Figure 20. Nucleolar protein levels tend to increase in IL-1 α MKs.

(A) The volcano plot depicts log2 fold changes versus –log10 q-values for proteins measured in immature MKs (day 3). Nucleolar proteins are highlighted, with those meeting both q-value (< 0.05) and fold change (> 1.5) criteria shown in bold and labelled. **(B)** The volcano plot for mature MKs (day 5) displays log2 fold changes against –log10 q-values. Nucleolar proteins are highlighted, with those satisfying both thresholds marked in bold and labelled.

4.2.3. IL-1α increases the number of UBF and Vps34 foci in the nucleoli of megakaryocytes with a moderate effect on total UBF expression

Given the novel finding that nucleolar Vps34 potentially functions together with UBF and is important for early MK development, we wanted to explore this further by investigating how Vps34 responds to IL-1α stimuli and the consequences on the nucleolus. Previously, nucleolar hypertrophy was observed in cells under chronic inflammation [181]. Therefore, we used the same model of BM MKs that were cultured *in vitro* with TPO or TPO together with IL-1α for three days (as described in Methods), giving rise to mostly immature MKs in which the highest percentage of cells displayed visible nucleoli. We blotted BM MK lysates and found similar expression levels of Vps34 and nucleolar proteins, B23, and fibrillarin in TPOcultured and IL-1α-cultured MKs (Figure 21A). We observed a slight upward trend in UBF expression, consistent with the presented proteomic data; however, this difference was not statistically significant. UBF is targeted by signaling pathways that regulate its activity through posttranslational modifications, phosphorylation, affecting its transcriptional function [182]. Because of this, we sought to investigate the expression of the phosphorylated UBF (P-UBF). However, we found that its levels were relatively stable in IL-1α MKs compared to TPO controls (Figure 21B).

To assess nucleolar morphology and changes in UBF/Vps34 localization, we performed immunofluorescent staining and confocal imaging. Since IL-1 α stimulation is considered an inflammatory insult, we aimed to observe the hallmark of nucleolar stress, namely the disruption of B23 (nucleophosmin). Interestingly, immunostaining for B23 revealed its partial translocation to the nucleoplasm in around 45% of IL-1 α MKs, significantly higher than in TPO, where around 25% of MKs showed this phenotype (**Figure 22A**). To assess the degree of nucleolar disruption, we co-stained MKs with UBF in parallel with B23 and found that, despite B23 being present in the nucleoplasm, the nucleolar borders (marked by B23) were mostly intact (**Figure 22B**).

Vps34 localized within the boundaries of B23 (**Figure 22A**) but was also present within other regions of the nucleoplasm and appeared equally distributed within nucleoli in both MK populations. However, after immunostaining with UBF, we identified numerous UBF/Vps34 foci in the nuclei of IL-1 α MKs (**Figure 22C**), displaying a stronger signal throughout the nucleus. UBF and Vps34 visibly colocalized in over 60% of TPO MKs, with even higher colocalization in IL-1 α MKs, where more than 80% of cells displayed visible colocalization (**Figure 22D**). We also examined and quantified the degree of UBF/Vps34 colocalization and found significantly higher values of colocalization coefficient in IL-1 α MKs, indicating their

higher localization to the same compartment (**Figure 22E**). In addition to an increased cell population with visible UBF/Vps34 colocalization, IL-1 α MKs exhibited a significantly higher number of UBF and Vps34 foci, indicating additional fibrillar centers of the nucleoli (**Figure 22F**).

A higher number of UBF foci indicates higher nucleolar activity and increased rRNA transcription as a result of inflammatory stimuli. It is interesting that IL-1 α stimulation was accompanied by a stronger presence of Vps34 in the nucleolus, though the total expression of Vps34, as well as other nucleolar proteins, remained mostly unchanged.

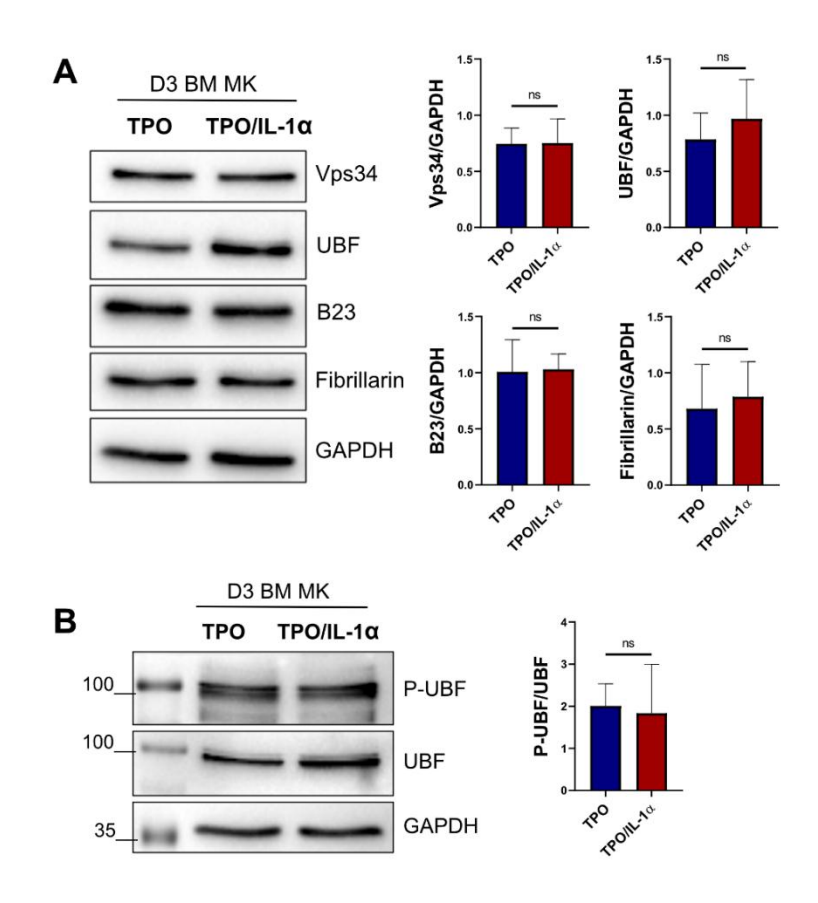


Figure 21. IL-1 α stimulation does not significantly alter nucleolar protein expression in megakaryocytes.

BM MKs were cultured for three days either with TPO or with TPO and IL-1α. MKs were enriched over a BSA gradient, lysed, and transferred to nitrocellulose membranes. They were then incubated with antibodies against the specified protein targets. (A) MKs cultured with IL-1α exhibit no significant changes in nucleolar protein expression, although UBF displays a slight upward trend. The graphs display quantified protein signal normalized over GAPDH in a minimum of eight independent experiments. (B) MKs were blotted for P-UBF to assess the phosphorylation status, but no significant differences were observed. The graphs display quantified protein signal normalized over GAPDH in

a minimum of three independent experiments. ImageJ was used for signal quantification. The graphs display data as means, with error bars indicating \pm SD. ns – not significant

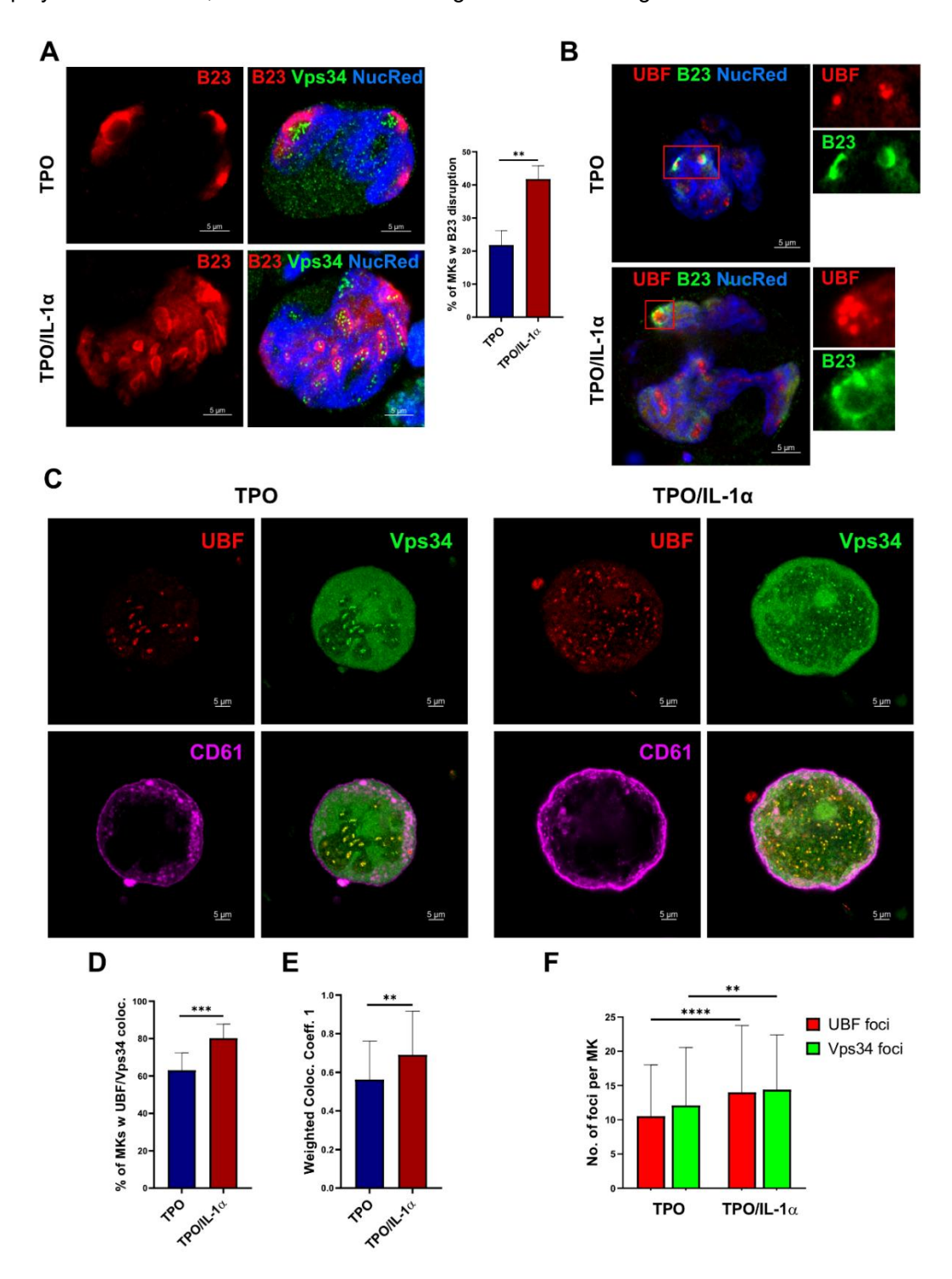


Figure 22. IL-1 α induces nucleolar stress and results in an increased number and colocalization of UBF/Vps34 nuclear foci in immature megakaryocytes.

BM MKs were cultured for three days with either TPO alone or TPO together with IL-1a. The cells were then fixed and immunostained for Vps34 and nucleolar markers. Cells were visualized using an LSM880 confocal microscope (Carl Zeiss) with a Plan-Apochromat 63×/1.40 oil DIC III objective. (A) B23 staining showed a greater percentage of MKs exhibiting B23 disruption/translocation to the nucleoplasm (NucRed positive staining indicates the nucleus) and/or cytoplasm after IL-1α treatment. The representative middle z-plane of the acquired stack is shown. At least 10 MKs were analyzed per condition across three independent experiments. (B) Nucleolar morphology marked by UBF and B23 staining. A close-up of the confocal images is extracted from a single z-plane of the acquired z-stack. (C) MKs were stained for UBF and Vps34, using CD61 as an MK lineage marker. (D) Following IL-1α treatment, a higher percentage of MKs exhibited visible UBF/Vps34 colocalization. Representative middle z-planes are shown, highlighting UBF/Vps34 localization in the nucleus and nucleolus. (E) Weighted colocalization coefficients were analyzed using ZEN Black software (Carl Zeiss). At least 20 MKs were analyzed for each condition across two independent experiments. (F) An increased number of both UBF and Vps34 foci in the MK nuclei accompanied this colocalization. At least 15 MKs were analyzed for each condition across a minimum of five independent experiments. Data in the graphs are presented as means, with error bars representing ± SD. ** p < 0.01, *** p < 0.001, **** p < 0.0001

4.2.4. Inhibition of Vps34 during early megakaryopoiesis inhibits megakaryocyte growth and disperses nucleolar UBF

The role of Vps34 in DMS development and proplatelet formation during MK maturation has already been established [68]. Several lines of research have studied the effects of both Vps34 knockdown and knockout [183-185], as well as the application of Vps34 inhibitors [186-188]. The common phenotype that was observed was the accumulation of large cytoplasmic vacuoles, described as swollen, dysfunctional late endosomes [185]. This is expected considering one of the main functions of Vps34 in endolysosomal trafficking. Since attempts to knockout Vps34 completely have been proven embryonically lethal [184], while others pointed out the reversal in Vps34 after shRNA knockdown [187], it is sufficient to state that Vps34 is an essential protein indispensable for cellular survival. In our experiments, we have opted for the pharmacological approach by using a potent and selective inhibitor, Vps34-IN1 (IN1). We cultured BM MKs in the presence or absence of IN1 (from day 0) in different concentration ranges. We imaged the cells in culture and observed that already at 0.1 µM concentrations, IN1 decreased MK size by approximately 50% compared to control MKs (in line with previous observations [68]) and around 66% in the case of IL-1α cultured MKs (**Figure 23B**). IL-1α MKs appeared more sensitive to Vps34 inhibition, as 1 µM IN1 reduced MK size by around 80% compared to approximately 60% size reduction in TPO MKs at the same concentration (Figure **23B**). We then immunostained and analyzed the cells for UBF, Vps34, and CD61 as MK marker (Figure 23A). After IN1 treatment, in both TPO control and IL-1α-cultured MKs, we found a significant dispersal of UBF/Vps34 foci in the nucleus (**Figure 23C**). This decrease in the number of foci was more drastic in IL-1a MKs, as even the lowest concentrations of IN1 significantly reduced their number (**Figure 23C**), indicating the decline of nucleoli and therefore decreased ability of the cell growth.

These results suggest that Vps34 is essential in supporting the growth and adequate development of BM MKs, both in the cases of physiological TPO- and IL-1 α - driven megakaryopoiesis mediated by ribosomal biogenesis. While IL-1 α MKs are significantly larger in size, they exhibit increased sensitivity to Vps34 inhibition. Pharmacological inhibition of Vps34 also leads to a more pronounced reduction of UBF/Vps34 foci in IL-1 α -treated cells, which may suggest a greater reliance on Vps34 activity to maintain nucleolar activity.

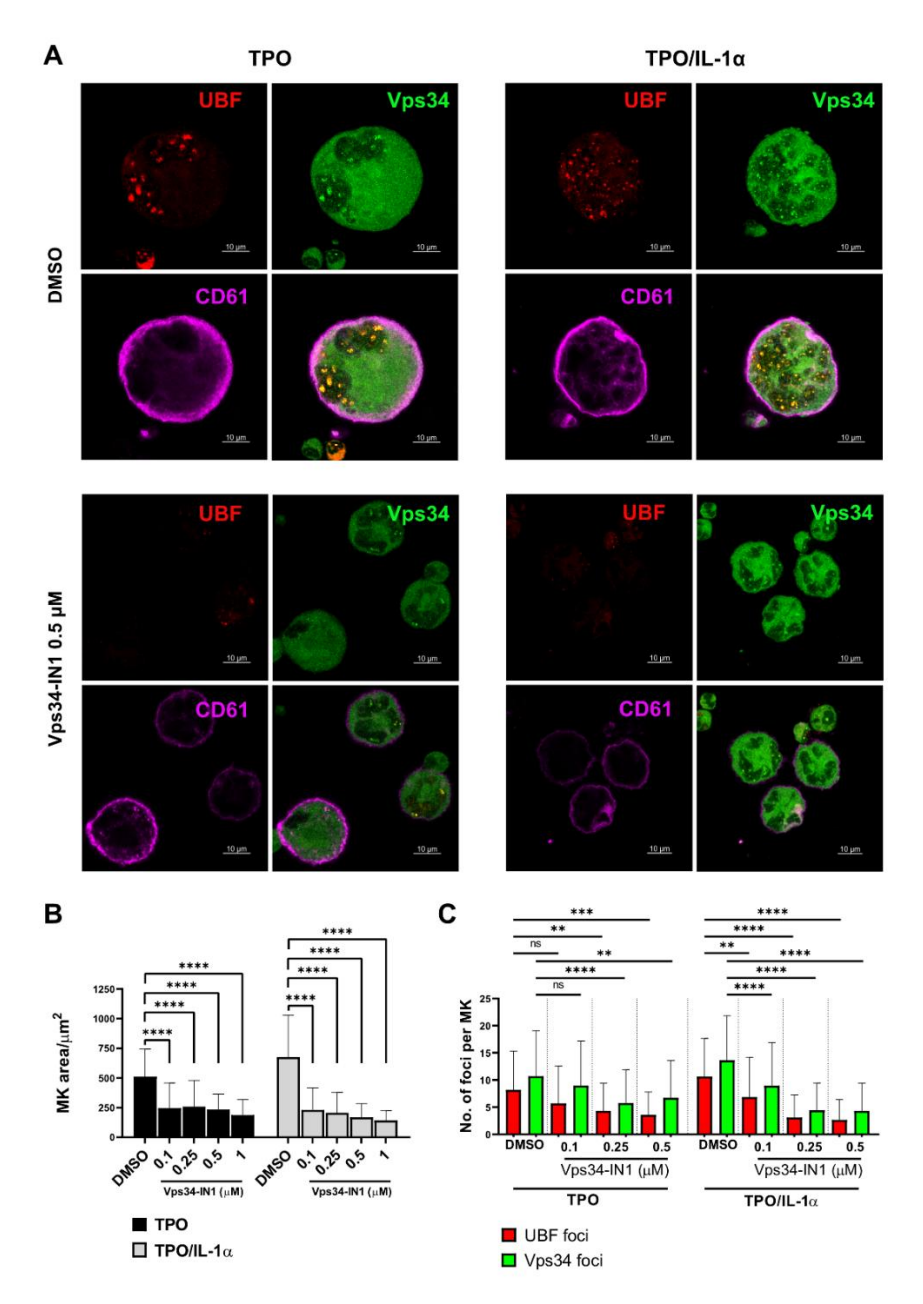


Figure 23. Pharmacological inhibition of Vps34 disperses UBF foci and impairs megakaryocyte expansion.

BM MKs were cultured in the presence of TPO or TPO and IL-1α for three days. Additionally, MKs were treated with a concentration range of Vps34 inhibitor (IN1). MKs were imaged using an LSM880 confocal microscope (Carl Zeiss) with a Plan-Apochromat 63×/1.40 oil DIC III objective. (A) MKs were stained for UBF, Vps34, and CD61 as MK marker. Immunofluorescence revealed the absence of UBF/Vps34 foci in the nucleus following IN1 treatment. Data quantified in graph (C). (B) Bright-field images of BM-derived MKs were captured using a 40x objective on an Axio Vert.A1 microscope (Carl Zeiss), and the MK area was quantified using ZEN software. The graph represents halted MK growth in dependence on increasing IN1 concentrations. Data in the graphs are presented as means, with

error bars representing \pm SD from a minimum of three independent experiments. ** p < 0.01, **** p < 0.0001, ns – not significant

4.3. IN VIVO MODEL OF THROMBOCYTOPENIA DEMONSTRATES CHANGES IN THE NUCLEOLUS AND VPS34 KINASE IN BONE MARROW MEGAKARYOCYTES

Our *in vitro* model with IL-1 α effectively simulated a controlled proinflammatory environment in BM cells. However, inducing thrombocytopenia *in vivo* gives us a more comprehensive insight into MKs' response. This model is well established, and previously it was shown that acute platelet depletion caused by anti-GPIb α antibody induces an increase in IL-1 α levels [51]. Thrombocytopenia could be considered a non-canonical cellular stressor, as it puts pressure on MKs to release more platelets to compensate for their low levels in circulation.

In the following experiments, we induced acute platelet depletion via anti-GPIb α antibody administration [162, 189], then collected and prepared BM cryosections. Immunostaining for Vps34 and GPIb β showed changes in MK size along with total Vps34 MFI after platelet depletion, although Vps34 did not show quantitative changes in foci formation in the nucleus.

4.3.1. Acute platelet depletion affects the size of bone marrow megakaryocytes and increases Vps34 fluorescence intensity

Given how Vps34 responded to IL-1α treatment *in vitro*, we were interested in exploring the molecular consequences of thrombocytopenia in MKs in mice.

Administration of anti-GPIbα antibody successfully depleted platelets (performed in collaboration with T. Bruketa and Dr. Markus Bender, Institute of Experimental Biomedicine, University Hospital Würzburg, Rudolf Virchow Center, Würzburg, Germany), and after the specified time points (6h, 24h, 48h) BM were collected. We immunostained BM sections for Vps34 and GPIbβ, which served as a marker for MKs (Figure 24A). Confocal microscopy analysis indicated a significant reduction in MK area 24 hours after platelet depletion. (Figure 24B). This reduction was temporary, as MK size returned to normal after 48 hours (Figure 24B). We also assessed the fluorescence intensity of Vps34 across the total cell area. Notably, Vps34 MFI in MKs from platelet-depleted sections showed a substantial increase at all time points (Figure 24C).

The presence of smaller MKs 24 hours after platelet depletion could indicate immature MKs progressing through early development to compensate for low platelet levels. While we can only speculate, the increase in Vps34 signal in MKs at all time points after the depletion of platelets might point to a role of Vps34 in the rapid recovery from platelet loss. Therefore, we took a closer look to analyse MKs at larger magnification and decipher the exact Vps34 localization.

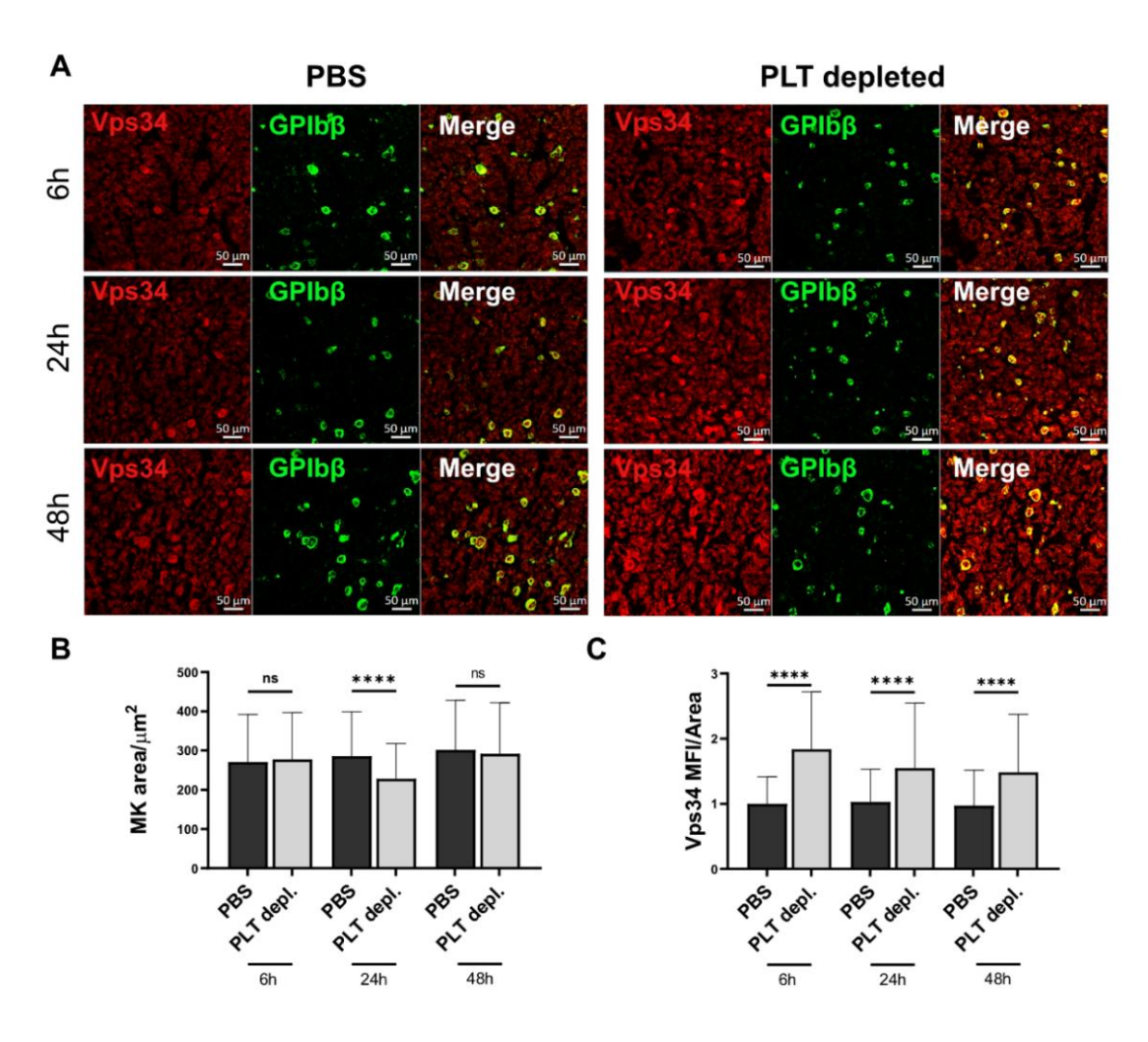


Figure 24. Changes in MK size and Vps34 signal in the bone marrow following platelet depletion.

Mice were depleted of circulating platelets, and BM was harvested at the indicated time points (6h, 24h, and 48h post-depletion). (A) BM sections were immunostained for MK marker (GPlb β), Vps34, and imaged by LSM880 (Carl Zeiss) confocal microscope equipped with a Plan-Apochromat 20×/0.8 M27 objective. Representative maximum projections are shown here. (B) The MK surface area was analyzed using Zeiss ZEN Black software and presented in the graph. (C) Vps34 mean fluorescence intensity (MFI) was analyzed using Zeiss ZEN Black software and expressed over the total MK surface area. MFI values in PLT-depleted samples were normalized according to respective PBS controls. Graphs represent mean values, with error bars indicating \pm SD from a minimum of three independent experiments. ns – non-significant, ***** p < 0.0001.

We sought to determine whether *in vivo* MKs show nuclear localization of Vps34 as we have observed *in vitro*. In parallel with Vps34 and GPlbβ immunostaining, we counterstained sections with NucRed for the nucleus (**Figure 25A**). Indeed, Vps34 was localized in the nucleus of *in situ* MKs, with foci-like staining also within the regions of the nucleus where NucRed staining was absent, indicative of the

xnucleolus (**Figure 25A**, white arrows). This phenotype was observed in both control BMs and BM after platelet depletion.

Since the number of Vps34 foci was increased after IL-1 α stimulation *in vitro*, we performed the same analysis in MKs in BM sections. However, there was no observable difference between the two conditions at the same time points (**Figure 25B**). Even more, the MFI of Vps34 in the nucleus showed a significant drop 6 hours post-platelet depletion (**Figure 25C**). This drop was transient, as the MFI normalized after the 24-hour point and remained consistent with the MFI values from control MKs (**Figure 25C**).

Unfortunately, we could not stain the sections with typical nucleolar markers since antibodies did not work in tissue sections, so we could not assess the nucleolar size and possible disruption. Nevertheless, considering that nuclear dyes for immunofluorescence have a strong affinity for DNA-rich regions, and since the nucleolar core is largely composed of RNA and proteins, nucleoli are excluded from DNA staining. Because the Vps34 signal was positive throughout the nucleus, even in those dark and unstained areas, this could imply its nucleolar localization. It's intriguing to consider if the discrepancies between total cell and nuclear MFI of Vps34 stem from active protein shuttling between the nucleus and the rest of the cell, especially given the early transient drop and normalization of nuclear Vps34 MFI in MKs after platelet depletion.

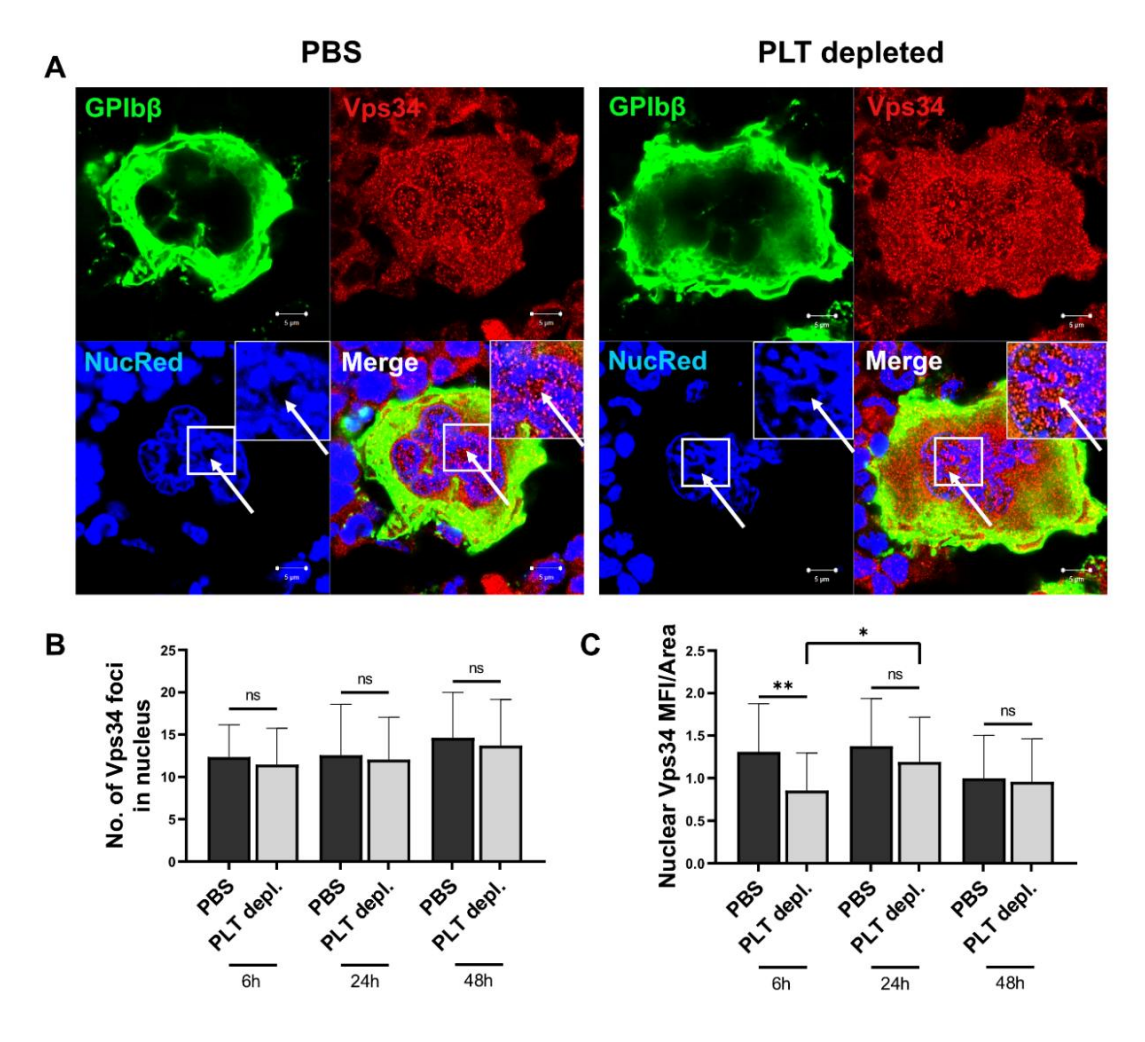


Figure 25. Vps34 localizes in the nucleus and nucleolus of bone marrow megakaryocytes.

(A) BM sections were immunostained for the MK marker (GPIb β), Vps34, counterstained for the nucleus (NucRed), and imaged by LSM880 (Carl Zeiss) confocal microscope equipped with a Plan-Apochromat 63×/1.40 oil DIC III objective. Representative maximum projections are shown here, indicating Vps34 localization in the nucleus and NucRed-negative regions resembling nucleoli. (B) The number of positive Vps34 dots (foci) in the nucleus per cell was counted manually in the middle z-plane of acquired confocal images and presented in the graph. (C) Vps34 mean fluorescence intensity (MFI) was analyzed using Zeiss ZEN Black software and expressed over the total nuclear surface area of MKs. MFI values in PLT-depleted samples were normalized according to respective PBS controls. Graphs represent mean values, with error bars indicating \pm SD from a minimum of three independent experiments. ns – non-significant, * p < 0.05, ** p < 0.01.

4.4. CHARACTERIZATION OF THE NUCLEOLUS AND VPS34 KINASE IN HUMAN MEGAKARYOCYTIC CELL LINES

Nucleolar dynamics have been studied in many cells and cell types. However, very little research exists on nucleolar dynamics during MK maturation. A higher number of NORs was found in primary rat megakaryoblasts and immature MKs, and this number gradually decreased along with MK maturation [190].

To build upon this limited research, we aimed to characterize the nucleolus in MK cell lines, an available model of human MK. For this, we used human megakaryoblastic cell lines DAMI and HEL, along with an immortalized myelogenous leukemia cell line K562. We induced megakaryocytic differentiation by treating the cells with phorbol 12-myristate 13-acetate (PMA) and assessed the nucleolar protein expression and localization. These PMA-treated cells achieved higher MK maturation and are regarded as differentiated cells throughout the thesis. Conversely, non-stimulated (NS) cells were allowed to proliferate and are considered immature MKs and are termed undifferentiated throughout this work.

Interestingly, we found that early PMA-induced differentiation significantly increased the number of visible nucleoli, while prolonged periods of proliferation caused the cells to exhibit signs of nucleolar stress. We also characterized Vps34 and its behavior in relation to nucleolar dynamics and discovered that it localizes in the nucleus of both undifferentiated and differentiated cells. Additionally, among all the nucleolar proteins, the highest degree of Vps34 colocalization was found with UBF, as in mouse primary MKs. Given the leukemic nature of the previously mentioned cell lines, we analyzed human mononuclear cells and also found Vps34 confined to the nucleolus, thus supporting our model for studying nucleolar changes in other cells.

4.4.1. PMA-induced differentiation of DAMI cells leads to an increase in nucleolar number and Vps34 localization in the nucleus

Because of its structural analogy to diacylglycerol, PMA is a potent activator of protein kinase C (PKC), activating downstream MEK/MAPK pathways [191]. This signaling pathway has been well characterized in DAMI and K562 cell lines, which have been used as a model to study MK differentiation [192-196]. PMA-induced differentiation of DAMI cells is accompanied by several important cellular changes. Notably, cells undergoing differentiation become polyploid and adhere to the surface on which they are cultured, while their proliferation decreases substantially [194, 195]. When stimulated by PMA and TPO, there was a significant upregulation of important MK transcription factors in DAMI cells, such as GATA1 and NF-E2 [196]. Furthermore, mature differentiated DAMI cells were found to release GPIb-positive

functional platelet-like particles containing both alpha and dense granules [196]. DAMI cells are also of interest when studying leukemic proliferation, given that they harbor constitutively active JAK2/STAT5 signaling [197].

In our experiments, we stimulated DAMI cells with 100 nM PMA for 24 to 72 hours. NS cells were allowed to proliferate within the same time frame. At each time point, cells were lysed, and total expression of Vps34 and nucleolar proteins was analyzed by Western blot (**Figure 26**). While we did not observe statisticly significant changes in Vps34 expression, we found that proliferating cells had significantly upregulated UBF, B23, and fibrillarin (**Figure 26**). On the other hand, although differentiated cells (PMA) displayed initial high expression levels of nucleolar proteins and Vps34 at 24h (compared to NS 0h), at later time points expression did not increase further or was generally lower. The difference was significant in the case of UBF, where differentiated cells had lower UBF content when compared to controls at the 48h time point (**Figure 26**).

These results could indicate that the upregulation of nucleolar proteins is important for accommodating the high protein turnover during cell proliferation. Conversely, the later lower expression of nucleolar proteins in differentiating cells aligns with the observed decreased number of NORs in mature MKs [190] and reported arrest in cellular growth following PMA treatment of DAMI cells [195].

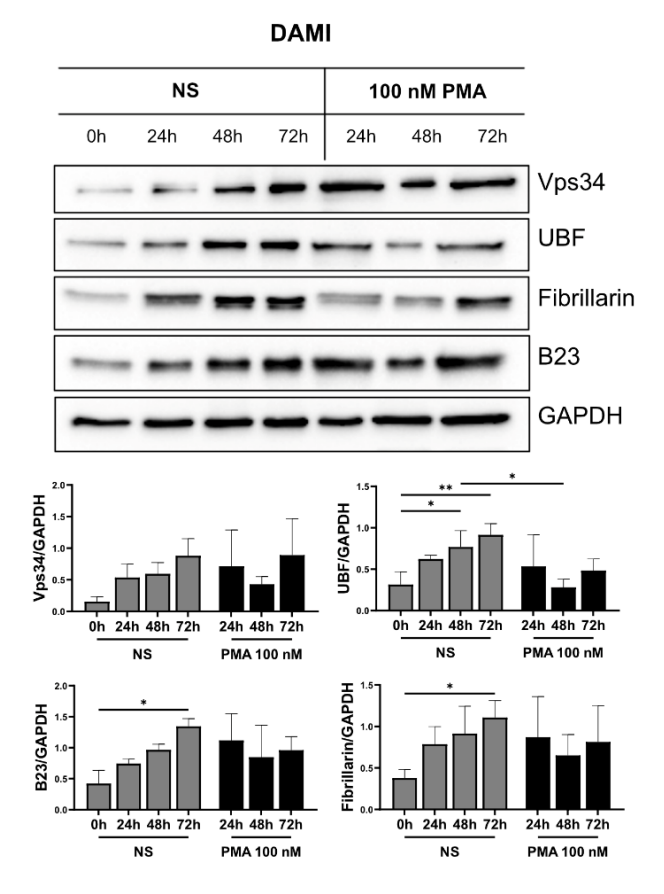


Figure 26. Effect of proliferation and PMAinduced differentiation on expression of nucleolar proteins and Vps34 in DAMI cells.

DAMI cells were seeded and treated with 100 nM concentrations of PMA for 24-72 hours. Control cells were allowed to proliferate within the same period. Cell lysates were subjected to SDS-PAGE, then blotted onto a nitrocellulose membrane and incubated with the indicated antibodies. Representative immunoblots show expression levels of Vps34, UBF, fibrillarin, B23, and GAPDH. Blots were analyzed by ImageJ, using GAPDH as a loading control. Graphs represent mean values, with error bars indicating ± SD from four independent experiments. * p < 0.05, ** p < 0.01.

In addition to total protein expression, we were interested in the localization of these proteins in the context of nucleolar morphology. Because B23 is localized at the rim of nucleoli and represents a marker of its granular component, it allows us to distinguish the outside borders of the nucleoli clearly.

In DAMI cells, we identified three major nucleolar phenotypes characterized by B23 staining: organized, disrupted, and the absence of staining (**Figure 27A**). Organized staining refers to structured nucleoli with clear borders, where the majority of the B23 signal originates from the nucleolus, a feature similarly observed in the majority of primary mouse MKs. Disrupted nucleoli are hallmarks of nucleolar stress, where B23 translocates to the nucleoplasm and/or cytoplasm and displays a diffused signal throughout the nucleus. This phenotype was rarely observed in primary mouse MKs. Lastly, the absence of staining means that the cell did not have visible nucleoli at the time of fixation, possibly pointing to nucleolar disassembly or a halt in ribosomal production [198].

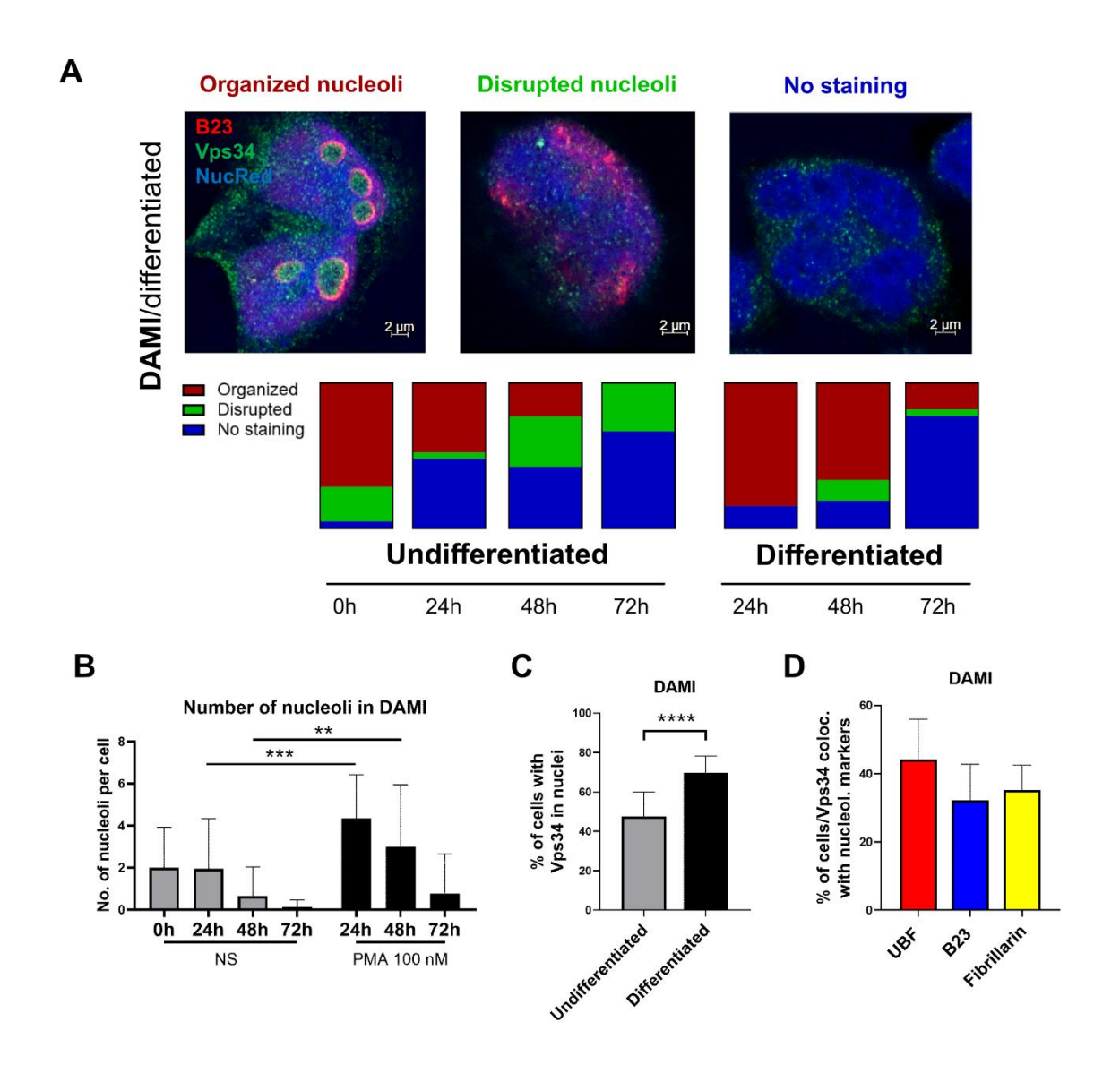


Figure 27. Nucleolar morphology and Vps34 localization are affected by PMA-induced differentiation in DAMI cells.

DAMI cells were seeded and treated with the indicated concentrations of PMA. (A) Cells were fixed and immunostained for B23 and Vps34 and counterstained for the nucleus. Confocal microscopy images were acquired using an LSM880 confocal microscope (Carl Zeiss) equipped with a Plan-Apochromat $63 \times /1.40$ oil DIC III objective. Representative images of maximum projections are shown, and nucleolar phenotypes are quantified and presented as percentages of total cell number in the color scheme below. (B) The number of organized B23-marked nucleolar structures per cell was quantified in acquired confocal images and plotted in the graph. (C) The percentage of undifferentiated and PMA-differentiated DAMI cells at the 24-hour time point showing positive Vps34 signal in the nucleus was quantified. (D) The colocalization pattern of nuclear Vps34 with nucleolar markers was quantified and expressed as the percentage of undifferentiated DAMI cells at the 24-hour time point that display positive colocalization of Vps34 with each nucleolar marker. Graphs represent mean values, with error bars indicating \pm SD from four independent experiments. ** p < 0.01, *** p < 0.001, **** p < 0.0001.

At the starting point (0h), over 70% of undifferentiated DAMI cells had organized nucleoli (**Figure 27A**, red bar). During proliferation, cells gradually lost organized nucleolar structures and showed signs of nucleolar disruption. This phenotype peaked at the 48h time point, with almost 40% of cells showing disruption (**Figure 27A**, green bar), while the other 40% had no positive B23 staining (**Figure 27A**, blue bar). Finally, the decrease of B23 staining was the dominant phenotype after 72h, with approximately 70% of cells having no visible nucleoli.

Cells undergoing differentiation displayed a higher number of organized nucleoli at early time points when compared to undifferentiated cells analyzed at the same time (**Figure 27A**, quantified in graph **27B**), with the difference being significant at 24 and 48 hours post-PMA treatment. This is in line with increased ploidy induced by PMA-differentiation and previous findings. While around 65% of differentiated cells retained organized nucleolar structures after 48h, at the 72h mark, almost 80% of cells showed no visible nucleoli (**Figure 27A**).

Interestingly, this higher number of nucleoli in differentiating cells was also accompanied by a higher percentage of cells exhibiting nuclear Vps34 localization. On average, more than 70% of differentiated cells had positive Vps34 staining in the nucleus (Figure 27A, quantified in 27C). In undifferentiated DAMI cells, Vps34 is localized in the nucleus and nucleolus, with the highest degree of colocalization observed with UBF in almost half of the cells, followed by fibrillarin and B23 (Figure **27D**). While observing UBF and Vps34 colocalization, we also noticed a somewhat different staining phenotype of UBF compared to primary MKs, where UBF is present in highly organized structures (Figure 28A). In undifferentiated and differentiated DAMI, at the 24-hour time point, more nucleoplasm was positive for UBF and displayed a more dispersed and diffused staining, similar to B23 (Figure 28A). We quantified the colocalization between UBF and Vps34, but found no significant difference between undifferentiated and differentiated DAMI 24 hours post PMA stimulation, indicating that Vps34 follows the pattern of UBF (Figure 28C). We also quantified the colocalization between B23 and Vps34 (Figure 28B). Interestingly, in differentiated DAMI cells, B23 colocalized more with Vps34 than in undifferentiated cells (Figure 28D). Vps34 was clearly visible localizing within B23 territories in differentiated cells (Figure 28E), indicating a shift of Vps34/UBF towards B23 in differentiated DAMI cells.

Collectively, a higher number of nucleoli during early differentiation is consistent with our data on primary MKs, where immature MKs cultured until day 3 exhibit the highest number of nucleoli. Differences observed in the disrupted nucleoli

phenotype, with increased B23, UBF, and Vps34 in the nucleoplasm, and somewhat different colocalization of Vps34 with nucleolar markers compared to primary MKs, could be due to the altered biology of the DAMI cell line, resulting from its leukemic origin. This is further supported by the diffused, unorganized UBF phenotype (as opposed to primary MKs) and by a stronger B23 signal and presence of multiple organized nucleolar structures in differentiated cells (24h time-point), which showed a significantly higher degree of colocalization between B23 and Vps34 than in undifferentiated DAMI cells.

Considering the points mentioned above, we focused on early differentiation (24h post-PMA treatment) in the immunofluorescence experiments with K562 and HEL cells.

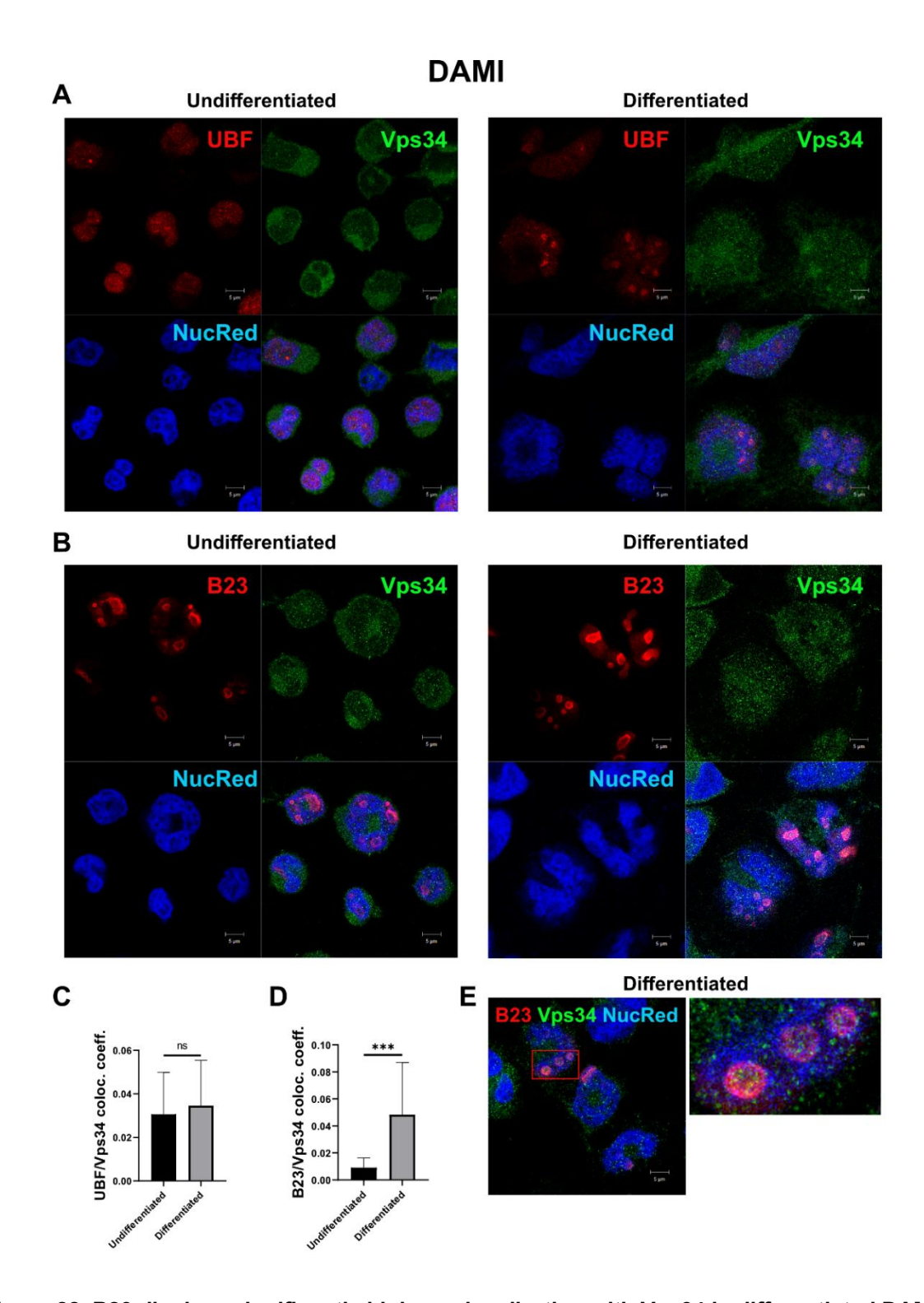


Figure 28. B23 displays significantly higher colocalization with Vps34 in differentiated DAMI cells.

(A) We immunostained DAMI cells for UBF, Vps34, and counterstained for the nucleus (NucRed) in undifferentiated and PMA-differentiated conditions. Cells were imaged using an LSM880 confocal microscope (Carl Zeiss) equipped with a Plan-Apochromat 63×1.40 oil DIC III objective. Representative maximum projections are shown, showcasing differences in the staining phenotype of UBF. **(B)** Immunostaining was performed for B23 and Vps34 with NucRed. Representative maximum projections show Vps34 localizing within B23-marked territories. **(C, D)** We quantified the colocalization of UBF with Vps34 and B23 with Vps34 using ZEN Black software (Carl Zeiss). A minimum of 10 cells were analyzed per condition across two independent experiments. **(E)** A close-up of the acquired confocal images with visible green signal (Vps34) within B23-marked nucleoli. Graphs represent mean values, with error bars indicating \pm SD from two independent experiments. **** p < 0.001, ns – not significant

4.4.2. K562 cells respond to PMA by decreasing nucleolar protein expression and subtly increasing the number of nucleoli

K562 cells were first derived from a patient with chronic myeloid leukemia (CML) in terminal blast crisis [199]. One of the key characteristics of these cells is the presence of the BCR-ABL fusion gene, also known as the Philadelphia chromosome [199, 200]. Apart from the capacity for megakaryocytic differentiation, K562 cells have been shown to differentiate into erythroid cells expressing hemoglobin under sodium butyrate stimulation [201].

To induce megakaryocytic differentiation of K562 cells, we used 20 nM PMA and stimulated the cells for 24 to 72 hours. First, we wanted to analyze the total expression of nucleolar proteins and Vps34 by Western blot (**Figure 29**). Proliferating K562 cells showed a similar trend to DAMI cells regarding upregulation of nucleolar proteins, including Vps34 (**Figure 29**). UBF was significantly upregulated after 24 hours, while B23 increased significantly after 48 hours of proliferation (**Figure 29**). Conversely, differentiated K562 cells had generally lower expression levels, and this difference was significant with UBF at 48 and 72 hours post-PMA treatment (**Figure 29**).

Based on these results, we can draw a similar conclusion that the increased activity of nucleolar proteins is crucial for managing the high rate of protein synthesis that occurs during cell proliferation.

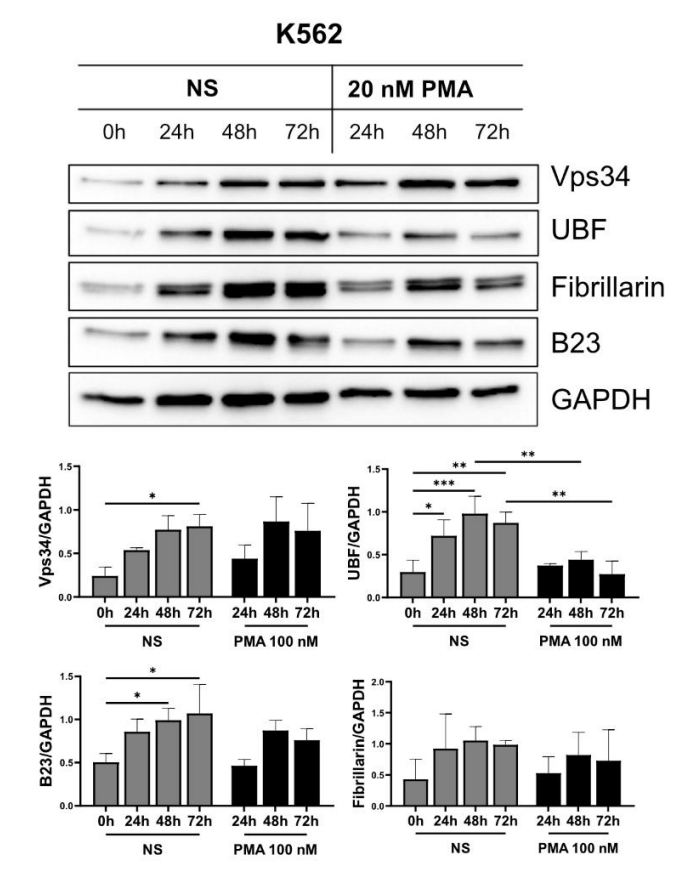


Figure 29. Impact of cell growth and PMA-triggered differentiation on the expression of nucleolar proteins and Vps34 in K562 cells.

K562 cells were seeded and treated with 20 nM concentrations of PMA for 24-72 hours. Control cells were permitted to proliferate during the same timeframe. Cell Ivsates underwent SDS-PAGE and were subsequently transferred nitrocellulose membrane, where they were incubated with the specified antibodies. Representative blots illustrate expression levels of Vps34 and nucleolar proteins. Blots were analyzed by ImageJ, using GAPDH as a loading control. Graphs represent mean values, with error bars indicating ± SD from four independent experiments. * p < 0.05, ** p < 0.01, *** p < 0.001.

Unlike DAMI cells, K562 displayed mild phenotypical changes in cell morphology and structure in response to PMA. The most prominent features were polyploidization and a slight increase in cell size. We stained K562 cells for nucleolar markers and Vps34 (**Figure 30A**) and found a modest, but not significant, increase in the number of nucleoli following PMA-induced differentiation (**Figure 30B**). Interestingly, while more than 70% of differentiated DAMI cells showed positive Vps34 signal in the nucleus (**Figure 27C**), in K562 cells this phenotype was undoubtedly dominant, with almost 100% of cells with Vps34 in the nucleus (**Figure 30B**). Furthermore, the nuclear Vps34 signal overlapped with UBF and was within the borders of B23, indicating that Vps34 was also present in the nucleolus (**Figure 30A**).

Megakaryocytic differentiation of K562 displayed similar traits to those in DAMI, such as polyploidy and a slight increase in size, but also had some unique features. While some K562 cells developed adherent properties, the majority remained in suspension. Additionally, apoptotic cells were also present after PMA treatment, and a similar finding was reported previously [202]. Although the differentiation did not significantly increase the number of nucleoli, this may be attributed to the different

origin and nature of these cells and their response to PMA stimuli. The unchanged number of nucleoli also agrees with only a slight increase in their size after PMA stimulation.

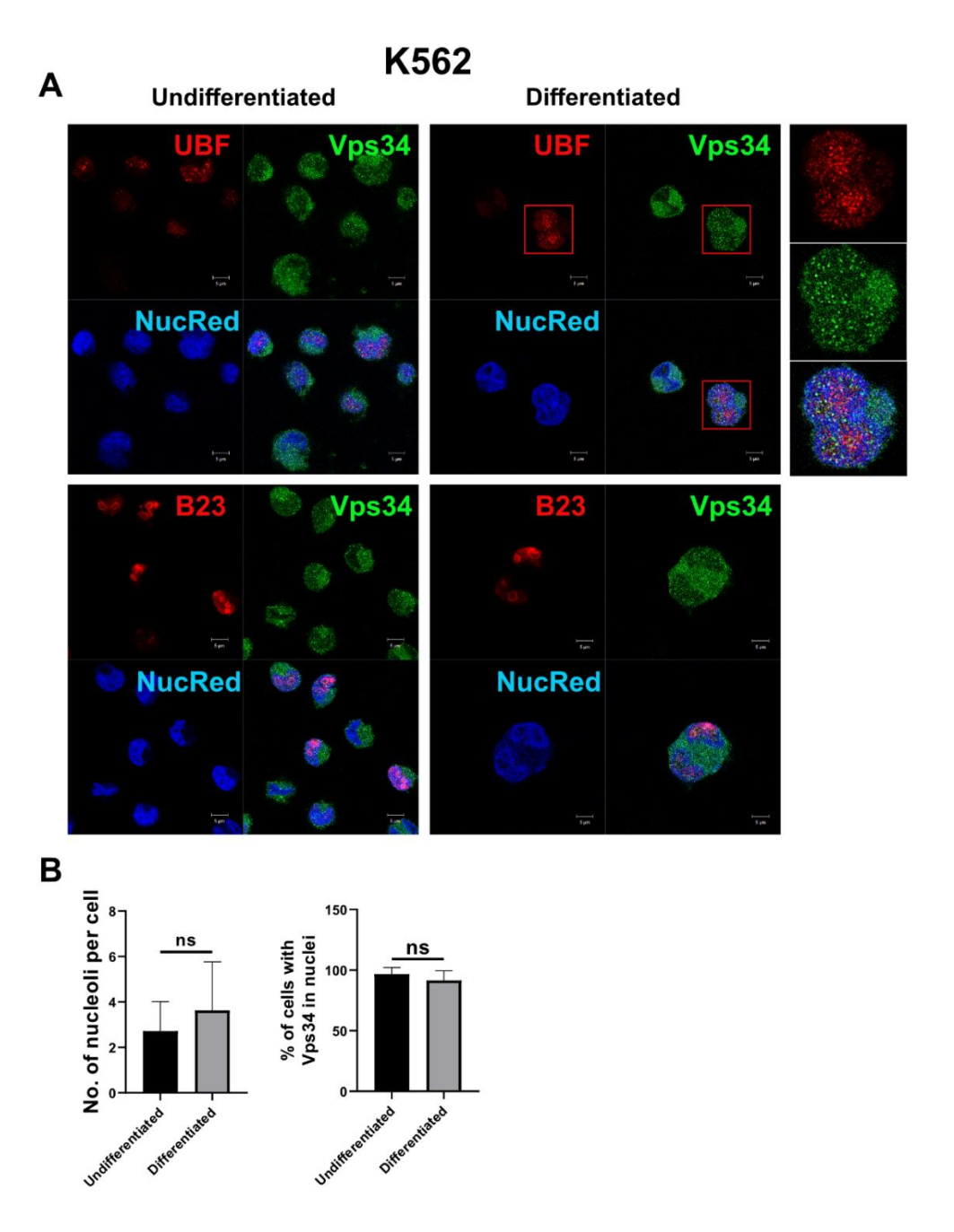


Figure 30. PMA-induced differentiation in K562 cells does not alter nucleoli number or nuclear Vps34 localization.

K562 cells were seeded and treated with 20 nM PMA for 24h. **(A)** Cells were fixed and immunostained for nucleolar markers (UBF, B23) and Vps34 and counterstained for the nucleus (NucRed). Confocal microscopy images were acquired using an LSM880 (Carl Zeiss) equipped with a Plan-Apochromat $63\times/1.40$ oil DIC III objective. Representative images of maximum projections are shown and UBF/Vps34 colocalization is enlarged. **(B)** The number of organized B23-marked nucleolar structures per cell was quantified throughout the acquired z-stack and plotted in the graph. The percentage of cells with a positive Vps34 signal in the nucleus was counted manually and presented in the graph. Graphs represent mean values, with error bars indicating \pm SD from three independent experiments. ns – not significant

4.4.3. Nucleoli number increases significantly in PMA-differentiated HEL cells

HEL cells are human erythroleukemia cells, first used to study erythroid differentiation and globin expression [203]. With the discovery that HEL are a triphenotypic cell line, they were also used to study MK differentiation and development [204-207]. Similar to DAMI cells, HEL also carry a JAK2 mutation (V617F), resulting in its constitutive activity [206]. A p53 mutation coexists in this cell line, which causes a loss of p53 function [206].

We used 100 nM PMA to induce megakaryocytic differentiation in HEL cells. Our aim was to characterize the morphology of the nucleoli via immunofluorescence and the relationship with Vps34, using UBF and B23 as nucleolar markers. Differentiated HEL cells respond to PMA similarly to DAMI cells regarding adherence and polyploidization (Figure 31A). Immunofluorescent staining revealed organized nucleolar structures and positive Vps34 staining in the nucleolus in undifferentiated and differentiated cells (Figure 31A). Differentiated cells had a significantly higher number of nucleoli when compared to undifferentiated cells (Figure 31B), similarly to DAMI cells. Both experimental conditions had a comparable rate of cells with a positive Vps34 signal in the nucleus (Figure 31B), as the percentage was close to 100. In this regard, HEL cells were more similar to K562. Interestingly, UBF was not dispersed as in DAMI cells, but rather more distinct and present in organized structures, both in undifferentiated and differentiated HEL cells. When quantifying the colocalization between UBF and Vps34 (Figure 31C), we found a significantly higher degree of colocalization, as these differentiated cells showed a pattern of UBF staining that was more similar to primary MKs. We also performed the same analysis for B23 and Vps34 colocalization (Figure 31D) and found significant colocalization.

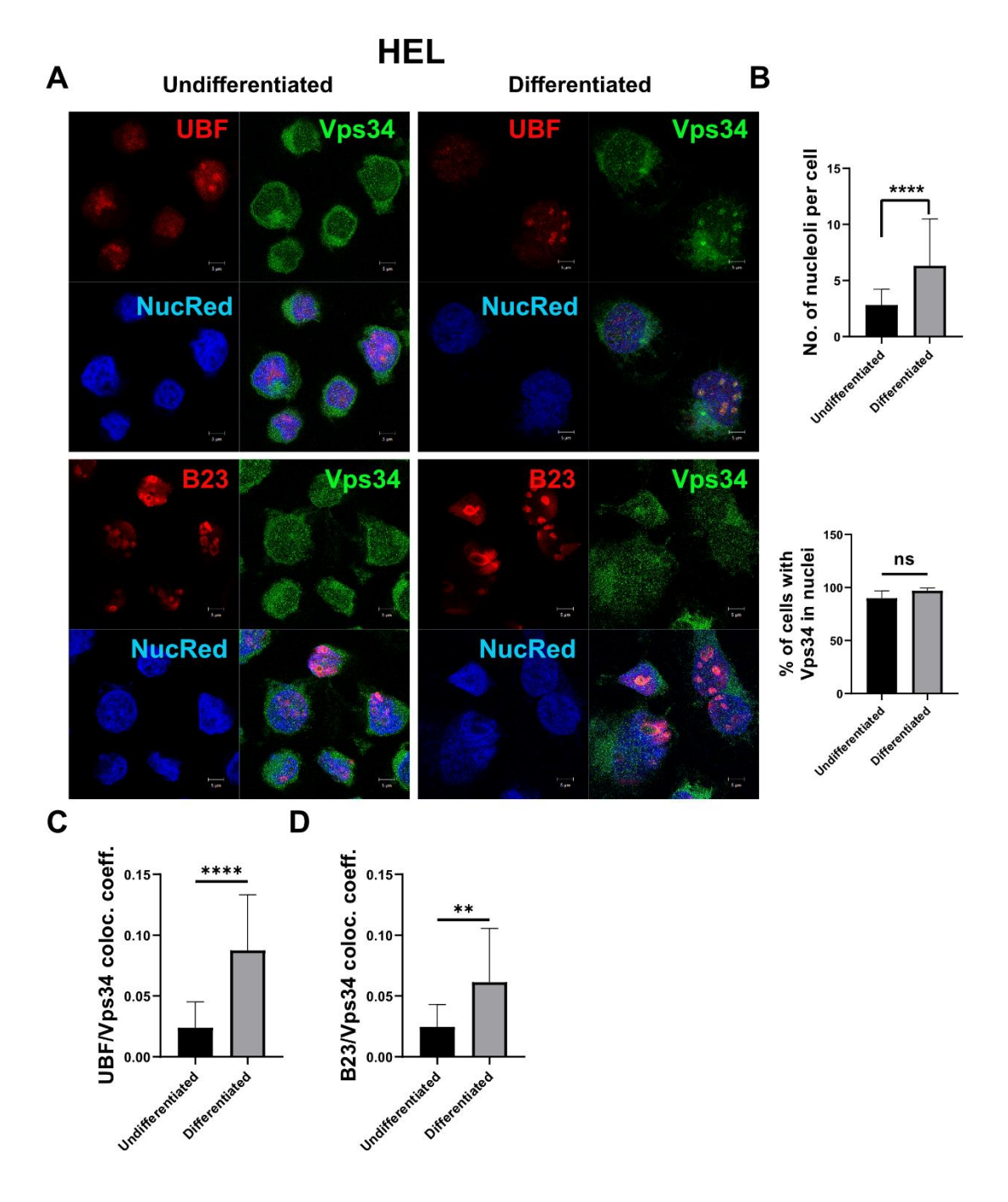


Figure 31. PMA-induced differentiation increases nucleolar activity in HEL cells.

HEL cells were seeded and treated with 100 nM PMA for 24h. **(A)** Cells were fixed and immunostained for nucleolar markers (UBF or B23), Vps34, and counterstained for the nucleus (NucRed). Confocal imaging was performed using an LSM880 (Carl Zeiss) equipped with a Plan-Apochromat 63×/1.40 oil DIC III objective. Representative images of maximum projections are shown. **(B)** The number of nucleoli was counted manually based on positive B23 staining throughout the z-stack and presented in the graph. Cells showing positive Vps34 staining in the nucleus were counted manually in both

populations of undifferentiated and differentiated cells and presented as a percentage of the total cell count in the graph. **(C, D)** Weighted colocalization coefficients were analyzed in ZEN Black software (Carl Zeiss) and shown in the graphs. At least 10 cells were analyzed per condition across two independent experiments. Graphs represent mean values, with error bars indicating \pm SD. ** p < 0.01, **** p < 0.0001, ns – not significant

4.4.4. Vps34 localizes in the nucleolus of human mononuclear cells

Since all three cell lines previously used were leukemic in nature, we wanted to confirm whether the observed nucleolar morphology and Vps34 localization would be found in healthy cells. For this purpose, we isolated mononuclear cells *via* Ficoll Paque from the blood of adult healthy donors, as outlined in Methods. We stained the cells for UBF, B23, and Vps34 (**Figure 32A**) and analyzed the frequency of nucleolar visibility, as well as Vps34 localization. Around 40% of isolated mononuclears displayed visible nucleoli, with UBF localizing inside the B23 nucleolar borders (**Figure 32A**, **B**). UBF localization within defined B23 borders in mononuclear cells was clearly different to what we observed in cell lines, where we often found scattered and diffused appearance of B23 and UBF, further confirming the aberrant nucleolar morphology present in malignant cells. Vps34 was present in the nucleus and nucleolus, and was shown to colocalize with both nucleolar markers (**Figure 32C**).

While it was definitely present inside the nucleolus, there was a high percentage of cells where Vps34 displayed a strong signal at the nucleolar borders, thus colocalizing with B23 (**Figure 32A, C**). Because of the somewhat rare visibility of the nucleoli and the fact that most mononuclear cells show only one nucleolus per cell, these features could contribute to the differences in observed Vps34 colocalizations.

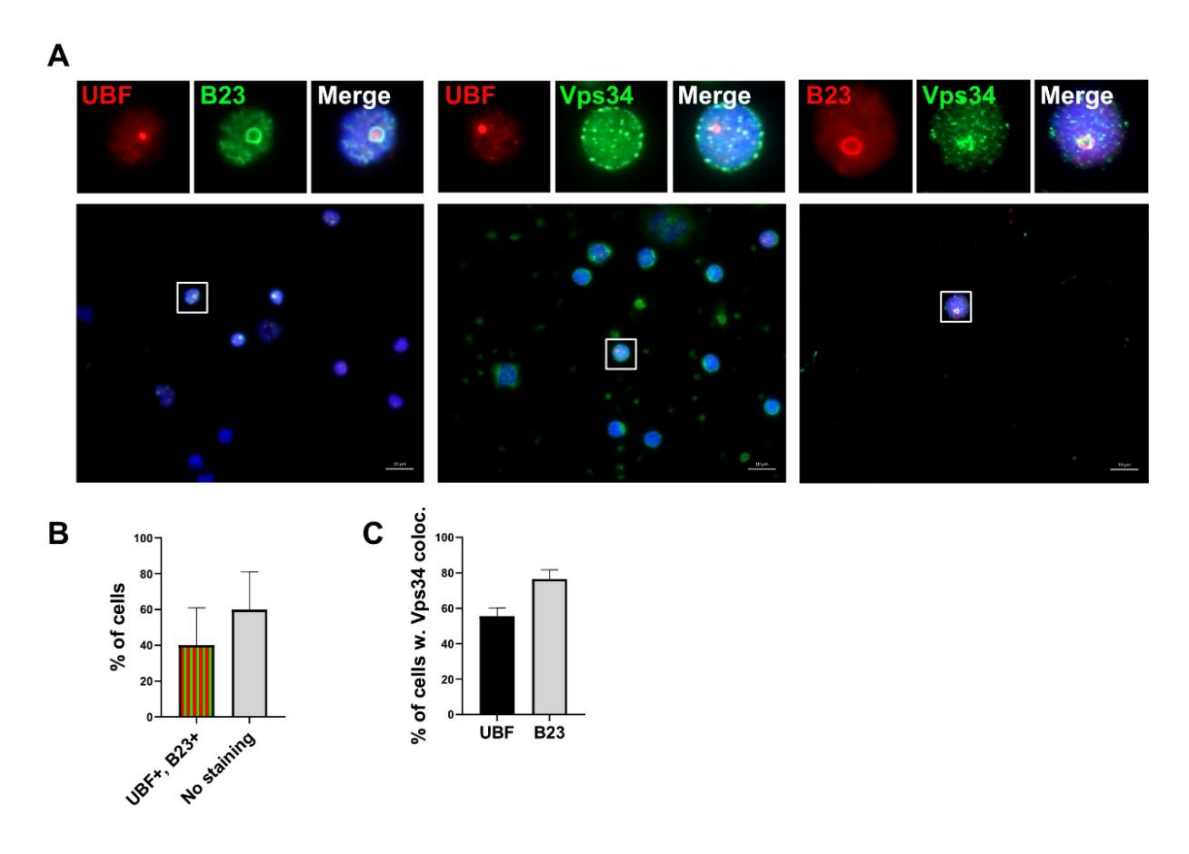


Figure 32. Vps34 is found in the nucleolus of human mononuclear cells.

Human mononuclear cells were isolated from the blood of adult, healthy donors following the Ficoll-Paque protocol. **(A)** Cells were fixed and immunostained for UBF, B23, and Vps34 and counterstained for the nucleus with DAMI. Fluorescence images were captured using a Zeiss Axio Observer.Z1 epifluorescence microscope (Carl Zeiss) equipped with Plan-Apochromat 63x/1.40 oil DIC M27 objective, 1.6x Tubelens Optovar lens, and Axiocam 506 imaging device. Representative images of mononuclears (white squares) are shown, highlighting nucleolar structure and Vps34 (co)localization. The scale bar is at 10 µm. **(B)** The percentage of mononuclears showing positive UBF and B23 staining was quantified and shown in the graph. **(C)** The rate of cells exhibiting visible colocalization of Vps34 with either UBF or B23 was quantified and shown in the graph. In total, at least 150 cells were analyzed per staining and experiment across three independent experiments. Graphs represent mean values, with error bars indicating \pm SD.

In summary, in the case of cell lines, the Vps34 signal clearly colocalized with UBF, a consistent observation across all three cell lines we examined. This also aligned with our findings in primary MKs, where the highest level of colocalization was seen between UBF and Vps34. Additionally, we found that inflammatory insult *via* IL-1α could cause nucleolar disruption in primary MKs (**Figure 22**), unlike DAMI cells, which showed some B23 presence in the nucleoplasm even under basal conditions and during prolonged proliferation (**Figure 27**). The most noticeable difference was in the UBF phenotype between primary MKs and cell lines. In primary MKs, the organization of UBF foci was focused, discrete, and concentrated (**Figure 22**).

Conversely, undifferentiated cell lines exhibited a more dispersed and diffused UBF staining throughout the nucleoplasm (**Figures 28, 30, 31**). These differences could be explained, at least partially, due to the leukemic nature of the cell lines. Because of the higher metabolic demand in cancer cells, nucleoli can be enlarged, disorganized, or altered even at basal levels [208, 209].

Nevertheless, in all cases, Vps34 was observed to be present in the nucleoli and to be confined to UBF and B23; however, this warrants further investigation. We have extensively characterized nucleolar phenotypes and their changes during proliferation and megakaryocytic differentiation in three human megakaryocytic cell lines. Additionally, we monitored alterations in the localization and expression of Vps34 in both primary cells and cell lines. Given the novel localization of Vps34 in the nucleolus, these findings lay a solid groundwork for future research into the previously unexplored role of nucleolar Vps34 in states of inflammation and cellular oncology.

4.5.VPS34 INHIBITION AFFECTS DNA DAMAGE OUTCOMES AND NUCLEOLAR PROTEIN EXPRESSION AFTER EXPOSURE TO GENOTOXIC INSULT

DNA damage is recognized as a trigger for the nucleolar stress response [103, 105, 109]. Considering the newly identified presence of Vps34 in the nucleolus, we aimed to examine how changes in the kinase's activity influence the DDR and the nucleolus. We chose a pharmacological method involving Vps34-IN1 to assess how DAMI, K562, and HEL cells respond to various DNA-damaging agents, including UV radiation and chemotherapeutic treatments, under conditions of Vps34 inhibition as well as with intact Vps34 functionality.

4.5.1. Vps34 inhibition alone induces DNA damage and downregulates UBF in a time- and dose-dependent manner in DAMI and HEL cells

It has been demonstrated that genotoxic insult results in an increase in PI3P in the nucleus [89]. Considering the localization of Vps34 in the nucleus of DAMI, K562, and HEL cells, we sought to investigate whether the nuclear pool of Vps34 plays a role in DDR.

Before treating the cells with known DNA-damaging agents, we wanted to be sure that Vps34 inhibition has no effect on cells. For this purpose, we used DAMI, K562, and HEL cells and treated the cells with a fixed concentration of the Vps34-IN1 (10 μ M) for varying time points (3, 6, 9, 18, and 24 hours) (**Figure 33**). In parallel, to evaluate the concentration dependency, cells were treated for 18 hours with increasing concentrations of the inhibitor (0.5, 1, 5, and 10 μ M) (**Figure 34**).

We used Western blot to analyse the total expression of γ -H2A.X as a measure of DDR in parallel with UBF. Surprisingly, we found significant upregulation of γ -H2A.X with IN1 (10 μ M) treatment after 18 and 24 hours in DAMI and HEL cells that was paralleled by downregulation of UBF (**Figure 33A, C**). K562 cells did not show significant upregulation of γ -H2A.X, nor did we observe significant changes in UBF expression (**Figure 33B**).

We further characterized the dose response and found that DAMI cells again responded similarly, with the upregulation of γ -H2A.X significant at 10 μ M of IN1 (**Figure 34A, C**), while in the case of HEL cells the DNA damage was significant at both 5 μ M and 10 μ M of IN1 (**Figure 34C**). Downregulation of UBF was significant after 18 hours of treatment with 10 μ M of IN1 in both DAMI and HEL (**Figure 34A, C**). K562 cells, on the other hand, displayed no significant changes in UBF or γ -H2A.X expression, indicating their higher tolerance on Vp34 inhibition (**Figure 34B**).

This dual approach enabled a more comprehensive characterization of the time- and dose-dependent effects of Vps34 inhibition on the induction of DNA damage (as measured by γ -H2A.X) and UBF downregulation. Notably, DAMI and HEL cells exhibited comparable responses across both treatment conditions, prompting further investigation into potential underlying factors. Given that both cell lines harbor the JAK2 V617F mutation [195, 197, 206], while K562 cells lack this mutation and do not exhibit similar sensitivity to Vps34 inhibition, we can assume that the shared mutational background may contribute to the observed phenotype.

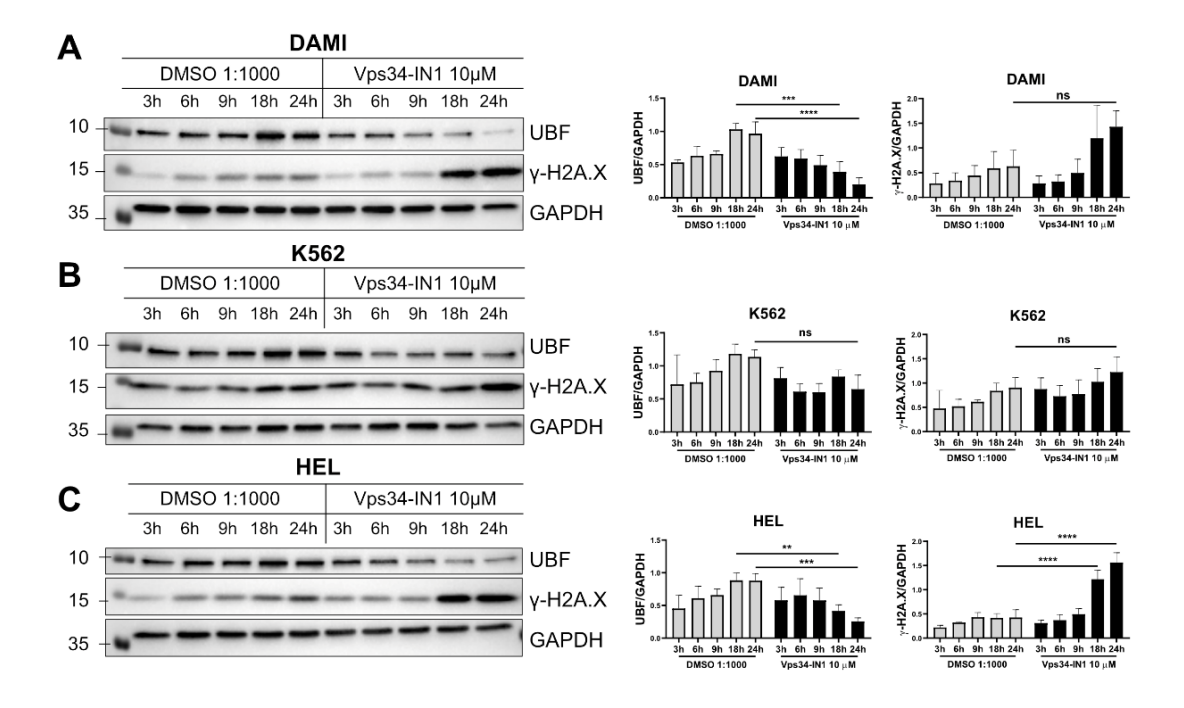


Figure 33. Pharmacological inhibition of Vps34 time-dependently upregulates γ -H2A.X and downregulates UBF in DAMI and HEL cells.

(A) DAMI, (B) K562, and (C) HEL cells were seeded and treated with 10 μ M Vps34-IN1 and lysed at the indicated time points. Cell lysates were analyzed by SDS-PAGE, then blotted onto a nitrocellulose membrane and incubated with the indicated antibodies. Representative immunoblots show expression levels of nucleolar marker (UBF) and DNA damage marker (γ -H2A.X). Blots were analyzed by ImageJ, using GAPDH as a loading control. Graphs represent mean values, with error bars indicating \pm SD from a minimum of three independent experiments. ** p < 0.01, *** p < 0.001, *** p < 0.0001, ns – non-significant

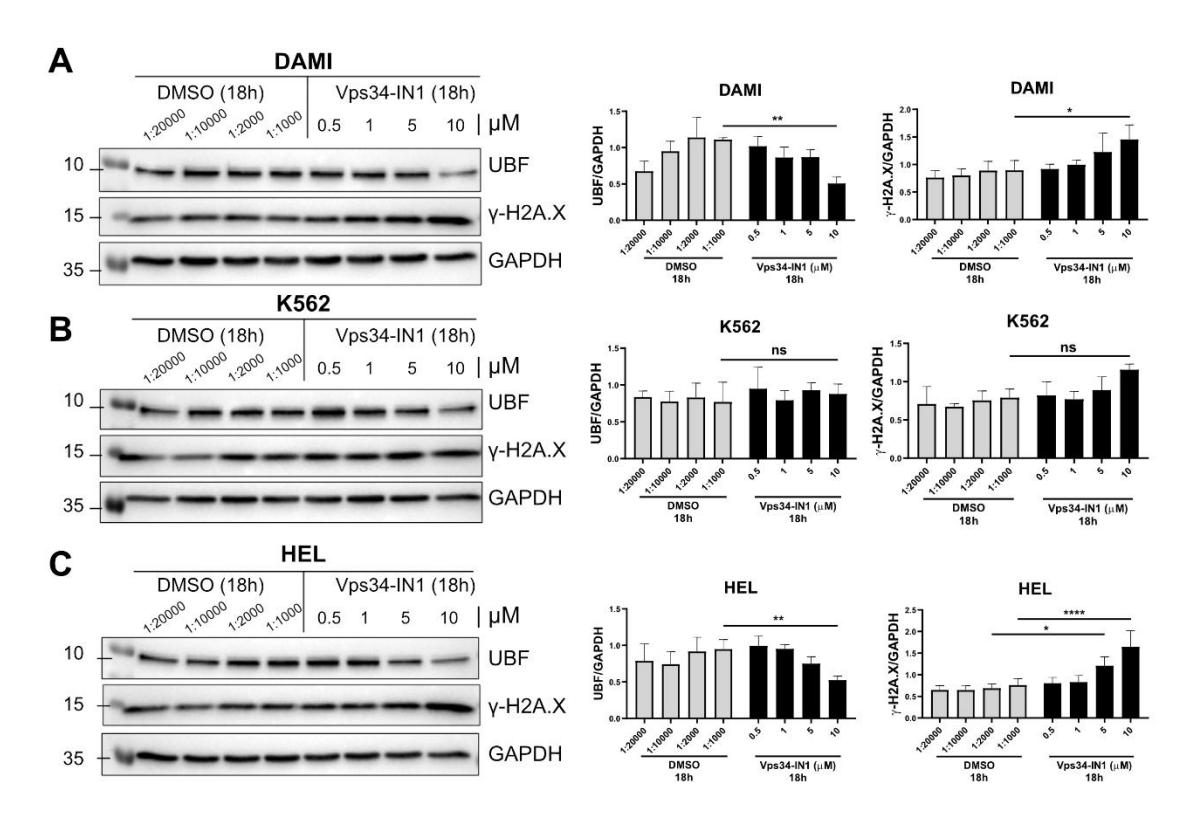


Figure 34. Pharmacological inhibition of Vps34 increases γ -H2A.X and decreases UBF expression in a dose-dependent manner in DAMI and HEL cells.

(A) DAMI, (B) K562, and (C) HEL cells were seeded and treated with indicated concentrations of Vps34-IN1 and lysed after 18h of treatment. Cell lysates were analyzed by SDS-PAGE, then blotted onto a nitrocellulose membrane and incubated with the indicated antibodies. Representative immunoblots show expression levels of nucleolar marker (UBF) and DNA damage marker (γ -H2A.X). Blots were analyzed by ImageJ, using GAPDH as a loading control. Graphs represent mean values, with error bars indicating \pm SD from a minimum of three independent experiments. * p < 0.05, ** p < 0.01, **** p < 0.0001, ns - non-significant

4.5.2. PI3P strongly localizes in the nucleus of cells positive for γ-H2A.X

Considering the γ -H2A.X upregulation in DAMI and HEL cells following Vps34 inhibition, we aimed to investigate the localization of the lipid produced by the kinase, PI3P. We used 10 μ M concentrations of Vps34-IN1 and treated the cells for 18 hours. In parallel, cells were also exposed to UV irradiation for 10 minutes, to induce DNA damage. Then, we processed them according to the protocol for immunostaining of phosphoinositides, as described in Methods.

In DAMI cells, we found PI3P to localize primarily in the cytoplasm, as well as in the nuclear periphery and nucleus, where it was faintly dispersed (Figure 35A). Upon Vps34 inhibition, as expected, we noticed a decline in PI3P in both cytoplasm and nuclei (Figure 35B), and some cells displayed positive y-H2A.X foci in the nucleus, indicating DNA damage sites (Figure 35A). The strong presence of y-H2A.X foci was also evident in the cells exposed to UV radiation. We measured the MFI of y-H2A.X; however, we found no significant difference between experimental conditions (Figure 35C). Interestingly, we found that PI3P was strongly localized in the nucleus of cells containing y-H2A.X foci, showing moderate colocalization, as evidenced by the yellow signals marked in red boxes (Figure 35A). To further characterize the occurrence of γ-H2A.X foci, we divided our cell populations into those positive for γ-H2A.X and those showing no y-H2A.X signal in the nucleus. We then measured the MFI of PI3P and found that, although the difference was not statistically significant, a noticeable trend of higher PI3P MFI was observed in cells positive for y-H2A.X (Figure 35D), supporting previous observations that genotoxic insults can increase PI3P in nuclei. The localization of PI3P in HEL cells was very similar to DAMI, with the lipid mainly localizing in the cytoplasm, but also present in the nuclear periphery and with discreet staining in the nucleus (Figure 35E). When exposed to Vps34-IN1, there was a significant decrease in PI3P MFI levels (Figure 35F), and we found a strong increase of y-H2A.X foci in the nucleus of these cells (Figure 35E). Consistent with our findings in DAMI, PI3P also localized strongly in the nucleus of γ-H2A.Xpositive cells, exhibiting some degree of colocalization, as observed after UV exposure (Figure 35E). Although we did not observe changes in the MFI of y-H2A.X (Figure 35G), when we measured total cell PI3P MFI in y-H2A.X-positive and negative cells, we found significantly higher MFI values of PI3P in cells containing y-H2A.X foci in the nucleus (Figure 35H).

The heightened presence of PI3P in the nuclei of cells undergoing DDR opens up a question on the role of this lipid in DDR and nucleolar stress. Additionally, some cells with a positive γ-H2A.X signal in the nucleus had a stronger presence of PI3P in the nucleus than in the cytoplasm, prompting future analysis into the dynamics of PI3P between multiple cell compartments in cells undergoing DDR.

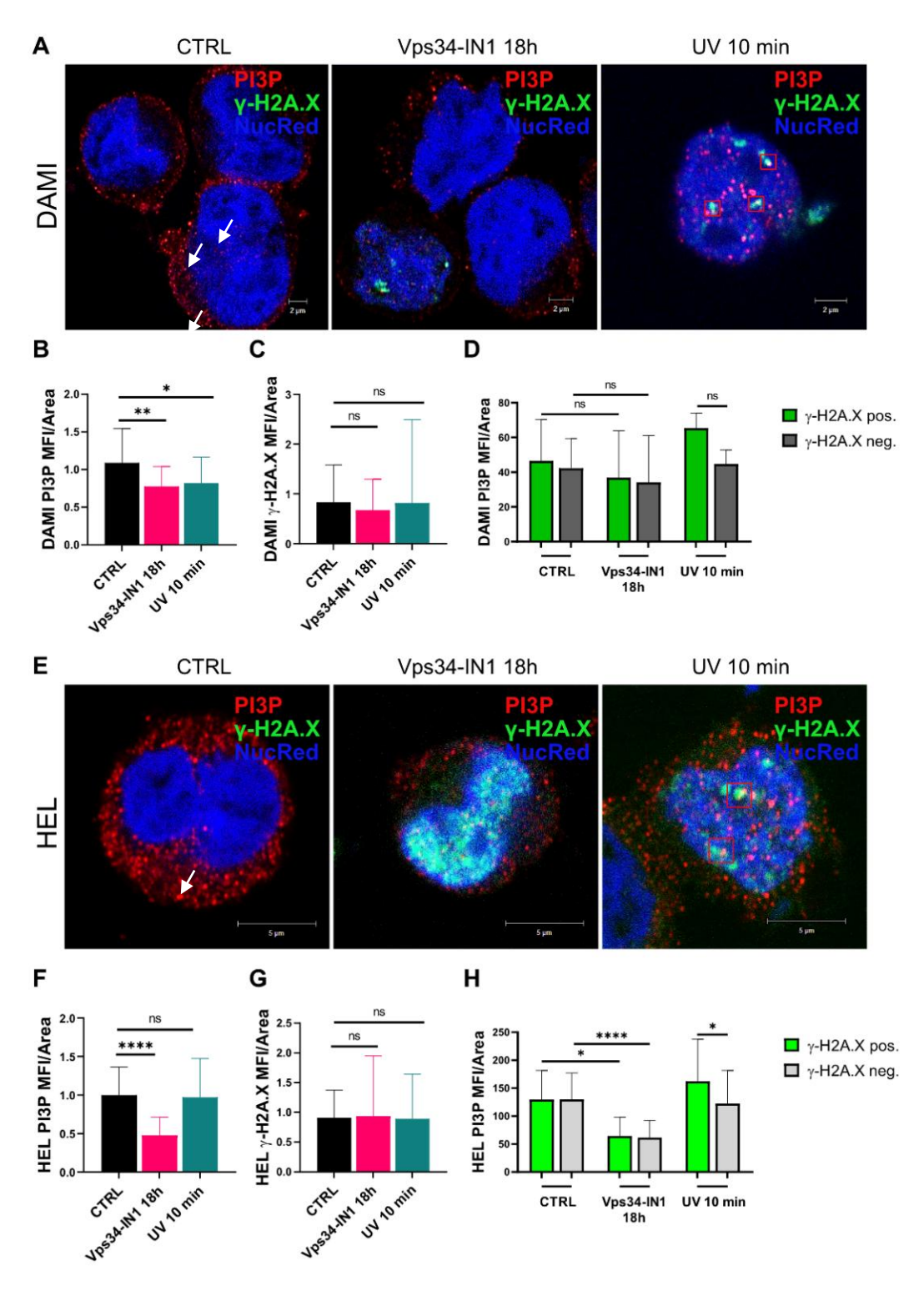


Figure 35. PI3P is present in the nucleus of DAMI and HEL cells undergoing DDR.

(A) DAMI and (E) HEL cells were seeded and treated with 10 μ M Vps34-IN1 (or an appropriate vehicle dilution; CTRL) for 18 hours at 37°C and 5% CO₂. Then, cells were processed for immunofluorescent

staining of phosphoinositides, as described in Methods. In parallel, cells were exposed to UV lamp irradiation for 10 minutes and processed thereafter in the same manner. Cells were imaged using an LSM880 (Carl Zeiss) equipped with a Plan-Apochromat $63\times/1.40$ oil DIC III objective, and representative middle z-plane images are shown. MFI analysis of **(B, F)** PI3P and **(C, G)** γ -H2A.X was performed using Zeiss ZEN Black software and expressed over the total cell area. **(D, H)** DAMI and HEL cells were divided into populations displaying positive γ -H2A.X foci in the nucleus and those with absent γ -H2A.X signal (negative) and the appropriate MFI values were expressed over each experimental condition. Graphs represent mean values, with error bars indicating \pm SD from two independent experiments. A minimum of 20 cells were analyzed per condition. * p < 0.05, ** p < 0.01, **** p < 0.001, **** p < 0.0001, ns - non-significant

4.5.3. Pre-treatment with Vps34 inhibitor attenuates UV-induced DNA damage in DAMI and HEL cells

The induction of DNA damage following Vps34 inhibition alone indicated that disruption of this kinase is sufficient to trigger a DDR. This observation led us to explore how inhibiting Vps34 might modulate the DDR in cells exposed to established DNA-damaging agents.

We pre-treated DAMI, K562, and HEL cells with 10 μ M IN1 for 2 hours and then exposed them to UV radiation as outlined in the Methods. We lysed the cells and performed a Western blot to detect possible changes in total expression of Vps34, nucleolar proteins, and γ -H2A.X (**Figure 36**). Although quantification of immunofluorescence did not show a difference (**Figure 35C, G**), Western blot analysis of all three cell lines revealed a significant upregulation of γ -H2A.X in DMSO-treated (control) cells following UV exposure (**Figure 36A-C**). Surprisingly, in DAMI and HEL cells that were pre-treated with IN1, there was a significant downregulation of γ -H2A.X after UV irradiation (**Figure 36A, C**). This phenotype of DDR was not observed in K562 cells, and there was no significant difference in γ -H2A.X expression (**Figure 36B**).

Short-term UV exposure and/or pre-treatment with IN1 were not sufficient to induce significant changes in Vps34, UBF, or fibrillarin levels. However, the observation that γ -H2A.X expression was downregulated in DAMI and HEL cells pre-treated with IN1 was unexpected, given that Vps34 inhibition alone was sufficient to induce DNA damage (**Figure 33, 34**). We anticipated that this pre-treatment would result in an even greater accumulation of DNA damage; however, this was not observed. Additionally, K562 cells pre-treated with IN1 did not show this attenuation of γ -H2A.X, raising more questions on the potential contribution of the JAK2 mutation to DDR.

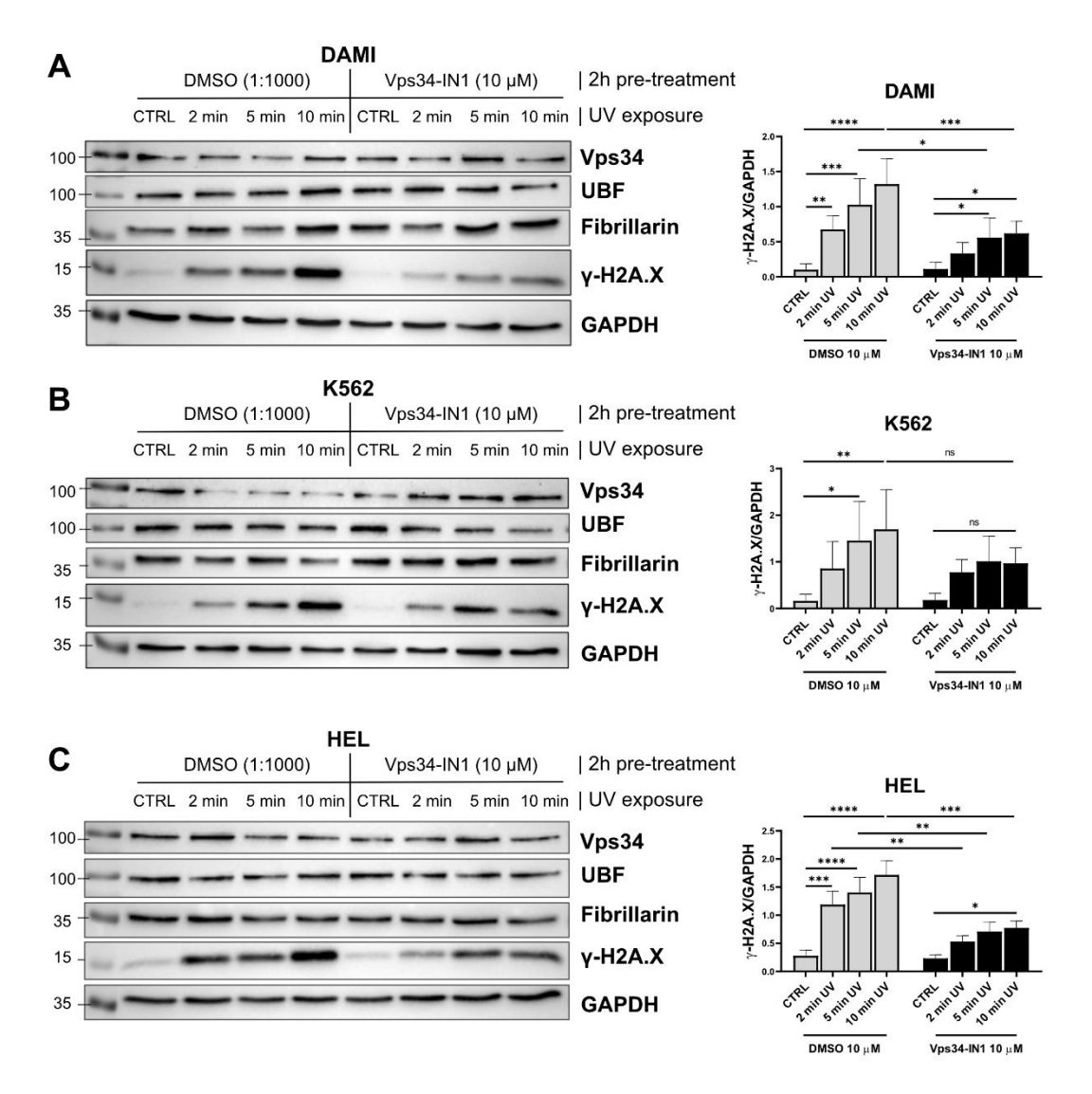


Figure 36. Inhibition of Vps34 prior to UV exposure dampens γ -H2A.X expression in DAMI and HEL cells.

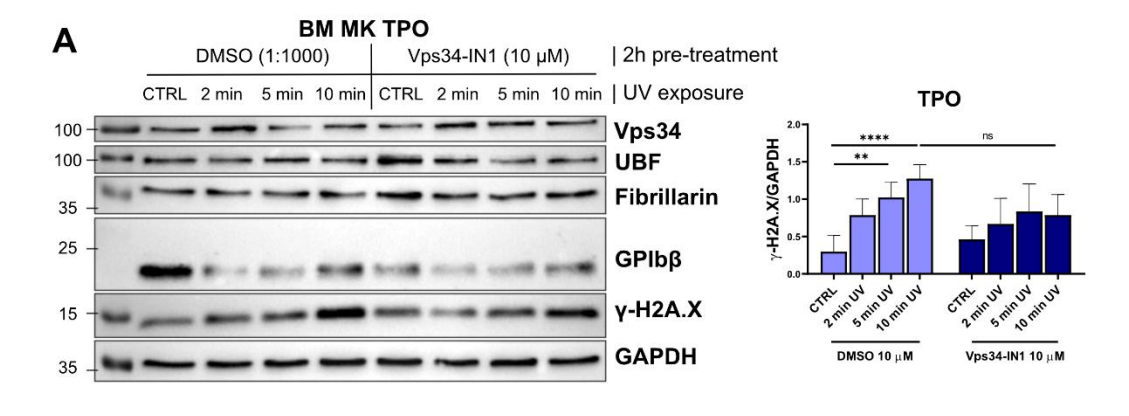
(A) DAMI, (B) K562, and (C) HEL cells were seeded and pre-treated with 10 μ M Vps34-IN1 (or appropriate vehicle dilution of DMSO) for 2 hours at 37°C, 5% CO₂. Then, cells were exposed to UV lamp irradiation for 2, 5, and 10 minutes. After each time point, cells were allowed to recover for 1 hour at 37°C, 5% CO₂. Cells were then lysed, analyzed by SDS-PAGE, then blotted onto a nitrocellulose membrane and incubated with the indicated antibodies. Representative immunoblots show expression levels of Vps34, nucleolar proteins (UBF, fibrillarin), and DNA damage marker (γ-H2A.X). Blots were analyzed by ImageJ, using GAPDH as a loading control. Graphs represent mean values, with error bars indicating ± SD from a minimum of three independent experiments. * p < 0.05, ** p < 0.01, *** p < 0.001, **** p < 0.0001, ns – non-significant

4.5.4. Primary megakaryocytes show a slight reduction in γ-H2A.X levels after Vps34 inhibition and before UV exposure

Given the results we observed in cell lines, our next aim was to investigate whether the modulating effect of Vps34 inhibition on DDR can also be reproduced in primary cells. For this purpose, we used our established model of BM-derived MKs. As we have already characterized a unique maturation phenotype of MKs cultured with IL- 1α in this work, we decided to use both TPO- and TPO/IL- 1α -cultured MKs to gain a better understanding of whether inflammatory insults can also contribute to the DDR.

After three days in culture, MKs were isolated *via* BSA gradient, then pre-treated with 10 μ M Vps34-IN1 and exposed to UV radiation for 2-, 5-, and 10 minutes. Cells were lysed and analyzed by Western blot. We noticed a steady upregulation of γ -H2A.X in control cells in both TPO- and IL-1 α -cultured MKs without a significant difference between the two (**Figure 37A, B**). MKs that were pre-treated with Vps34-IN1 showed a slight increase in γ -H2A.X expression. Although the downregulation of γ -H2A.X was observed in both MK populations with Vps34-IN1, this difference did not reach statistical significance (**Figure 37A, B**). We have also tracked the expression of nucleolar proteins, such as UBF and fibrillarin, as well as the Vps34 kinase, although we did not observe significant changes in their expression.

Primary MKs are physiological models and do not harbour mutations, as opposed to the cell lines we used in previous experiments. The lack of a strong effect with the Vps34 inhibitor in primary MKs, compared to DAMI and HEL cell lines, on DDR could suggest a role for JAK2 in mediating Vps34 signals, as JAK2 V617F is a common mutation in DAMI and HEL cells. Nevertheless, the trend of γ -H2A.X downregulation in which Vps34 was inhibited before DNA damage still warrants further investigation in shedding light on the role of this kinase and its lipid product in DDR.



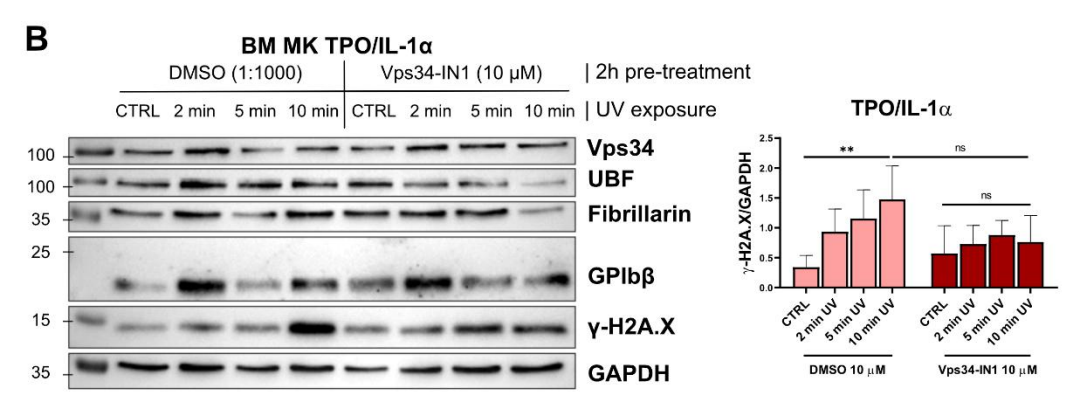


Figure 37. Inhibiting Vps34 before UV exposure slightly reduces γ -H2A.X expression in primary murine megakaryocytes.

BM progenitor cells were isolated and cultured in the presence of either (A) TPO or (B) TPO together with IL-1 α for three days as described in the Methods. Cells were lysed, analyzed by SDS-PAGE, then blotted onto nitrocellulose membranes and incubated with antibodies against nucleolar proteins (UBF, fibrillarin), Vps34, GAPDH, and γ -H2A.X. Blots were analyzed using ImageJ, and GAPDH was used as a loading control. Graphs represent mean values, with error bars indicating \pm SD from five independent experiments. ** p < 0.01, **** p < 0.0001, ns - non-significant

5. DISCUSSION

5.1. INTERLEUKIN-1 ALPHA AS A PROINFLAMMATORY MODULATOR OF MEGAKARYOCYTE MATURATION

Proplatelet formation, driven by extensive microtubular reorganization, is thought to facilitate physiological thrombopoiesis [36, 37, 210]. However, other lines of research propose membrane budding of MKs as the dominant source of platelets under homeostatic conditions [42], supported by other lines of evidence [211, 212]. A recent study has even proposed that MKs develop different types of intravascular protrusions based on the level of platelet demand [213]. Variations in platelet demand are common during inflammation and infection, conditions in which activated platelets are known to mediate cell interactions between immune cells and take part in the innate immune response [6]. Platelet activation can lead to increased platelet consumption and, consequently, thrombocytopenia. Thrombocytopenic conditions were also shown to induce the rupture of MKs [51], an alternative model of platelet release able to rapidly compensate for low platelet counts, mainly through the mediation of the proinflammatory cytokine IL-1 α .

In this thesis, we explored the effects of IL-1 α on early megakaryopoiesis and demonstrated that IL-1 α has a profound impact on MK maturation. We thoroughly characterized the maturation phenotype of BM MKs cultured in the presence of IL-1 α *in vitro*, as well as the functional consequences on molecular profile and platelet production capacity. We have shown that IL-1 α promotes emperipolesis, resulting in MKs with a distinct immune-related proteomic signature.

Our study demonstrated that IL-1 α stimulation resulted in the increased release of PLPs from BM MKs and induced structural changes in the proplatelet shape. Proplatelets from IL-1 α lacked proper branching, were often detached from MK cell bodies, and had noticeably larger tips. While microtubule appearance remained preserved, lining the shafts and ending in coils, some IL-1 α proplatelets displayed thicker shafts. Proteomic analysis revealed a notable rise in β 1-tubulin (Tubb1) expression on day 5 in BM MKs cultured with IL-1 α , consistent with earlier observations in FL MKs [51]. It has been shown that β 1-tubulin dynamics are crucial for proplatelet formation *in vitro* [214]. Therefore, the rise in β 1-tubulin levels might offset the proplatelet formation in IL-1 α MKs. The detection of proplatelet fragments in IL-1 α samples implies these fragments may have detached more readily from MK cell bodies, indicating an increased tendency to break, as previously suggested [51]. Another possibility is that increased PLPs are released directly from MKs *via* membrane rupture. However, we could not observe these membrane changes due

to the absence of high-resolution live cell imaging, and possibly because this process happens quickly [51].

Nishimura *et al.* also showed that IL-1 α induced higher expression of Gata1, caspase-3, and Akt/Erk phosphorylation [51]. At the proteome level, we observed a notable increase in Gata1 and caspase-3 levels in MKs cultured with IL-1 α up to day 5. Moreover, Erk phosphorylation in response to IL-1 α stimulation was significantly higher, while c-Mpl and IL-1R1 levels remained stable. Our findings indicate that Erk activity is essential for proper MK development in response to both TPO and IL-1 α , as inhibiting Erk decreased MK growth and polyploidization, with a stronger effect seen in MKs cultured with IL-1 α .

We also demonstrated that IL-1α-stimulated MKs exhibit distinct morphological and molecular characteristics. They were larger in size and had higher ploidy, features usually indicative of higher levels of maturity. However, they also showed lower expression of hemostatic proteins, such as vWF and GPIbB, that would usually favor immature MKs. In adults, mature MKs are typically large, polyploid cells that express higher levels of maturation markers like the GPIb receptor complex, vWF, and fibrinogen. However, in neonatal and fetal MKs, both in humans and mice, the correlation of the size or ploidy and cytoplasmic maturity is disrupted: fetal/neonatal MKs are smaller with lower ploidy compared to adult MKs, but they still show high levels of cytoplasmic maturation [24]. Recent studies indicate that platelet reactivity decreases in platelets formed during acute thrombocytopenia, accompanied by a reduced response to GPVI [215, 216]. These hyporeactive platelets may be formed during stress thrombopoiesis, consistent with our observations of IL-1α-treated MKs showing reduced expression of hemostatic proteins. Based on recent studies, we propose that IL-1α causes MKs to mature at a faster pace, potentially at the cost of their hemostatic capacity, thereby avoiding hyperreactivity associated with inflammation. The variability in platelet production mechanisms might be a universal feature of all MKs or limited to specific subsets, which requires further research.

Several studies have shown that a subset of HSCs is biased towards MK lineage and is primed for platelet production [217-219]. As previously suggested, extrinsic factors alone can induce a different cell profile, such as MKs found in lungs, which acquire the immune phenotype [220]. MK progenitors have also been identified in the spleen, where splenic megakaryopoiesis is essential during acute systemic inflammation, like sepsis [21]. Authors have demonstrated that IL-3 promotes the maturation of splenic MKs during septic conditions, with MKs exhibiting an immune-related transcriptional profile [221].

In a chronic inflammatory environment, IL-1 β has been shown to contribute to abnormal MK maturation [168]. Earlier studies showed that IL-1 β can increase the number of MKs in the BM and spleen, leading to thrombocytosis in mice [170]. Later, another group of authors studied the impact of IL-1 β on human megakaryocytic cell lines, finding it increases TPO and transcription factors such as c-Jun, c-Fos, GATA-1, and NF-E2 [169]. Our proteomic analysis revealed a significant increase in Runx1 transcription factor levels in IL-1 α -treated MKs on day 3, potentially contributing to the accelerated growth and polyploidy observed in these cells.

IL-1α acts as an early trigger for inflammatory signaling by binding to IL-1R1, similar to IL-1β, and activating downstream pathways such as NF-κB. Additionally, IL-1α stimulation has been shown to increase IL-1β expression, and the reverse can occur in other cells [222]. The mutual sustained expression of IL-1α and IL-1β is mediated by NF-κB signaling [222-224], and NF-κB family members have been reported to be expressed in human MKs and platelets [225]. Our proteomic analyses showed that by day 5 of IL-1α stimulation, NF-κB subunit 100 and IL-1β were significantly more abundant. This indicates activation of NF-κB signaling, likely enhancing IL-1β production to boost the immune response. However, confirmation in future studies is necessary.

Although the BM is generally viewed as an immune-suppressive tissue environment, there is considerable heterogeneity within the MK population, with a notable presence of immune MKs. In humans, a subset of CD148+CD48+ MKs (hBM-MK5, ~7% of MKs) was found to be enriched for immune pathways and expressing chemokines, cytokines, and pathogen-recognition receptors. These cells expand rapidly after bacterial infection or LPS stimulation and localize near neutrophils, suggesting a role in immune surveillance [226]. In mice, an analogous cluster was described (~5% of MKs), marked by CD53, lymphocyte-specific protein 1 (Lsp1), and CD48 expression, predominantly of low-ploidy and regulated by transcription factors PU.1 and IRF8, with transcriptional programs linked to phagocytosis, antigen presentation, and inflammatory signaling [227]. Functionally, murine CD53⁺ MKs can engulf bacteria and stimulate T-cell proliferation, while human CD148+CD48+ MKs show chemokine-mediated neutrophil recruitment and can expand in response to infection [226, 227]. Despite species-specific marker usage (CD148 vs. CD53), both subsets share CD48 expression, infection-driven expansion, and immune functional specialization, supporting the idea of a conserved immune MK lineage distinct from platelet-producing MKs. Our data indicate that on day 3, MKs cultured with IL-1a exhibit high levels of neutrophil-related proteins and antimicrobial peptides, such as Lcn2, S100a9, and Ltf. Previous research has shown that immune MKs, identified by markers like CD148 and CD48, tend to interact more closely with Ly6G-positive neutrophils *in vitro* [9] compared to MKs not expressing these immune receptors. In our study, we observed that Ly6G+ cells were located within IL-1α-cultured MKs, indicating emperipolesis. This process was previously described as an unusual example of multicellular interaction that benefits both MKs and neutrophils [179]. Neutrophils were observed to exchange membrane material with MKs, and this process enhanced platelet production [228]. Interestingly, patients with gray platelet syndrome, a condition marked by bleeding and low platelet counts, exhibited a higher rate of emperipolesis in their human BM [229, 230], and the same was observed in patients with myelofibrosis [231] and immune thrombocytopenia [232].

Proteomic profiling of MKs stimulated with IL-1α for five days revealed that, although not highly emperipoletic, these cells maintained a significantly different abundance of neutrophil-related proteins. MKs and platelets have been previously shown to express some of the neutrophil proteins identified in our proteomic studies, such as CXCL5 or Camp; however, others were not previously reported until now (e.g., Lcn2, Ltf). This suggests that there may be an active protein transfer between neutrophils and MKs within an IL-1α-driven pro-inflammatory environment. Additionally, a recent study employing intravital microscopy demonstrated that neutrophils actively pull on intravascular MK extensions to promote the formation of proplatelets [233]. This interaction was found to be mediated via β2 integrin/ICAM1 interactions, and disrupting this interaction reduced the neutrophil-MK contact and downstream platelet production [233]. Interestingly, in mouse models of vascular injury and inflammation, enhanced neutrophil "plucking" led to elevated platelet output, which in turn resulted in the worsening of cardiovascular complications [233]. Therefore, this neutrophil-driven "plucking" mechanism of platelet release was proposed to be the link between inflammation and enhanced platelet production and, consequently, increased cardiovascular risk.

Our approach has several limitations, primarily the use of an *in vitro* culture system. Conducting inflammation induction with IL-1 α in vivo would provide a more comprehensive understanding of MK maturation and their interactions with neutrophils. However, our advantage was studying the effects of IL-1 α in a controlled setting, ensuring only BM cells responded to the stimuli. This minimized the influence of other peripheral cells, allowing for a detailed examination of IL-1 α -driven changes in MK maturation and function. We demonstrated that IL-1 α 's role goes beyond promoting platelet release; it can also alter the maturation phenotype of BM MKs toward an immune-related profile, increasing emperipolesis and interactions with neutrophils. Overall, our results illuminate the cellular dynamics of MKs during inflammation, showing how IL-1 α -mediated inflammation influences MK maturation.

5.2. THE NUCLEOLUS AND VPS34 IN THE MEGAKARYOCYTE RESPONSE TO INFLAMMATORY-MEDIATED STRESS AND THROMBOCYTOPENIA

MK maturation is accompanied by a massive increase in MK size, significant cytoplasmic expansion, including granule and DMS synthesis [29, 234], as well as nuclear polyploidization that enhances RNA and protein production [235]. Protein synthesis in MKs is tightly coupled to pathways that sense nutrient status, growth factors, and stress signals, all of which are critical for sustaining the high biosynthetic demand of platelet biogenesis. Given the extensive cellular growth that characterizes maturing MKs, we investigated how inflammatory stress and acute platelet demand impact the nucleolus and Vps34 in BM MKs.

Besides their role in platelet production, MKs have been identified as a diverse and heterogeneous cell population, as described in the introduction and the previous section [236]. We have already discussed the role of IL-1α as a modulator of MK maturation, promoting an immune MK phenotype. Under stress conditions such as inflammation and infection, MKs express immune receptors like MHC class II and are capable of secreting cytokines and chemokines, including platelet factor 4 (PF4), TGFβ, and IL-8 [237]. MKs can also sense inflammation through the expression of toll-like receptors (TLRs) [237]. Megakaryocytic cell lines were found to release IL-1α and IL-6, among others, after stimulation [238, 239], while primary human MKs were found to release IL-1a, IL-3, IL-6, and granulocyte-macrophage colonystimulating factor (GM-CSF) even in basal conditions [90]. Additionally, MKs can secrete microparticles rich in protein and RNA, which may result from high protein turnover in MKs as a response to stress stimuli [240-242]. Our research reveals that, in addition to an immune proteomic signature, IL-1α-derived MKs are enriched in ribosomal and nucleolar proteins. We also observed that IL-1α stimulation increases the number of UBF foci, which could suggest enhanced nucleolar activity. However, this needs to be further confirmed by evaluating pre-rRNA transcription.

Vps34 colocalizes with UBF and increases in the nucleolus of IL-1 α -cultured MKs alongside UBF. It has already been demonstrated that Vps34 is vital for normal MK development [68]. An unpublished study by Bertović *et al.* demonstrated that inhibiting Vps34 significantly reduced nascent RNA synthesis and 45S pre-rRNA levels. These findings establish Vps34 as an essential regulator of rRNA transcription and ribosome production in MKs. We also discovered that it contributes to IL-1 α -mediated MK maturation, as its inhibition results in significantly smaller MKs and nucleolar dispersion. This dispersion was evident in both control BM MKs and those treated with IL-1 α . Our immunofluorescence data from IL-1 α -stimulated MKs showed that inflammatory stimuli increased the presence of UBF foci in the nucleus of BM MKs, along with Vps34, and UBF displayed a significantly higher degree of

colocalization with Vps34. We have also noticed changes in the nucleolar morphology, particularly the partial translocation of B23 to the nucleoplasm, in response to IL-1α treatment. In BALB3T3 cells, Bertović *et al.* found PI3P to be present in nucleoplasmic and perinucleolar regions. Several other PI species have already been identified in the nucleolus, as elaborated in the introduction. Notably, PI(4,5)P₂ has been implicated in the regulation of RNA polymerase activity and the organization of nucleolar architecture [86, 243], while PI(3,4,5)P₃ is involved in the recruitment of proteins to the nucleolus [244, 245]. Given the emerging role of Vps34 in regulating rRNA transcription and the dynamic formation of UBF/Vps34 foci following inflammatory stimuli, it is plausible that Vps34, and/or Vps34-derived PI3P, facilitate the recruitment of nucleolar proteins that boost ribosome biogenesis and overall protein synthesis.

Recent studies also highlight the flexible changes in nucleolar structure during inflammation. In macrophages stimulated with LPS, viral mimics like poly I:C, or CpG-DNA, nucleoli merge, grow larger, and decrease in number, all of which revert when the stimulus is removed [117, 118]. This suggests a reversible nucleolar stress response linked to immune activation. In non-dividing monocytes activated with interferon-γ, the authors observed enlarged nucleoli and increased silver-stained NOR signals [246]. These features are common to dividing cells, despite no cell division. These findings imply that NOR activation indicates increased ribosomal gene activity tied to immune function, rather than proliferation.

Given that ribosome production consumes approximately 80% of a cell's total energy, it is tightly regulated and can be influenced by external factors [247-249]. In many cells, external signals and disruptions that lead to cellular stress can often result in growth arrest [250]. This is due to energy conservation, which allows for the activation of other recovery pathways [251]. In contrast, rapidly proliferating cells like hematopoietic, immune, and even cancer cells can respond differently to external stressors and even enhance protein production, thus promoting their growth and expansion [248, 252-255]. In our experiments, we found that IL-1 α stimulation resulted in 26 differentially abundant ribosomal proteins on day 3 of MK culture and 93 ribosomal proteins on day 5. Over 60% of ribosomal proteins differentially abundant in day 3 IL-1 α MKs constitute the large ribosomal subunit, such as Rpl35 and Rpl29.

Furthermore, we have also profiled a number of nucleolar proteins in our proteomic studies and found them also to be highly abundant in IL-1 α MKs, although with a moderate fold-change difference. One of the differentially abundant nucleolar proteins in IL-1 α -stimulated MKs was Noc3I. Noc3I has been implicated in chromatin

organization and the regulation of rDNA transcription [256], suggesting that inflammatory stimulation may enhance nucleolar activity and ribosome biogenesis at early stages of MK maturation. In mature IL-1 α -stimulated MKs (day 5), two nucleolar proteins (Nol8 and Urb1) showed similar differential abundance. These proteins are known to participate in rRNA processing and ribosomal subunit assembly [257, 258], a process that appears responsive to inflammatory stimuli in mature MKs.

In our experiments on cell lines, we noted changes in nucleolar dynamics even under baseline conditions. We observed a significant increase in the number of nucleoli in DAMI and HEL cells during PMA-induced differentiation, which correlated with the increasing ploidy of the cells. Additionally, Vps34 appeared to follow the nucleolar dynamics and was found in the nucleolus throughout the proliferation and differentiation of the cell lines. Furthermore, it exhibited a low but comparable degree of colocalization with UBF and B23 in differentiated DAMI and HEL cells.

Another feature we have observed is aberrant UBF staining present in the nucleoplasm. Compared to primary MKs, which harboured discreet UBF foci, often grouped in clusters, our megakaryocytic cell lines (DAMI, K562, and HEL) demonstrated a diffused UBF signal throughout the nucleoplasm. This is consistent with several studies on leukemic and cancer cell lines, such as in cell lines harbouring B23 mutations, which show disrupted nucleolar architecture characterized by loss of the nucleolar rim structure, distorted shape, and formation of protein aggregates [259]. A large-scale imaging screen, even in untreated conditions, reveals that colorectal carcinoma cell lines such as HCT116 and DLD1 maintain larger and more amorphous nucleoli [260]. Additionally, in small cell lung cancer (SCLC) lines, fast-growing high-MYC expression cell lines display prominent and enlarged nucleoli at baseline, contrasting with slow-growing lines that have small, inconspicuous nucleoli [261].

Although some of the observed nucleolar alterations under baseline conditions may stem from the malignant nature of the megakaryocytic cell lines used in our model, additional stimuli likely contribute to the dynamic changes in nucleolar activity. Colchicine-induced polyploidization in megakaryocytic cell lines such as DAMI, HEL, and K562 showed a notable increase (up to about 5.6-fold) in AgNOR counts, signifying heightened rDNA transcription during endomitotic DNA replication [262]. It is intriguing to speculate that IL-1 α stimulation triggers early polyploidization in MKs and that the resulting genomic amplification enhances the number of active NORs, thereby increasing UBF foci. Our data clearly demonstrates that IL-1 α -treated MKs exhibit significantly higher ploidy levels than TPO MKs. A study in yeast

demonstrated that the RNA Pol I transcription rate increases proportionally with genome copy number and cell size in polyploid cells [263]. Multiple tumour analyses have revealed that aneuploid or polyploid cancers exhibit higher AgNOR staining, reflecting increased numbers of NOR-bearing chromosomes and NORs [264]. In breast cancer models, more aggressive (high-ploidy or high-growth) cell lines show increased average number and size of nucleoli, higher rates of ribosome biogenesis measured by [³H]-uridine uptake, and more fibrillar centers per nucleolus, which collectively indicate enhanced rDNA transcription and processing machinery [265]. Therefore, the connection between polyploidy, increased NOR activity, and likely higher ribosomal output provides a plausible mechanism in favor of heightened platelet production during IL-1α-mediated stress thrombopoiesis and acute platelet demand.

Thrombocytopenia refers to a condition characterized by low circulating platelet counts, defined as $< 150 \times 10^9 / L$ [266, 267]. It can arise as a symptom of various underlying disorders or as an independent clinical entity. We have already elaborated on how thrombocytopenia can occur as a symptom of acute inflammation, and other studies also highlight its association with infections [268]. The pathophysiology of thrombocytopenia often involves impaired platelet production as well as increased platelet destruction and/or sequestration. Given the pressure thrombocytopenia exerts on MKs to meet the body's demand for platelets, we can consider it as a source of cellular stress.

In our *in vivo* model of acute platelet depletion, we observed a transient reduction in nuclear Vps34 MFI at 6 hours post-depletion, followed by normalization by 24 hours. This dynamic localization, especially given that the total Vps34 signal was elevated at all time points, could suggest active shuttling of Vps34 between cytoplasm and nucleus in MKs. Although we were unable to stain for nucleolar-specific markers, the Vps34 signal diffusely filled nuclear regions devoid of DAPI, which likely correspond to nucleoli, suggesting localization within or around these organelles in MKs. Vps34 and PI3P nuclear localization has been demonstrated in primary MKs and other cell types by our laboratory (Bertović *et al*, unpublished), and nuclear PI3P has been observed previously in other cells [82, 93, 153, 154]. Acute platelet loss may elevate ribosomal demands in MKs to accelerate platelet production, thus triggering nucleolar stress signaling mediated *via* nuclear Vps34/PI3P. PI3P is known to recruit a variety of FYVE and PX domain-containing effectors, which are core regulators of autophagy and stress adaptation pathways [269, 270], and it has been shown to increase in the nuclei of cells under genotoxic stress [158].

Another observation we have made is the transient drop in MK size 24 hours after platelet depletion. Since platelet production relies on MKs, thrombocytopenic conditions may alter MK numbers and morphology in the BM. Although in immune thrombocytopenia (ITP) BM examinations are often inconclusive, there are cases where the number of MKs is increased [271]. This could be in support of our observation, potentially indicating the presence of immature MKs that are rapidly maturing in order to compensate for low platelet levels.

Our data suggest that nucleolar activity in MKs may be increased under inflammatory and regenerative stress, potentially leading to enhanced ribosome production that meets the needs of increased platelet production. IL-1α-stimulated MKs show elevated UBF and Vps34 nuclear foci, while Vps34 inhibition disperses these foci, further supporting its role in nucleolar organization. Differentiation of DAMI and HEL cells increases the nucleolar number and colocalization of UBF/Vps34. Leukemic cells show basal nucleolar disruption, emphasizing the changes in nucleolar architecture in disease. *In vivo*, platelet depletion transiently reduces MK size and increases Vps34 in BM MKs, suggesting a role for Vps34 in the thrombocytopenic stress response. These findings propose that Vps34 is involved in nucleolar dynamics during stress megakaryopoiesis, though the exact mechanisms remain to be clarified and researched further.

5.3. VPS34 ACTIVITY MODULATES THE DNA DAMAGE RESPONSE TO GENOTOXIC INSULTS IN MEGAKARYOCYTES

Megakaryopoiesis is closely linked with DDR signaling, which plays a role in both maintaining genomic integrity in normal conditions, as well as in guiding cell commitment and maturation into the MK lineage [272].

Studies in murine HSCs show that even moderate DNA damage and the resulting activation of the G₂-M checkpoint are enough to prime these cells toward becoming MKs. This process triggers the expression of key markers like CD41 and GATA-1 and initiates endomitotic differentiation, bypassing the need for intermediate progenitor stages [273]. This "damage-priming" mechanism likely plays an essential role in helping the body quickly restore platelets after myelosuppressive injury. Newer studies have also proposed how moderate DNA damage in MKs and their progenitors enhances megakaryopoiesis and increases platelet production in vivo [274]. This may also help explain the expansion of MK-HSC during aging, which is closely linked to the accumulation of DNA damage [275]. In parallel, TPO primes HSCs metabolically by boosting mitochondrial activity and managing reactive oxygen species [276]. This enhances cell survival and steers differentiation toward the MK lineage, both under normal conditions and in response to stress [276]. This metabolic activation probably affects the cell's redox balance and causes mild replication stress, which then activates the DDR pathways. Within the BM environment, mature MKs also play a supportive role for stressed HSCs by secreting niche factors, extracellular vesicles, and cytokines that help maintain stem cell quiescence, as well as manage local oxidative and replicative stress levels [272].

Given the supporting role of DDR pathways in regulating MK lineage commitment and maturation, it is important to consider the broader molecular networks that intertwine with DDR machinery. While historically associated with cytoplasmic membrane dynamics, recent studies have revealed that PI metabolism extends into the nucleus [277, 278]. In this thesis, we examined the potential role of Vps34 and PI3P in DDR and their influence on DDR in DAMI, K562, and HEL cells, as well as primary MKs.

Nuclear PIs dynamically accumulate at sites of DNA damage and actively regulate DDR signaling cascades. Sequestering nuclear PI species, such as PI(4,5)P2 or PI(3,4,5)P3, impairs ATR/ATRIP recruitment and downstream Chk1 activation, even when upstream RPA binding remains intact [89, 154, 279]. PI(3,4,5)P3 localizes to the nucleolus and interacts with DNA damage-responsive proteins like PARP1 through basic lysine-rich motifs [279]. Interestingly, recent evidence demonstrates that Vps34-generated PI3P binds directly to the repair endonuclease FEN1 (*via* its

R378 residue), facilitating FEN1 recruitment to DNA lesions and promoting efficient double-strand break repair [280]. Loss of this Vps34-Pl3P-FEN1 axis sensitizes cells to genotoxic stress and disrupts chromosomal stability [280].

On the other hand, nucleolar stress, which is often triggered by rDNA damage or suppression of Pol I transcription, shuts down ribosome biogenesis and redistributes nucleolar proteins such as B23 and Treacle, initiating a nucleolar DDR program that includes p53 activation or induction of autophagy [281-283]. However, nucleolar protein redistribution is not limited to B23. For instance, treatment of RPE-1 and cancer cell lines with Pol I inhibitors like CX-5461 or flavopiridol triggers a distinctive nucleolar stress state. UBF redistributes into peripheral stress caps, disengages from rDNA promoters, and transcription halts, even though total UBF protein levels remain largely unchanged under short-term exposure [260]. In a different stress setting, under conditions such as UV or oxidative stress, the intracellular domain (ICD) of β-dystroglycan is released from the membrane, enters the nucleus, and accumulates in the nucleolus [284]. There, it binds UBF and B23, reduces UBF levels, disrupts rRNA transcription, and alters nucleolar structure, acting as a regulator of nucleolar stress [284]. Additionally, partial knockdown of UBF itself mimics nucleolar perturbation by activating cytosolic stress signaling via NF-κB and provoking p53-mediated cell-cycle arrest [285].

Interestingly, we found that inhibition of Vps34 in DAMI and HEL cells causes accumulation of γ -H2A.X and progressive downregulation of UBF, which could be indicative of DNA damage-associated nucleolar stress. The intense nuclear PI3P signal co-localizing with γ -H2A.X foci may suggest that Vps34-generated PI3P could serve as a scaffold for repair complexes. When Vps34 is inhibited before UV exposure, the downregulation of γ -H2A.X implies that PI3P is required not only for damage sensing but also to sustain DDR signaling.

Intriguingly, we observed some discrepancies between Western blot and immunofluorescence assessments of γ -H2A.X in DAMI, K562, and HEL cell lines. Western blot consistently revealed high upregulation of γ -H2A.X, whereas in immunofluorescence, we did not observe a related increase in γ -H2A.X foci in the same cells. This discrepancy likely reflects inherent methodological differences. Western blot measures cumulative γ -H2A.X protein across the entire cell population, while immunofluorescence relies on visually detectable, spatially clustered foci. In leukemic contexts, where basal DNA damage may be present, Western blot provides greater sensitivity than foci counting. This interpretation is supported by literature in hematologic malignancies, where high basal γ -H2A.X levels detected by Western blot often correspond to ongoing replication stress and chromosomal instability, even

when discrete foci are sparse or absent by microscopy [286-289]. Other authors also emphasize how γ -H2A.X is commonly phosphorylated under various physiological conditions, including endogenous oxidative stress, replication-associated lesions, hypoxia, and cellular aging, generating a detectable basal γ -H2A.X level even in the absence of external damage [290, 291]. Collectively, this highlights methodological limitations in γ -H2A.X detection: while immunofluorescence foci enumeration is highly sensitive at low damage levels, it may fail when the γ -H2A.X signal is diffuse or widespread. In contrast, Western blotting provides higher sensitivity to overall phosphorylation but lacks spatial resolution.

Given that γ-H2A.X upregulation and UBF downregulation following Vps34 inhibition occurred in DAMI and HEL cells, but not significantly in K562 cells or primary MKs, we hypothesized that the genetic background of these cell lines may play a role. The differential sensitivity of DAMI and HEL cells (both harboring JAK2 mutations) versus K562 cells (JAK2 wild-type) to Vps34 inhibition highlights the potential interaction between JAK2-mediated signaling and DDR.

study demonstrates that JAK2-V617F mutations, One characteristic myeloproliferative neoplasms (MPNs), induce replication stress and DNA doublestrand breaks [292]. In response, cells upregulate the DNA helicase RECQL5 via JAK2-Pl3K signaling, which is essential to maintain genomic stability [292]. Knockdown of RECQL5 in JAK2-V617F tumor cells increases sensitivity to hydroxyurea and other replication stressors, leading to fork stalling, increased y-H2A.X, and apoptosis [292]. In primary MPN models, despite JAK2-driven proliferative and inflammatory signaling, basal DDR markers such as y-H2A.X and phospho-ATR remain low, likely due to compensatory mechanisms [293]. The upregulation of DUSP1, a member of dual-specificity MAPK phosphatases and a negative regulator of MAPK signaling in mammalian cells, and RECQL5 keeps reactive oxygen species and DNA stress under control [293]. DDR markers increase only during progression to myelofibrosis [293], implying that protective feedback is gradually lost as the disease advances. Another study shows that JAK2-V617Fexpressing progenitors depend on DUSP1 to suppress DDR activation under oxidative and inflammatory stress [294]. Inhibition of DUSP1 in HEL cells triggers JNK/p38 reactivation, increases y-H2A.X foci, and apoptosis [294].

In this context, our finding that Vps34 inhibition significantly upregulates γ -H2A.X and downregulates UBF in DAMI and HEL cells (but not in K562) suggests that JAK2-mutant cells rely more critically on Vps34-mediated PI3P signaling to buffer intrinsic DNA damage and preserve nucleolar integrity. This reliance may arise from the pre-existing replication stress caused by JAK2 activation, which renders these

cells more susceptible when essential nuclear repair mechanisms are disrupted. The fact that UBF suppression accompanies γ -H2A.X induction supports a nucleolar DDR model, where rDNA transcription is halted as damage signaling is activated. Building on this, previous studies have shown that Vps34 inhibition in acute myeloid leukemia impairs autophagy, vesicular trafficking, and mTORC1 signaling, selectively inducing apoptosis in malignant cells while sparing normal hematopoietic progenitors, highlighting VPS34 as a potential therapeutic target [187]. Additionally, the broader role of autophagy in cancer emphasizes that modulating these pathways can influence tumor progression and therapeutic response [295]. Neither study specifically monitored DNA damage, so combining DNA damage and nucleolar stress, as we have done with γ H2A.X and UBF, could provide useful insight into cancer cell vulnerability and provide a platform for future mechanism-based treatments.

6. CONCLUSIONS

In our experiments on the effect of IL-1 α on MKs and MK maturation, we found:

- TPO and IL-1α stimulation produced larger MKs of higher ploidy, with shorter and less branched proplatelets, and released more numerous and larger PLPs.
- Hemostatic protein downregulation (vWF, GPIbβ, GPIbα, GPIX) was confirmed across multiple methods, showing robust, matrix-independent effects.
- IL-1α promoted MK maturation through enhanced Erk-MAPK signaling without changing receptor expression; Erk inhibition reduced MK size and ploidy, confirming pathway involvement.
- IL-1α increased emperipolesis in immature MKs with numerous internalized neutrophils, and proteomics showed downregulation of platelet proteins and upregulation of neutrophil-related proteins like CXCL5, lactoferrin, cathelicidin, S100a9, and lipocalin-2, inducing an inflammatory shift.

Our work on the nucleolar characterization and the role of Vps34 in nucleolar stress revealed:

- IL-1α increased ribosomal and nucleolar activity in MKs, with proteomic data pointing to abundant ribosomal proteins in immature and mature MKs.
- Vps34 colocalized with UBF in nucleoli, and IL-1α boosted nucleolar Vps34 and UBF foci, indicating heightened nucleolar function under inflammation.
- Vps34 inhibition (IN1) impaired MK growth, reduced size, and disrupted nucleolar foci, showing that Vps34 supports nucleolar integrity.
- In vivo, Vps34 was found in the nucleoli of BM MKs, and platelet depletion in mice caused a transient MK size reduction and increased the cytoplasmic pool of Vps34, confirming the importance of Vps34 during thrombocytopenic stress.
- DAMI, K562, and HEL cell lines and mononuclear cells also showed Vps34 in nucleoli with UBF and B23, demonstrating similarity in localization across different cell types; Differentiation increased cell ploidy, nucleolar number, and nuclear Vps34 foci, though leukemic cells displayed distinct nucleolar stress phenotypes.

Our experiments on the role of Vps34 in the DDR:

- Vps34 inhibition upregulated γ-H2A.X and downregulated UBF in DAMI and HEL, but not in K562, showing cell line-specific sensitivity
- PI3P localized in nuclei of cells with γ-H2A.X foci.
- Vps34 inhibition before UV exposure reduced γ-H2A.X expression in DAMI and HEL but not in K562, suggesting JAK2-based DDR modulation.

7. REFERENCES

- 1. Orkin, S.H. and L.I. Zon, *Hematopoiesis: an evolving paradigm for stem cell biology.* Cell, 2008. **132**(4): p. 631-44.
- 2. Quach, M.E., W. Chen, and R. Li, *Mechanisms of platelet clearance and translation to improve platelet storage*. Blood, 2018. **131**(14): p. 1512-1521.
- 3. Versteeg, H.H., et al., *New fundamentals in hemostasis*. Physiol Rev, 2013. **93**(1): p. 327-58.
- 4. Bye, A.P., A.J. Unsworth, and J.M. Gibbins, *Platelet signaling: a complex interplay between inhibitory and activatory networks.* J Thromb Haemost, 2016. **14**(5): p. 918-30.
- 5. van der Meijden, P.E.J. and J.W.M. Heemskerk, *Platelet biology and functions: new concepts and clinical perspectives.* Nat Rev Cardiol, 2019. **16**(3): p. 166-179.
- 6. Semple, J.W., J.E. Italiano, Jr., and J. Freedman, *Platelets and the immune continuum.* Nat Rev Immunol, 2011. **11**(4): p. 264-74.
- 7. Shannon, O., *The role of platelets in sepsis.* Res Pract Thromb Haemost, 2021. **5**(1): p. 27-37.
- 8. Smyth, S.S., et al., *Platelet functions beyond hemostasis*. J Thromb Haemost, 2009. **7**(11): p. 1759-66.
- 9. Morrell, C.N., et al., *Emerging roles for platelets as immune and inflammatory cells*. Blood, 2014. **123**(18): p. 2759-67.
- 10. Zhou, L., et al., *The critical role of platelet in cancer progression and metastasis*. Eur J Med Res, 2023. **28**(1): p. 385.
- 11. Ebaugh, F.G., Jr. and R.M. Bird, *The normal megakaryocyte concentration in aspirated human bone marrow.* Blood, 1951. **6**(1): p. 75-80.
- 12. Doulatov, S., et al., *Hematopoiesis: a human perspective.* Cell Stem Cell, 2012. **10**(2): p. 120-36.
- 13. Noetzli, L.J., S.L. French, and K.R. Machlus, *New Insights Into the Differentiation of Megakaryocytes From Hematopoietic Progenitors*. Arterioscler Thromb Vasc Biol, 2019. **39**(7): p. 1288-1300.
- 14. Behrens, K. and W.S. Alexander, *Cytokine control of megakaryopoiesis*. Growth Factors, 2018. **36**(3-4): p. 89-103.
- 15. de Sauvage, F.J., et al., Stimulation of megakaryocytopoiesis and thrombopoiesis by the c-Mpl ligand. Nature, 1994. **369**(6481): p. 533-8.
- 16. Li, J., Y. Xia, and D.J. Kuter, *Interaction of thrombopoietin with the platelet c-mpl receptor in plasma: binding, internalization, stability and pharmacokinetics*. Br J Haematol, 1999. **106**(2): p. 345-56.

- 17. Long, M.W., N. Williams, and S. Ebbe, *Immature megakaryocytes in the mouse: physical characteristics, cell cycle status, and in vitro responsiveness to thrombopoietic stimulatory factor.* Blood, 1982. **59**(3): p. 569-75.
- 18. Michelson, A.D., *Platelets*. 2019: Academic Press.
- 19. Lindemann, A., et al., *Biologic effects of recombinant human interleukin-3 in vivo.* J Clin Oncol, 1991. **9**(12): p. 2120-7.
- 20. Burstein, S.A., *Effects of interleukin 6 on megakaryocytes and on canine platelet function.* Stem Cells, 1994. **12**(4): p. 386-93.
- 21. Lazzari, L., et al., Interleukin-6 and interleukin-11 act synergistically with thrombopoietin and stem cell factor to modulate ex vivo expansion of human CD41+ and CD61+ megakaryocytic cells. Haematologica, 2000. **85**(1): p. 25-30.
- 22. Turner, K.J., et al., *The role of recombinant interleukin 11 in megakaryocytopoiesis*. Stem Cells, 1996. **14 Suppl 1**: p. 53-61.
- 23. Nagata, Y., Y. Muro, and K. Todokoro, *Thrombopoietin-induced polyploidization of bone marrow megakaryocytes is due to a unique regulatory mechanism in late mitosis.* J Cell Biol, 1997. **139**(2): p. 449-57.
- 24. Davenport, P., Z.J. Liu, and M. Sola-Visner, *Changes in megakaryopoiesis over ontogeny and their implications in health and disease.* Platelets, 2020. **31**(6): p. 692-699.
- 25. Bluteau, D., et al., Regulation of megakaryocyte maturation and platelet formation. J Thromb Haemost, 2009. **7 Suppl 1**: p. 227-34.
- 26. Ravid, K., et al., *Roads to polyploidy: the megakaryocyte example.* J Cell Physiol, 2002. **190**(1): p. 7-20.
- 27. Raslova, H., et al., *Megakaryocyte polyploidization is associated with a functional gene amplification.* Blood, 2003. **101**(2): p. 541-4.
- 28. Yamada, E., *The fine structure of the megakaryocyte in the mouse spleen.* Acta Anat (Basel), 1957. **29**(3): p. 267-90.
- 29. Eckly, A., et al., *Biogenesis of the demarcation membrane system (DMS) in megakaryocytes*. Blood, 2014. **123**(6): p. 921-30.
- 30. Gerrard, J.M., et al., Localization of platelet prostaglandin production in the platelet dense tubular system. Am J Pathol, 1976. **83**(2): p. 283-98.
- 31. Handagama, P.J., et al., *Incorporation of a circulating protein into megakaryocyte and platelet granules.* Proc Natl Acad Sci U S A, 1987. **84**(3): p. 861-5.
- 32. Jones, O.P., *Origin of megakaryocyte granules from Golgi vesicles*. Anat Rec, 1960. **138**: p. 105-13.

- 33. Battinelli, E.M., et al., *Megakaryocytes package contents into separate alpha-granules that are differentially distributed in platelets.* Blood Adv, 2019. **3**(20): p. 3092-3098.
- 34. Heijnen, H.F., et al., *Multivesicular bodies are an intermediate stage in the formation of platelet alpha-granules.* Blood, 1998. **91**(7): p. 2313-25.
- Wright, J.H., *The Origin and Nature of the Blood Plates.* Boston Med Surg J, 1906. **154**: p. 643-645.
- 36. Italiano, J.E., Jr., et al., *Blood platelets are assembled principally at the ends of proplatelet processes produced by differentiated megakaryocytes.* J Cell Biol, 1999. **147**(6): p. 1299-312.
- 37. Patel, S.R., J.H. Hartwig, and J.E. Italiano, Jr., *The biogenesis of platelets from megakaryocyte proplatelets*. J Clin Invest, 2005. **115**(12): p. 3348-54.
- 38. Thon, J.N., et al., *Cytoskeletal mechanics of proplatelet maturation and platelet release.* J Cell Biol, 2010. **191**(4): p. 861-74.
- 39. Kemble, S., et al., *Analysis of preplatelets and their barbell platelet derivatives by imaging flow cytometry.* Blood Adv, 2022. **6**(9): p. 2932-2946.
- 40. Zhao, X., et al., *Highly efficient platelet generation in lung vasculature reproduced by microfluidics*. Nat Commun, 2023. **14**(1): p. 4026.
- 41. Furniss, J.A., N. Tarassova, and A.W. Poole, *Platelet generation in vivo and in vitro*. Blood, 2024. **144**(22): p. 2283-2294.
- 42. Potts, K.S., et al., *Membrane budding is a major mechanism of in vivo platelet biogenesis*. J Exp Med, 2020. **217**(9).
- 43. Ihzumi, T., et al., *Megakaryocyte and platelet formation: a scanning electron microscope study in mouse spleen.* Arch Histol Jpn, 1977. **40**(4): p. 305-20.
- 44. Italiano, J.E., et al., *Microvesicles, but not platelets, bud off from mouse bone marrow megakaryocytes.* Blood, 2021. **138**(20): p. 1998-2001.
- 45. Kosaki, G., *Platelet production by megakaryocytes: protoplatelet theory justifies cytoplasmic fragmentation model.* Int J Hematol, 2008. **88**(3): p. 255-267.
- 46. Lefrancais, E., et al., *The lung is a site of platelet biogenesis and a reservoir for haematopoietic progenitors.* Nature, 2017. **544**(7648): p. 105-109.
- 47. Kosaki, G., *In vivo platelet production from mature megakaryocytes: does platelet release occur via proplatelets?* Int J Hematol, 2005. **81**(3): p. 208-19.
- 48. Ouzegdouh, Y., et al., *The physical and cellular conditions of the human pulmonary circulation enable thrombopoiesis.* Exp Hematol, 2018. **63**: p. 22-27 e3.
- 49. Zucker-Franklin, D. and S. Petursson, *Thrombocytopoiesis--analysis by membrane tracer and freeze-fracture studies on fresh human and cultured mouse megakaryocytes.* J Cell Biol, 1984. **99**(2): p. 390-402.

- 50. Zucker-Franklin, D. and C.S. Philipp, *Platelet production in the pulmonary capillary bed: new ultrastructural evidence for an old concept.* Am J Pathol, 2000. **157**(1): p. 69-74.
- 51. Nishimura, S., et al., *IL-1alpha induces thrombopoiesis through megakaryocyte rupture in response to acute platelet needs.* J Cell Biol, 2015. **209**(3): p. 453-66.
- 52. Cavalli, G., et al., *Interleukin 1alpha: a comprehensive review on the role of IL-1alpha in the pathogenesis and treatment of autoimmune and inflammatory diseases*. Autoimmun Rev, 2021. **20**(3): p. 102763.
- 53. Garlanda, C., C.A. Dinarello, and A. Mantovani, *The interleukin-1 family: back to the future.* Immunity, 2013. **39**(6): p. 1003-18.
- 54. Kaneko, N., et al., *The role of interleukin-1 in general pathology.* Inflamm Regen, 2019. **39**: p. 12.
- 55. Chiu, J.W., et al., *IL-1alpha Processing, Signaling and Its Role in Cancer Progression*. Cells, 2021. **10**(1).
- 56. Li, Y. and Q. Jiang, *Uncoupled pyroptosis and IL-1beta secretion downstream of inflammasome signaling.* Front Immunol, 2023. **14**: p. 1128358.
- 57. Huang, M., et al., *Interleukins in Platelet Biology: Unraveling the Complex Regulatory Network.* Pharmaceuticals (Basel), 2024. **17**(1).
- 58. Burzynski, L.C., et al., *The Coagulation and Immune Systems Are Directly Linked through the Activation of Interleukin-1alpha by Thrombin.* Immunity, 2019. **50**(4): p. 1033-1042 e6.
- 59. Luis, T.C., et al., *Perivascular niche cells sense thrombocytopenia and activate hematopoietic stem cells in an IL-1 dependent manner.* Nat Commun, 2023. **14**(1): p. 6062.
- 60. Lolicato, F., et al., *Phosphoinositide switches in cell physiology From molecular mechanisms to disease.* J Biol Chem, 2024. **300**(3): p. 105757.
- 61. Falkenburger, B.H., et al., *Phosphoinositides: lipid regulators of membrane proteins.* J Physiol, 2010. **588**(Pt 17): p. 3179-85.
- 62. Posor, Y., W. Jang, and V. Haucke, *Phosphoinositides as membrane organizers*. Nat Rev Mol Cell Biol, 2022. **23**(12): p. 797-816.
- 63. Ohashi, Y., *Activation Mechanisms of the VPS34 Complexes.* Cells, 2021. **10**(11).
- 64. Ohashi, Y., S. Tremel, and R.L. Williams, *VPS34 complexes from a structural perspective.* J Lipid Res, 2019. **60**(2): p. 229-241.
- 65. Rostislavleva, K., et al., Structure and flexibility of the endosomal Vps34 complex reveals the basis of its function on membranes. Science, 2015. **350**(6257): p. aac7365.

- 66. Liu, Y., et al., *Targeting VPS34 in autophagy: An update on pharmacological small-molecule compounds.* Eur J Med Chem, 2023. **256**: p. 115467.
- 67. Severin, S., et al., *Phosphoinositides take a central stage in regulating blood platelet production and function.* Adv Biol Regul, 2024. **91**: p. 100992.
- 68. Bertovic, I., et al., *Vps34 derived phosphatidylinositol 3-monophosphate modulates megakaryocyte maturation and proplatelet production through late endosomes/lysosomes.* J Thromb Haemost, 2020. **18**(7): p. 1756-1772.
- 69. Valet, C., et al., A dual role for the class III PI3K, Vps34, in platelet production and thrombus growth. Blood, 2017. **130**(18): p. 2032-2042.
- 70. Mujalli, A., et al., *Profiling of phosphoinositide molecular species in human and mouse platelets identifies new species increasing following stimulation.*Biochim Biophys Acta Mol Cell Biol Lipids, 2018. **1863**(9): p. 1121-1131.
- 71. Bura, A., et al., The intracellular and plasma membrane pools of phosphatidylinositol-4-monophosphate control megakaryocyte maturation and proplatelet formation. Res Pract Thromb Haemost, 2023. **7**(4): p. 100169.
- 72. Caux, M., et al., *PIKfyve-Dependent Phosphoinositide Dynamics in Megakaryocyte/Platelet Granule Integrity and Platelet Functions.* Arterioscler Thromb Vasc Biol, 2022. **42**(8): p. 987-1004.
- 73. Katan, M. and S. Cockcroft, *Phosphatidylinositol(4,5)bisphosphate: diverse functions at the plasma membrane.* Essays Biochem, 2020. **64**(3): p. 513-531.
- 74. Wang, Y., et al., Loss of PIP5KIgamma, unlike other PIP5KI isoforms, impairs the integrity of the membrane cytoskeleton in murine megakaryocytes. J Clin Invest, 2008. **118**(2): p. 812-9.
- 75. Min, S.H., et al., Loss of PIKfyve in platelets causes a lysosomal disease leading to inflammation and thrombosis in mice. Nat Commun, 2014. **5**: p. 4691.
- 76. Durrant, T.N., et al., *Identification of PtdIns(3,4)P(2) effectors in human platelets using quantitative proteomics*. Biochim Biophys Acta Mol Cell Biol Lipids, 2020. **1865**(2): p. 158575.
- 77. Bobe, R., et al., *Phosphatidylinositol 3-kinase-dependent translocation of phospholipase Cgamma2 in mouse megakaryocytes is independent of Bruton tyrosine kinase translocation.* Blood, 2001. **97**(3): p. 678-84.
- 78. Ribes, A., et al., *Phosphoinositide 3-kinases in platelets, thrombosis and therapeutics.* Biochem J, 2020. **477**(22): p. 4327-4342.
- 79. Ivana Bertović, S.B., Siniša Volarević, Antonija Jurak Begonja, *Vps34 localizes to the nucleolus and regulates rRNA transcription and early megakaryocyte development.* unpublished; Laboratory for Hematopoiesis, Faculty of Biotechnology and Drug Development, University of Rijeka

- 80. Manzoli, F.A., et al., *Chromatin phospholipids in normal and chronic lymphocytic leukemia lymphocytes*. Cancer Res, 1977. **37**(3): p. 843-9.
- 81. Rose, H.G. and J.H. Frenster, *Composition and metabolism of lipids within repressed and active chromatin of interphase lymphocytes*. Biochim Biophys Acta, 1965. **106**(3): p. 577-91.
- 82. Vidalle, M.C., et al., *Nuclear Phosphoinositides as Key Determinants of Nuclear Functions*. Biomolecules, 2023. **13**(7).
- 83. Audhya, A. and S.D. Emr, *Regulation of PI4,5P2 synthesis by nuclear-cytoplasmic shuttling of the Mss4 lipid kinase*. EMBO J, 2003. **22**(16): p. 4223-36.
- 84. Bunce, M.W., K. Bergendahl, and R.A. Anderson, *Nuclear PI(4,5)P(2): a new place for an old signal.* Biochim Biophys Acta, 2006. **1761**(5-6): p. 560-9.
- 85. Osborne, S.L., et al., *Nuclear PtdIns*(4,5)P2 assembles in a mitotically regulated particle involved in pre-mRNA splicing. J Cell Sci, 2001. **114**(Pt 13): p. 2501-11.
- 86. Sobol, M., et al., *Nuclear phosphatidylinositol 4,5-bisphosphate islets contribute to efficient RNA polymerase II-dependent transcription.* J Cell Sci, 2018. **131**(8).
- 87. Faberova, V., et al., Super-Resolution Localisation of Nuclear PI(4)P and Identification of Its Interacting Proteome. Cells, 2020. **9**(5).
- 88. Fiume, R., et al., *Nuclear Phosphoinositides: Their Regulation and Roles in Nuclear Functions.* Int J Mol Sci, 2019. **20**(12).
- 89. Wang, Y.H., et al., *DNA damage causes rapid accumulation of phosphoinositides for ATR signaling.* Nat Commun, 2017. **8**(1): p. 2118.
- 90. Alkhoury, C., et al., Class 3 PI3K coactivates the circadian clock to promote rhythmic de novo purine synthesis. Nat Cell Biol, 2023. **25**(7): p. 975-988.
- 91. Bunney, T.D., et al., Association of phosphatidylinositol 3-kinase with nuclear transcription sites in higher plants. Plant Cell, 2000. **12**(9): p. 1679-88.
- 92. Gaur, N.A., et al., *Vps factors are required for efficient transcription elongation in budding yeast.* Genetics, 2013. **193**(3): p. 829-51.
- 93. Gillooly, D.J., et al., *Localization of phosphatidylinositol 3-phosphate in yeast and mammalian cells.* EMBO J, 2000. **19**(17): p. 4577-88.
- 94. Boisvert, F.M., et al., *The multifunctional nucleolus*. Nat Rev Mol Cell Biol, 2007. **8**(7): p. 574-85.
- 95. Pederson, T., *The plurifunctional nucleolus*. Nucleic Acids Res, 1998. **26**(17): p. 3871-6.
- 96. Raska, I., P.J. Shaw, and D. Cmarko, *New insights into nucleolar architecture and activity.* Int Rev Cytol, 2006. **255**: p. 177-235.
- 97. Pederson, T., *The nucleolus*. Cold Spring Harb Perspect Biol, 2011. **3**(3).

- 98. Shaw, P. and J. Brown, *Nucleoli: composition, function, and dynamics.* Plant Physiol, 2012. **158**(1): p. 44-51.
- 99. Cooper, G., *The Nucleolus*, in *The Cell: A Molecular Approach*. 2000, Sinauer Associates 2000.
- 100. Ni, C. and M. Buszczak, *Ribosome biogenesis and function in development and disease*. Development, 2023. **150**(5).
- 101. Schmidt, E.V., *The role of c-myc in cellular growth control.* Oncogene, 1999. **18**(19): p. 2988-96.
- 102. Granneman, S. and D. Tollervey, *Building ribosomes: even more expensive than expected?* Curr Biol, 2007. **17**(11): p. R415-7.
- 103. Maehama, T., et al., *Nucleolar stress: Molecular mechanisms and related human diseases*. Cancer Sci, 2023. **114**(5): p. 2078-2086.
- 104. Kubbutat, M.H., S.N. Jones, and K.H. Vousden, *Regulation of p53 stability by Mdm2*. Nature, 1997. **387**(6630): p. 299-303.
- 105. James, A., et al., *Nucleolar stress with and without p53.* Nucleus, 2014. **5**(5): p. 402-26.
- 106. Russo, A. and G. Russo, *Ribosomal Proteins Control or Bypass p53 during Nucleolar Stress.* Int J Mol Sci, 2017. **18**(1).
- 107. Zhang, Z., et al., Stabilization of E2F1 protein by MDM2 through the E2F1 ubiquitination pathway. Oncogene, 2005. **24**(48): p. 7238-47.
- 108. Takagi, M., et al., Regulation of p53 translation and induction after DNA damage by ribosomal protein L26 and nucleolin. Cell, 2005. **123**(1): p. 49-63.
- 109. Yang, K., J. Yang, and J. Yi, *Nucleolar Stress: hallmarks, sensing mechanism and diseases.* Cell Stress, 2018. **2**(6): p. 125-140.
- 110. Perry, R.P. and D.E. Kelley, *Persistent synthesis of 5S RNA when production of 28S and 18S ribosomal RNA is inhibited by low doses of actinomycin D.* J Cell Physiol, 1968. **72**(3): p. 235-46.
- 111. Zhang, Y., et al., *Ribosomal protein L11 negatively regulates oncoprotein MDM2 and mediates a p53-dependent ribosomal-stress checkpoint pathway.*Mol Cell Biol, 2003. **23**(23): p. 8902-12.
- 112. Jandhyala, D.M., C.M. Thorpe, and B. Magun, *Ricin and Shiga toxins: effects on host cell signal transduction*. Curr Top Microbiol Immunol, 2012. **357**: p. 41-65.
- 113. Sinha, N.K., et al., *The ribotoxic stress response drives UV-mediated cell death.* Cell, 2024. **187**(14): p. 3652-3670 e40.
- 114. Vind, A.C., et al., ZAKalpha Recognizes Stalled Ribosomes through Partially Redundant Sensor Domains. Mol Cell, 2020. **78**(4): p. 700-713 e7.

- 115. Vind, A.C., et al., *The ribotoxic stress response drives acute inflammation, cell death, and epidermal thickening in UV-irradiated skin in vivo.* Mol Cell, 2024. **84**(24): p. 4774-4789 e9.
- 116. Brighenti, E., et al., *Interleukin 6 downregulates p53 expression and activity by stimulating ribosome biogenesis: a new pathway connecting inflammation to cancer.* Oncogene, 2014. **33**(35): p. 4396-406.
- 117. Lee, T.A., et al., *The nucleolus is the site for inflammatory RNA decay during infection.* Nat Commun, 2022. **13**(1): p. 5203.
- 118. Mladineo, I. and J. Hrabar, *Leukocyte Nucleolus and Anisakis pegreffii-When Falling Apart Means Falling in Place.* Genes (Basel), 2020. **11**(6).
- 119. Chen, J. and L.A. Stark, *Insights into the Relationship between Nucleolar Stress and the NF-kappaB Pathway.* Trends Genet, 2019. **35**(10): p. 768-780.
- 120. Khandelwal, N., et al., *Nucleolar NF-kappaB/RelA mediates apoptosis by causing cytoplasmic relocalization of nucleophosmin.* Cell Death Differ, 2011. **18**(12): p. 1889-903.
- 121. Mayer, C. and I. Grummt, *Cellular stress and nucleolar function*. Cell Cycle, 2005. **4**(8): p. 1036-8.
- 122. Lafita-Navarro, M.C. and M. Conacci-Sorrell, *Nucleolar stress: From development to cancer.* Semin Cell Dev Biol, 2023. **136**: p. 64-74.
- 123. Kang, H. and J.H. Shin, Repression of rRNA transcription by PARIS contributes to Parkinson's disease. Neurobiol Dis, 2015. **73**: p. 220-8.
- 124. Yung, B.Y., H. Busch, and P.K. Chan, *Translocation of nucleolar phosphoprotein B23 (37 kDa/pl 5.1) induced by selective inhibitors of ribosome synthesis.* Biochim Biophys Acta, 1985. **826**(4): p. 167-73.
- 125. Chan, P.K., M. Aldrich, and H. Busch, *Alterations in immunolocalization of the phosphoprotein B23 in HeLa cells during serum starvation.* Exp Cell Res, 1985. **161**(1): p. 101-10.
- 126. Kurki, S., et al., *Nucleolar protein NPM interacts with HDM2 and protects tumor suppressor protein p53 from HDM2-mediated degradation.* Cancer Cell, 2004. **5**(5): p. 465-75.
- 127. Yang, K., et al., A redox mechanism underlying nucleolar stress sensing by nucleophosmin. Nat Commun, 2016. **7**: p. 13599.
- Ma, T.S., et al., Hypoxia-induced transcriptional stress is mediated by ROS-induced R-loops. Nucleic Acids Res, 2023. 51(21): p. 11584-11599.
- 129. Sapio, R.T., C.J. Burns, and D.G. Pestov, *Effects of Hydrogen Peroxide Stress on the Nucleolar Redox Environment and Pre-rRNA Maturation.* Front Mol Biosci, 2021. **8**: p. 678488.

- 130. Chan, P.K., Characterization and cellular localization of nucleophosmin/B23 in HeLa cells treated with selected cytotoxic agents (studies of B23-translocation mechanism). Exp Cell Res, 1992. **203**(1): p. 174-81.
- 131. Chan, P.K. and F.Y. Chan, A study of correlation between NPM-translocation and apoptosis in cells induced by daunomycin. Biochem Pharmacol, 1999. **57**(11): p. 1265-73.
- 132. Kuter, D.J., *Treatment of chemotherapy-induced thrombocytopenia in patients with non-hematologic malignancies.* Haematologica, 2022. **107**(6): p. 1243-1263.
- 133. Whaun, J.M. and H.D. Clarke, *The effect of daunomycin on platelets in vitro*. Arch Int Pharmacodyn Ther, 1989. **300**: p. 292-304.
- 134. Ma, W., et al., Doxorubicin-Induced Platelet Activation and Clearance Relieved by Salvianolic Acid Compound: Novel Mechanism and Potential Therapy for Chemotherapy-Associated Thrombosis and Thrombocytopenia. Pharmaceuticals (Basel), 2022. **15**(12).
- 135. Narla, A. and B.L. Ebert, *Ribosomopathies: human disorders of ribosome dysfunction*. Blood, 2010. **115**(16): p. 3196-205.
- 136. Draptchinskaia, N., et al., *The gene encoding ribosomal protein S19 is mutated in Diamond-Blackfan anaemia*. Nat Genet, 1999. **21**(2): p. 169-75.
- 137. Van den Berghe, H., et al., *Distinct haematological disorder with deletion of long arm of no. 5 chromosome.* Nature, 1974. **251**(5474): p. 437-8.
- 138. Jadersten, M., *Pathophysiology and treatment of the myelodysplastic syndrome with isolated 5q deletion.* Haematologica, 2010. **95**(3): p. 348-51.
- 139. Ebert, B.L., et al., *Identification of RPS14 as a 5q- syndrome gene by RNA interference screen.* Nature, 2008. **451**(7176): p. 335-9.
- 140. Vardiman, J.W., N.L. Harris, and R.D. Brunning, *The World Health Organization (WHO) classification of the myeloid neoplasms*. Blood, 2002. **100**(7): p. 2292-302.
- 141. Feng, G., et al., A systematic classification of megakaryocytic dysplasia and its impact on prognosis for patients with myelodysplastic syndromes. Exp Hematol Oncol, 2015. **5**: p. 12.
- 142. Goasguen, J.E., et al., Quality control initiative on the evaluation of the dysmegakaryopoiesis in myeloid neoplasms: Difficulties in the assessment of dysplasia. Leuk Res, 2016. **45**: p. 75-81.
- 143. Gupta, G., et al., Myelodysplastic syndromes/neoplasms: recent classification system based on World Health Organization Classification of Tumors International Agency for Research on Cancer for Hematopoietic and Lymphoid Tissues. J Blood Med, 2010. 1: p. 171-82.

- 144. van Dooijeweert, B., et al., *GATA-1 Defects in Diamond-Blackfan Anemia:* Phenotypic Characterization Points to a Specific Subset of Disease. Genes (Basel), 2022. **13**(3).
- 145. Liu, Y.L., et al., *Animal models of Diamond-Blackfan anemia: updates and challenges.* Haematologica, 2023. **108**(5): p. 1222-1231.
- 146. Jackson, S.P. and J. Bartek, *The DNA-damage response in human biology and disease.* Nature, 2009. **461**(7267): p. 1071-8.
- 147. Bian, L., et al., MRE11-RAD50-NBS1 complex alterations and DNA damage response: implications for cancer treatment. Mol Cancer, 2019. **18**(1): p. 169.
- 148. Marechal, A. and L. Zou, *DNA damage sensing by the ATM and ATR kinases*. Cold Spring Harb Perspect Biol, 2013. **5**(9).
- 149. Mah, L.J., A. El-Osta, and T.C. Karagiannis, gammaH2AX: a sensitive molecular marker of DNA damage and repair. Leukemia, 2010. 24(4): p. 679-86.
- 150. Ivashkevich, A., et al., Use of the gamma-H2AX assay to monitor DNA damage and repair in translational cancer research. Cancer Lett, 2012. **327**(1-2): p. 123-33.
- 151. Sanchez-Flores, M., et al., gammaH2AX assay as DNA damage biomarker for human population studies: defining experimental conditions. Toxicol Sci, 2015. **144**(2): p. 406-13.
- 152. Valdiglesias, V., et al., gammaH2AX as a marker of DNA double strand breaks and genomic instability in human population studies. Mutat Res, 2013. **753**(1): p. 24-40.
- 153. Shah, Z.H., et al., *Nuclear phosphoinositides and their impact on nuclear functions*. FEBS J, 2013. **280**(24): p. 6295-310.
- 154. Wang, Y.H. and M.P. Sheetz, When PIP(2) Meets p53: Nuclear Phosphoinositide Signaling in the DNA Damage Response. Front Cell Dev Biol, 2022. **10**: p. 903994.
- 155. Jacobsen, R.G., et al., *Polyphosphoinositides in the nucleus: Roadmap of their effectors and mechanisms of interaction.* Adv Biol Regul, 2019. **72**: p. 7-21.
- 156. Cocco, L., et al., Synthesis of polyphosphoinositides in nuclei of Friend cells. Evidence for polyphosphoinositide metabolism inside the nucleus which changes with cell differentiation. Biochem J, 1987. **248**(3): p. 765-70.
- 157. Smith, C.D. and W.W. Wells, *Phosphorylation of rat liver nuclear envelopes.*II. Characterization of in vitro lipid phosphorylation. J Biol Chem, 1983.

 258(15): p. 9368-73.
- 158. Choi, S., et al., *A nuclear phosphoinositide kinase complex regulates p53.* Nat Cell Biol, 2019. **21**(4): p. 462-475.

- 159. Yokogawa, T., et al., Evidence that 3'-phosphorylated polyphosphoinositides are generated at the nuclear surface: use of immunostaining technique with monoclonal antibodies specific for PI 3,4-P(2). FEBS Lett, 2000. **473**(2): p. 222-6.
- 160. Mishkind, M., et al., *Heat stress activates phospholipase D and triggers PIP accumulation at the plasma membrane and nucleus*. Plant J, 2009. **60**(1): p. 10-21.
- 161. Thon, J.N., et al., *High-content live-cell imaging assay used to establish mechanism of trastuzumab emtansine (T-DM1)--mediated inhibition of platelet production.* Blood, 2012. **120**(10): p. 1975-84.
- 162. Gupta, S., et al., *GPVI signaling is compromised in newly formed platelets after acute thrombocytopenia in mice.* Blood, 2018. **131**(10): p. 1106-1110.
- 163. Rueden, C.T., et al., *ImageJ2: ImageJ for the next generation of scientific image data*. BMC Bioinformatics, 2017. **18**(1): p. 529.
- 164. Hughes, C.S., et al., Single-pot, solid-phase-enhanced sample preparation for proteomics experiments. Nat Protoc, 2019. **14**(1): p. 68-85.
- 165. Uhlen, M., et al., *Proteomics. Tissue-based map of the human proteome.* Science, 2015. **347**(6220): p. 1260419.
- 166. Kolberg, L., et al., g:Profiler-interoperable web service for functional enrichment analysis and gene identifier mapping (2023 update). Nucleic Acids Res, 2023. **51**(W1): p. W207-W212.
- 167. Zhang, Q.Y., et al., *Antimicrobial peptides: mechanism of action, activity and clinical potential.* Mil Med Res, 2021. **8**(1): p. 48.
- 168. Beaulieu, L.M., et al., Interleukin 1 receptor 1 and interleukin 1beta regulate megakaryocyte maturation, platelet activation, and transcript profile during inflammation in mice and humans. Arterioscler Thromb Vasc Biol, 2014. **34**(3): p. 552-64.
- 169. Chuen, C.K., et al., Interleukin-1beta up-regulates the expression of thrombopoietin and transcription factors c-Jun, c-Fos, GATA-1, and NF-E2 in megakaryocytic cells. J Lab Clin Med, 2004. **143**(2): p. 75-88.
- 170. Kimura, H., et al., *Interleukin-1 beta (IL-1 beta) induces thrombocytosis in mice:* possible implication of IL-6. Blood, 1990. **76**(12): p. 2493-500.
- 171. van den Oudenrijn, S., et al., A combination of megakaryocyte growth and development factor and interleukin-1 is sufficient to culture large numbers of megakaryocytic progenitors and megakaryocytes for transfusion purposes. Br J Haematol, 1999. **106**(2): p. 553-63.
- 172. Yang, M., et al., Expression of interleukin (IL) 1 type I and type II receptors in megakaryocytic cells and enhancing effects of IL-1beta on

- megakaryocytopoiesis and NF-E2 expression. Br J Haematol, 2000. **111**(1): p. 371-80.
- 173. Schick, P.K., et al., Synthesis and secretion of von Willebrand factor and fibronectin in megakaryocytes at different phases of maturation. Arterioscler Thromb Vasc Biol, 1997. **17**(4): p. 797-801.
- 174. Luo, S.Z., et al., Glycoprotein Ibalpha forms disulfide bonds with 2 glycoprotein Ibbeta subunits in the resting platelet. Blood, 2007. **109**(2): p. 603-9.
- 175. Mo, X., et al., *Transmembrane domains are critical to the interaction between platelet glycoprotein V and glycoprotein Ib-IX complex.* J Thromb Haemost, 2012. **10**(9): p. 1875-86.
- 176. Huizinga, E.G., et al., Structures of glycoprotein Ibalpha and its complex with von Willebrand factor A1 domain. Science, 2002. **297**(5584): p. 1176-9.
- 177. Bertovic, I., A. Bura, and A. Jurak Begonja, *Developmental differences of in vitro cultured murine bone marrow- and fetal liver-derived megakaryocytes*. Platelets, 2022. **33**(6): p. 887-899.
- 178. Rojnuckarin, P., J.G. Drachman, and K. Kaushansky, *Thrombopoietin-induced activation of the mitogen-activated protein kinase (MAPK) pathway in normal megakaryocytes: role in endomitosis.* Blood, 1999. **94**(4): p. 1273-82.
- 179. Cunin, P. and P.A. Nigrovic, *Megakaryocyte emperipolesis: a new frontier in cell-in-cell interaction*. Platelets, 2020. **31**(6): p. 700-706.
- 180. Munoz-Velasco, I., A.K. Herrera-Escamilla, and A. Vazquez-Salazar, *Nucleolar origins: challenging perspectives on evolution and function.* Open Biol, 2025. **15**(3): p. 240330.
- 181. Penzo, M., et al., *The Ribosome Biogenesis-Cancer Connection*. Cells, 2019. **8**(1).
- 182. Voit, R. and I. Grummt, *Phosphorylation of UBF at serine 388 is required for interaction with RNA polymerase I and activation of rDNA transcription.* Proc Natl Acad Sci U S A, 2001. **98**(24): p. 13631-6.
- 183. Devereaux, K., et al., Regulation of mammalian autophagy by class II and III PI 3-kinases through PI3P synthesis. PLoS One, 2013. **8**(10): p. e76405.
- 184. Jaber, N. and W.X. Zong, Class III PI3K Vps34: essential roles in autophagy, endocytosis, and heart and liver function. Ann N Y Acad Sci, 2013. **1280**: p. 48-51.
- 185. Johnson, E.E., et al., Gene silencing reveals a specific function of hVps34 phosphatidylinositol 3-kinase in late versus early endosomes. J Cell Sci, 2006. **119**(Pt 7): p. 1219-32.

- 186. Bago, R., et al., Characterization of VPS34-IN1, a selective inhibitor of Vps34, reveals that the phosphatidylinositol 3-phosphate-binding SGK3 protein kinase is a downstream target of class III phosphoinositide 3-kinase. Biochem J, 2014. **463**(3): p. 413-27.
- 187. Meunier, G., et al., Antileukemic activity of the VPS34-IN1 inhibitor in acute myeloid leukemia. Oncogenesis, 2020. **9**(10): p. 94.
- 188. Ronan, B., et al., *A highly potent and selective Vps34 inhibitor alters vesicle trafficking and autophagy.* Nat Chem Biol, 2014. **10**(12): p. 1013-9.
- 189. Morodomi, Y., et al., *Mechanisms of anti-GPlbalpha antibody-induced thrombocytopenia in mice.* Blood, 2020. **135**(25): p. 2292-2301.
- 190. Janoutova, J. and Z. Likovsky, *Nucleoli and argyrophil nucleolus organizer regions (AgNORs) of cells of the megakaryocytic line in the rat.* Physiol Res, 1995. **44**(3): p. 193-6.
- 191. Kang, C.D., et al., Signaling mechanism of PMA-induced differentiation of K562 cells. Biochem Biophys Res Commun, 1996. **221**(1): p. 95-100.
- 192. Butler, T.M., A. Ziemiecki, and R.R. Friis, Megakaryocytic differentiation of K562 cells is associated with changes in the cytoskeletal organization and the pattern of chromatographically distinct forms of phosphotyrosyl-specific protein phosphatases. Cancer Res, 1990. **50**(19): p. 6323-9.
- 193. Huang, R., et al., *Megakaryocytic differentiation of K562 cells induced by PMA reduced the activity of respiratory chain complex IV.* PLoS One, 2014. **9**(5): p. e96246.
- 194. Wilhide, C.C., et al., Overexpression of cyclin D1 in the Dami megakaryocytic cell line causes growth arrest. Blood, 1995. **86**(1): p. 294-304.
- 195. Greenberg, S.M., et al., *Characterization of a new megakaryocytic cell line:* the Dami cell. Blood, 1988. **72**(6): p. 1968-77.
- 196. Lev, P.R., et al., *Production of functional platelet-like particles by the megakaryoblastic DAMI cell line provides a model for platelet biogenesis.* Platelets, 2011. **22**(1): p. 28-38.
- 197. Liu, R.Y., et al., Constitutive activation of the JAK2/STAT5 signal transduction pathway correlates with growth factor independence of megakaryocytic leukemic cell lines. Blood, 1999. **93**(7): p. 2369-79.
- 198. Correll, C.C., J. Bartek, and M. Dundr, *The Nucleolus: A Multiphase Condensate Balancing Ribosome Synthesis and Translational Capacity in Health, Aging and Ribosomopathies.* Cells, 2019. **8**(8).
- 199. Lozzio, C.B. and B.B. Lozzio, *Human chronic myelogenous leukemia cell-line with positive Philadelphia chromosome*. Blood, 1975. **45**(3): p. 321-34.

- 200. Rowley, J.D., Letter: A new consistent chromosomal abnormality in chronic myelogenous leukaemia identified by quinacrine fluorescence and Giemsa staining. Nature, 1973. **243**(5405): p. 290-3.
- 201. Andersson, L.C., M. Jokinen, and C.G. Gahmberg, *Induction of erythroid differentiation in the human leukaemia cell line K562.* Nature, 1979. **278**(5702): p. 364-5.
- 202. Hirose, K., et al., *Megakaryocytic differentiation in human chronic myelogenous leukemia K562 cells induced by ionizing radiation in combination with phorbol 12-myristate 13-acetate.* J Radiat Res, 2013. **54**(3): p. 438-46.
- 203. Martin, P. and T. Papayannopoulou, *HEL cells: a new human erythroleukemia cell line with spontaneous and induced globin expression.* Science, 1982. **216**(4551): p. 1233-5.
- 204. Hu, L., et al., *EloA promotes HEL polyploidization upon PMA stimulation through enhanced ERK1/2 activity.* Platelets, 2022. **33**(5): p. 755-763.
- 205. Long, M.W., et al., Regulation of megakaryocyte phenotype in human erythroleukemia cells. J Clin Invest, 1990. **85**(4): p. 1072-84.
- 206. Zhao, W., et al., *JAK2V617F* and p53 mutations coexist in erythroleukemia and megakaryoblastic leukemic cell lines. Exp Hematol Oncol, 2012. **1**(1): p. 15.
- 207. Zauli, G., et al., *PMA-induced megakaryocytic differentiation of HEL cells is accompanied by striking modifications of protein kinase C catalytic activity and isoform composition at the nuclear level.* Br J Haematol, 1996. **92**(3): p. 530-6.
- 208. Stepinski, D., *The nucleolus, an ally, and an enemy of cancer cells.* Histochem Cell Biol, 2018. **150**(6): p. 607-629.
- 209. Orsolic, I., et al., *The relationship between the nucleolus and cancer: Current evidence and emerging paradigms.* Semin Cancer Biol, 2016. **37-38**: p. 36-50.
- 210. Schwer, H.D., et al., A lineage-restricted and divergent beta-tubulin isoform is essential for the biogenesis, structure and function of blood platelets. Curr Biol, 2001. **11**(8): p. 579-86.
- 211. Brown, E., et al., *Multiple membrane extrusion sites drive megakaryocyte migration into bone marrow blood vessels.* Life Sci Alliance, 2018. **1**(2).
- 212. Ellis, M.L., et al., *GPIbalpha-filamin A interaction regulates megakaryocyte localization and budding during platelet biogenesis.* Blood, 2024. **143**(4): p. 342-356.

- 213. Kowata, S., et al., *Platelet demand modulates the type of intravascular protrusion of megakaryocytes in bone marrow.* Thromb Haemost, 2014. **112**(4): p. 743-56.
- 214. Bornert, A., et al., *Cytoskeletal-based mechanisms differently regulate in vivo and in vitro proplatelet formation.* Haematologica, 2021. **106**(5): p. 1368-1380.
- 215. Hyslop, S.R., et al., *A glycoprotein VI signaling defect in newly formed platelets generated in stress thrombopoiesis.* J Thromb Haemost, 2025. **23**(6): p. 1996-2009.
- 216. Pirabe, A., et al., *Impaired hemostatic and immune functions of platelets after acute thrombocytopenia.* J Thromb Haemost, 2025. **23**(3): p. 1052-1065.
- 217. Nishikii, H., et al., *Unipotent Megakaryopoietic Pathway Bridging Hematopoietic Stem Cells and Mature Megakaryocytes.* Stem Cells, 2015. **33**(7): p. 2196-207.
- 218. Sanjuan-Pla, A., et al., *Platelet-biased stem cells reside at the apex of the haematopoietic stem-cell hierarchy.* Nature, 2013. **502**(7470): p. 232-6.
- 219. Shin, J.Y., et al., *High c-Kit expression identifies hematopoietic stem cells with impaired self-renewal and megakaryocytic bias.* J Exp Med, 2014. **211**(2): p. 217-31.
- 220. Yeung, A.K., et al., *Lung megakaryocytes display distinct transcriptional and phenotypic properties.* Blood Adv, 2020. **4**(24): p. 6204-6217.
- 221. Valet, C., et al., Sepsis promotes splenic production of a protective platelet pool with high CD40 ligand expression. J Clin Invest, 2022. **132**(7).
- 222. Singh, A.K., et al., *Critical role of IL-1alpha in IL-1beta-induced inflammatory responses: cooperation with NF-kappaBp65 in transcriptional regulation.* FASEB J, 2019. **33**(2): p. 2526-2536.
- 223. Hiscott, J., et al., Characterization of a functional NF-kappa B site in the human interleukin 1 beta promoter: evidence for a positive autoregulatory loop. Mol Cell Biol, 1993. **13**(10): p. 6231-40.
- 224. Mori, N. and D. Prager, *Transactivation of the interleukin-1alpha promoter by human T-cell leukemia virus type I and type II Tax proteins.* Blood, 1996. **87**(8): p. 3410-7.
- 225. Spinelli, S.L., et al., *Platelets and megakaryocytes contain functional nuclear factor-kappaB.* Arterioscler Thromb Vasc Biol, 2010. **30**(3): p. 591-8.
- 226. Liu, C., et al., Characterization of Cellular Heterogeneity and an Immune Subpopulation of Human Megakaryocytes. Adv Sci (Weinh), 2021. **8**(15): p. e2100921.

- 227. Sun, S., et al., Single-cell analysis of ploidy and the transcriptome reveals functional and spatial divergency in murine megakaryopoiesis. Blood, 2021. **138**(14): p. 1211-1224.
- 228. Cunin, P., et al., *Megakaryocyte emperipolesis mediates membrane transfer from intracytoplasmic neutrophils to platelets.* Elife, 2019. **8**.
- 229. Di Buduo, C.A., et al., *Abnormal proplatelet formation and emperipolesis in cultured human megakaryocytes from gray platelet syndrome patients.* Sci Rep, 2016. **6**: p. 23213.
- 230. Larocca, L.M., et al., *Megakaryocytic emperipolesis and platelet function abnormalities in five patients with gray platelet syndrome.* Platelets, 2015. **26**(8): p. 751-7.
- 231. Schmitt, A., et al., *Pathologic interaction between megakaryocytes and polymorphonuclear leukocytes in myelofibrosis.* Blood, 2000. **96**(4): p. 1342-7.
- 232. Sharma, S. and A. Rawat, *Increased emperipolesis in megakaryocytes in a case of idiopathic thrombocytopenic purpura*. Indian J Pathol Microbiol, 2006. **49**(4): p. 631.
- 233. Petzold, T., et al., Neutrophil "plucking" on megakaryocytes drives platelet production and boosts cardiovascular disease. Immunity, 2022. **55**(12): p. 2285-2299 e7.
- 234. Machlus, K.R. and J.E. Italiano, Jr., *The incredible journey: From megakaryocyte development to platelet formation.* J Cell Biol, 2013. **201**(6): p. 785-96.
- 235. Zimmet, J. and K. Ravid, *Polyploidy: occurrence in nature, mechanisms, and significance for the megakaryocyte-platelet system.* Exp Hematol, 2000. **28**(1): p. 3-16.
- 236. Khatib-Massalha, E. and S. Mendez-Ferrer, *Megakaryocyte Diversity in Ontogeny, Functions and Cell-Cell Interactions*. Front Oncol, 2022. **12**: p. 840044.
- 237. Cunin, P. and P.A. Nigrovic, *Megakaryocytes as immune cells.* J Leukoc Biol, 2019. **105**(6): p. 1111-1121.
- 238. Avraham, H., et al., *Cytokine gene expression and synthesis by human megakaryocytic cells.* Int J Cell Cloning, 1992. **10**(2): p. 70-9.
- 239. Jiang, S., et al., *Cytokine production by primary bone marrow megakaryocytes.* Blood, 1994. **84**(12): p. 4151-6.
- 240. Flaumenhaft, R., et al., *Megakaryocyte-derived microparticles: direct visualization and distinction from platelet-derived microparticles.* Blood, 2009. **113**(5): p. 1112-21.

- 241. Italiano, J.E., Jr., A.T. Mairuhu, and R. Flaumenhaft, *Clinical relevance of microparticles from platelets and megakaryocytes*. Curr Opin Hematol, 2010. **17**(6): p. 578-84.
- 242. Melki, I., et al., *Platelet microvesicles in health and disease.* Platelets, 2017. **28**(3): p. 214-221.
- 243. Yildirim, S., et al., *Involvement of phosphatidylinositol 4,5-bisphosphate in RNA polymerase I transcription.* J Cell Sci, 2013. **126**(Pt 12): p. 2730-9.
- 244. Mazloumi Gavgani, F., et al., *Nuclear upregulation of class I phosphoinositide* 3-kinase p110beta correlates with high 47S rRNA levels in cancer cells. J Cell Sci, 2021. **134**(3).
- 245. Okada, M., S.W. Jang, and K. Ye, Akt phosphorylation and nuclear phosphoinositide association mediate mRNA export and cell proliferation activities by ALY. Proc Natl Acad Sci U S A, 2008. **105**(25): p. 8649-54.
- 246. Schedle, A., et al., *Nucleolar morphology and rDNA in situ hybridisation in monocytes*. Cell Tissue Res, 1992. **269**(3): p. 473-80.
- 247. Gebauer, F. and M.W. Hentze, *Molecular mechanisms of translational control*. Nat Rev Mol Cell Biol, 2004. **5**(10): p. 827-35.
- 248. Chaillou, T., T.J. Kirby, and J.J. McCarthy, *Ribosome biogenesis: emerging evidence for a central role in the regulation of skeletal muscle mass.* J Cell Physiol, 2014. **229**(11): p. 1584-94.
- 249. Vadivel Gnanasundram, S. and R. Fahraeus, *Translation Stress Regulates Ribosome Synthesis and Cell Proliferation*. Int J Mol Sci, 2018. **19**(12).
- 250. Verheyden, Y., L. Goedert, and E. Leucci, *Control of nucleolar stress and translational reprogramming by IncRNAs.* Cell Stress, 2018. **3**(1): p. 19-26.
- 251. Boulon, S., et al., *The nucleolus under stress.* Mol Cell, 2010. **40**(2): p. 216-27.
- 252. Chang, C.Y., et al., *Ribosome Biogenesis Serves as a Therapeutic Target for Treating Endometriosis and the Associated Complications.* Biomedicines, 2022. **10**(1).
- 253. Hwang, S.P. and C. Denicourt, *The impact of ribosome biogenesis in cancer:* from proliferation to metastasis. NAR Cancer, 2024. **6**(2): p. zcae017.
- 254. Paulsen, M.T., et al., Coordinated regulation of synthesis and stability of RNA during the acute TNF-induced proinflammatory response. Proc Natl Acad Sci U S A, 2013. **110**(6): p. 2240-5.
- 255. Roweth, H.G., et al., *Pro-inflammatory megakaryocyte gene expression in murine models of breast cancer.* Sci Adv, 2022. **8**(41): p. eabo5224.
- 256. Cheung, M.H., et al., *Human NOC3 is essential for DNA replication licensing in human cells.* Cell Cycle, 2019. **18**(5): p. 605-620.

- 257. Dez, C., et al., Npa1p, a component of very early pre-60S ribosomal particles, associates with a subset of small nucleolar RNPs required for peptidyl transferase center modification. Mol Cell Biol, 2004. **24**(14): p. 6324-37.
- 258. Sekiguchi, T., et al., *NOP132 is required for proper nucleolus localization of DEAD-box RNA helicase DDX47.* Nucleic Acids Res, 2006. **34**(16): p. 4593-608.
- 259. Grundy, M., et al., *Abnormal nucleoli architecture and aggregate formation in nucleophosmin mutated acute myeloid leukaemia.* J Cell Sci, 2025. **138**(10).
- 260. Potapova, T.A., et al., *Distinct states of nucleolar stress induced by anticancer drugs.* Elife, 2023. **12**.
- 261. Matsumoto, T., et al., Relation between nucleolar size and growth characteristics in small cell lung cancer cell lines. Jpn J Cancer Res, 1991. **82**(7): p. 820-8.
- 262. Baatout, S., et al., Augmentation of the number of nucleolar organizer regions in human megakaryocyte cell lines after induction of polyploidization by a microtubule inhibitor. Eur J Clin Invest, 1998. **28**(2): p. 138-44.
- 263. Perez-Ortin, J.E., et al., *Cell volume homeostatically controls the rDNA repeat copy number and rRNA synthesis rate in yeast.* PLoS Genet, 2021. **17**(4): p. e1009520.
- 264. Matos-Perdomo, E. and F. Machin, *Nucleolar and Ribosomal DNA Structure under Stress: Yeast Lessons for Aging and Cancer.* Cells, 2019. **8**(8).
- 265. Belin, S., et al., Dysregulation of ribosome biogenesis and translational capacity is associated with tumor progression of human breast cancer cells. PLoS One, 2009. **4**(9): p. e7147.
- 266. Santoshi, R.K., et al., *A Comprehensive Review of Thrombocytopenia With a Spotlight on Intensive Care Patients.* Cureus, 2022. **14**(8): p. e27718.
- 267. Zarychanski, R. and D.S. Houston, *Assessing thrombocytopenia in the intensive care unit: the past, present, and future.* Hematology Am Soc Hematol Educ Program, 2017. **2017**(1): p. 660-666.
- 268. Rasizadeh, R., et al., *Viruses and thrombocytopenia*. Heliyon, 2024. **10**(6): p. e27844.
- 269. Polson, H.E., et al., *Mammalian Atg18 (WIPI2) localizes to omegasome-anchored phagophores and positively regulates LC3 lipidation.* Autophagy, 2010. **6**(4): p. 506-22.
- 270. Proikas-Cezanne, T., et al., *WIPI proteins: essential PtdIns3P effectors at the nascent autophagosome.* J Cell Sci, 2015. **128**(2): p. 207-17.
- 271. Mahabir, V.K., et al., *A blinded study of bone marrow examinations in patients with primary immune thrombocytopenia*. Eur J Haematol, 2013. **90**(2): p. 121-6.

- 272. Du, C., J. Chen, and J. Wang, *New insights into the generation and function of megakaryocytes in health and disease.* Haematologica, 2025. **110**(7): p. 1500-1512.
- 273. Garyn, C.M., et al., *G2 arrest primes hematopoietic stem cells for megakaryopoiesis*. Cell Rep, 2024. **43**(7): p. 114388.
- 274. Camacho, V., et al., *Induction of Moderate DNA Damage Enhances Megakaryopoiesis and Platelet Production.* Blood Adv, 2025.
- 275. Rundberg Nilsson, A., et al., *Human and Murine Hematopoietic Stem Cell Aging Is Associated with Functional Impairments and Intrinsic Megakaryocytic/Erythroid Bias.* PLoS One, 2016. **11**(7): p. e0158369.
- 276. Nakamura-Ishizu, A., et al., *Thrombopoietin Metabolically Primes Hematopoietic Stem Cells to Megakaryocyte-Lineage Differentiation.* Cell Rep, 2018. **25**(7): p. 1772-1785 e6.
- 277. Hifdi, N., et al., *Phosphoinositide signaling in the nucleus: Impacts on chromatin and transcription regulation.* Biol Cell, 2025. **117**(1): p. e2400096.
- 278. Chen, M., et al., *The nuclear phosphoinositide response to stress.* Cell Cycle, 2020. **19**(3): p. 268-289.
- 279. Mazloumi Gavgani, F., et al., *Nuclear Phosphatidylinositol 3,4,5-Trisphosphate Interactome Uncovers an Enrichment in Nucleolar Proteins.*Mol Cell Proteomics, 2021. **20**: p. 100102.
- 280. Zhang, X., et al., *Identification of VPS34-PI(3)P-FEN1-mediated DNA repair pathway as a potential drug target to overcome chemoresistance*. Biochem Biophys Res Commun, 2023. **674**: p. 27-35.
- 281. Eliopoulos, A.G., S. Havaki, and V.G. Gorgoulis, *DNA Damage Response and Autophagy: A Meaningful Partnership.* Front Genet, 2016. **7**: p. 204.
- 282. Gal, Z., et al., *Treacle Sticks the Nucleolar Responses to DNA Damage Together.* Front Cell Dev Biol, 2022. **10**: p. 892006.
- 283. Urbancokova, A., et al., *Topological stress triggers persistent DNA lesions in ribosomal DNA with ensuing formation of PML-nucleolar compartment.* Elife, 2024. **12**.
- 284. Azuara-Medina, P.M., et al., *The intracellular domain of beta-dystroglycan mediates the nucleolar stress response by suppressing UBF transcriptional activity.* Cell Death Dis, 2019. **10**(3): p. 196.
- 285. Chen, J., et al., *Identification of a novel TIF-IA-NF-kappaB nucleolar stress response pathway.* Nucleic Acids Res, 2018. **46**(12): p. 6188-6205.
- 286. Ji, J., et al., *Phosphorylated fraction of H2AX as a measurement for DNA damage in cancer cells and potential applications of a novel assay.* PLoS One, 2017. **12**(2): p. e0171582.

- 287. Walters, D.K., et al., Evidence for ongoing DNA damage in multiple myeloma cells as revealed by constitutive phosphorylation of H2AX. Leukemia, 2011. **25**(8): p. 1344-53.
- 288. Leifert, W.R. and S.M. Siddiqui, *gammaH2AX* is a biomarker of modulated cytostatic drug resistance. Cytometry A, 2015. **87**(8): p. 692-5.
- 289. Willitzki, A., et al., Fully automated analysis of chemically induced gammaH2AX foci in human peripheral blood mononuclear cells by indirect immunofluorescence. Cytometry A, 2013. **83**(11): p. 1017-26.
- 290. Reddig, A., D. Roggenbuck, and D. Reinhold, *Comparison of different immunoassays for γH2AX quantification*. Journal of Laboratory and Precision Medicine, 2018. **3**.
- 291. Valente, D., et al., Factors to Consider for the Correct Use of gammaH2AX in the Evaluation of DNA Double-Strand Breaks Damage Caused by Ionizing Radiation. Cancers (Basel), 2022. **14**(24).
- 292. Chen, E., et al., *RECQL5 Suppresses Oncogenic JAK2-Induced Replication Stress and Genomic Instability.* Cell Rep, 2015. **13**(11): p. 2345-2352.
- 293. Stetka, J., et al., Role of DNA Damage Response in Suppressing Malignant Progression of Chronic Myeloid Leukemia and Polycythemia Vera: Impact of Different Oncogenes. Cancers (Basel), 2020. **12**(4).
- 294. Stetka, J., et al., Addiction to DUSP1 protects JAK2V617F-driven polycythemia vera progenitors against inflammatory stress and DNA damage, allowing chronic proliferation. Oncogene, 2019. **38**(28): p. 5627-5642.
- 295. Lee, M.J., et al., Enhancing Anti-Cancer Therapy with Selective Autophagy Inhibitors by Targeting Protective Autophagy. Biomol Ther (Seoul), 2023. **31**(1): p. 1-15.

8. LIST OF FIGURES

Figure 1. Schematic representation of canonical megakaryopoiesis	2
Figure 2. Schematic representation of proplatelet formation.	6
Figure 3. Schematic representation of IL-1α-mediated cytoplasmic rupture vs.	
proplatelet formation	7
Figure 4. The interconversion of phosphoinositide species.	9
Figure 5. Schematic representation of the structural subunits of Vps34 complexes	
and II	10
Figure 6. Schematic representation of the nucleolus and nucleolar	
subcompartments	13
Figure 7. Schematic overview of the mechanism of histone H2A.X phosphorylation	n
in the early phase of DDR	19
Figure 8. IL-1α significantly enlarges megakaryocytes, modifies proplatelet	
structures, and promotes the release of platelet-like particles in vitro	40
Figure 9. Evaluation of platelet production capacity of IL-1α-cultured	
megakaryocytes	41
Figure 10. IL-1 α modulates megakaryocyte maturation by decreasing GPIb β and	
vWF levels while enhancing ploidy	43
Figure 11. Influence of Matrigel on in vitro IL-1α-induced megakaryocyte	
maturation	45
Figure 12. IL-1α modulates Erk signaling in megakaryocytes following TPO	
stimulation, and inhibiting Erk leads to halted megakaryocyte growth and ploidy	48
Figure 13. IL-1α induces emperipolesis in megakaryocytes in vitro	50
Figure 14. Characterization of megakaryocytes cultured with IL-1α until day 5	52
Figure 15. The localization and distribution of the GPIb receptor and CD61 in	
megakaryocytes cultured with IL-1α until day 5	53
Figure 16. IL-1 $lpha$ alters the megakaryocyte proteome and protein expression durir	ng
early maturation	57
Figure 17. Heatmap of key proteins involved in hemostasis, immunity, and	
megakaryocyte development in immature megakaryocytes	58
Figure 18. Hemostatic and neutrophil-related proteome changes in IL-1 α -treated	
mature megakaryocytes.	
Figure 19. Ribosomal proteins show a q-value-significant differential abundance	in
IL-1α MKs	
Figure 20. Nucleolar protein levels tend to increase in IL-1α MKs	
Figure 21. IL-1 α stimulation does not significantly alter nucleolar protein expressi	on
in megakaryocytes	
Figure 22. IL-1 $lpha$ induces nucleolar stress and results in an increased number and	
colocalization of UBF/Vps34 nuclear foci in immature megakaryocytes	74

9. LIST OF TABLES

Table 1. Overview of PIs, related enzymes, and their localization and roles in MK
biology10
Table 2. Pls that localize in the nucleus and their functions in cellular stress response
Table 3. List of chemicals22
Table 4. List of reagents for cell culture
Table 5. List of cytokines
Table 6. List of buffers used for cell lysis, SDS-PAGE, and Western blot 24
Table 7. List of buffers used for immunofluorescence staining of BM cryosections 25
Table 8. List of buffers used for immunofluorescence staining of cells25
Table 9. List of buffers used for murine platelet isolation
Table 10. List of primary antibodies
Table 11. List of secondary antibodies
Table 12. List of q-value significant ribosomal proteins with higher abundance in
TPO/IL-1α cultured MKs on day 361
Table 13. List of q-value significant ribosomal proteins with higher abundance in
TPO/IL-1α cultured MKs on day 5
Table 14. List of nucleolar and functionally related proteins identified in the day 3 MK
proteome with corresponding q-values and fold changes (TPO/IL-1 α vs. TPO) 67
Table 15. List of nucleolar and functionally related proteins identified in the day 5 MK
proteome with corresponding q-values and fold changes (TPO/IL-1 α vs. TPO) 69

10. LIST OF ABBREVIATIONS

ADP adenosine diphosphate

ATM ataxia-telangiectasia mutated kinase

ATP adenosine triphosphate

BM bone marrow

BSA bovine serum albumin

Camp cathelicidin antimicrobial peptide
CFU-MKs colony-forming unit-megakaryocytes
CLP common lymphoid progenitor cell
CMP common myeloid progenitor cell
DAPI 4'.6-diamidino-2-phenylindole

DDR DNA damage response
DFC dense fibrillar component

DMEM Dulbecco's Modified Eagle Medium
DMS demarcation membrane system

DSBs double-strand breaks

EEA1 early endosomal antigen 1

filamin A

FBS fetal bovine serum
FC fibrillar center
FL fetal liver

FSC forward side scatter GC granular component

GMP granulocyte-macrophage progenitor cell

HSC hematopoietic stem cell

IL interleukin JAK Janus kinase

FInA

LAMP1 lysosomal-associated membrane protein 1

Lcn2 lipocalin-2

LPS lipopolysaccharide

Ltf lactoferrin

LT-HSC long-term hematopoietic stem cell MAPK mitogen-activated protein kinase

MEP megakaryocyte-erythroid progenitor cell

MFI mean fluorescent intensity

MK megakaryocyte

MPNs myeloproliferative neoplasms
MPP multipotent progenitor cell

Ncf1 neutrophilic cytosol factor 1

NF-κB nuclear factor κB

NORs nucleolar organizing regions PCA principal component analysis

Pglyrp peptidoglycan recognition protein 1

PI phosphoinositide

 $PI(3,4)P_2$ phosphatidylinositol 3,4-bisphosphate $PI(3,4,5)P_3$ phosphatidylinositol 3,4,5-trisphosphate $PI(3,5)P_2$ phosphatidylinositol 3,5-bisphosphate $PI(4,5)P_2$ phosphatidylinositol 4,5-bisphosphate

PI3K phosphoinositide-3 kinase

PI3P phosphatidylinositol 3-monophosphate PI4P phosphatidylinositol 4-monophosphate PI5P phosphatidylinositol 5-monophosphate

PKC protein kinase C PLL poly-L-lysine

PLPs platelet-like-particles

PLT platelet

PMA phorbol 12-myristate 13-acetate

Pol I RNA polymerase I

RPMI Roswell Park Memorial Institute

RT room temperature

S100a9 S100 calcium-binding protein A9 SDF1α stromal cell-derived factor 1 alpha

STAT signal transducers and activators of transcription

ST-HSC short-term hematopoietic stem cell

TPO thrombopoietin

UBF upstream binding factor Vps34 vacuolar protein sorting 34

vWF von Willebrand factor

11. BIOGRAPHY

Curriculum vitae – Robert Kolman

ROBERT KOLMAN

Date of birth: 18/04/1996 | Place of birth: Zagreb, Croatia | Nationality: Croatian

Gender: Male | Email address: kolman.robert@outlook.com

Work experience

VISITING SCIENTIST | 05/2024 – 08/2024

INSTITUTE FOR EXPERIMENTAL IMMUNOLOGY AND IMAGING, UNIVERSITY HOSPITAL ESSEN – ESSEN, GERMANY

- Visiting PhD student at the Department of Immunodynamics; research training in the field of mass spectrometry-based proteomics during research mobility (MOBDOK-2023-2199)
- UNIVERSITY RESEARCH ASSISTANT | 2021 CURRENT
 UNIVERSITY OF RIJEKA, FACULTY OF BIOTECHNOLOGY AND DRUG DEVELOPMENT – RIJEKA, CROATIA
 - PhD Student working on the project of American Society of Hematology: Nucleolar control of megakaryopoiesis; funded by Croatian Science Foundation ("Young Researchers' Career Development Project", DOK-2020-01-4154) under the supervision of Prof. Antonija Jurak Begonja, PhD
- MEDICAL BIOCHEMIST INTERN | 2020 2021

UNIVERSITY HOSPITAL FOR TUMORS, SESTRE MILOSRDNICE UNIVERSITY HOSPITAL CENTER – ZAGREB, CROATIA

- Mandatory clinical internship for medical biochemists (fields: clinical chemistry, laboratory hematology and coagulation, analytical toxicology) under the supervision of Assistant Prof. Ljiljana Mayer, PhD
- State exam passed in October 2021 Ministry of Health, Zagreb, Croatia

Education and training

- Ph.D. in MEDICINAL CHEMISTRY | Faculty of Biotechnology and Drug Development, University of Rijeka, Rijeka, Croatia
 2021 – CURRENT
- MSc in MEDICAL BIOCHEMISTRY AND LABORATORY MEDICINE | Faculty of Pharmacy and Biochemistry, University of Zagreb, Zagreb, Croatia 2014 – 2019

Conferences and seminars

Kolman R, Bertović I, Peradinović J, Mohović N, Munitić I, Jurak Begonja A
 Effect of interleukin-1 alpha on megakaryopoiesis and platelet formation in vitro | Poster presentation

FEBS3+ Meeting: Exploring Molecular Frontiers 25/09/2024 – 28/09/2024 Pula, Croatia

Kolman R, Bertović I, Peradinović J, Mohović N, Munitić I, Jurak Begonja A
 Interleukin-1 alpha modulates megakaryocyte maturation and platelet
 production in vitro | Poster presentation

European Hematology Association (EHA) Annual Congress 13/06/2024 – 16/06/2024 Madrid, Spain

- Kolman R, Bertović I, Jurak Begonja A
 Interleukin-1 alpha affects megakaryocyte maturation in vitro | Oral presentation Won best presentation prize
 Ph.D. Student Days of the Doctoral Programme "Medicinal Chemistry" 14/09/2023 15/09/2023 Rijeka, Croatia
- Kolman R, Bertović I, Jurak Begonja A
 Class III PI3-kinase Vps34 is involved in the cellular stress response in human leukemic cell lines | Poster presentation
 27th Wilhelm Bernhard Workshop on the Cell Nucleus
 19/06/2023 23/06/2023 Prague, Czech Republic
- Kolman R, Bertović I, Bruketa T, Spindler M, Bender M, Jurak Begonja A
 Acute platelet needs mediated through interleukin-1 alpha affect Vps34
 kinase in mouse megakaryocytes | Poster presentation Won "Young Career
 Researcher" fellowship from Selvita
 International Congress of the Croatian Society of Biochemistry and Molecular
 Biology (HDBMB22) "From Science to Knowledge"
 28/09/2022 01/10/2022 Brela, Croatia
- Kolman R, Bertović I, Bruketa T, Bender M, Jurak Begonja A
 Vps34 kinase in megakaryocyte response to high platelet needs through interleukin-1 alpha | Oral presentation
 1st Biomedicine and Health Ph.D Students Congress "Science and Us" 19/05/2022 20/05/2022 Rijeka, Croatia

Bertović I, Kolman R, Bruketa T, Jurak Begonja A
 Vps34 localizes to the nucleolus and mediates early megakaryopoiesis |
 Poster presentation

American Society of Cell Biology (ASCB) Virtual Conference 01/12/2021 – 10/12/2021 Virtual Conference

Projects

05/2024 – 07/2024

Outbound Mobility of Research Assistants (MOBDOK-2023)

MOBDOK-2023-2199, Croatian Science Foundation

Project leader: Robert Kolman, MSc

2021 – CURRENT

Young Researchers' Career Development Project – Training New Doctoral Students

DOK-2020-01-4154, Croatian Science Foundation

Project leader: Prof. Antonija Jurak Begonja, PhD

Professional courses

• 12/09/2024 – 12/09/2024 (Split, Croatia)

EMBO Workshop on Communicating Research

EMBO training workshop facilitated by EMBO Solutions; Designed to empower and inspire, this workshop gave invaluable insights into the fundamentals of scientific publication and effective research communication.

10/09/2024 – 11/09/2024 (Split, Croatia)

Fellowsherpa Workshop on Fellowship Application

A comprehensive course organized by Fellowsherpa, which guides students and early postdoctoral scholars through the fellowship application process.

04/10/2022 – 06/10/2022 (Trieste, Italy) | Won ICGEB travel grant support

Fluorescence microscopy and high-throughput imaging

Practical course in fluorescence microscopy and high-throughput imaging organized by the International Centre for Genetic Engineering and Biotechnology (ICGEB)

12/05/2022 – 15/05/2022

9th Translational Research E-Conference "Myeloproliferative Neoplasms"

Organized by European School of Hematology (ESH)

Publications

Kolman R, Voß H, Bertović I, et al. Interleukin-1 alpha alters megakaryocyte maturation, promotes emperipolesis, and induces a distinct proteomic profile. *J Thromb Haemost*. Published online September 17, 2025. doi:10.1016/j.jtha.2025.08.037

Parchure A, Cesarec M, Braut A, <u>Kolman R</u> et al. **ADAR1 p150 prevents HSV-1** from triggering PKR/elF2α-mediated translational arrest and is required for efficient viral replication. *PLoS Pathog*. 2025;21(4):e1012452. Published 2025 Apr 8. doi:10.1371/journal.ppat.1012452

Networks and memberships

- 2024 CURRENT European Hematology Association (EHA)
- 2022 CURRENT International Society on Thrombosis and Hemostasis (ISTH)
- 2021 CURRENT
 Croatian Chamber of Medical Biochemists
- 2021 CURRENT
 Croatian Society of Biochemistry and Molecular Biology
- 2020 CURRENT
 Croatian Society of Medical Biochemistry and Laboratory Medicine

Honours and awards

26/09/2017 | **Dean's Award for Academic Achievement** – Faculty of Pharmacy and Biochemistry, University of Zagreb

Teaching activity

2022 – CURRENT

Assistant - course "Cell and Molecular Biology"

Undergraduate programme "Biotechnology and Drug Research" Faculty of Biotechnology and Drug Development, University of Rijeka

• 2021 – CURRENT

Assistant – course "Medical Physiology and Pathophysiology"

Undergraduate programme "Biotechnology and Drug Research" Faculty of Biotechnology and Drug Development, University of Rijeka

2021 – CURRENT

Assistant - course "Tissue Engineering"

Graduate programme "Biotechnology in Medicine", Faculty of Biotechnology and Drug Development, University of Rijeka

Popularization of Science

19/02/2024 – 19/02/2024 Rijeka, Croatia

Presenter: Megakaryocyte response to stress: a bloody challenge

Popularization of science; "PhD Café" organized by Croatian Science Foundation

03/05/2022 – 03/05/2022 Rijeka, Croatia

Workshop: What is blood?

Kolman R, Knight L, Bura A, Jurak Begonja A - organizers of the workshop during the Open Day of the Department of Biotechnology, University of Rijeka

12/12/2020 – 12/12/2020 Zagreb, Croatia

Volunteering

Presenter: Clinical chemistry diagnostics in oncology

Kolman R, Sinožić T - presenters at the Student Congress on Cancer, organized by the Faculty of Chemical Engineering and Technology

• 22/11/2020 – 22/11/2020 Zagreb, Croatia

Presenter: Working in a hospital for tumors and biochemical diagnostics in oncology

Held a presentation for younger students at the ProfessionalDays2020 event organized by the Croatian Pharmacy and Medical Biochemistry Students' Association

• 01/06/2019 – 01/06/2019 Zagreb, Croatia

Member of the Organizing Committee

9th Pharmacy and Medical Biochemistry Student Symposium

• 25/05/2019 – 26/05/2019 Zagreb, Croatia

Member of the Education Committee

6th Congress of Croatian Pharmacy and Medical Biochemistry Students' Association

Licenses and certificates

- 10/2021 - CURRENT | Licensed medical biochemist

Registered medical biochemist under the Croatian Chamber of Medical Biochemists

- 05/07/2021 - CURRENT | Certificate of qualification for conducting animal experiments (Category C)

Issued by the Faculty of Veterinary Medicine, University of Zagreb